April 2013

Particle Fluidization in Upward and Inverse Liquid-Solid Circulating Fluidized Bed

Long Sang
The University of Western Ontario

Supervisor
Dr. Jesse Zhu
The University of Western Ontario

Graduate Program in Chemical and Biochemical Engineering

A thesis submitted in partial fulfillment of the requirements for the degree in Doctor of Philosophy

Particle Fluidization in Upward and Inverse Liquid-Solid Circulating Fluidized Bed

(Thesis format: Integrated Article)

by

Long Sang

Graduate Program in Chemical and Biochemical Engineering

A thesis submitted in partial fulfillment
of the requirements for the degree of
Doctor of Philosophy

The School of Graduate and Postdoctoral Studies
The University of Western Ontario
London, Ontario, Canada

Abstract

The fluidization of particles in upwards and inverse Liquid-Solid Circulating Fluidized Bed is carried out to investigate the hydrodynamic characteristics when using “heavy” and “light” particles, whose densities are higher and lower than that of the surrounding liquid respectively. Generally, the solids are fluidized upwards in the former case, whereas, the downwards fluidization is preferred in the latter scenario.

In the Liquid-Solid Circulating Fluidized Bed (LSCFB) riser, where the upwards fluidization takes place, the effects of particle properties on solids holdup are investigated experimentally based on three parameters: superficial liquid velocity, normalized superficial liquid velocity and excess superficial liquid velocity. The results show that the excess superficial liquid velocity (U_l-U_t), among those three parameters, is a more appropriate parameter to evaluate the effects of the particle properties on the solids holdup, facilitating general comparisons for different types of particles. Then such particle property effects are studied analytically by incorporating operating parameters and particle properties into a mathematical model, showing excellent agreement with the experimental results. By this model, the transition velocity demarcating the circulating fluidization regime and the transport regime is determined to complete the flow regime map in liquid-solid fluidization systems.

In the Inverse Liquid-Solid Circulating Fluidized Bed (ILSCFB) downer, where the inverse fluidization takes place, under the circulating fluidization regime, the hydrodynamic characteristics are investigated experimentally by the fluidization of Styrofoam and Hollow Glassbeads. For both types of particles, axial solids holdup distribution is quite uniform, while radial solids holdup distribution is slightly non-uniform with slight increase adjacent to the wall under various operating conditions, but no obvious “core-annulus” structure is observed. Such solids holdup distribution pattern is closely related to the solids circulation rate, superficial liquid velocity, local liquid and particle velocity which are also measured for Styrofoam particles. It is shown that the radial profiles of both liquid and particle velocities are slightly non-uniform, higher at the center region while lower adjacent to the wall, influenced by solids circulation rate and superficial liquid velocity. The local slip velocity derived from local liquid and particle velocities is found to be very close to the single particle

terminal velocity and one-dimensional slip velocity deduced from the superficial liquid, solids velocities and cross-sectional average solids holdup, suggesting that there is no obvious clustering phenomenon and solids segregation in ILSCFB downer under various operating conditions.

The hydrodynamics under the inverse conventional fluidization regime are also studied by examining the bed voidage and dimensionless bed expansion. A new mathematical model correlating Archimedes and Reynolds number is proposed for the prediction of the bed voidage and dimensionless bed expansion in both inverse and upwards liquid-solid fluidization system, exhibiting better accuracy than that of the well known Richardson and Zaki equation.

The comparisons of the hydrodynamics in ILSCFB and LSCFB are also made based on the force balance discussion, enabling the comparison of inverse and upwards circulating fluidization of particles. Then the generalized flow regime map is developed in terms of dimensionless superficial velocity and dimensionless particle size by determining the demarcations of different flow regimes quantitatively.

Keywords

Liquid-Solid Circulating Fluidized Bed (LSCFB), Inverse Liquid-Solid Circulating Fluidized Bed (ILSCFB), solids holdup, particle properties, liquid velocity, particle velocity, slip velocity, flow regime map

Co-Authorship Statement

Title: Experimental Investigation of the Effects of Particle Properties on Solids Holdup in an LSCFB Riser

Author: Long Sang, Jesse Zhu

Long Sang designed and performed the major part of the experiment and carried out data analysis under the guidance of advisor Dr. Jesse Zhu. All drafts of this manuscript were written by Long Sang. Modifications were carried out under close supervision of advisor Dr. J. Zhu. The final version of this article was published in Chemical Engineering Journal, 197 (2012) 322 – 329

Title: Prediction of Average Solids Holdup and Slip Velocity in Liquid-Solid Circulating Fluidized Bed Riser

Author: Long Sang, Jesse Zhu

Long Sang designed and performed the major part of the experiment and carried out data analysis under the guidance of advisor Dr. Jesse Zhu. All drafts of this manuscript were written by Long Sang. Modifications were carried out under close supervision of advisor Dr. J. Zhu. The final version of this article is ready for submission.

Title: Generalized Fluidization in Inverse and Upwards Liquid-Solid Fluidized Bed

Author: Long Sang, Jesse Zhu

The experimental setup of Inverse Liquid-Solid Circulating Fluidized Bed was designed and modified by Long Sang together with Jianzhang Wen under the guidance of advisor Dr. J. Zhu. All the experimental work was undertaken by Long Sang. All drafts of this manuscript were written by Long Sang. Modifications were carried out under close supervision of advisor Dr. J. Zhu. The final version of this article is ready for submission.

Title: Hydrodynamics in Inverse Liquid-Solid Circulating Fluidized Bed Downer

Author: Long Sang, Jesse Zhu

The experimental setup of Inverse Liquid-Solid Circulating Fluidized Bed was designed and modified by Long Sang together with Jianzhang Wen under the guidance of advisor Dr. J. Zhu. All the experimental work was undertaken by Long Sang. All drafts of this manuscript were written by Long Sang. Modifications were carried out under close supervision of advisor Dr. J. Zhu. The final version of this article is ready for submission.

Title: Local Slip Velocity Behavior in Inverse Liquid-Solid Circulating Fluidized Bed Downer

Author: Long Sang, Jesse Zhu

The experimental setup of Inverse Liquid-Solid Circulating Fluidized Bed was designed and modified by Long Sang together with Jianzhang Wen under the guidance of advisor Dr. J. Zhu. All the experimental work was undertaken by Long Sang. All drafts of this manuscript were written by Long Sang. Modifications were carried out under close supervision of advisor Dr. J. Zhu. The final version of this article is ready for submission.

Title: Advances in (Gas)-Liquid-Solid Circulating Fluidized Bed- A Comprehensive Review

Author: Long Sang, Jesse Zhu

All drafts of this manuscript were written by Long Sang. Modifications were carried out under close supervision of advisor Dr. J. Zhu. The final version of this article is ready for submission.

Acknowledgments

I would like to take this opportunity to express the gratitude and appreciation to those who have always been helping and supporting me in the academic and daily life.

My sincerest thank to my Supervisor Dr. Zhu, for believing in my potential, supporting me not only on research but also on daily life during my whole period of Ph.D. study, and setting a role model for me, which ensured my successful fulfillment of this study.

Much appreciation is extended to Dr. D. Karamanev and Dr. Hui Zhang for their helpful discussion and encouragement.

My gratefulness is directed to Mr. Jianzhang Wen for being a good friend beyond age and his help designing and constructing the experimental equipment. Many thanks go to Mr. Michael Zhu for his help addressing the electrical issues during the experiments.

Thanks are also extended to my friends in the research group, Ying Ma, Quan He, Jing Xu, Yuanyuan Shao, Qing Mu, Liqiang Zhang, Jing Fu, Tang Li, Yong Liu, Tracy Wang and Shan Gao, for their help, advice and friendship.

Many thanks to George Zhang, Kara Malott, Kristen Hunt for their service.

The financial assistance from National Science of Engineering Foundation of Canada and the Western Engineering Scholarship is gratefully acknowledged.

Great gratitude is to my parents. Without their consistent and unreserved support, I could not have done this mission thus far a success.

Finally, my special thank to my lovely wife, Danni Bao, for being a loyal friend and life partner. I cannot thank her enough for loving and supporting me unconditionally.

Table of Contents

List of Tables

List of Figures

Chapter 1

1 General Introduction

1.1 Introduction

Liquid-Solid Circulating Fluidized Beds (LSCFBs) are gaining in popularity for their wide range of potential applications because of their many advantages including significantly high mass and heat transfer rates, improved liquid-solid contact efficiency, easy control of large quantity of particles etc (Zhu et al. 2000). The design, scale up and operation of such liquid-solid continuous systems require information of phase holdup and flow patterns referred to as the hydrodynamic characteristics. Intensive studies have been carried out to investigate the axial and radial solids holdup distributions (Liang et al. 1996; Liang et al. 1997; Zheng et al. 1999; Zheng et al. 2002), local liquid velocity profiles (Liang et al. 1996; Zheng 1999), slip velocity behaviors (Natarajan et al. 2011).

In the above mentioned LSCFBs, solids are fluidized upwards as their densities are larger than that of the surrounding liquid. Whereas, when the density of the solids is lower than that of the surrounding liquid, the downwards fluidization is necessary, referred to as the inverse fluidization. Compared with other light particle systems, inverse conventional fluidization has its advantages, including the efficient control of the process (Nikolov and Karamanev 1987; Karamanev and Nikolov 1996) and biofilm thickness (Karamanev and Nikolov 1992), higher rate of mass transfer (Nikolov and Nikov 1994) and possibility for re-fluidization (Renganathan and Krishnaiah 2003). Some previous experimental and modeling studies have been done to investigate the hydrodynamics of the Inverse Liquid-Solid Fluidized Bed (ILSFB), for example, the bed voidage (Karamanev and Nikolov 1992; Renganathan and Krishnaiah 2005), the minimum fluidization velocity (Karamanev and Nikolov 1992; Vijaya et al. 2000; Renganathan and Krishnaiah 2003), particle terminal velocity in Newtonian (Karamanev and Nikolov 1992) and non-Newtonian fluids (Dewsbury et al. 2000), flow regimes and pressure drops across the bed (Ulaganathan and Krishnaiah 1996), voidage waves (Howley and Glasser 2004), layer inversion of binary particle system (Escudie et al. 2007), liquid circulation velocity in the

inverse fluidized bed airlift reactor (Kawalec-Pietrenko 2000). Some other characteristics such as heat transfer (Cho et al. 2002; Lu et al. 2006) and mass transfer (Nikolov and Nikov 1994) were also studied.

A detailed literature review on previous hydrodynamic studies in LSCFB and conventional inverse fluidized bed as presented in Chapter 2, reveals the following issues all of which are addressed in this study:

1. Although the effects of the particle properties have been studied, more comprehensive understandings on such effects are still needed.
2. While in an effort to develop the mathematical models to predict the average solids holdup under the circulating fluidization regime, a more sophisticated model that incorporates particle properties is still necessary.
3. All research on the inverse fluidization only focused on conventional fluidization regime. No research work has ever been conducted to study the hydrodynamics under the circulating fluidization regime in the inverse fluidization systems.
4. No research work has been carried out to generalize the fluidization in both inverse and upwards liquid-solid circulating fluidized bed.

1.2 Objectives

In order to further enhance the understanding of the circulating fluidization, the effects of particles are investigated in the upwards LSCFB:

1. Investigate the effects of the particle density, size and sphericity on the hydrodynamics in LSCFB based on three parameters: superficial liquid velocity, normalized superficial liquid velocity and excess superficial liquid velocity.
2. Propose a mathematical expression valid in circulating fluidization regime to predict the solids holdup and slip velocity, then identify the effects of particle properties.

To combine the benefits of both inverse fluidization and the concept of circulating fluidization, a new type of liquid-solid circulating fluidized bed, which is called Inverse Liquid-Solid Circulating Fluidized Bed (ILSCFB), should be developed.

1. Design and install a new type of inverse fluidized bed that is able to fluidize and circulate the particles continuously inside the inverse fluidized bed when the fluidization velocity is larger than the particle terminal velocity.
2. Conduct a comprehensive study on the hydrodynamics of ILSCFB, including the axial/radial solids holdup profile, local liquid velocity, local particle velocity and slip velocity in the downer under a wide range of operating conditions.
3. Propose a flow regimes map for ILSCFBs in terms of dimensionless particle diameter vs. dimensionless liquid velocity.
4. Compare the fluidization in both ILSCFB and LSCFB by proposing analytical mathematical expressions under different fluidization regimes.

1.3 Thesis structure

This thesis follow the “integrated article” format as outlined in UWO Thesis Guide.

Chapter 1 is a general introduction followed by detailed literature review in Chapter 2.

Chapter 3 provides the details about the experimental apparatus, including the structures of LSCFB and ILSCFB, the measurement techniques and experimental procedures in this study. The information on the particles used in this study is also provided.

Chapter 4 and Chapter 5 reports the experimental studies in the upwards LSCFB system.

Chapter 4 discusses the effects of particle properties (density and size) on solids holdup in the riser of Liquid-Solid Circulating Fluidized Bed (LSCFB) experimentally based on three parameters: the superficial liquid velocity, the normalized superficial liquid velocity

and the excess superficial liquid velocity. A straightforward mathematical expression is also proposed based on the force balance analysis.

Chapter 5 further studies the effects of particle properties (density, size and sphericity) on solids holdup and slip velocity in the LSCFB riser through analytical model. The proposed model incorporates slip velocity, operational parameters and particle properties to predict average solids holdup under the circulating fluidization regime. This model is valid for a wide range of riser dimensions and particle properties with adequate accuracy (>80%) so that it enables the quantitative investigation of the effects of particle properties on average solids holdup and average particle slip velocity. By this model, the transition velocity demarcating the circulating fluidization regime and the transport regime is determined to complete the flow regime map in the liquid-solid fluidization system.

Chapter 6, 7 and 8 report the experimental studies in inverse conventional fluidization and circulating fluidization, respectively.

Chapter 6 reports the experimental results on the bed voidage and dimensionless bed expansion under the inverse conventional fluidization regime. New mathematical equations for the prediction of the bed voidage and dimensionless bed expansion are proposed based on force balance of particle in terms of Archimedes number and Reynolds number for both inverse and upwards liquid-solid fluidization systems.

Chapter 7 presents the hydrodynamic characteristics in the downer of an Inverse Liquid-Solid Circulating Fluidized Bed (ILSCFB) by fluidization of Styrofoam and Hollow Glassbeads whose densities are lower than that of fluidization media. For both types of particles, the axial and radial solids holdup distribution is discussed and the comparisons of the hydrodynamics in ILSCFB and LSCFB are also made based on the force balance discussion, enabling a comparison of inverse and upwards circulating fluidization of particles. Then the generalized flow regime map suggesting different flow regimes for the both liquid-solid fluidization system is developed in terms of dimensionless superficial

velocity and dimensionless particle size by quantitatively determining the demarcations of different flow regimes.

Chapter 8 reports the local particle and liquid velocities in the downer of an Inverse Liquid-Solid Circulating Fluidized Bed (ILSCFB). The radial profiles of particle velocity, liquid velocity and slip velocity under various operating conditions are presented. The local slip velocities derived from local particle and liquid velocities are also compared with the single particle terminal velocity and the one-dimensional slip velocity deduced from the superficial liquid and solids velocities and cross-sectional average solids holdup.

Chapter 9 gives the general conclusions of above studies and recommendations for future work on LSCFB and ILSCFB.

References

Cho, Y. J., H. Y. Park, S. W. Kim, Y. Kang and S. D. Kim (2002). Heat transfer and hydrodynamics in two- and three-phase inverse fluidized beds. Industrial and Engineering Chemistry Research 41(8): 2058-2063.

Dewsbury, K. H., D. G. Karamanev and A. Margaritis (2000). Dynamic behavior of freely rising buoyant solid spheres in non-newtonian liquids. AIChE Journal 46(1): 46-51.

Escudie, R., N. Epstein, J. R. Grace and H. T. Bi (2007). Layer inversion and bed contraction in down-flow binary-solid liquid-fluidized beds. Canadian Journal of Chemical Engineering 85(1): 25-35.

Howley, M. A. and B. J. Glasser (2004). A comparison of one-dimensional traveling waves in inverse and normal fluidized beds, Austin, TX, United states, American Institute of Chemical Engineers.

Karamanev, D. G. and L. N. Nikolov (1992). Bed Expansion of Liquid-Solid Inverse Fluidization. Aiche Journal 38(12): 1916-1922.

Karamanev, D. G. and L. N. Nikolov (1996). Application of inverse fluidization in wastewater treatment: From laboratory to full-scale bioreactors. Environmental Progress 15(3): 194-196.

Kawalec-Pietrenko, B. (2000). Liquid circulation velocity in the inverse fluidized bed airlift reactor. Bioprocess and Biosystems Engineering 23(4): 397-402.

Liang, W., S. Zhang, J.-X. Zhu, Y. Jin, Z. Yu and Z. Wang (1997). Flow characteristics of the liquid-solid circulating fluidized bed. Powder Technology 90(2): 95-102.

Liang, W. G., J. X. Zhu, Y. Jin, Z. Q. Yu, Z. W. Wang and J. Zhou (1996). Radial nonuniformity of flow structure in a liquid-solid circulating fluidized bed. Chemical Engineering Science 51(10 pt A): 2001-2010.

Lu, P., Y. Cao, A. Wu and W.-P. Pan (2006). Experimental study of heat transfer in a horizontal swirling fluidized bed, Pittsburgh, PA, United states, International Pittsburgh Coal Conference.

Natarajan, P., V. Ramalingam, G. Ramadoss and R. V. Seeniraj (2011). Study of slip velocity and application of drift-flux model to slip velocity in a liquid-solid circulating fluidized bed. Advanced Powder Technology 22(Compendex): 77-85.

Nikolov, L. and D. Karamanev (1987). Experimental Study of the Inverse Fluidized Bed Biofilm Reactor. Canadian Journal of Chemical Engineering 65(2): 214-217.

Nikolov, V. R. and I. Nikov (1994). Liquid-solid mass transfer in three-phase inverse fluidized bed (TPIFB). Hungarian Journal of Industrial Chemistry 22(2): 125-128.

Renganathan, T. and K. Krishnaiah (2003). Prediction of minimum fluidization velocity in two and three phase inverse fluidized beds. Canadian Journal of Chemical Engineering 81(3-4): 853-860.

Renganathan, T. and K. Krishnaiah (2005). Voidage characteristics and prediction of bed expansion in liquid-solid inverse fluidized bed. Chemical Engineering Science 60(10): 2545-2555.

Ulaganathan, N. and K. Krishnaiah (1996). Hydrodynamic characteristics of two-phase inverse fluidized bed. Bioprocess and Biosystems Engineering 15(3): 159-164.

Vijaya, L. A. C., M. Balamurugan, M. Sivakumar, S. T. Newton and M. Velan (2000). Minimum fluidization velocity and friction factor in a liquid-solid inverse fluidized bed reactor. Bioprocess and Biosystems Engineering 22(5): 461-466.

Zheng, Y. (1999). Flow Structure in a Liquid Solid Circulating Fluidized Bed. Chemical and Biochemical Engineering. London, University of Western Ontario. Ph.D.

Zheng, Y., J.-X. Zhu, N. S. Marwaha and A. S. Bassi (2002). Radial solids flow structure in a liquid-solids circulating fluidized bed. Chemical Engineering Journal 88(1-3): 141-150.

Zheng, Y., J.-X. Zhu, J. Wen, S. A. Martin, A. S. Bassi and A. Margaritis (1999). The axial hydrodynamic behavior in a liquid-solid circulating fluidized bed. Canadian Journal of Chemical Engineering 77(Compendex): 284-290.

Zhu, J.-X., D. G. Karamanev, A. S. Bassi and Y. Zheng (2000). (Gas-)liquid-solid circulating fluidized beds and their potential applications to bioreactor engineering. The Canadian Journal of Chemical Engineering 78(1): 82-94.

Chapter 2

2 Literature Review

The hydrodynamic studies in the liquid-solid circulating fluidization systems have popularities due to a number of attractive features of the LSCFB, such as significantly high mass and heat transfer rates, improved liquid-solid contact efficiency, easy control of large quantity of particles etc. (Zhu et al. 2000), enabling Liquid-Solid Circulating Fluidized Beds (LSCFBs) to have a wide range of potential applications, such as ion exchange system for the continuous recovery protein from cheese whey (Lan et al. 2000), bioconversion of agri-waste into lactic acid (Patel et al. 2008), bioreactors (Chowdhury et al. 2009; Li et al. 2012) and other applications (Felice 1995; Zhu et al. 2000). In the above mentioned LSCFBs, the solids are fluidized upwards as their densities are higher than that of the surrounding liquid, whereas, when the density of the solids is lower than that of the surrounding liquid, the downwards fluidization is necessary, referred to as the inverse fluidization. Compared to other light particle systems, the inverse conventional fluidization has its advantages, including the efficient control of the bioprocess (Nikolov and Karamanev 1987; Karamanev and Nikolov 1996) and of biofilm thickness (Karamanev and Nikolov 1992), higher rate of mass transfer (Nikolov and Nikov 1994), and possibility for re-fluidization (Renganathan and Krishnaiah 2003). In most research papers, the downwards fluidization is called inverse fluidization, which have some applications in the waste water treatment (Karamanev and Nikolov 1996; Sowmeyan and Swaminathan 2008). In order to combine the benefits of inverse fluidization and concept of circulating fluidization, a new type of liquid-solid circulating fluidized bed, which is called Inverse Liquid-Solid Circulating Fluidized Bed (ILSCFB), is developed in this research. Therefore, the review of previous studies related to the hydrodynamics of LSCFB and inverse conventional fluidization are essential to establish better understandings of flow characteristics in ILSCFB.

2.1 Hydrodynamics in Liquid-Solid Circulating Fluidized Bed

2.1.1 Flow regimes

The flow regimes in liquid-solid systems are dependent on the liquid flow rate. With increasing liquid flow rate, defined by superficial liquid velocity (U_l), the liquid-solid system experiences several flow regimes as shown in Fig. 2.1a. When the superficial liquid velocity (U_l) is lower than the minimum fluidization velocity (U_{mf}), the bed is in the fixed bed regime. Increasing the superficial liquid velocity (U_l) beyond the minimum fluidization velocity (U_{mf}), the liquid-solid system enters the conventional fluidization regime, where there exists a clear boundary between the bottom dense region and the top freeboard region. Within this regime, an increase in the liquid flow rate causes the dense phase to expand more and raises the dense-dilute phase boundary. With a further increase of the liquid velocity, the boundary between the two phases becomes unclear while the height of the dense phase increases further. Then some particles begin to be entrained out of the bed. At this time, the fluidized bed is in the transition from conventional fluidization to circulating fluidization (Liang et al., 1997; Zheng et al., 1999). With increasing solid-liquid density ratio, the above transition becomes more obvious (Zheng and Zhu, 1999). When the liquid velocity is sufficiently high, large quantity of particles are transported out of the bed and particle circulation rate is increased sharply. At this point, the bed has entered the circulating fluidization regime and it is essential to continuously feed particles into the riser bottom to maintain the bed.

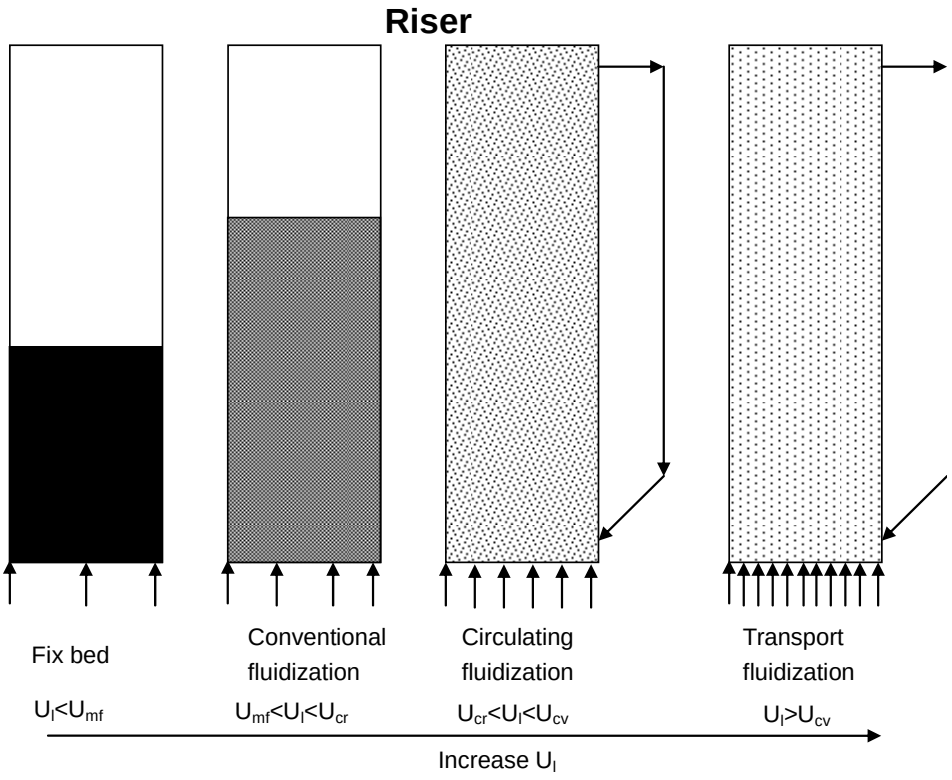

(a)

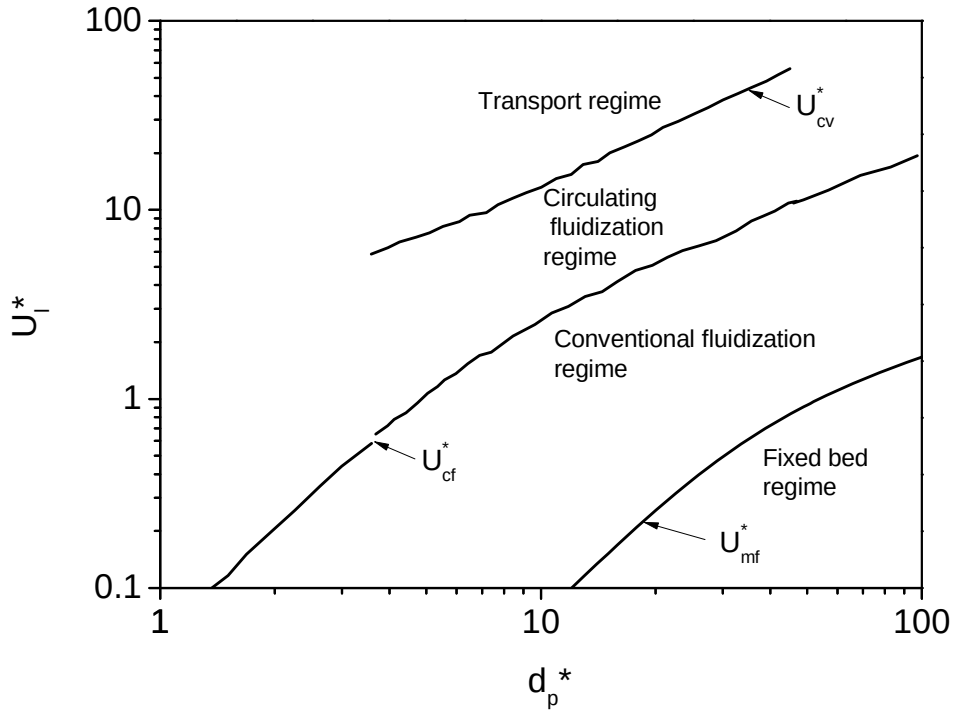

(b)

Fig. 2.1 Flow regimes and flow regime map

As shown in Fig. 2.1b, the transitions of those flow regimes could be determined by the flow regime map (Liang et. al., 1997; Zheng and Zhu, 1999) in terms of dimensionless superficial velocity and dimensionless particle size which are defined as $U_l^* = U_l\left[\rho_l^2/(\mu g \Delta\rho)\right]^{1/3} = Re/Ar^{1/3}$ and $d_p^* = d_p\left(\rho_s g \Delta\rho/\mu^2\right)^{1/3} = Ar^{1/3}$ (Grace 1986) respectively. The fixed bed flow regime and the conventional fluidization regime are demarcated by the minimum fluidization velocity (U_{mf}). For the minimum transition velocity (U_{cf}) demarcating the conventional fluidization regime and the circulating fluidization regime, Liang et. al. (Liang et al. 1993) found that such transition velocity is only 0.6 times of the particle terminal velocity. Later on, Zheng and Zhu (1999), reported that this transition velocity (U_{cf}) is about 1.1~1.2 times of the particle terminal velocity (U_t). The latter reports seem to be more reasonable because they measured such transition velocity is determined by the emptying bed method and independent of operating conditions such as the solids inventory and the feeding system. For the transition velocity (U_{cv}) from the circulating fluidization regime to the transport regime, Liang et. al. (1997) reported that U_{cv} is related to both the liquid velocity and the solids circulating rate.

2.1.2 Axial solids holdup distribution

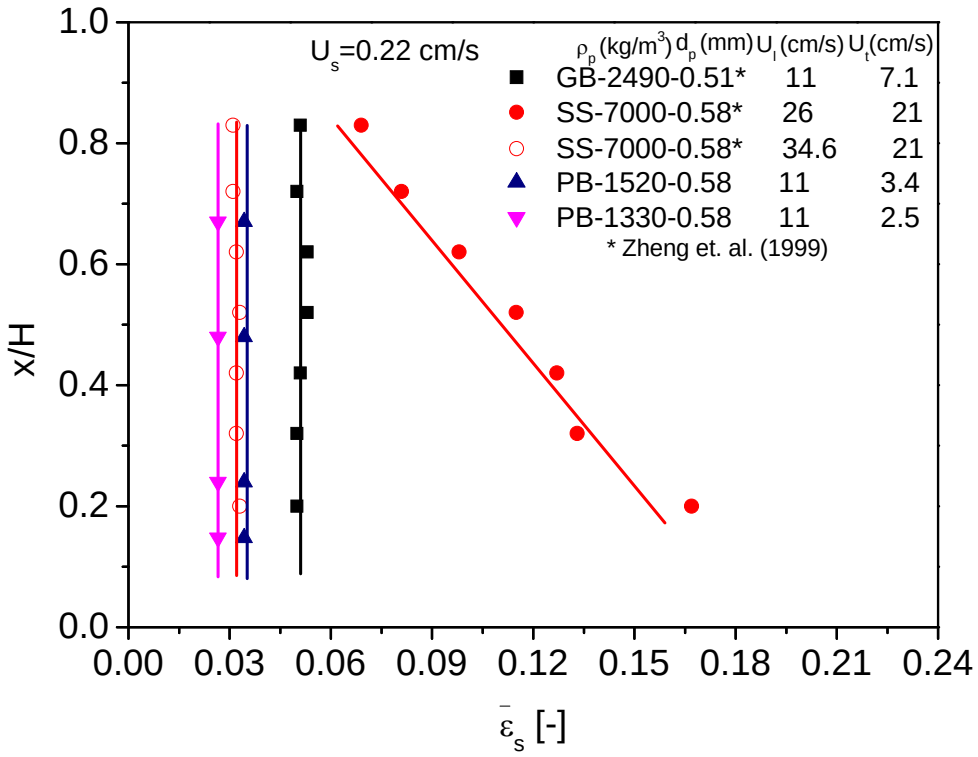

Fig. 2.2 Solids holdup at different positions of the riser for 4 types of particles in same size but different density.

The axial solids holdup distribution in the terms of dimensionless height vs. average solids holdup ($\bar{\varepsilon}_s$) is plotted in Fig. 2.2 under similar superficial liquid velocity (U_l) and superficial solids velocity (U_s). It is shown that the axial profiles for the lighter particles (Glassbeads and plastic beads) are uniform in the entire riser (Zheng et. al., 1999). However, for the heavy particles (steel shot), the axial distribution of solid holdups is not uniform, denser at riser bottom while diluter at riser top, even when U_l=26 cm/s (U_t=21 cm/s). This non-uniformity could be eliminated by further increasing the liquid velocity (Zheng et. al., 1999). Clearly, the effect of the particle density is crucial to the axial solids distribution.

2.1.3 Radial solids holdup distribution

Zheng et. al. (2002) measured the local solids holdup at 7 radial positions and 4 axial locations of LSCFB riser. The radial distribution of solids holdup in LSCFB riser is non-uniform at lower liquid velocity: dilute in the center and denser near the riser wall. This non-uniformity pattern is also observed at four different heights. Meanwhile, for a given liquid velocity, both the radial non-uniformity and the average solids holdup increase with increasing solids circulation rate (in term of the superficial solids velocity U_s). By further increasing the liquid velocity, the radial non-uniformity decreases significantly. This is because the flow regime has transited from the circulating fluidization regime to the dilute transport regime (Liang et. al., 1997). The radial non-uniformity is also related to the particle density (Zheng et. al., 1999).

The non-uniform distribution of the solid holdup actually can be quantified by introducing the concepts of Standard Deviation and Intermittency Index (Brereton and Grace, 1993), which is classified into the micro flow structures (Zhu et. al., 2000). For both parameters, higher values appear in the wall region. With an increase to the solids circulation rate, the magnitudes of the both parameters also increase. This indicates that fluctuations in the solids movement become more vigorous in the wall region and at higher particle circulation rate, due to the increase in solids holdup in both cases. Although the both parameters can be employed as an indicator of the non-uniform distribution of the solids holdup, Standard Deviation is not easily interpreted because the time-mean density varies from point to point; whereas the intermittency Index is a normalized standard deviation, so that it is more meaningful for the direct comparisons for different operating conditions.

2.1.4 Liquid velocity

The radial distribution of liquid velocity was only reported by very few researchers (Liang et. al., 1996, 1997; Zheng and Zhu, 1999). The typical local liquid velocity is non-uniformly distributed along the radial direction: higher liquid velocity at the riser center and lower liquid velocity near the riser wall. With increasing the liquid velocity under the

same solids circulation rate, this non-uniformity decreases because the flow regime transfers from the circulating regime to the dilute transport regime (Zhu et. al., 2000). Furthermore, Zheng and Zhu (1999) reported that solids circulation rate can significantly affect the radial profile of local liquid velocity. Adding more particles leads to an increase in local liquid velocity at the axis but a decrease at the wall. They argued that particle concentration in the vicinity of the wall increases more quickly with increasing solids circulation rate in comparison with that at the central region (Zheng et al., 1999). To balance this variation, liquid velocity in the wall region decreases while that in the central region tends to rise.

Such non-uniformity in radial liquid velocity distribution can be quantified by introducing the concept of Radial Non-uniformity Index (RNI), the normalized standard deviation of the cross-sectional average liquid velocity, which varies between 0 and 1, with larger values indicating more non-uniformity in flow structures (Zheng and Zhu 2003). The higher value of RNI indicates larger non-uniform radial liquid velocity distribution. According to their research, RNI value equals to 0 under the conventional fluidization regime because the uniform solids distribution. However, under the circulating fluidization regime, the RNI value increases first and then decreases with increasing liquid velocity until the flow enters the transport regime, where the RNI value is constant and slightly larger than 0.

2.1.5 Particle velocity

Roy and his research team (Roy et al. 1997; Roy et al. 2005) was the first group to measure the radial distribution of particle velocity with larger particles. The increasing liquid superficial velocity steepens the radial profiles of particle velocity in the operating range of their study. They also found that the radial profiles of particle velocity do not change significantly with the axial position. Later, another group of researchers (Zhang et al. 2003) reported that the liquid distributor significantly affects the non-uniformity of the local particle velocity at the lower part of riser, however, at higher axial position, the effect of the liquid distributor becomes minor. They also investigated the radial local

particle velocity under different solids circulation rate and found that with increasing solids circulation rate, the non-uniformity of the radial local particle velocity also increases. Unfortunately, there has been no attempt to investigate the effects of the particle properties on the particle velocity distribution in their reported works.

2.1.6 Slip velocity

The slip velocity in LSCFB have been reported by several groups of researchers (Liang et al. 1997; Zheng 1999; Natarajan et al. 2011), who all found that the calculated apparent slip velocity is larger than the calculated average slip velocity based on the Kwauk (1963) theory extended from the Richardson and Zaki equation, which is valid for the conventional fluidization regime. In order to improve the existing correlations, Natarajan et. al. (2011) and Sang and Zhu (2012, Chapter 4) proposed two mathematical correlations to predict the average slip velocity independently. However, all the above mentioned studies only investigated the average slip velocity. There was no attempt to study the radial local slip velocity in LSCFB, because there are no experimental data of both local liquid velocity and local particle velocity under the same condition by those researchers. The local slip velocity can be one direction for future research.

2.1.7 Modeling

Generally, the modeling studies on LSCFB can be classified into two categories: analytical methods which are based on flow mechanics, classic correlations and assumptions, and numerical methods, which are based on computational fluid dynamics (CFD). Besides, an artificial neural network (ANN) approach, is developed to model and study the phase holdup distributions in a LSCFB system (Razzak et al. 2012).

For the analytical method, there is a simple one-dimensional model (Richardson and Zaki 1954; Kwauk 1963) to predict the solids holdup and slip velocity in homogenous fluidization. However, it is found that this one dimensional model is not valid in the circulating flow regime (Liang et. al., 1997) due to the non-uniform profile in radial direction. In order to predict such non-uniformity, a core-annulus model (Liang and Zhu

1997) is proposed to consider such non-uniformity. In this type of model, the riser is divided into two parts: a core region in the center and an annulus region adjacent to the wall. Within each region, the fluidization is considered homogeneous and the flow conditions such as liquid and solids holdups, particle and liquid velocities are assumed constant. The radial non-uniformity is then taken care of by the flow segregation between the two regions. By this model, in each region, the average solids holdup, liquid velocity, particle velocity and slip velocity can be predicted under different operating conditions. One limitation of this model is that such predictions are still in terms of average values, so that it cannot provide the precise radial profile. To overcome this limitation, a method based on drift-flux model successfully predicted the flow phenomenon observed in experiments at the cost of introducing one extra empirical parameter called distribution coefficient which is not a flow parameter, making this model rather empirical (Palani et al. 2007) .

For numerical work, Roy and Dudukovic (Roy and Dudukovic 2001) simulated the liquid and solids residence time distributions in the riser, as well as the solids velocity and holdup pattern, based on a CFD two-fluid Euler-Lagrange model. The predicted results were validated with the experimental data and showed its application in predicting the extent of solids backmixing in the reactor. Then Cheng and Zhu (Cheng and Zhu 2005) developed a CFD model based on Eularian-Eularian two phase approach and simulated the hydrodynamics in the riser of an LSCFB under different operating conditions, different particle properties and different riser dimensions. The model predictions had good agreement with the experimental data in the literature. Moreover, the simulation results provided detailed radial profiles of solids holdup, liquid velocity and particle velocity at any axial position as well as the turbulence intensity that are hard to measure in the experiments. Later, the same group of researchers (Cheng and Zhu 2008) investigated the scale-up issue in LSCFB by the CFD model and compared with the similitude method. Their work showed a combination of a reliable CFD model with the proper similitude scale-up is more promising in facilitating better reactor design, scale-up and operation.

Comparing the both methods, each has advantageous and limitations. For example, the analytical method can provide quick estimation of the flow characteristics in LSCFB but such information is limited to certain conditions. While the CFD method can simulate the "real" flow map inside LSCFB and provide very detailed information of the flow field, the simulation process is time consuming by involving huge amount of calculations. Therefore, the analytical model is usually used for the reactor design due to its simplicity and the CFD is used for optimizing the reactor design because of its robust simulation.

2.2 Hydrodynamics in conventional inverse fluidized bed

As early as 1982, the flow characteristics in a three-phase inverse fluidized bed have been studied (Fan et. al., 1982). Since then the research work on the inverse liquid-solid fluidized bed has never stopped.

Similar to the upwards fluidization system, the dimensionless bed expansion (H_T/H_0) is independent of the initial bed height for the whole range of operation starting from packed bed to fully fluidized bed (Ulaganathan and Krishnaiah 1996), while the pressure drop increases with increase in liquid velocity till the bed is completely fluidized and remains almost constant (Ulaganathan and Krishnaiah 1996). For the bed expansion, the situation is more complex and intensive studies were conducted.

The different models for correlation of bed expansion with superficial fluid velocity can be classified into three main categories (Fan et al. 1982) in the traditional fluidized bed. Type I model is based on correlations between U/U_i and ε. The Richardson and Zaki model is the most popular in this group. Type II gives ε as a function of *Ar* and *Re*. The models of Ramamurthy and Subbaraju (Ramamurthy and Subbaraju 1973) is typical for this group. The third group of models is based on the dependence between ε and the main variables of the fluidized bed as in the Wen and Yu correlation (Wen and Yu 1966). Among all the models, the Richardson and Zaki model (Richardson and Zaki 1954) is most popular due to its simplicity and its accuracy of predicting the experimental data. Theoretically, the flow behavior of free rising particles is identical to the free settling

ones. Ideally, the Richardson and Zaki equation in the upwards fluidization system is suppose to be valid in the inverse fluidization system as well. However, Karamanev and Nikolov (1992) found that there were large deviations between the experimental results and the predicted ones by Richardson and Zaki equation in the inverse system, because the free rising of the lighter particles deviate from the standard drag curve when $Re > 130$ or $\rho_p < 300\text{Kg/m}^3$, due to its smaller inertia, resulting a horizontal movement by the turbulent in the flow field. . The same group of researchers also made proper modifications on the calculation of the drag coefficient to enable the Richardson and Zaki equation to be valid in the inverse system again.

Inspired by those differences in calculation of drag coefficient, Karamanev (Karamanev 1996) proposed an explicit way to determine it based on Archimedes number instead of Reynolds number for both “heavy” and “light” particles, facilitating the calculation of the particle terminal velocity and application of the Richardson and Zaki equation. This is important because the definition of *Re* denotes the ratio of dynamic pressure to shear stress on a moving particle, whereas the definition of *Ar* denotes the ratio of effective gravitational force to viscous force, which are directly exerted to a free falling or free rising particle. Thus, the definitions of drag coefficient C_D and bed expansion index (n) for falling particles, as well as rising bubbles, would be theoretically more rational and scientific to be based on *Ar* rather than *Re*.

Other experimental and modeling works also have been carried out to investigate the hydrodynamics of the inverse fluidization system, for example, the minimum fluidization velocity (Karamanev and Nikolov 1992; Vijaya et al. 2000; Renganathan and Krishnaiah 2003), particle terminal velocity in Newtonian (Karamanev and Nikolov 1992) and non-Newtonian fluids (Dewsbury et al. 2000), flow regimes and pressure drops across the bed (Ulaganathan and Krishnaiah 1996), voidage waves (Howley and Glasser 2004), layer inversion of binary particle system (Escudie et al. 2007) were well studied experimentally and mathematically. These studies were compared in the Table 2.1. Some other characteristics such as the heat transfer (Cho et al. 2002; Lu et al. 2006), mass transfer (Nikolov and Nikov 1994) were also studied.

Table 2.1 Tabulation of different studies conducted earlier on inversed fluidization

Researcher	H (m)	*d*/*D*	Density (kg/m^3)	Re_{mf} or Re_t	*Ar*
Fan et al (1982)	2.7	0.062~0.251 (*d*/0.0762m)	388~930		1.1×10^5 ~ 7.65×10^6
Karamanev and Nikolov (1992)	1.3	0.016~0.091 (*d*/0.08m)	75~930	4.5~150 83~2350	0.008×10^6 ~ 3.39×10^6
Ulaganathan and Krishnaiah (1996)	1.8	0.166~0.266 (*d*/0.0753m)	126~534	453.5~575	3.32×10^6 ~ 5.18×10^6
Renganathan and Krishnaiah (2003)	2.2	0.002~0.142 (*d*/0.089m)	250~917	0.009~810	18 ~ 15.4×10^6
Renganathan and Krishnaiah (2005)	2.2	0.002~0.142 (*d*/0.089m)	250~917	0.009~810	1.76 ~ 8.21×10^6

2.3 Hydrodynamics in inverse circulating fluidized bed

Currently, most of the hydrodynamic investigations in the inverse fluidization system are focusing on the two-phase inverse fluidized bed. In the former system, three flow regimes named “Packed Bed” “Semi-Fluidized Bed” and “Fully Fluidized Bed” were proposed (Ulaganathan and Krishnaiah 1996). However, when the bed is fully fluidized, further increasing the liquid velocity beyond the terminal velocity, the flow will enter a new regime similar to the circulating fluidization regime in the traditional LSCFB (Liang et al. 1997). There are no relevant research studies in this new flow regime and the new pattern of inverse fluidized bed in the inverse fluidization system.

References

Cheng, Y. and J.-X. Zhu (2005). CFD modelling and simulation of hydrodynamics in liquid-solid circulating fluidized beds. Canadian Journal of Chemical Engineering 83(2): 177-185.

Cheng, Y. and J. Zhu (2008). Hydrodynamics and scale-up of liquid-solid circulating fluidized beds: Similitude method vs. CFD. Chemical Engineering Science 63(12): 3201-3211.

Cho, Y. J., H. Y. Park, S. W. Kim, Y. Kang and S. D. Kim (2002). Heat transfer and hydrodynamics in two- and three-phase inverse fluidized beds. Industrial and Engineering Chemistry Research 41(8): 2058-2063.

Chowdhury, N., J. Zhu, G. Nakhla, A. Patel and M. Islam (2009). A novel liquid-solid circulating fluidized-bed bioreactor for biological nutrient removal from municipal wastewater. Chemical Engineering and Technology 32(3): 364-372.

Dewsbury, K. H., D. G. Karamanev and A. Margaritis (2000). Dynamic behavior of freely rising buoyant solid spheres in non-newtonian liquids. AIChE Journal 46(1): 46-51.

Escudie, R., N. Epstein, J. R. Grace and H. T. Bi (2007). Layer inversion and bed contraction in down-flow binary-solid liquid-fluidized beds. Canadian Journal of Chemical Engineering 85(1): 25-35.

Fan, L.-S., K. Muroyama and S. H. Chern (1982). Hydrodynamic Characteristics of Inverse Fluidization in Liquid-Solid and Gas-Liquid-Solid Systems. The Chemical Engineering Journal V 24(N 2): 143-150.

Felice, R. D. (1995). Hydrodynamics of liquid fluidisation, Review article number 47 Chemical Engineering Science 50(8): 1213-1245.

Grace, J. R. (1986). Contacting modes and behaviour classification of gas-solid and other two-phase suspensions. The Canadian Journal of Chemical Engineering 64(3): 353-363.

Howley, M. A. and B. J. Glasser (2004). A comparison of one-dimensional traveling waves in inverse and normal fluidized beds, Austin, TX, United states, American Institute of Chemical Engineers.

Karamanev, D. G. (1996). Equations for calculation of the terminal velocity and drag coefficient of solid spheres and gas bubbles. Chemical Engineering Communications 147: 75-84.

Karamanev, D. G. and L. N. Nikolov (1992). Bed Expansion of Liquid-Solid Inverse Fluidization. Aiche Journal 38(12): 1916-1922.

Karamanev, D. G. and L. N. Nikolov (1996). Application of inverse fluidization in wastewater treatment: From laboratory to full-scale bioreactors. Environmental Progress 15(3): 194-196.

Kwauk, M. (1963). Generalized fluidization I, steady state motion. Scienta Sinica 12: 587-612.

Lan, Q., J. X. Zhu, A. S. Bassi, A. Margaritis, Y. Zheng and G. E. Rowe (2000). Continuous protein recovery using a liquid - Solid circulating fluidized bed ion exchange system: Modelling and experimental studies. Canadian Journal of Chemical Engineering 78(Compendex): 858-866.

Li, M., G. Nakhla and J. Zhu (2012). Simultaneous carbon and nitrogen removal with enhanced bioparticle circulation in a Circulating Fluidized Bed Biofilm Reactor. Chemical Engineering Journal 181-182: 35-44.

Liang, W.-G. and J.-X. Zhu (1997). A core-annulus model for the radial flow structure in a liquid-solid circulating fluidized bed (LSCFB). Chemical Engineering Journal 68(1): 51-62.

Liang, W., S. Zhang, J.-X. Zhu, Y. Jin, Z. Yu and Z. Wang (1997). Flow characteristics of the liquid-solid circulating fluidized bed. Powder Technology 90(2): 95-102.

Liang, W. G., S. L. Zhang, Z. Q. Yu, Y. Jin and Q. W. Wu (1993). Liquid-Solid circulating fluidized bed (I): studies on the phase holdups and solid circulating rate. Journal of Chemical Industry and Engineering (China) 44: 666-671.

Lu, P., Y. Cao, A. Wu and W.-P. Pan (2006). Experimental study of heat transfer in a horizontal swirling fluidized bed, Pittsburgh, PA, United states, International Pittsburgh Coal Conference.

Natarajan, P., V. Ramalingam, G. Ramadoss and R. V. Seeniraj (2011). Study of slip velocity and application of drift-flux model to slip velocity in a liquid-solid circulating fluidized bed. Advanced Powder Technology 22(Compendex): 77-85.

Nikolov, L. and D. Karamanev (1987). Experimental Study of the Inverse Fluidized Bed Biofilm Reactor. Canadian Journal of Chemical Engineering 65(2): 214-217.

Nikolov, V. R. and I. Nikov (1994). Liquid-solid mass transfer in three-phase inverse fluidized bed (TPIFB). Hungarian Journal of Industrial Chemistry 22(2): 125-128.

Palani, N., R. Velraj and R. V. Seeniraj (2007). A model to predict radial solids holdup and liquid velocity distributions in liquid-solid circulating fluidized bed. Chemical Product and Process Modeling 2(3).

Patel, M., A. S. Bassi, J. J. X. Zhu and H. Gomaa (2008). Investigation of a dual-particle liquid-solid circulating fluidized bed bioreactor for extractive fermentation of lactic acid. Biotechnology Progress, 2540 Olentangy River Road, P.O. Box 3337, Columbus, OH 43210-3337, United States, American Chemical Society.

Ramamurthy, K. and K. Subbaraju (1973). Bed Expansion Characteristics of Annular Liquid Fluidized. 12(2): 184-189.

Razzak, S. A., S. M. Rahman, M. M. Hossain and J. Zhu (2012). Investigation of artificial neural network methodology for modeling of a liquid-solid circulating fluidized bed riser. Powder Technology 229: 71-77.

Renganathan, T. and K. Krishnaiah (2003). Prediction of minimum fluidization velocity in two and three phase inverse fluidized beds. Canadian Journal of Chemical Engineering 81(3-4): 853-860.

Richardson, J. and W. Zaki (1954). Sedimentation and fluidization: Part I. Transactions of the Institution of Chemical Engineers 32(8): 35-53.

Richardson, J. F. and W. N. Zaki (1954). Sedimentation and fluidisation. Institution of Chemical Engineers -- Transactions 32(1): 35-52.

Roy, S., J. Chen, S. B. Kumar, M. H. Al-Dahhan and M. P. Dudukovic (1997). Tomographic and particle tracking studies in a liquid-solid riser. Industrial and Engineering Chemistry Research 36(11): 4666-4669.

Roy, S. and M. P. Dudukovic (2001). Flow mapping and modeling of liquid-solid risers, American Chemical Society.

Roy, S., A. Kemoun, M. H. Al-Dahhan and M. P. Dudukovic (2005). Experimental investigation of the hydrodynamics in a liquid-solid riser. AIChE Journal 51(3): 802-835.

Sowmeyan, R. and G. Swaminathan (2008). Performance of inverse anaerobic fluidized bed reactor for treating high strength organic wastewater during start-up phase. Bioresource Technology 99(14): 6280-6284.

Ulaganathan, N. and K. Krishnaiah (1996). Hydrodynamic characteristics of two-phase inverse fluidized bed. Bioprocess and Biosystems Engineering 15(3): 159-164.

Vijaya, L. A. C., M. Balamurugan, M. Sivakumar, S. T. Newton and M. Velan (2000). Minimum fluidization velocity and friction factor in a liquid-solid inverse fluidized bed reactor. Bioprocess and Biosystems Engineering 22(5): 461-466.

Wen, C. Y. and Y. H. Yu (1966). Mechanics of fluidization. Chemical Engineering Progress Symposium, 1966.

Zhang, H., T. Wang, J. Wang and Y. Jin (2003). Particle velocity field in liquid-solid circulating fluidized beds. Huagong Xuebao/Journal of Chemical Industry and Engineering (China) 54(10): 1355-1360.

Zheng, Y. (1999). Flow Structure in a Liquid Solid Circulating Fluidized Bed. Chemical and Biochemical Engineering. London, University of Western Ontario. Ph.D.

Zheng, Y. and J. Zhu (2003). Radial Distribution of Liquid Velocity in a Liquid-Solids Circulating Fluidized Bed. International Journal of Chemical Reactor Engineering 1.

Zhu, J.-X., D. G. Karamanev, A. S. Bassi and Y. Zheng (2000). (Gas-)liquid-solid circulating fluidized beds and their potential applications to bioreactor engineering. The Canadian Journal of Chemical Engineering 78(1): 82-94.

Chapter 3

3 Experimental Apparatus and Measurement Methods

Two different liquid-solid circulating fluidized beds were designed and installed in this project, including the upwards Liquid-Solid Circulating Fluidized Bed (LSCFB) and downwards Inverse Liquid-Solid Circulating Fluidized Bed (ILSCFB). In this chapter, the detailed descriptions of the experimental setup and the measurement techniques are presented.

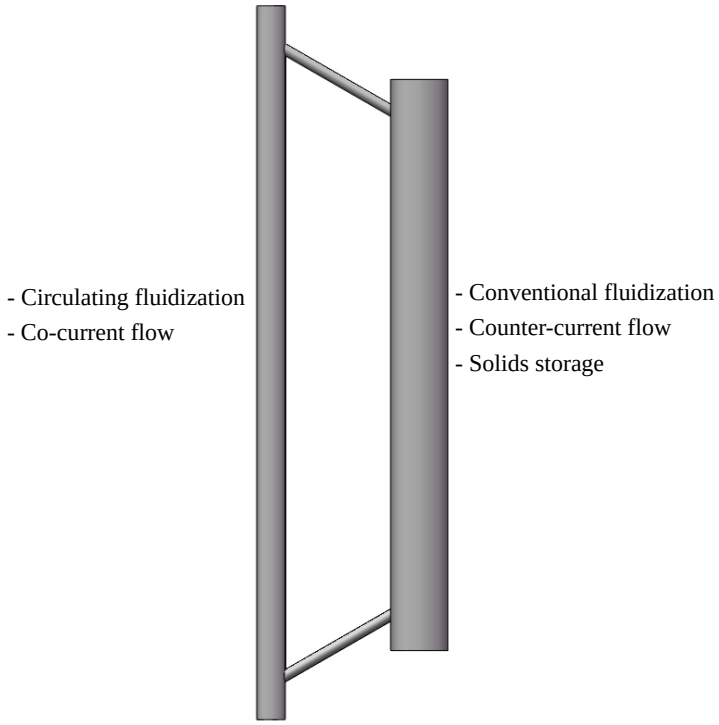

Fig. 3.1 The schematic structure of LSCFB and ILSCFB.

A schematic structure of the LSCFB and ILSCFB is shown in Fig. 3.1. The two types of circulating fluidized bed consist of two major columns connected by two feeding pipes. In the smaller diameter column, there is circulating fluidization regime with solids and liquid flow upward/downwards co-currently, so that the smaller diameter column is characterized by short retention time of both solid particles and liquid and a high degree of shear stress. While in the larger diameter column, there is conventional fluidization regime with solids flow downwards/upwards and liquid flow upwards/downwards

counter-currently, so that this column is characterized by large solids retention time, low shear stress and longer liquid retention time.

In LSCFB, because the density of particles is higher than that of water, the particles should be fluidized upwards therefore the column is called riser. While, when the density of particles is lower than that of water, the particles then should be fluidized downwards in the same column therefore it is called downer. Accordingly, the downer in LSCFB then becomes riser in ILSCFB. The detailed comparisons are conducted in Table 3.1.

Table 3.1 Comparison of LSCFB and ILSCFB structure

Devices	LSCFB	ILSCFB	Functions
Fluidization column	Riser (0.076 m)	Downer (0.076 m)	Circulating fluidization Conventional fluidization
Particle storage column	Downer (0.2 m)	Storage (riser) (0.2 m)	Particle storage Conventional fluidization
Liquid distributors	Bottom of riser	Top of downer	Uniformly distribute liquid stream
Liquid-solid separator	Top of riser	Bottom of downer	Separate liquid and particles
Solids circulating measuring device	Top of downer	Bottom of storage (riser)	Measure the solids circulation rate
Gas evacuation device	Separator	Auxiliary distributor Gas evacuation pipe	Eliminate gas
Anti-siphon device	N/A	At the top of ILSCFB	

3.1 The structure of LSCFB and ILSCFB

3.1.1 Upwards LSCFB

Two different liquid-solid circulating fluidized beds were designed and installed in this study, including the upwards Liquid-Solid Circulating Fluidized Bed (LSCFB) and downwards Inverse Liquid-Solid Circulating Fluidized Bed (ILSCFB). In this chapter, the detailed descriptions of the experimental setup and the measurement techniques are presented.

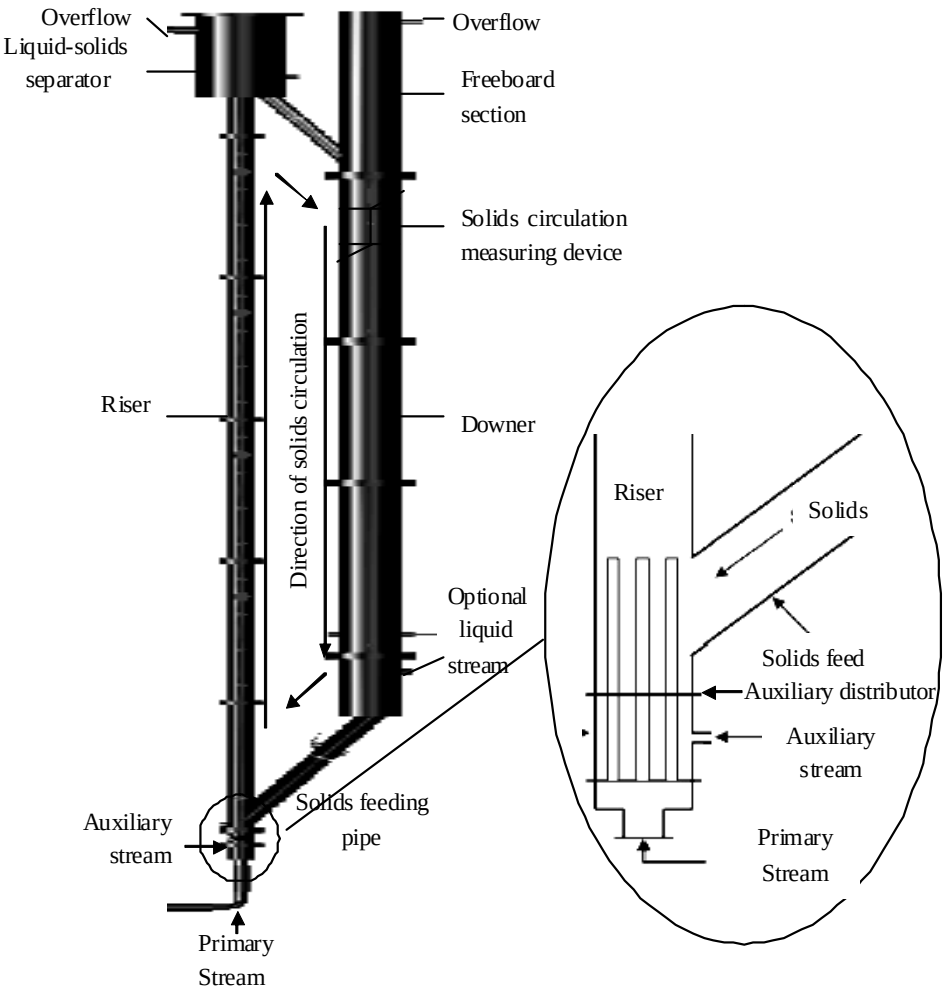

Fig. 3.2 The schematic diagram of LSCFB apparatus.

The set-up of the upwards LSCFB system is shown schematically in Fig. 3.2. The system mainly consists of a Plexiglas riser column of 0.076 m ID and 5.4 m in height, a liquid–solid separator, downer, freeboard section on top of downer and a device for measuring the solids circulation rate. This riser is connected to the 0.2 m ID Plexiglas downer through a solids returning pipe at the top and a solids feeding pipe at the bottom. At the bottom of the riser, there are two distributors: the main liquid distributor made of seven stainless steel tubes occupying 19.5% of the total riser cross-sectional area and extending 0.2 m into the riser, and the auxiliary liquid distributor made of a porous plate with 4.8% opening area at the base of the riser.

The liquid and solids flow rates can be controlled independently by adjusting the main and the auxiliary liquid flow rates. The auxiliary liquid stream controls the quantity of the particles recirculating from the downer to the riser: when the auxiliary flow is set to zero, no particles are able to enter the riser and no continuous particle circulation could be formed. Introducing the auxiliary liquid flow, solids do not begin to flow immediately. Only when the auxiliary liquid flow reaches a threshold flow rate, solids will begin to flow. After that, additional liquid added to the riser bottom cause more particles to enter the riser. Particles introduced into the riser bottom are carried up to the top of the riser by the combined liquid flow (the main liquid flow plus the auxiliary liquid flow) and separated by the large cone based cylindrical liquid–solid separator at the top. Liquid is then returned to the liquid reservoir for reuse and the particles are returned to the downer after passing through the solids circulation rate measuring device.

3.1.2 Downwards ILSCFB

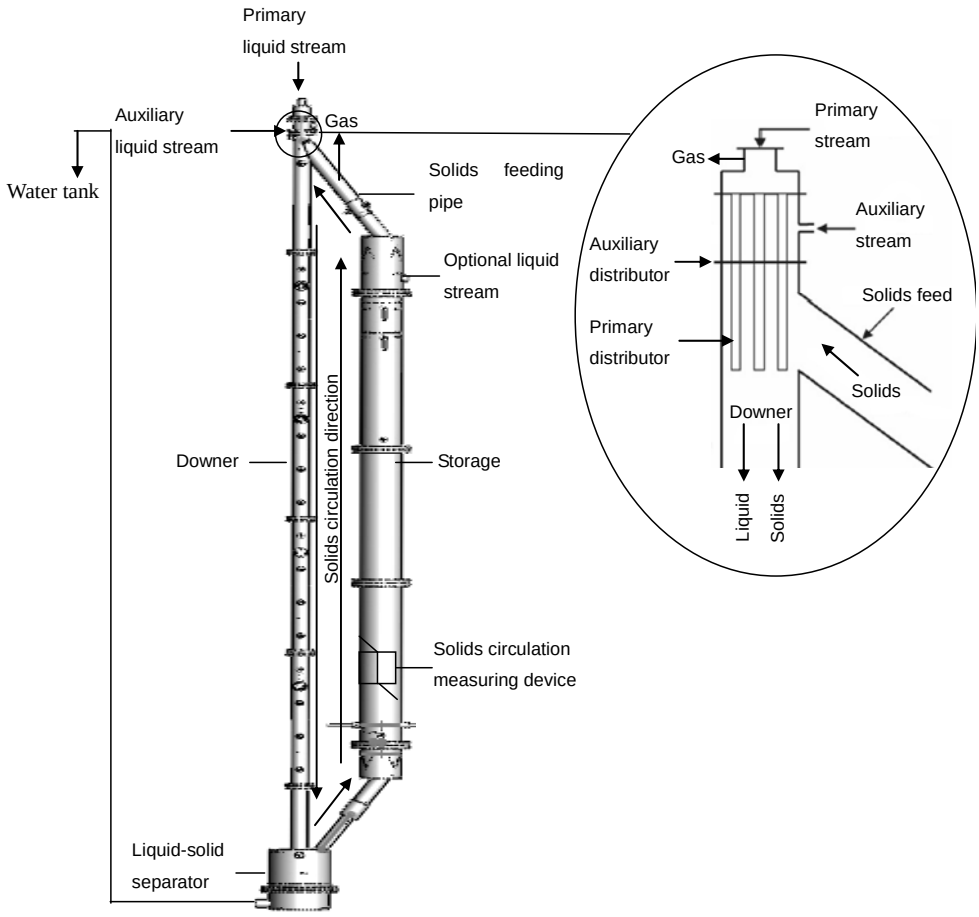

Fig. 3.3 The schematic diagram of ILSCFB apparatus.

The set-up of ILSCFB system is shown schematically in Fig. 3.3. The system mainly consists of a 0.076 m ID Plexiglas downer column, where the inverse fluidization takes place, a liquid–solid separator, storage column, and a device for measuring the solids circulation rate at the bottom of storage. This downer is connected to the 0.2 m ID Plexiglas storage column through a solids returning pipe at the bottom and a solids feeding pipe at the top. There are two distributors: the main liquid distributor made of seven stainless steel tubes occupying 19.5% of the total downer cross-sectional area and extending 0.2 m down to the downer, and the auxiliary liquid distributor made of a porous plate with 4.8% opening area at the top of the downer. With such configuration, particles introduced into the downer top are carried down to the bottom of the downer by the combined liquid flow (the primary liquid flow plus the auxiliary liquid flow) and

separated by the cylindrical liquid–solid separator at the bottom. Liquid is then returned to the liquid reservoir for reuse while the particles are returned to the storage column after passing through the solids circulation rate measuring device and re-introduced into the downer top via the solid feeding pipe to re-fluidize. Therefore, the light particles are continuously circulating inside ILSCFB system.

The liquid and solids flow rates can be controlled independently by adjusting the primary and the auxiliary liquid flow rates. The auxiliary liquid stream controls the quantity of the particles recirculating from the riser to the downer: when the auxiliary flow is set to zero, no particles are able to enter the downer and no continuous particle circulation could be formed. Introducing the auxiliary liquid flow, solids do not begin to flow immediately. Only when the auxiliary liquid flow reaches a threshold flow rate, solids begin to flow. After that, additional liquid added to the downer top cause more particles to enter the downer.

Some specific characteristics in ILSCFB but not observed in upwards LSCFB must be stressed.

The liquid entering the fluidized bed through the liquid distributor often carries gas bubbles. When such bubbles goes in an upflow fluidized bed, it leaves the bed rapidly from the separator at the top of riser because the direction of its free rise is the same as the direction of liquid flow and therefore it does not change significantly the hydrodynamics in the riser. However, in ILSCFB, those gas bubbles may act like “light” particles and move downwards with the liquid, the flow direction of which is opposite to the bubble rising direction. Such phenomenon will affect the hydrodynamics in ILSCFB downer because of the gas bubbles accumulation. It is very important to evacuate the gas bubble form the fluidized bed. The gas bubbles were removed from the auxiliary liquid distributor before each experimental run.

3.2 Measurement procedures

Key parameters are measured in this study, including average solids holdup ($\bar{\varepsilon}_s$), local solids holdup (ε_s), local liquid velocity (V_l), local particle velocity (V_p) and superficial solids velocity (U_s). Their corresponding measuring devices are listed in Table 3.2.

Table 3.2 Measurement methods for different parameters

Parameters	Measuring devices
Average solids holdup	Optical fiber probe, manometer
Local solids holdup	Optical fiber probe
Local particle velocity	Optical fiber probe
Local liquid velocity	Dual conductivity probe and conductivity meter
Superficial solids velocity	Half butterfly valve

3.2.1 Measurement of average solids concentration

The average solids holdup is obtained from the measuring of pressure drop with monometers. Eight pressure ports are installed along the riser/downer column and connected to eight monometers respectively to obtain the pressure at different riser/downer heights. The detailed sampling positions are listed in Table 3.3. With the following equation, the average solids holdup can be calculated based on the pressure drop due to the density difference between the particles and fluidization liquid: $\bar{\varepsilon}_s = \rho_l \Delta h / (\Delta\rho \Delta H)$, where Δh is the water level difference between two monometers, ΔH is the height difference between two probes and $\Delta\rho = \rho_s - \rho_l$ in LSCFB and $\Delta\rho = \rho_l - \rho_s$ in ILSCFB.

Table 3.3 Measurement positions on axial and radial directions

Distance from main liquid distributor (cm) Riser/downer (7.6 cm I.D.)	Radial sampling positions, *r*/*R* (-) Riser/downer (7.6 cm I.D.)
10	0
61.5	0.2034
80.5	0.492
183.8	0.6396
260.3	0.7615
311.1	0.8641
387.8	0.9518
438.8	----

3.2.2 Measurement of local solids concentration

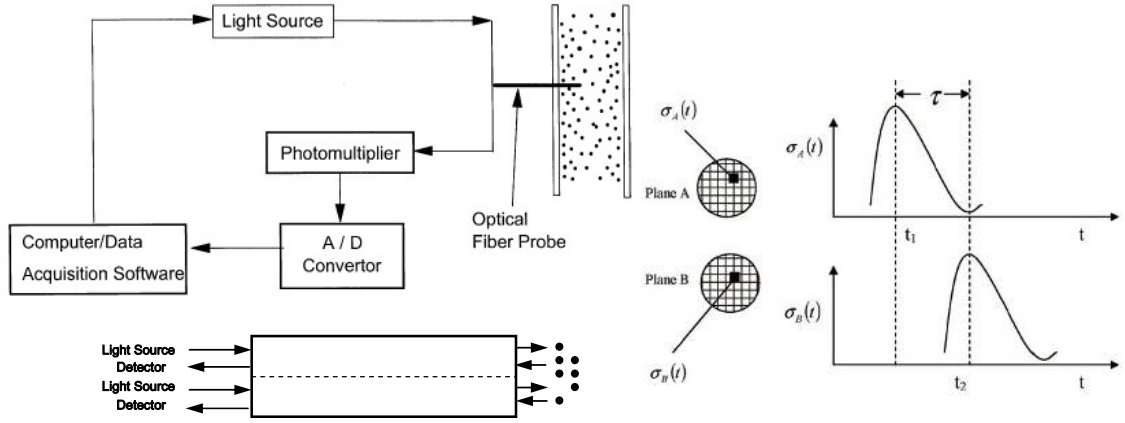

Fig. 3.4 The schematic diagram of solids holdup and particle velocity measurement with optical fiber probe.

The local solids concentration is measured with the multi-fiber type fiber optic concentration probe as shown in Fig. 3.4. The 3.8 mm diameter probe tip consists of approximately 8000 emitting and receiving quartz fibers, each having a diameter of $15\,\mu m$. The active area, where the fibers are located, is approximately 1 mm by 1 mm. A small volume of particles are illuminated by the emitted light, and reflect the light back to the receiving fiber. The reflected light intensity, which is correlated to the volumetric concentration within the volume, is then converted into electrical impulses and integrated

over time, so that a quantitative measure of the local solids concentration is achieved with prior accurate calibration.

These probes, which are a type of intrusive measurement, are simple and practical, effective for local properties and for highly turbulent and denser systems. Moreover, they are nearly free of interference by temperature, humidity, electrostatics and electromagnetic fields. The major difficulty in using this reflective optical fiber probe is that precise calibration is required prior to carrying out prior solids concentration measurements.

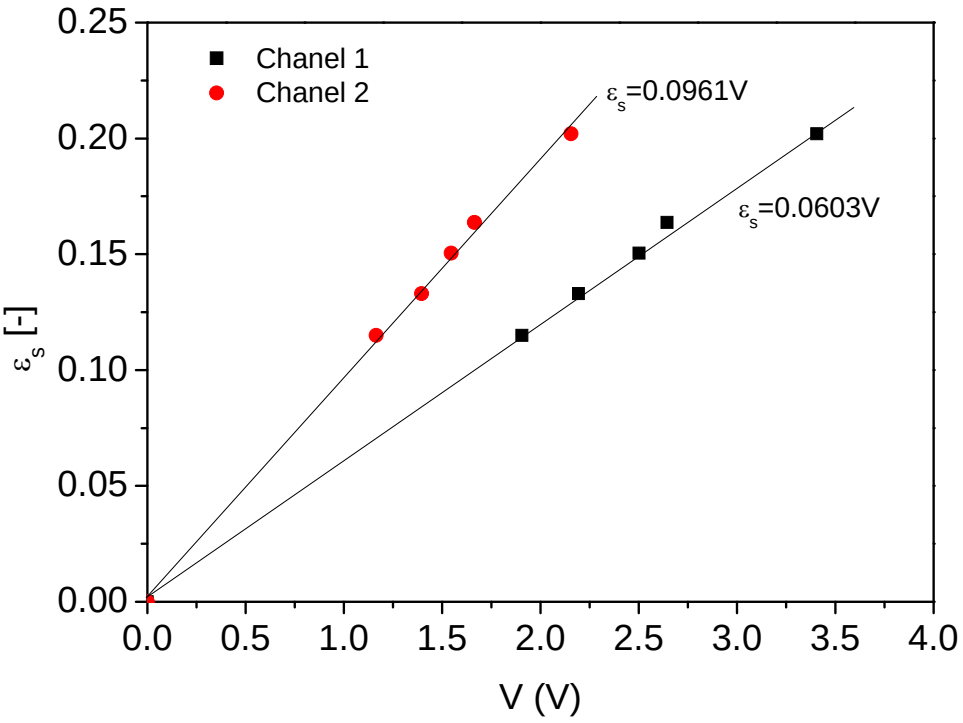

Fig. 3.5 The typical calibration curve for the optical fiber probe.

The calibration of optical fiber probe for the liquid–solid systems could be carried out on site. With the fluidized bed operated in the conventional fluidization regime, where the solids holdup is considered homogeneous in both the axial and the radial direction. Under each flow rate condition, the optical fiber probe is applied to measure the solids reflecting light intensity. This is matched with the solids holdup data obtained from manometers, to

build up a full calibration curve. Once the solids concentration calibration curve is obtained, the measurement voltage signals can be easily related to the solids holdups. Fig. 3.5 shows a typical calibration curve for the optical fiber probe.

3.2.3 Measurement of local particle velocity

The multiple-fiber optical probe is a type of probe, which can be used to measure solids concentration and particle velocity simultaneously. To attain the particle velocity, a cross-correlation between two light receiving channels is required to be applied. The particles in the downer move downward to reflect the light emitted by the probe back to channel B and channel A respectively, which are two bundles of receiving fibers. The particle velocity can be determined by

$$V_p = L_e / T_{AB} \tag{3.1}$$

where L_e is the effective distance between channel A and B, which is calibrated by the manufacturer (1.69 mm in this study). T_{AB} is the time lag between the signal of one particle detected by channel B and channel A. The cross-correlation of

$$\phi_{AB}(\tau) = \lim_{T\to\infty} \frac{1}{T} \int_0^T A(t)B(t+\tau)dt \tag{3.2}$$

is applied to determine T_{AB} (Horio et al. 1988).

If both signals are narrow impulses separated by a fixed time delay, ϕ_{AB} will peak sharply.

3.2.4 Measurement of local liquid velocity

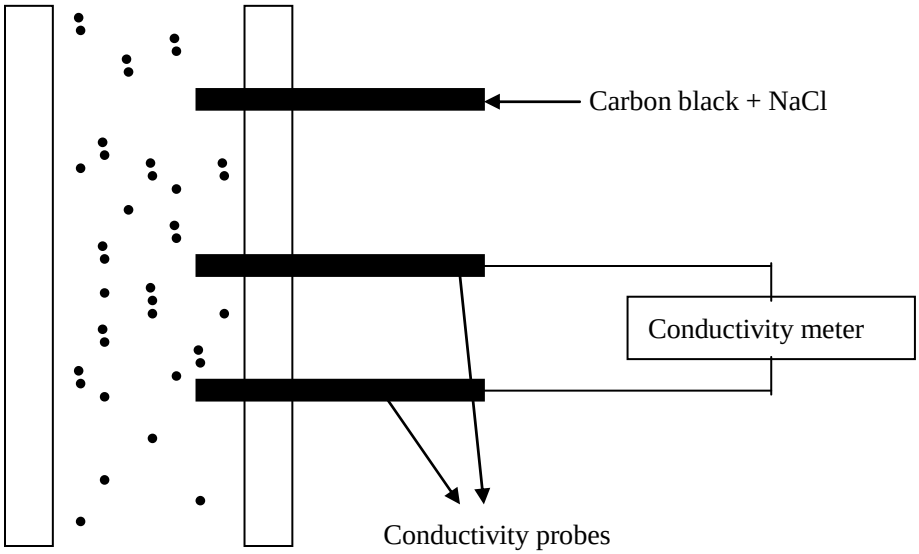

Fig. 3.6 Schematic of local liquid velocity measurement

The local liquid velocity was measured with a pulse injection of saturated NaCl and carbon black electrolyte solution at the upstream of two bronze conductivity probes connecting to a conductivity meter, as shown in Fig. 3.6. Given the very small volume of the injection (about 0.5 ml), the effects of injection on the flow structure is negligible. The distance between the injection point and the upper conductivity probe is 25 cm. When the electrolyte solution is just injected into the downer, there is no signal change indicated by the conductivity meter. Then when the electrolyte solution travels downstream and reaches the point of conductivity probe, the signal indicated by the conductivity meter starts to change. The traveling of the electrolyte solution can also be observed from the traveling of the carbon black. By recording the time interval of the signal change and knowing the distance from the injection point to the conductivity probe, the local liquid velocity at various locations in the bed can be obtained. The injection was traversed in the radial direction to obtain the radial distribution of liquid velocity. All the radial distributions of liquid velocity reported in this study were at the axial position of 4 m below the main distributor, which is in the fully developed flow region.

3.2.5 Measurement of superficial solids velocity

Superficial solids velocity is measured by a half butterfly valve as shown in Fig. 3.2 and 3.3. The 0.2 m diameter storage column is divided into two halves by a central vertical plate with two half butterfly valves fixed at the top and the bottom. By appropriately flipping the top/bottom valve, all the falling/rising particles are induced to pass through the other half column, which is sealed by the bottom/top valve. Thus, all the particles are collected in one half column and increase the packed bed height with time elapsing. A certain distance from the closed valve is marked with a line. Once the particles bed surface passes the line, the accumulative time is recorded. The superficial solids velocity in the storage column can then be obtained by knowing the time period for solids accumulation and the solids packed height.

3.3 Particle properties

All experiments were carried out at ambient temperature. Tap water was used as the fluidizing liquid. The physical properties of the 3 types of particles employed in LSCFB and Styrofoam and Hollow Glassbeads used in ILSCFB are listed in Table 3.4 and Table 3.5 respectively. The terminal particle velocity is determined by the following equation (Karamanev 1996):

$$U_t = \sqrt{\frac{4\left(\rho_p - \rho_l\right) gd}{3\rho_l C_D}} \tag{3.3}$$

$$C_D = \frac{432}{Ar}\left(1 + 0.0470 Ar^{\frac{2}{3}}\right) + \frac{0.517}{1 + 154 Ar^{-\frac{1}{3}}} \tag{3.4}$$

valid for both free falling and free rising particles, but when $Ar > 1.18 \times 10^6 d_p^2$, $C_D = 0.95$ for free rising particles

Table 3.4 Physical properties of particles used in LSCFB

Particles	Density (kg/m^3)	Size (mm)	*Ar*	U_t (cm/s)
Plastic beads	1330	0.58	632	2.47
Plastic beads	1520	0.58	995	3.39
Plastic beads	1520	1.19	8600	6.41

Table 3.5 Physical properties of particles used in ILSCFB

Particles	Density (kg/m^3)	Size (mm)	*Ar*	U_t (cm/s)
Styrofoam I	46	0.8	9000	10.8
Hollow Glassbeads	790	2.5	320000	9.63
Styrofoam II	15	5	3310000	30.8
HDPE	940	3.5	25200	5.89

References

Horio, M., K. Morishita, O. Tachibana and N. Murata (1988). Solids distribution and movement in circulating fluidized beds. Circulating Fluidized Bed Technology II, Toronto, Pergamon Press.

Karamanev, D. G. (1996). Equations for calculation of the terminal velocity and drag coefficient of solid spheres and gas bubbles. Chemical Engineering Communications 147: 75-84.

Chapter 4

4 Experimental Investigation of the Effects of Particle Properties on Solids Holdup in an LSCFB Riser

4.1 Introduction

Liquid-Solid Circulating Fluidized Beds (LSCFBs) are gaining in popularity for their wide range of potential applications, such as ion exchange system for the continuous recovery protein from cheese whey (Lan et al. 2000), bioconversion of agri-waste into lactic acid (Patel et al. 2008), liquid-solid circulating fluidized bed bioreactors (Chowdhury et al. 2008) and other applications (Felice 1995; Zhu et al. 2000).

The design, scale up and operation of such liquid-solid continuous systems require information of phase holdup and flow patterns referred to as the hydrodynamic characteristics. Numerous papers have reported that the solids holdup is dependent on operating conditions, e.g. the superficial liquid velocity, the auxiliary liquid velocity and the solids circulation rate (Liang et al. 1997; Zheng et al. 1999). Unfortunately, however, little research has been conducted to investigate the effects of particle properties on hydrodynamics in LSCFBs with inconclusive results. Zheng et. al. (1999,2002) and Liang et. al. (1997) reported the hydrodynamics for different types of particles (seen in Table 1) in LSCFBs in both axial and radial directions, but the effects of particle density and size were not discussed. While Natarajan et. al. (2008) did try to study the effects of particle density and size on the solids holdup, their experimental comparison was unfortunately based on the same auxiliary liquid velocity, which could lead to different solids circulation rate for different types of particles (Zheng et al. 1999), so that such comparison is invalid. Meanwhile, Natarajan et. al. (2008) did not consider the terminal velocity (U_t) which could be different when comparing the solids holdup of different types of particles with different densities and sizes. Zheng et. al.(2002) took the terminal velocity (U_t) into consideration when plotting experimental solids holdup against the normalized superficial liquid velocity (U_l/U_t). However, there is no research work comparing the solids holdup based on another parameter, the excess superficial liquid

velocity (U_l-U_t), which incorporated the terminal velocity (U_t). Also limited studies on the mathematical models that could relate the solids holdup and particle properties are reported for LSCFB systems. Though there is a model based on the drift flux theory to estimate solids holdup in LSCFB risers (Natarajan et al. 2008), an extra empirical parameter (distribution coefficient) was introduced to make their model rather empirical and parameter dependent.

In this paper, the average and local solids holdups of 5 different types of particles are examined to conduct systematic studies on the effects of the particle properties based on the 3 parameters: the superficial liquid velocity (U_l), the normalized superficial liquid velocity (U_l/U_t) and the excess superficial liquid velocity (U_l-U_t). This paper then discusses the generalized effects of the particle properties on the solids holdup and to propose a mathematical equation to predict the average solids holdup directly from the operating conditions and particle properties for LSCFB risers.

Table 4.1 Riser dimensions and particle physical properties used in Zheng et. al. (1999, 2002) and current study

Researchers	Riser ID (m)	Riser height (m)	Particles	Particle density (kg/m^3)	Particle size (mm)	Particle sphericity	U_t (cm/s) Calculated by Clift et. al. (1978)[*1] for spherical particles and Haider et. al. (1989)[*2] for non-sphrical particles	Re_t	Ar
Zheng et. al. (1999,2002)	0.076	3	Glassbeads	2490	0.51	~1	7.1	36.1	1920
			Steel shot	7000	0.58	--	21	113.1	11500
Current research	0.076	5.4	Plastic beads	1330	0.58	~0.7	2.47	14.5	632
			Plastic beads	1520	0.58	~0.7	3.39	19.7	995
			Plastic beads	1520	1.19	~0.7	6.41	76.3	8600

*1 $\log Re_t = -1.814 + 1.347\log N_D - 0.1243(\log N_D)^2 + 0.00634(\log N_D)^3$ with $N_D = C_D Re_t^2 = \frac{4\rho_l(\rho_p - \rho_l)gd^3}{3\mu^2} = \frac{4}{3}Ar$

*2 $u^* = \left[\frac{18}{\left(d^*\right)^2} + \frac{2.3348 - 1.7439\phi}{4\left(d^*\right)^{0.5}}\right]^{-1}$ with $u^* = U_l\left[\rho_l^2/(\mu g\Delta\rho)\right]^{1/3} = Re/Ar^{1/3}$, $d^* = d_p\left(\rho_p g\Delta\rho/\mu^2\right)^{1/3}$, $\phi = 0.5 \sim 1$

4.2 Materials and methods

The set-up of LSCFB system is shown schematically in Fig. 4.1. The system mainly consists of a Plexiglas riser column of 7.62 cm ID and 5.4 m in height, a liquid–solids separator, downer, freeboard section on top of downer and a device for measuring the solids circulation rate. This riser is connected to the 20 cm ID Plexiglas downer through a solids returning pipe at the top and a solids feeding pipe at the bottom. At the bottom of the riser, there are two distributors: the main liquid distributor made of seven stainless steel tubes occupying 19.5% of the total riser cross-sectional area and extending 0.2 m into the riser, and the auxiliary liquid distributor made of a porous plate with 4.8% opening area at the base of the riser.

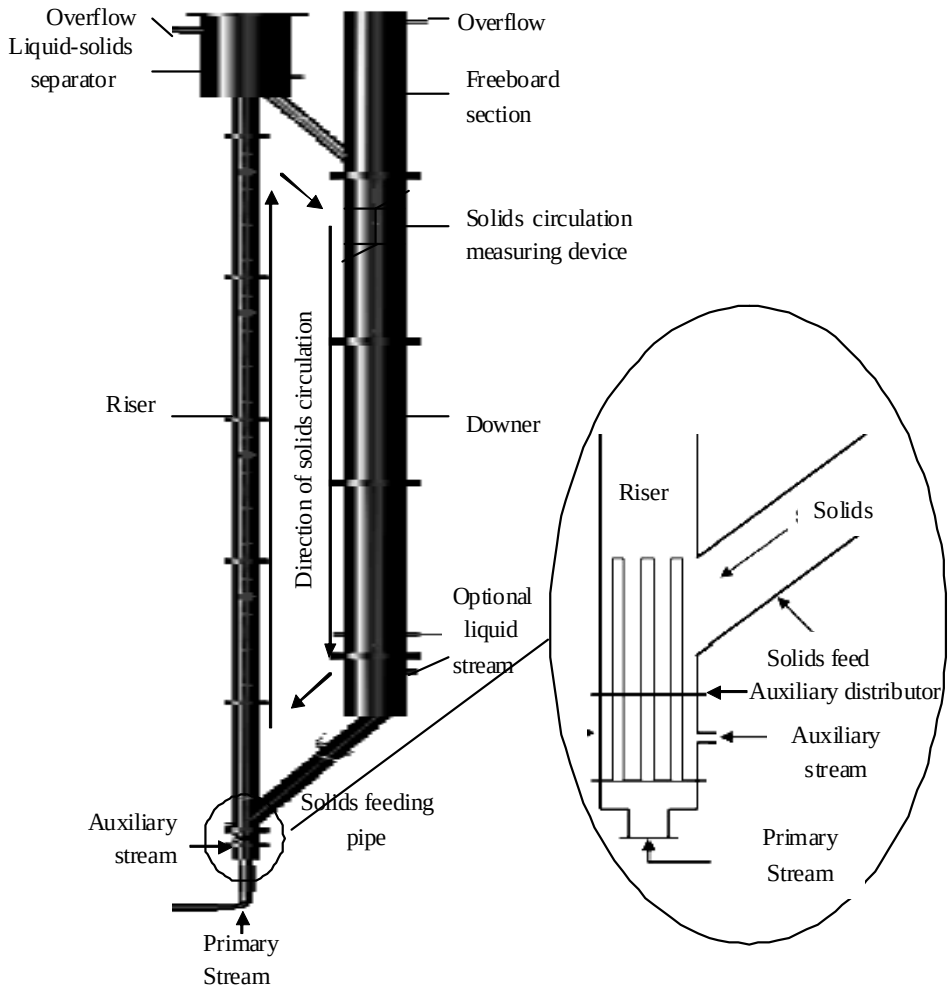

Fig. 4.1 The schematic diagram of LSCFB apparatus.

The liquid and solids flow rates can be controlled independently by adjusting the main and the auxiliary liquid flow rates. The auxiliary liquid stream controls the quantity of the particles recirculating from the downer to the riser: when the auxiliary flow is set to zero, no particles could enter the riser and no continuous particle circulation could be formed. Introducing the auxiliary liquid flow, solids do not begin to flow immediately. Only when the auxiliary liquid flow reaches a threshold flow rate, solids begin to flow. After that, additional liquid added to the riser bottom cause more particles to enter the riser. Particles introduced into the riser bottom are carried up to the top of the riser by the combined liquid flow (the main liquid flow plus the auxiliary liquid flow) and separated by the large cone based cylindrical liquid–solids separator at the top. Liquid is then returned to the liquid reservoir for reuse and the particles are returned to the downer after passing through the solids circulation rate measuring device.

The local solids holdup is measured by using an optical fiber solids concentration probe model PV-5, produced by the Institute of Process Engineering, Chinese Academy of Sciences. For details of this probe, please refer to (Zhang et al. 1998) and (Zheng et al. 2002). The calibration of this probe for the liquid–solids systems could be carried out on site. With the fluidized bed operated in the conventional particulate regime, where the solids holdup is considered homogeneous in both the axial and the radial direction, the output voltage signal from the probe is calibrated against the solids holdup data obtained from pressure gradient measurements. Such calibration is always conducted in the middle section of the fluidized bed so that the “end effect” is eliminated. Linear relationship was found between the voltage signal and the solids holdup for each type of the particles.

All experiments were carried out at ambient temperature. Tap water was used as the fluidizing liquid. The physical properties of the 3 types of particles employed in current study and 2 types of particles in the study of Zheng et. al. (1999) are listed in Table 4.1. In each run, local solids holdup was measured at different radial positions but given axial position by traversing the probe horizontally, after LSCFB unit was brought to a steady operation. In initial measurements, the probe was traversed from one wall to the other and

no significant asymmetry was found in the radial holdup profile. Therefore, measurements were taken only at one side of the riser, at seven radial locations between the center and the wall (r/R =0, 0.2034, 0.492, 0.6396, 0.7615, 0.8641, 0.9518). At 4 different levels the same procedure was repeated for different solids circulation rates and liquid velocities. For each measurement location, a 0.6 m around measurement section was enwrapped with a black plastic sheet to prevent external light interfering with the measurements.

4.3 Superficial solids velocity U_S and its control

Superficial solids velocity (U_s) is defined as the upward velocity of the solids phase alone where there is no liquid present in the riser. Solids circulation rate (G_s) is the mass flow rate of solids circulating between the riser and the downer at steady-state operation and the relation between the two is $U_s = G_s / \rho_p$. Although both parameters could be employed to describe the amount of solids circulating from the downer to the riser at unit time per unit area, it is more reasonable to use the superficial solids velocity (U_s) when different types of particles with different solids densities (ρ_p) are involved. This is important because when conducting the comparisons, such as solids holdup under different operating conditions, one must make sure the superficial solids velocity (U_s) is same. Otherwise the comparisons are not on the same basis, because the superficial solids velocity (U_s) could be different even when solids circulation rate (G_s) is set to be the same for particles of different density.

The variations of the superficial solids velocity (U_s) with the combined superficial liquid velocity (U_l) and the auxiliary liquid velocity (U_a) are shown in Fig. 4.2 for 5 types of particles. For all particles at different auxiliary liquid velocities (U_a), superficial solids velocity (U_s) initially increases with combined superficial liquid velocity (U_l) because solids circulation tends to be limited by the entrainment capacity of the combined liquid velocity, rather than the particle mobility at the exit of the feeding pipe at the riser bottom controlled by the auxiliary liquid velocity (U_a). Beyond the initial stage, the solids circulation is more controlled by the auxiliary liquid velocity (U_a), so that the superficial

solids velocity (U_s) is constant for each auxiliary liquid velocity (U_a) though the combined superficial liquid velocity (U_l) keeps increasing, and the solids circulation is considered to be fully developed. On the other hand, at this stage, the superficial solids velocity (U_s) increases with the auxiliary liquid velocity (U_a) for a fixed superficial liquid velocity (U_l) since more particles are introduced into the riser with higher auxiliary liquid velocity (U_a).

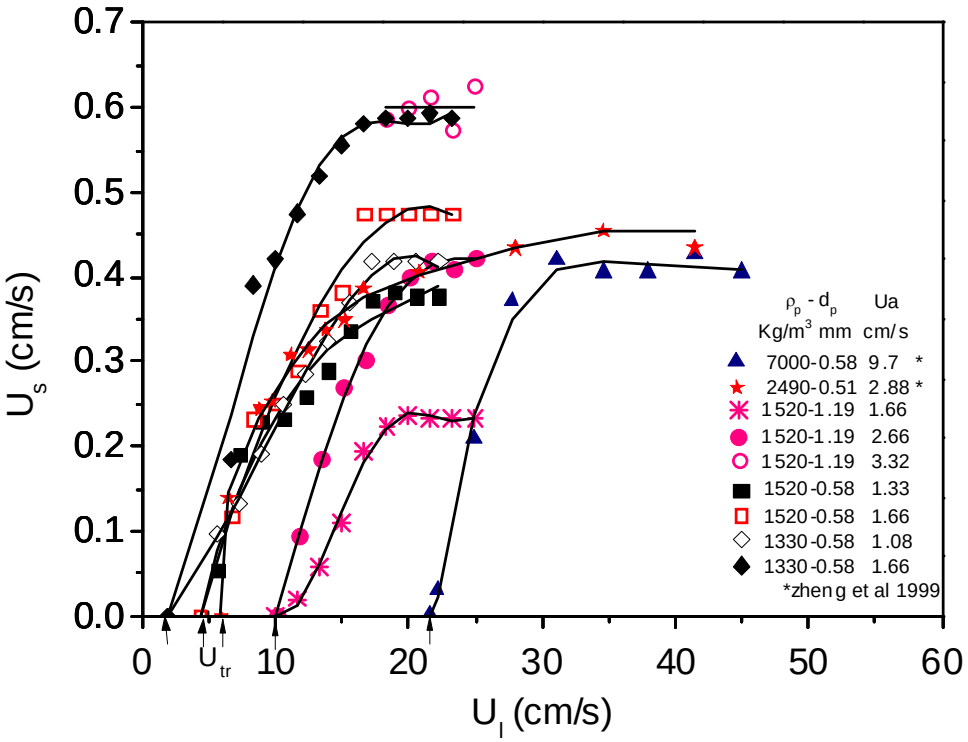

Fig. 4.2 The superficial solids velocity (U_s) as a function of combined superficial liquid velocity (U_l) for 5 types of particles under different auxiliary liquid velocity.

By adjusting the auxiliary liquid velocity (U_a), similar superficial solids velocity (U_s) could be achieved for all 5 types of particles. It can be seen from Fig. 4.2 that the superficial solids velocity (U_s) is around 0.4 cm/s when U_a=1.08, 1.33, 2.66, 2.88 and 9.7 cm/s for PB1330-0.58, PB1520-0.58, PB1520-1.19, GB2490-0.51 and SS7000-0.58 particles respectively. Therefore, in LSCFB systems, for different types of particles, the superficial solids velocity (U_s) could be different even if under the same auxiliary liquid velocity, e.g. U_a=1.66 cm/s, the superficial solids velocity (U_s) for PB1330-0.58,

PB1520-0.58 and PB1520-1.19 particles are 0.58 cm/s, 0.47 cm/s and 0.24 cm/s respectively shown in Fig. 4.2. As a result, when conducting the comparisons, it is important to keep the superficial solids velocity (U_s) fixed, rather than the auxiliary liquid velocity (U_a). Otherwise the comparisons are not valid since the solids holdup increase with the superficial solids velocity (U_s) when other operating conditions are the same. In the current study, the superficial solids velocity (U_s) is fixed for each set of comparison when investigating the effects of the particle properties.

It can also be noted that there is a critical superficial liquid velocity (U_l) existing, below which there is no particle circulation between the riser and the downer (U_s=0). Beyond the critical superficial liquid velocity (U_l), the flow enters the circulating fluidization regime (U_s>0). This critical superficial liquid velocity is referred to as the transition velocity (U_{tr}) (Liang et al. 1997; Zheng and Zhu 2001) which demarcates the conventional particulate regime and circulating fluidization regime (Liang et al. 1997; Zheng et al. 1999). As seen in Fig. 4.2, the transition velocity (U_{tr}) is higher with larger particle density or size. Many studies (Liang et al. 1997; Zheng et al. 1999) have proved that this transition velocity (U_{tr}) is almost equal to the particle terminal velocity (U_t) expressed as $U_t = \left[\left(4(\rho_p - \rho_l)gd_p\right)/\left(3\rho_l C_D\right)\right]^{1/2}$ (Denn 1980). This equation could explain why larger particle density or size will lead to higher particle terminal velocity (U_t) or higher transition velocity (U_{tr}) quantitatively.

4.4 The effects of particle properties on the hydrodynamics in LSCFB riser

In order to investigate the effects of particle properties (density and size) on the hydrodynamics in LSCFB riser, the experimental results of 3 types of particles in the current study and 2 types of particles in the studies by Zheng et. al. (1999, 2002) are compared under similar fluidization conditions (U_s =0.1~0.4 cm/s, U_l =11~45 cm/s). The selected particle densities range from 1330 kg/m^3 to 7000 kg/m^3 and particle sizes range from 0.51 mm to 1.19 mm, as shown in Table 4.1. As discussed in Section 4.3, the transition velocities (U_{tr}) (or particle terminal velocities (U_t)) for the 5 different types of

particles are different, such differences in the transition velocity (U_{tr}) should be considered when comparing the solids holdup. Beside the superficial liquid velocity (U_l), another two parameters, which incorporated the particle terminal velocity (U_t) (or transition velocity (U_{tr})), the normalized superficial liquid velocity (U_l/U_t) and the excess liquid velocity (U_l-U_t) are also introduced to investigate the effects of particle properties on the hydrodynamics in LSCFB riser.

4.4.1 The effect of the particle density

Solids holdup variations based on the superficial liquid velocity (U_l)

The average solids holdups of 5 different types of particles are plotted against the superficial liquid velocity (U_l) in Fig. 4.3 under the same superficial solids velocity U_s =0.4 cm/s. For all particles, the average solids holdup decreases when the superficial liquid velocity (U_l) increases because much energy is provided to entrain the particles, which leads to a lower solids concentration. For the particles having similar size, heavier particles lead to larger solids holdup under similar superficial liquid velocity (U_l). In other words, to achieve the same solids holdup, heavier particles require higher superficial liquid velocity (U_l). This phenomenon is not surprising because particles with similar size but higher density possess larger mass which makes them hard to fluidize. In order to show the particle density effect explicitly, Fig. 4.3 is replotted in terms of the average solids holdup ($\bar{\varepsilon}_s$) against the particle density (ρ_p) in Fig. 4.4a. It is clear that for all superficial liquid velocity (U_l), the average solids holdup ($\bar{\varepsilon}_s$) increases with particle density (ρ_p) monotonically. Clearly larger particle density leads to higher solids holdup in LSCFB riser when the comparison is based on the superficial liquid velocity (U_l).

The radial solids distributions for particles of different densities are compared in Fig. 4.4b for U_s=0.4 cm/s and U_l=28 cm/s. For all 3 types of particles, solids distribution is non-uniform across radial positions: lower at the riser centre but higher near the riser wall. At all radial locations, local solids holdup increases with particle density. For

example, local solids holdup for GB2490-0.51 is larger than that for PB1520-0.58 across the radius. Therefore, the larger particle density leads to higher solids concentration across the radius in LSCFB riser when the comparison is based on the superficial liquid velocity (U_l). As there are no experimental data of local solids concentration in the radial position for the SS7000-0.58 particles from the study of Zheng et. al. (1999), the data set is not included in this figure.

However, the above discussed comparison is based only on the superficial liquid velocity (U_l). It is insufficient because this parameter does not incorporate the terminal velocity (U_t) which is different for various types of particles. For further comparisons, the parameters that incorporate the terminal velocity (U_t) should be proposed. One way to incorporate the terminal velocity (U_t) is to use the normalized superficial liquid velocity (U_l/U_t) or the excess liquid velocity (U_l-U_t). In the following two subsections, the comparisons are conducted based on these two parameters respectively.

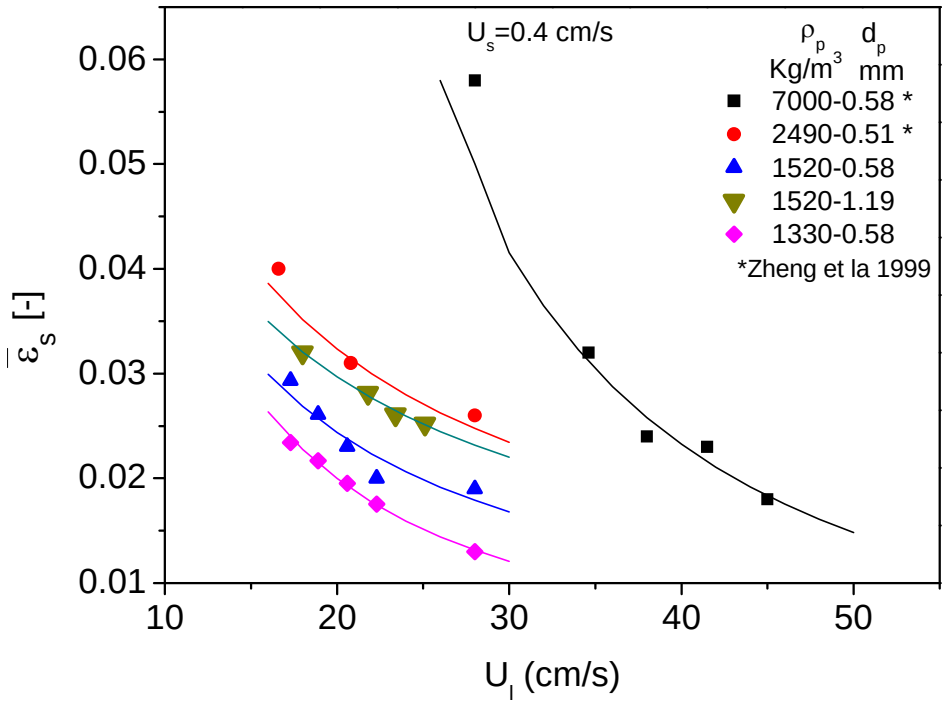

Fig. 4.3 The average solids holdup of 5 types of particles against the superficial liquid velocity under U_s=0.4 cm/s.

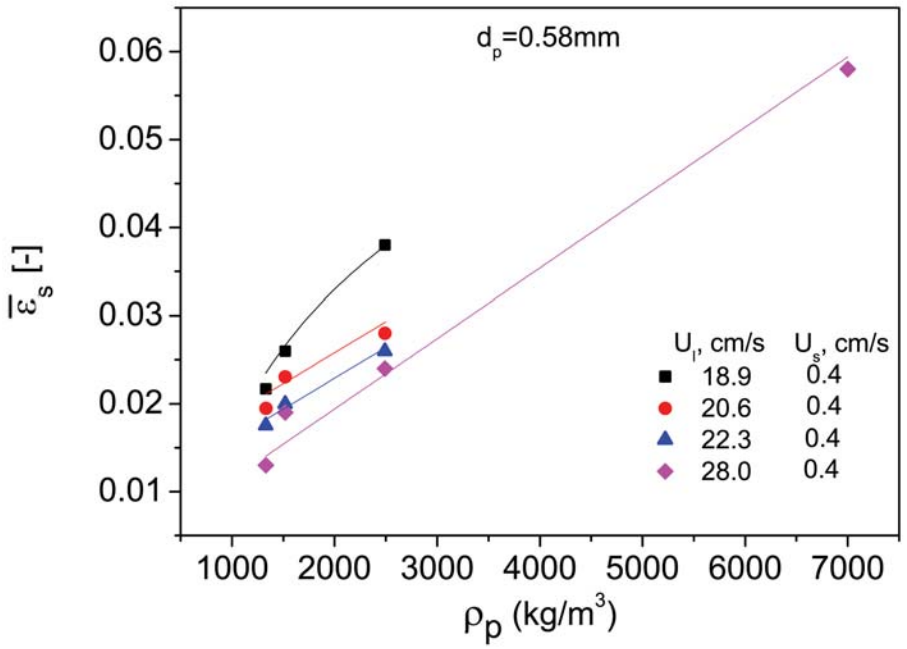

(a)

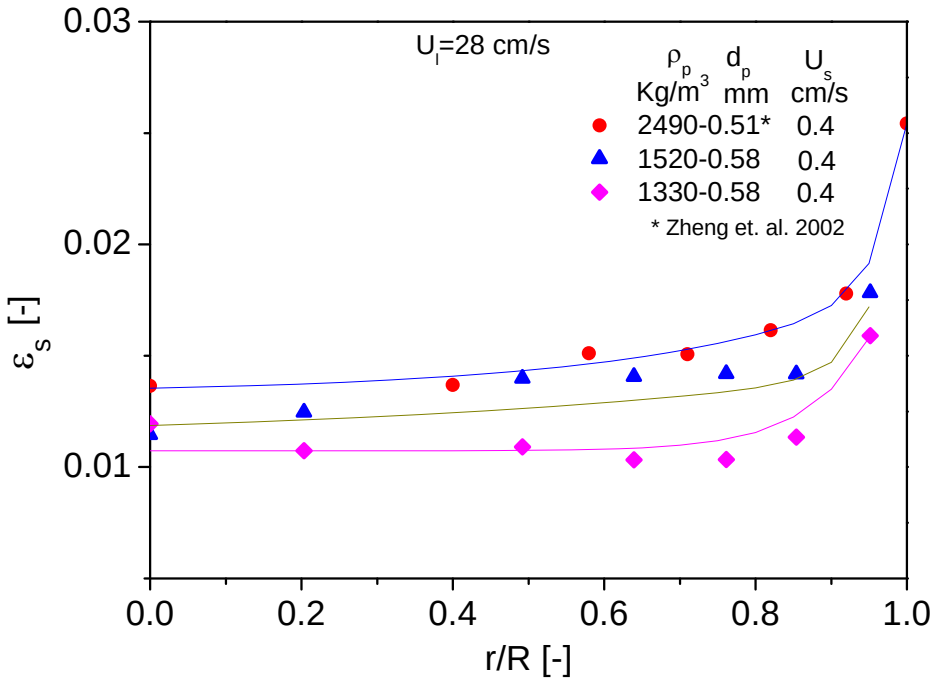

(b)

Fig. 4.4 The effect of the particle density on (a) the average solids holdup ($\bar{\varepsilon}_s$) based on the superficial liquid velocity (U_l) and (b) the corresponding local solids holdup across the radial position for 3 types of particles under U_s=0.4 cm/s and U_l=28 cm/s.

Solids holdup variations based on the normalized superficial liquid velocity (U_l/U_t)

The average solids concentrations of 5 different types of particles are plotted against the normalized superficial liquid velocity (U_l/U_t) in Fig. 4.5 under the same superficial solids velocity U_s =0.4 cm/s. For each type of particles, the average solids holdup decreases with the increasing normalized superficial liquid velocity (U_l/U_t), which is in accordance with the observation made from Fig. 4.3. However, for different types of particles, the effects of the particle density shown in Fig.4.5 are different from that shown in Fig. 4.3. To show the differences explicitly, the average solids holdups for 4 different types of particles with similar size as a function of particle density are shown in Fig. 4.6a, based on the normalized superficial liquid velocity (U_l/U_t). Under the same normalized superficial liquid velocity (U_l/U_t), the higher the particle density the lower the solids holdup. This decreasing trend of the average solids holdup ($\overline{\varepsilon}_s$) with increasing normalized superficial liquid velocity (U_l/U_t) is just contradictory to the results compared based on the superficial liquid velocity (U_l) shown in Fig. 4.4a. The different variation trends of the average solids holdup are related to the average particle velocity. The detailed explanations will be discussed after examining the force balance stated later.

The same trend shown in Fig. 4.6a could also be observed for the radial profile from Fig. 4.6b which shows the local solids holdup also decreasing with increasing particle density. Local solids holdup of heavier particles is smaller than that of lighter particles across the radius. Therefore, one can conclude from Fig. 4.6a and Fig. 4.6b that particles of higher density lead to lower solids concentration in LSCFB riser when compared to others based on the normalized superficial liquid velocity (U_l/U_t).

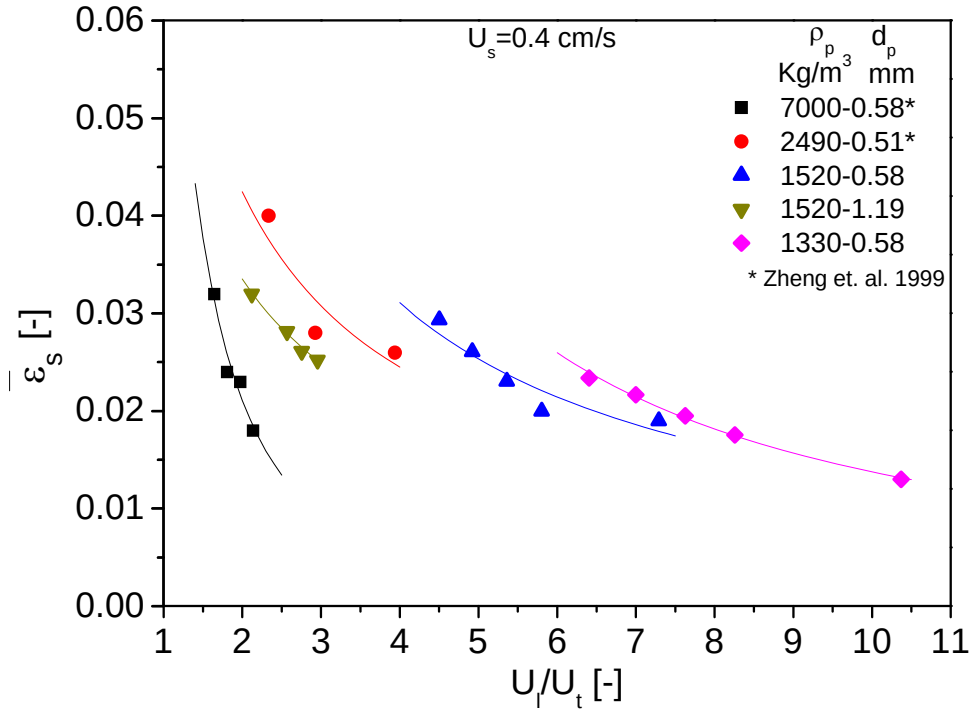

Fig. 4.5 The average solids holdup ($\bar{\varepsilon}_s$) of 5 types of particles against the normalized superficial liquid velocity (U_l/U_t) under U_s=0.4 cm/s

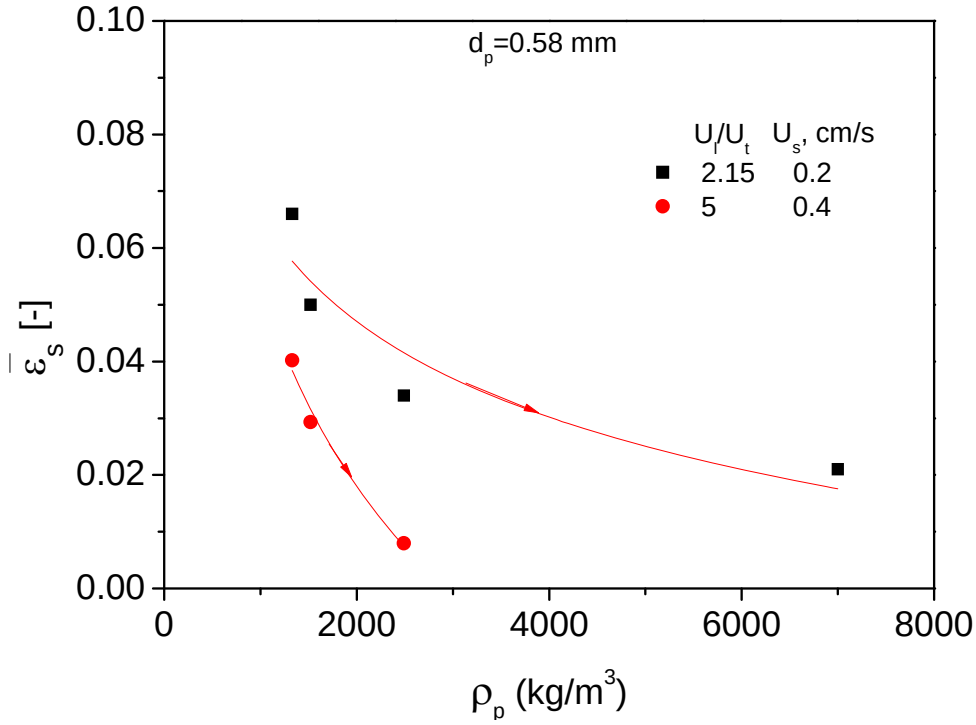

(a)

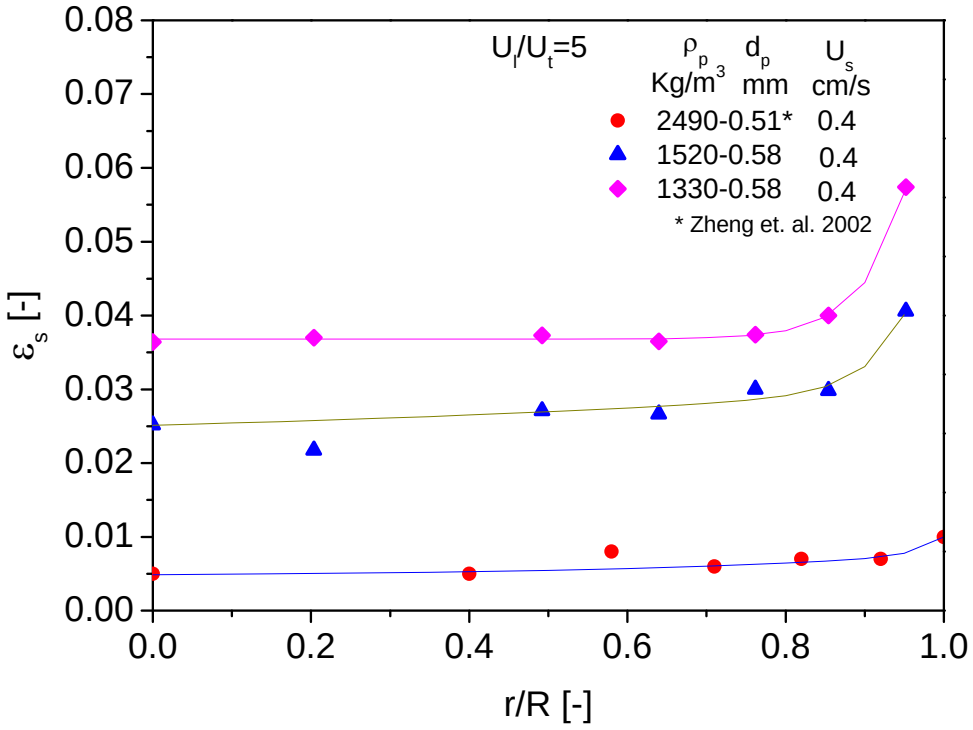

(b)

Fig. 4.6 The effect of the particle density on (a) the average solids holdup ($\bar{\varepsilon}_s$) based on the normalized superficial liquid velocity (U_l/U_t) and (b) the corresponding local solids holdup across the radial position when U_s=0.4 cm/s and U_l/U_t=5.

Solids holdup variations based on the excess superficial liquid velocity (U_l-U_t)

The average solids holdups for the same 4 types of particles with similar size are plotted against particle density in Fig. 4.7a based on the excess superficial liquid velocity (U_l-U_t). At fixed superficial solids velocity (U_s), when the excess superficial liquid velocity (U_l-U_t) is the same, the solids holdups are almost the same, suggesting particle density has little effect on the solids holdup when the excess liquid velocity (U_l-U_t) is fixed, though particle density increases from 1330 kg/m^3 to 7000 kg/m^3. In other words, for the same superficial solids velocity (U_s), the average solids holdup ($\bar{\varepsilon}_s$) is a function of the excess superficial liquid velocity (U_l-U_t). The similar trend is also observed for the local solids holdup shown in Fig. 4.7b. In the radial direction, at fixed superficial solids velocity (U_s), when the excess superficial liquid velocity (U_l-U_t) is the same, the solids holdups of 2 types of particles are almost identical at each radial position. Therefore, the effects of particle density are not obvious when the comparisons are based on the excess superficial liquid velocity (U_l-U_t). Further explanation will be provided after discussing the force balance.

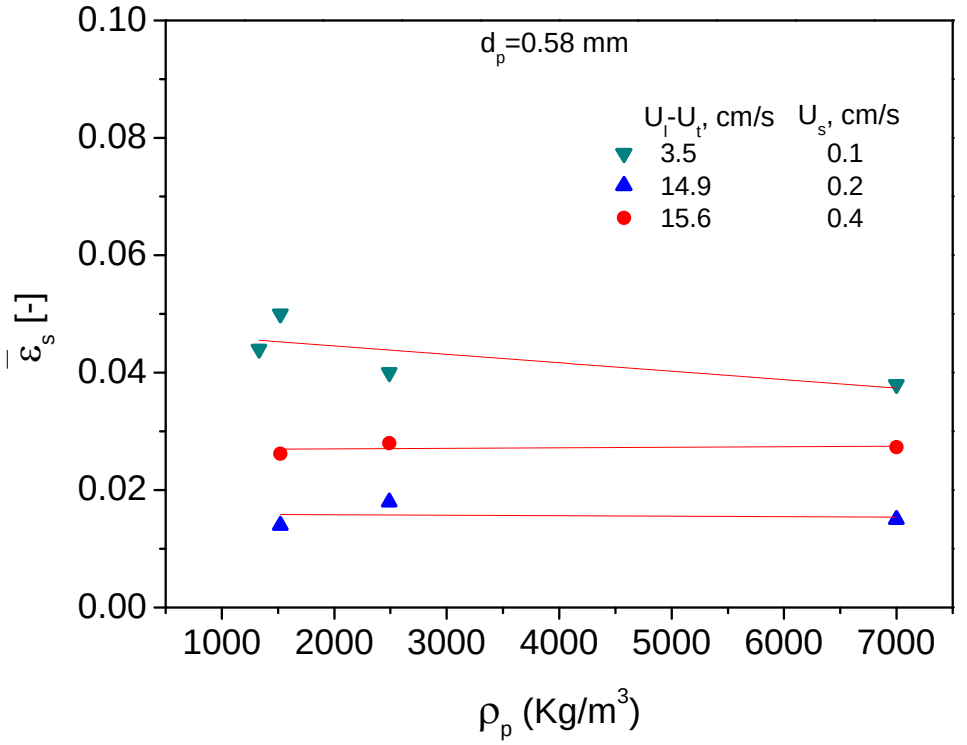

(a)

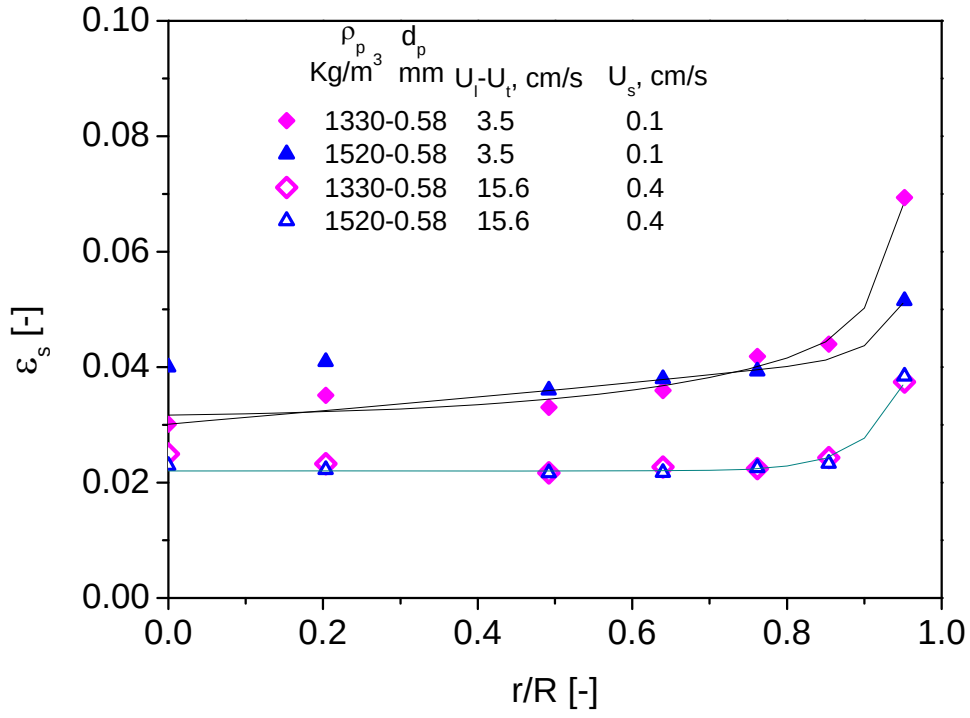

(b)

Fig. 4.7 The effect of particle density on (a) the average solids holdup ($\bar{\varepsilon}_s$) based on the excess superficial liquid velocity (U_l-U_t) and (b) the corresponding local solids holdup across the radial position under different U_s.

Force balance

From the above discussions, the effects of particle density on the solids holdup are distinct when the comparisons are based on those 3 parameters with regard to the superficial liquid velocity (U_l). At fixed superficial solids velocity (U_s), the solids holdup increases with increasing particle density when based on the superficial liquid velocity (U_l); the solids holdup decreases with increasing particle density when based on the normalized superficial liquid velocity (U_l/U_t); and the solids holdup is almost independent of the particle density when based on the excess superficial liquid velocity (U_l-U_t). In order to reveal the mechanism behind those different trends, a force balance exerted on particles needs to be examined. As it is very difficult to analyze the forces exerted on each particle due to the large number of particles used in fluidization, especially when considering all the inter-particle forces, the force balance for a single particle is considered first.

When particles are entrained upward in the fluid, the forces acting on each particle include the downward force of gravity (F_g) and the upward forces of drag force (F_d) and buoyancy (F_b). As known, the drag force is the main factor to accelerate the particles and is strongly dominated by the relative velocity which is referred to as slip velocity and defined as $U_{slip} = V_l - V_p$. When the flow is fully developed, the force balance could be achieved. Then the slip velocity is equal to the particle terminal velocity (U_t). The particle velocity (V_p) is expressed as:

$$V_p = V_l - U_t \tag{4.1}$$

In LSCFB, the solids holdup is limited and there is no significant clustering phenomena (Chen et al. 1991) so that there is no strong interparticle force existing, the following equation may be used to relate the average particle velocity ($\overline{V}_P$) with the superficial liquid velocity (U_l) (Kwauk 1963):

$$\overline{V}_p = \frac{U_l}{1-\overline{\varepsilon}_s} - U_t \tag{4.2}$$

When $\overline{\varepsilon}_s$ is small, e.g. less than 0.1, Eq. (4.2) may be simplified to

$$\overline{V}_p = U_l - U_t \tag{4.3}$$

On the other hand, in LSCFB, the average particle velocity ($\overline{V}_P$) could be expressed as:

$$\overline{V}_P = \frac{U_s}{\overline{\varepsilon}_s} \tag{4.4}$$

With Eq. (4.4), the average particle velocity ($\overline{V}_P$) can be calculated based on the average solids holdup ($\overline{\varepsilon}_s$) from the study by Zheng et. al. (1999) and current study. The average particle velocities ($\overline{V}_P$) as calculated by Eq. (4.3) and Eq. (4.4) are shown in Fig. 4.8 for conditions where the average solids holdup ($\overline{\varepsilon}_s$) is less than 0.1. One could note that the average particle velocity ($\overline{V}_P$) is almost equivalent to the parameter U_l-U_t with deviations under 20% for low solids holdup (less than 0.1). Therefore, the parameter U_l-U_t may be used to represent the average particle velocity ($\overline{V}_P$) that is $\overline{V}_p \approx U_l - U_t$. Fig. 4.7a can now be explained more clearly: when the excess superficial liquid velocity (U_l-U_t) is constant, the average particle velocity ($\overline{V}_P$) in the riser is also constant. Via continuity, a constant particle velocity under a given extend solids circulation flow (as represented by the superficial solids velocity (U_s)) will lead to a constant solids holdup in the riser. This also suggests that the excess superficial liquid velocity (U_l-U_t) should be the best parameter to study the effect of particle properties. Therefore, Fig. 4.7a is more appropriate than Fig. 4.4a and Fig. 4.6a to eliminate the effect of particle density.

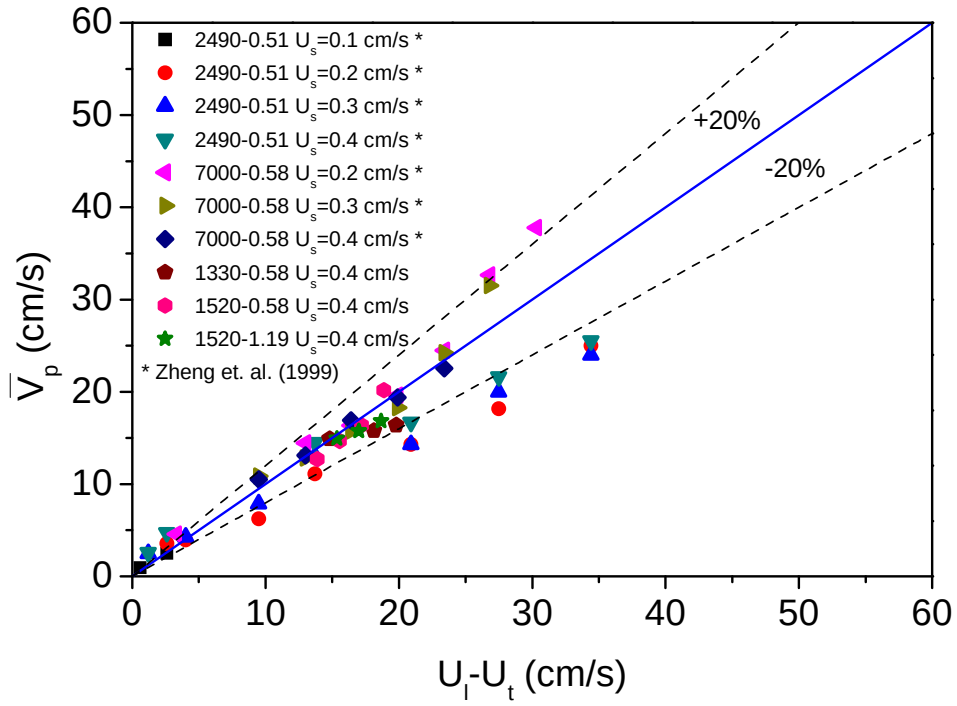

Fig. 4.8 The average particle velocity ($\overline{V}_P$) calculated from Eq. (4.4) vs. the excess superficial liquid velocity (U_l-U_t) for different types of particles from Zheng et. al. (1999) and current study.

For further investigation, the experimental data shown in Fig. 4.3 and Fig. 4.5 are replotted in terms of average solids holdup ($\overline{\varepsilon}_s$) vs. the excess superficial liquid velocity (U_l-U_t) as shown in Fig. 4.9. It can be clearly seen that the scattered data in Fig. 4.3 and Fig. 4.5 are nicely lined up in Fig. 4.9, indicating that the solids holdup is only a function of the excess superficial liquid velocity (U_l-U_t) under the same superficial solids velocity (U_s), regardless of the particle properties.

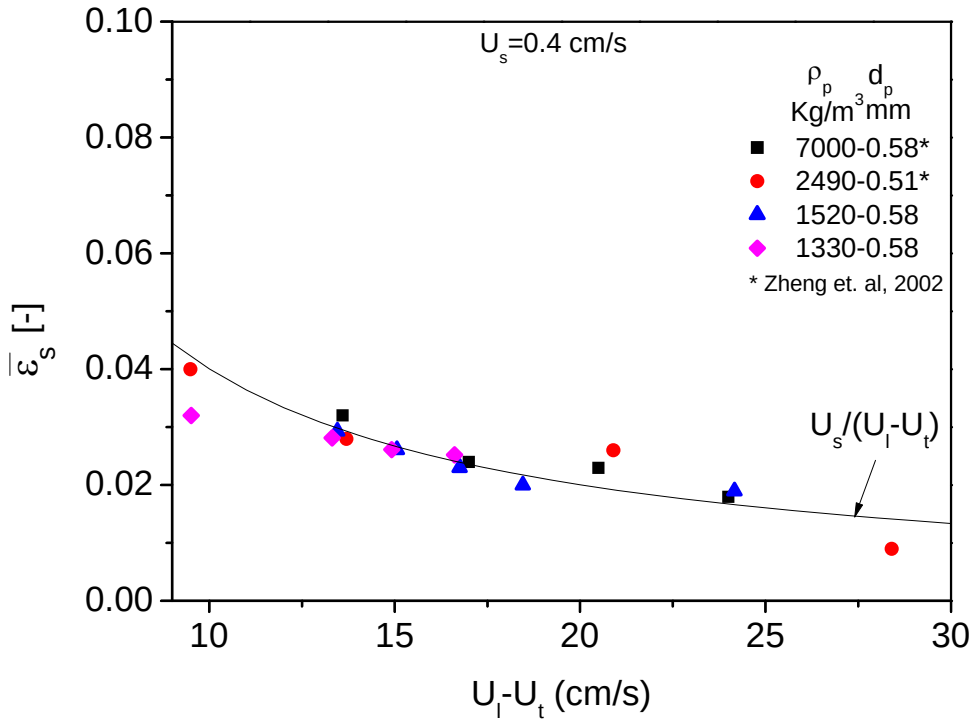

Fig. 4.9 The average solids holdup ($\bar{\varepsilon}_s$) as a function of the excess superficial liquid velocity (U_l-U_t) for 4 different types of particles when U_s=0.4 cm/s.

4.4.2 The effect of the particle size

The solids holdups of 2 types of particles with similar density but different sizes from Fig. 4.3 are plotted in Fig. 4.10a against the superficial liquid velocity (U_l). The average solids holdup increases with the particle size under similar operating conditions. This is expected as the particles having the same density but larger size possess larger mass which makes them hard to entrain under similar superficial liquid velocity (U_l), such effects being quite similar to those of the particle density as shown in Fig. 4.3. The same data from Fig. 4.10a is then plotted in Fig. 4.10b against the excess superficial liquid velocity (U_l-U_t), where the two distinct lines in Fig. 4.10a collapse well into a single line. This is similar to the observation made from Fig. 4.9, reinforcing the understanding that the solids holdup is only a function of the excess superficial liquid velocity (U_l-U_t) under the same superficial solids velocity (U_s), regardless of the particle properties.

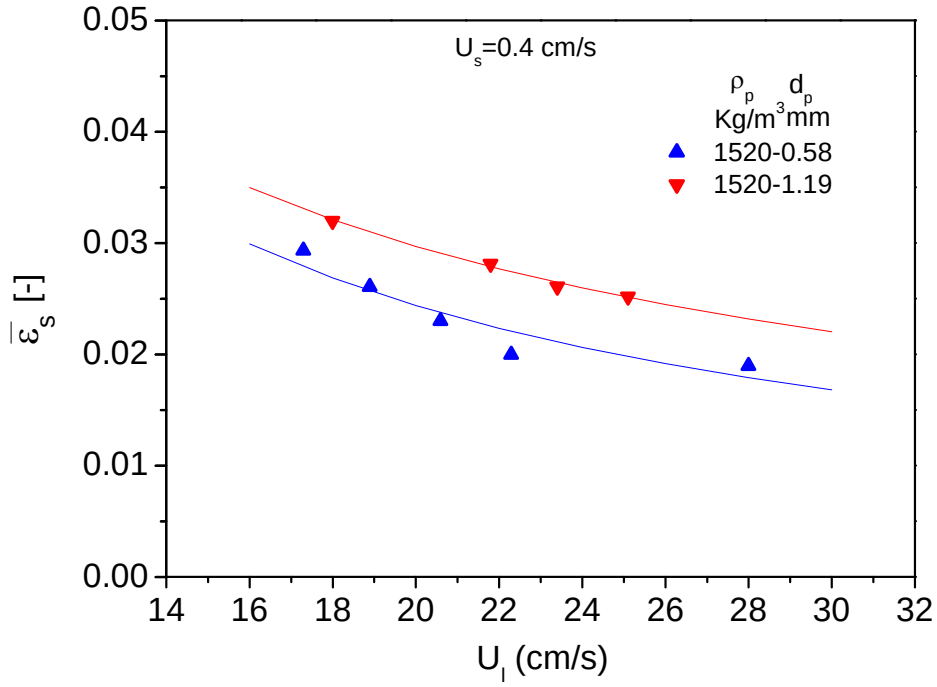

(a)

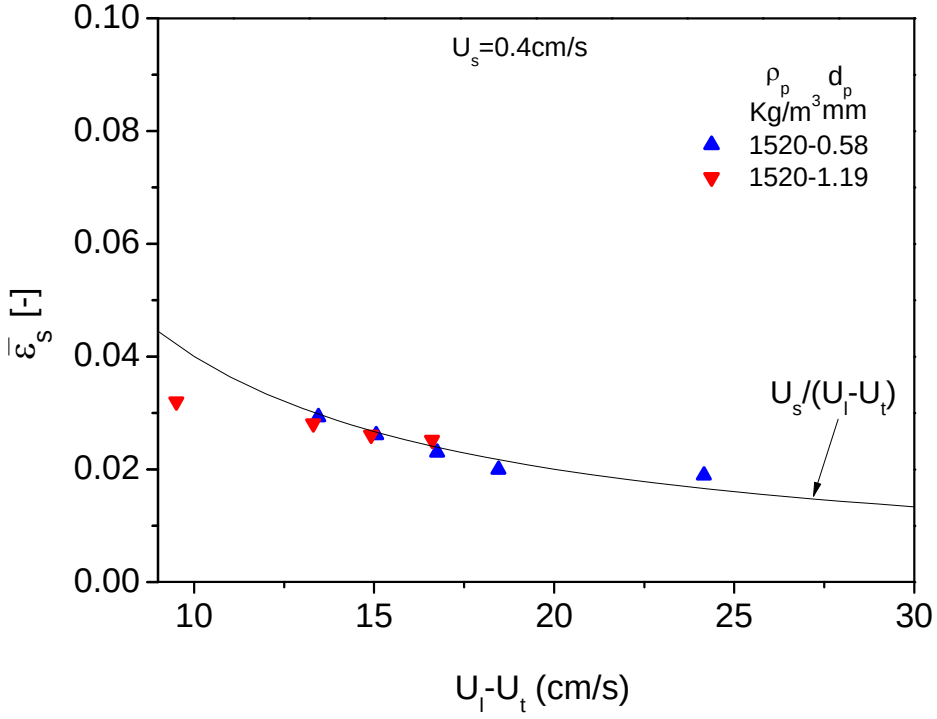

(b)

Fig. 4.10 The average solids holdup ($\bar{\varepsilon}_s$) versus (a) the superficial liquid velocity (U_l) and (b) the excess superficial liquid velocity (U_l-U_t) for 2 types of particles when U_s=0.4 cm/s.

4.4.3 The generalized effects of particle properties

According to the above analyses, the average particle velocity ($\overline{V}_P$) is approximately equivalent to the parameter U_l-U_t when the solids holdup is less than 0.1. Then combining Eq. (4.3) and Eq. (4.4), the following equation could be obtained:

$$\overline{\varepsilon}_s = \frac{U_s}{U_l - U_t} \tag{4.5}$$

With Eq. (4.5), the average solids holdup could be predicted directly from the operating conditions when it is less than 0.1. The validation of Eq. (4.5) with the experimental results is shown in Fig. 4.11. One can note that Eq. (4.5) predicts the average solids holdup in LSCFB riser with enough accuracy when the solids holdup is lower than 0.1. Eq. (4.5) also enables the direct comparison between two types of particles having both different densities and sizes because the effects of the particle density and size have already been incorporated into the terminal velocity (U_t). In other words, the terminal velocity (U_t) is a proper parameter to conduct the direct comparisons among different types of particles when both their densities and sizes are different. For example, in Fig. 4.3, the average solids holdup for the PB1520-1.19 particles is lower than that for the GB2490-0.51 particles under similar operating conditions due to its lower terminal velocity. Therefore, Eq. (4.5) facilitates a quick estimation to the average solids holdup of different types of particles in industrial LSCFB systems. However, there would be larger deviations with higher solids concentration ($\overline{\varepsilon}_s > 0.1$) because the parameter U_l-U_t is not equivalent to the average particle velocity ($\overline{V}_P$) any more due to the significant deviation of the solids holdup from unity. To more accurately predict the solids holdup values at higher solids holdup condition, more sophisticated model needs to be developed.

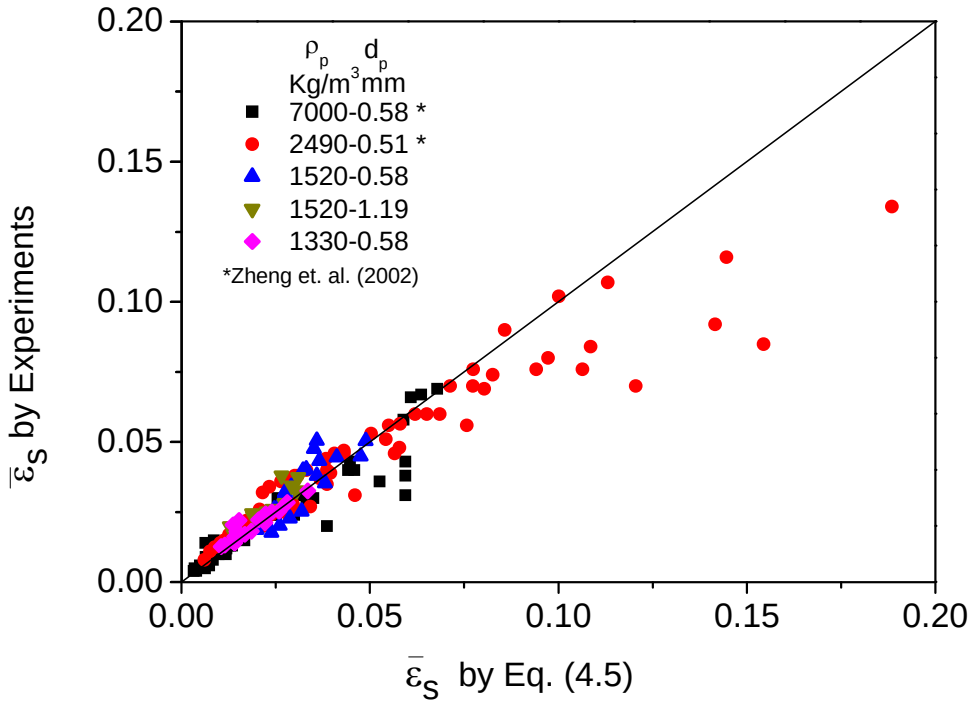

Fig. 4.11 Comparison of the predicted average solids holdup from Eq. (4.5) with the experimental data from the study of Zheng et. al. (1999) and current study.

4.5 Conclusions

The average and local solids holdups of 5 different types of particles are compared under various operating conditions to investigate the effects of the particle properties based on 3 parameters: the superficial liquid velocity (U_l), the normalized superficial liquid velocity (U_l/U_t) and the excess superficial liquid velocity (U_l-U_t). At fixed superficial solids velocity (U_s), the solids holdup increases with increasing particle density or size based on the superficial liquid velocity (U_l); whereas, the solids holdup decreases with increasing particle density or size based on the normalized superficial liquid velocity (U_l/U_t). When the comparison is based on the excess superficial liquid velocity (U_l-U_t), particle properties has little effects on the solids holdup, so that the excess superficial liquid velocity (U_l-U_t) is a more appropriate parameter to evaluate the effects of the particle properties compared to the superficial liquid velocity (U_l) and the normalized superficial liquid velocity (U_l/U_t).

A discussion on the force balance of the particles reveals that the excess superficial liquid velocity (U_l-U_t) is approximately equivalent to the average particle velocity ($\overline{V}_P$) when the average solids holdup is less than 0.1. Furthermore, the solids holdup is a function of the particle velocity (V_p) and the superficial solids velocity (U_s), which could be expressed quantitatively as $\overline{\varepsilon}_s = U_s / \left(U_l - U_t\right)$ when $\overline{\varepsilon}_s < 0.1$. This equation enables the quick estimation of the average solids holdup directly from the operation conditions in the industrial LSCFB systems for different types of particles having different densities and sizes. However, when $\overline{\varepsilon}_s > 0.1$, the predicted results would deviate from the experimental results. A more sophisticated model will be developed in our follow-up studies.

Nomenclature

Ar	Archimedes number defined by $d_p^3 g(\rho_p - \rho_l)\rho_l / \mu_l^2$
C_D	Particle drag coefficient
d_p	Particle diameter (mm)
D	Column diameter (m)
F_b, F_d, F_g	Buoyancy, drag force and gravity
G_s	Solids circulation rate (kg/ (m^2s))
g	Gravity acceleration
Re	Reynolds number defined by $U_l d_p \rho_l / \mu_l$
Re_t	Particle terminal Reynolds number defined by $U_t d_p \rho_l / \mu_l$
U_a	Auxiliary liquid velocity (cm/s)
U_l	Superficial liquid velocity (cm/s)
U_s	Superficial solids velocity (cm/s)
U_{slip}	Slip velocity (cm/s)
U_t	Particle terminal velocity (cm/s)
U_{tr}	Transition velocity demarcate the conventional particulate regime and circulating fluidization regime (cm/s)
V_l, V_p	Local liquid velocity and local particle velocity (cm/s)
$\overline{V}_p$	Average particle velocity (cm/s)

Greek letters

$\overline{\varepsilon}$	Average bed voidage
$\overline{\varepsilon}_s$	Average solids holdup
μ_l	Liquid viscosity (mPas)
ρ_p	Particle density (kg/m^3)

Subscripts

l	Liquid
p	Particle
s	Solids

References

Chen, Y.-M., C.-S. Jang, P. Cai and L.-S. Fan (1991). On the formation and disintegration of particle clusters in a liquid-solid transport bed. Chemical Engineering Science 46(9): 2253-2268.

Chowdhury, N., G. Nakhla and J. Zhu (2008). Load maximization of a liquid-solid circulating fluidized bed bioreactor for nitrogen removal from synthetic municipal wastewater. Chemosphere 71(Compendex): 807-815.

Clift, R., J. R. Grace and M. E. Weber (1978). Bubbles, drops, and particles. New York, Academic Press.

Denn, M. M. (1980). Process fluid mechanics, Prentice Hall.

Felice, R. D. (1995). Hydrodynamics of liquid fluidisation, Review article number 47 Chemical Engineering Science 50(8): 1213-1245.

Haider, A. and O. Levenspiel (1989). Drag coefficient and terminal velocity of spherical and nonspherical particles. Powder Technology 58(1): 63-70.

Kwauk, M. (1963). Generalized fluidization I, steady state motion. Scienta Sinica 12: 587-612.

Lan, Q., J. X. Zhu, A. S. Bassi, A. Margaritis, Y. Zheng and G. E. Rowe (2000). Continuous protein recovery using a liquid - Solid circulating fluidized bed ion exchange system: Modelling and experimental studies. Canadian Journal of Chemical Engineering 78(Compendex): 858-866.

Liang, W., S. Zhang, J.-X. Zhu, Y. Jin, Z. Yu and Z. Wang (1997). Flow characteristics of the liquid-solid circulating fluidized bed. Powder Technology 90(2): 95-102.

Natarajan, P., R. Velraj and R. V. Seeniraj (2008). Application of drift-flux model in liquid-solid circulating fluidized bed. Chemical Engineering Communications 195(Compendex): 1144-1158.

Patel, M., A. S. Bassi, J. J. X. Zhu and H. Gomaa (2008). Investigation of a dual-particle liquid-solid circulating fluidized bed bioreactor for extractive fermentation of lactic acid. Biotechnology Progress, 2540 Olentangy River Road, P.O. Box 3337, Columbus, OH 43210-3337, United States, American Chemical Society.

Zhang, H., P. M. Johnston, J. X. Zhu, H. I. de Lasa and M. A. Bergougnou (1998). A novel calibration procedure for a fiber optic solids concentration probe. Powder Technology 100(2-3): 260-272.

Zheng, Y. and J.-X. Zhu (2001). The onset velocity of a liquid-solid circulating fluidized bed. Powder Technology 114(1-3): 244-251.

Zheng, Y., J.-X. Zhu, N. S. Marwaha and A. S. Bassi (2002). Radial solids flow structure in a liquid-solids circulating fluidized bed. Chemical Engineering Journal 88(1-3): 141-150.

Zheng, Y., J.-X. Zhu, J. Wen, S. A. Martin, A. S. Bassi and A. Margaritis (1999). The axial hydrodynamic behavior in a liquid-solid circulating fluidized bed. Canadian Journal of Chemical Engineering 77(Compendex): 284-290.

Zhu, J.-X., D. G. Karamanev, A. S. Bassi and Y. Zheng (2000). (Gas-)liquid-solid circulating fluidized beds and their potential applications to bioreactor engineering. The Canadian Journal of Chemical Engineering 78(1): 82-94.

Chapter 5

5 Prediction of Average Solids Holdup and Slip Velocity in LSCFB Riser

5.1 Introduction

Interest in the area of Liquid-Solid Circulating Fluidized Beds (LSCFBs) research is growing based on the wide range of potential applications (Zhu et al. 2000). The design, scale up and operation of such liquid-solid continuous system require the information of the hydrodynamic characteristics, such as flow patterns, particle slip velocity and solids holdup. Many experimental studies (summarized in Table 5.1) have reported that the solids holdup is dependent on flow conditions, e.g. superficial liquid velocity, auxiliary liquid velocity and solids circulation rate etc. Unfortunately, there are few studies focused on mathematical models and correlations to predict solids holdup and particle slip velocity in LSCFB riser. Though the Richardson and Zaki equation (Richardson and Zaki 1954) and Kwauk theory (Kwauk 1963) are found to be the best correlation to predict the solids holdup and slip velocity directly from the operating conditions, they failed to predict solid holdup under high velocity fluidization due to either the non-uniformity of radial solids distribution (Liang et. al.,1997), or the larger slip velocity between the solids phase and the liquid phase (Natarajan et al. 2011). Some researchers (Lan et al. 2000; Mazumder et al. 2009) predicted average solids holdup in their own LSCFB systems, however, those empirical correlations are dependent on LSCFB structures and particle properties, so that they are not valid in other LSCFB. Two different groups of researchers Natarajan et al. (Natarajan et al. 2008), and Sang and Zhu (Chapter 4) tried to provide a better estimation of the solids holdup in LSCFB riser based on drift flux model and force balance respectively. However, the former model introduced an extra empirical parameter (distribution coefficient) making their model rather empirical and parameter dependent, and the latter was only valid when the average solids holdup was smaller than 0.1. A more sophisticated model is necessary to provide an accurate prediction of the solids holdup in LSCFB systems.

In this paper, an analytical model incorporating particle properties and slip velocity is developed to determine the average solids holdup. The predicted results are validated with the experimental data in different LSCFB risers in this research and in the literature. Then, based on this model, the effects of the particle properties on solids holdup are studied quantitatively and the transition velocity demarcating the circulating fluidization regime and the transport regime is determined to complete the flow regime map in liquid-solid fluidization systems.

Table 5.1 Riser dimensions and physical properties of particles used in existing literature and current work

Researchers	Riser ID (m)	Riser height (m)	Particles	Particle density (kg/m^3)	Particle size (mm)	Particle sphericity	*n*	Reported U_t (cm/s)	U_t by Eq. (5.3-5.4) (cm/s)	U_t by Eq. (5.5) (cm/s)	Re_t	*Ar*
Zheng et. al. (1999, 2002)	0.076	3	Glassbeads	2490	0.508	~1	3.15	5.9	7.1	8.6	36.1	1920
			Steel shot	7000	0.58	--	2.80	21.6	21	19.5	113.1	11500
Liang et. al. (1997)	0.14	3	Glassbeads	2460	0.405	~1	3.28	5.3	5.31	6.5	21.5	951
Natarajan et al (2011)	0.094	2.4	Sand	2700	0.55	-	3.05	8.9	8.9	8.3	49.0	2770
			Sand	2700	0.46	-	3.17	7	7	7.3	32.2	1660
Current research	0.076	5.4	Plastic beads	1330	0.58	~0.7	3.47	-	2.7	2.47	14.5	632
			Plastic beads	1520	0.58	~0.7	3.37	-	3.84	3.39	19.7	995
			Plastic beads	1520	1.19	~0.7	3.03	-	8.48	6.41	76.3	8600

5.2 Materials and methods

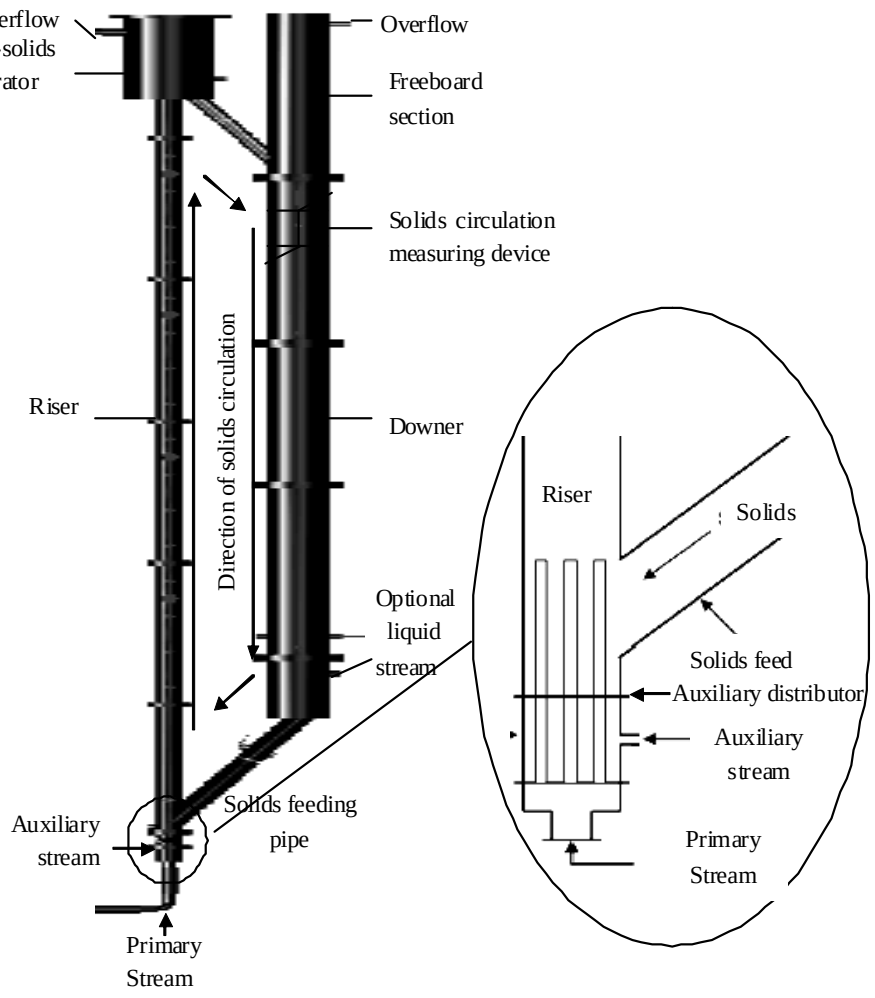

Fig. 5.1 The schematic diagram of LSCFB apparatus.

The set-up of LSCFB system is shown schematically in Fig. 5.1. The system mainly consists of a Plexiglas riser column of 7.62 cm ID and 5.4 m in height, a liquid–solids separator, freeboard section, a device for measuring the solids flow rate and downer. This riser was connected to the 0.2 m ID Plexiglas downer through a solids returning pipe at the top and a solids feeding pipe at the bottom. At the bottom of the riser, there are two distributors: the main liquid distributor made of seven stainless steel tubes occupying 19.5% of the total riser cross-sectional area and extending 0.2 m into the riser and the auxiliary liquid distributor, a porous plate with 4.8% opening area at the base of the riser.

The liquid and solids flow rates can be controlled independently by adjusting the main and the auxiliary liquid flow rates. The auxiliary liquid stream controls the quantity of the particles recirculating from the downer to the riser: when the auxiliary flow is set to zero, no particles could enter the riser and no continuous particle circulation could be formed. Introducing the auxiliary liquid flow, solids do not begin to flow immediately. Only when the auxiliary liquid flow reaches a threshold flow rate, solids begin to flow. After that, additional liquid added to the riser bottom cause more particles to enter the riser. Particles introduced into the riser bottom are carried up to the top of the riser by the combined liquid flow (the main liquid flow plus the auxiliary liquid flow) and separated by the large cone based cylindrical liquid–solids separator at the top. Liquid is then returned to the liquid reservoir and the particles are returned to the particle storage vessel after passing through the solids flow-rate measuring device.

The local solids holdup is measured by using an optical fiber solids concentration probe model PV-5, produced by the Institute of Process Engineering, Chinese Academy of Sciences. For the details of this probe, please refer to previous papers from our group (Zhang et al. 1998; Zheng et al. 2002). The calibration of this probe for the liquid–solids systems were carried out on site. With the fluidized bed operated in the conventional particulate regimes, where the solids holdup is the considered homogeneous in both the axial and the radial direction, the output voltage signal from the probe was calibrated against the solids holdup data obtained from pressure gradient measurements. Such calibration is always conducted in the middle section of the fluidized bed so that the “end effect” is eliminated. A linear relationship was found between the voltage signal and the solids holdup for each type of particle.

All experiments were carried out at ambient temperature with tap water being used as the fluidizing liquid. The physical properties of the three types of particles used are listed in Table 5.1. In each run, local solids holdup was measured at different radial positions by traversing the probe horizontally, after LSCFB unit was brought to a steady operation. In several early experiments, the probe was traversed from one wall to the other and no significant asymmetry was found in the radial holdup profile. Therefore, measurements in

this work were taken only at one side of the riser, at seven radial locations between the center and the wall at r/R =0, 0.2034, 0.492, 0.6396, 0.7615, 0.8641, 0.9518. The same procedure was repeated for different solids flow rates and liquid velocities at different axial locations. For each measurement location, the column section from about 0.3 m above to 0.3 m below the probe was wrapped with a black plastic sheet to prevent external light from penetrating into the riser and interfering with the measurements.

5.3 The control of superficial solids velocity U_s

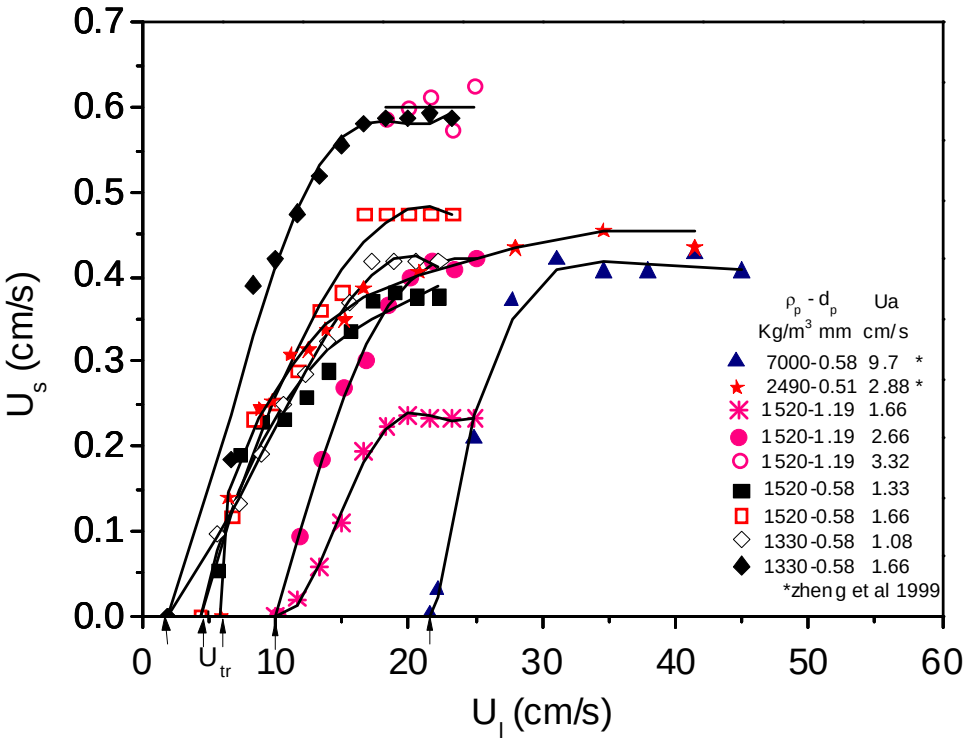

Fig. 5.2 The superficial solids velocity (U_s) as a function of combined superficial liquid velocity (U_l) for 5 types of particles under different auxiliary liquid velocity.

Superficial solids velocity (U_s) is defined as the upward velocity of the solids phase alone when there is no liquid present in the riser. Solids circulation rate (G_s) is the mass flow rate of solids circulating between the riser and the downer at steady-state operation and the relation between the two is $U_s = G_s / \rho_p$. Although both parameters could be employed to describe the amount of solids circulating from the downer to the riser at unit time per

unit area, it is more reasonable to use the superficial solids velocity (U_s) when different types of particles with different solids densities (ρ_p) are involved. This is important because when conducting the comparisons, such as solids holdup under different operating conditions. One must make sure the superficial solids velocity (U_s) is the same because otherwise the comparisons are not on the same basis, and the superficial solids velocity (U_s) could be different even when solids circulation rate (G_s) is set to be the same for particles of different density.

The variations of the superficial solids velocity (U_s) with the combined superficial liquid velocity (U_l) and the auxiliary liquid velocity (U_a) are shown in Fig. 5.2 for 5 types of particles. For all particles at different auxiliary liquid velocities (U_a), superficial solids velocity (U_s) initially increases with combined superficial liquid velocity (U_l) because solids circulation tends to be limited by the entrainment capacity of the combined liquid velocity, rather than the particle mobility at the exit of the feeding pipe at the riser bottom controlled by the auxiliary liquid velocity (U_a). Beyond the initial stage, the solids circulation is more controlled by the auxiliary liquid velocity (U_a), so that the superficial solids velocity (U_s) is constant for each auxiliary liquid velocity (U_a) though the combined superficial liquid velocity (U_l) keeps increasing and the solids circulation is considered to be fully developed. On the other hand, at this stage, the superficial solids velocity (U_s) increases with the auxiliary liquid velocity (U_a) for a fixed superficial liquid velocity (U_l) since more particles are introduced into the riser with higher auxiliary liquid velocity (U_a).

5.4 Average solids holdups

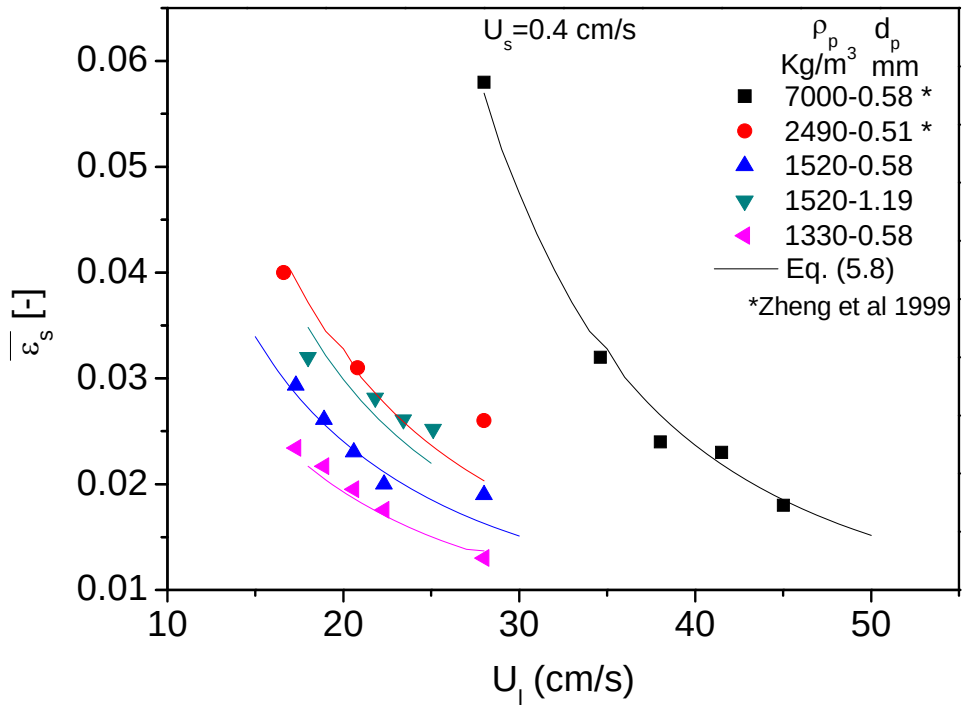

Fig. 5.3 The experimental and predicted average solids holdups of 5 types of particles against the superficial liquid velocity under U_s=0.4 cm/s.

The average solids holdups of 5 different types of particles are plotted against the superficial liquid velocity (U_l) in Fig. 5.3 under the same superficial solids velocity U_s=0.4 cm/s. For all particles, the average solids holdup ($\overline{\varepsilon}_s$) decreases when the superficial liquid velocity (U_l) increases because much energy is provided to entrain the particles, leading to a lower solids concentration. The detailed experimental results can be referred to Chapter 4.

5.5 Analytical model and discussion

According to the existing hydrodynamic studies in LSCFB risers, solids distribution along the axial direction is homogeneous (Liang et. al., 1997, Zheng et. al., 1999). In radial direction, the ratio between the minimum solids holdup at the core region and the

maximum solids holdup at the annulus region is only around 0.8~1, which is reasonable to be considered as uniform compared with its counter parts in gas-solids system and the gas-liquid-solid system. With such assumptions, average solids holdup in LSCFB riser can be written as the ratio between the superficial solids velocity and average particle velocity:

$$\bar{\varepsilon}_s = \frac{U_s}{\bar{V}_p} \tag{5.1}$$

where U_s is superficial solids velocity and $\bar{V}_p$ is average particle velocity. As average liquid velocity is $\bar{V}_l = \frac{U_l}{1-\bar{\varepsilon}_s}$, particle velocity in terms of liquid velocity and slip velocity is $\bar{V}_p = \frac{U_l}{1-\bar{\varepsilon}_s} - U_{slip}$, then Eq. (5.1) becomes

$$\bar{\varepsilon}_s = \frac{U_s}{\frac{U_l}{1-\bar{\varepsilon}_s} - U_{slip}} \tag{5.2}$$

with U_{slip} being a function of U_t.

It can be seen from Eq. (5.2) that the average solids holdup ($\bar{\varepsilon}_s$) can be expressed by superficial solids velocity (U_s), superficial liquid velocity (U_l), slip velocity (U_{slip}) and particle terminal velocity (U_t). As superficial solids velocity (U_s) and superficial liquid velocity (U_l) are measureable, to obtain a reasonable estimation from the Eq. (5.2), the particle terminal velocity (U_t) and slip velocity (U_{slip}) should be determined in advance.

Determination of U_t

For a free falling spherical particle, its terminal velocity (U_t) could be calculated as (Denn 1980):

$$U_t = \sqrt{\frac{4\left(\rho_p - \rho_l\right) gd}{3\rho_l C_D}} \tag{5.3}$$

where the drag coefficient C_D can be determined from the standard drag curve ln C_D~ln Re (Denn 1980) implicitly or the drag curve C_D~Ar (Karamanev 1996) explicitly. For the simplicity, the Karamanev equation is used due to its explicitly on C_D. The following equation based on a correlation of the drag coefficient C_D and Ar can be used for calculating the particle terminal velocity:

$$C_D = \frac{432}{Ar}(1+0.0470Ar^{\frac{2}{3}}) + \frac{0.517}{1+154Ar^{-\frac{1}{3}}} \tag{5.4}$$

For non-spherical particles, the terminal velocity can be determined by the following equation (Haider and Levenspiel 1989):

$$u^* = \left[\frac{18}{\left(d^*\right)^2} + \frac{2.3348-1.7439\phi}{4\left(d^*\right)^{0.5}}\right]^{-1} \tag{5.5}$$

where $U_l^* = U_l\left[\rho_l^2/(\mu g\Delta\rho)\right]^{1/3} = Re/Ar^{1/3}$, $d_p^* = d_p\left(\rho_s g\Delta\rho/\mu^2\right)^{1/3} = Ar^{1/3}$, $\phi = 0.5\sim 1$

It can be noted that particle sphericity (ϕ) is introduced when determine the terminal velocity (U_t), so that the effect of particle shape is considered when calculating average holdup in Eq. (5.2).

Table 5.1 summarizes the calculated U_t by Eq. (5.3) and (5.4) for spherical particles and Eq. (5.5) for non-spherical particles. It is shown that both sets of equations can serve well to predict the particle terminal velocity because the predicted U_t agrees well with the reported U_t reported by different researchers.

Determination of U_{slip}

Ideally, the slip velocity between the particles and the liquids equals to the particle terminal velocity. However, in multi-particle system, under the circulating fluidization regime, Zheng (1999) found that the onset velocity that demarcates the conventional

fluidization regime and the circulating fluidization regime is about 1.1~1.2 times of particle terminal velocity. By introducing this factor into the equation that predicting slip velocity based on Richardson and Zaki theory (Richardson and Zaki 1954), the slip velocity under the circulating fluidization regime is then calculated as:

$$\bar{U}_{slip} = 1.2U_t(1-\bar{\varepsilon}_s)^{n-1} \tag{5.6}$$

where *n* is the Richardson and Zaki index summarized in Table 5.1.

Meanwhile, slip velocity also can be determined from the superficial liquid velocity, superficial solids velocity and the measured average solids holdup in the bed:

$$\bar{U}_{slip} = \frac{U_l}{1-\bar{\varepsilon}_s} - \frac{U_s}{\bar{\varepsilon}_s} \tag{5.7}$$

The predicted slip velocity of Eq. (5.6) is validated with that by Eq. (5.7) from experimental data of this work and other research reports (Zheng et. al., 1999; Natarajan et. al, 2011). Fig. 5.4 shows the experimental and predicted slip velocity of Eq. (5.6) and Eq. (5.7) respectively as a function of the solids holdup for the glassbeads in the reported work of Zheng et. al (1999). It is shown that slip velocity predicted by Eq. (5.6) agrees very well with the Eq. (5.7) calculated from experimental results. Then the comparisons are extended by plotting slip velocity predicted from Eq. (5.6) with the calculated slip velocity from experimental data by Eq. (5.7) in literatures and in this work as seen in Fig. 5.5, showing that Eq. (5.6) can be employed to predict slip velocity in LSCFB riser with adequate accuracy.

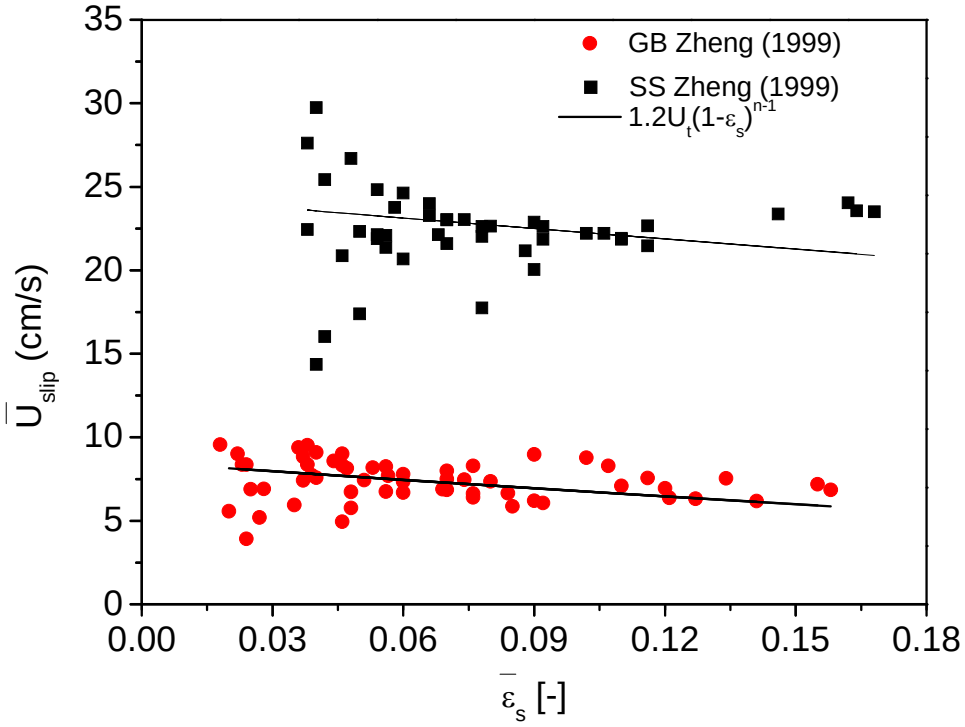

Fig. 5.4 Predicted slip velocity as a function of the solids holdup of glassbeads and steel shots by Zheng et. al. (1999).

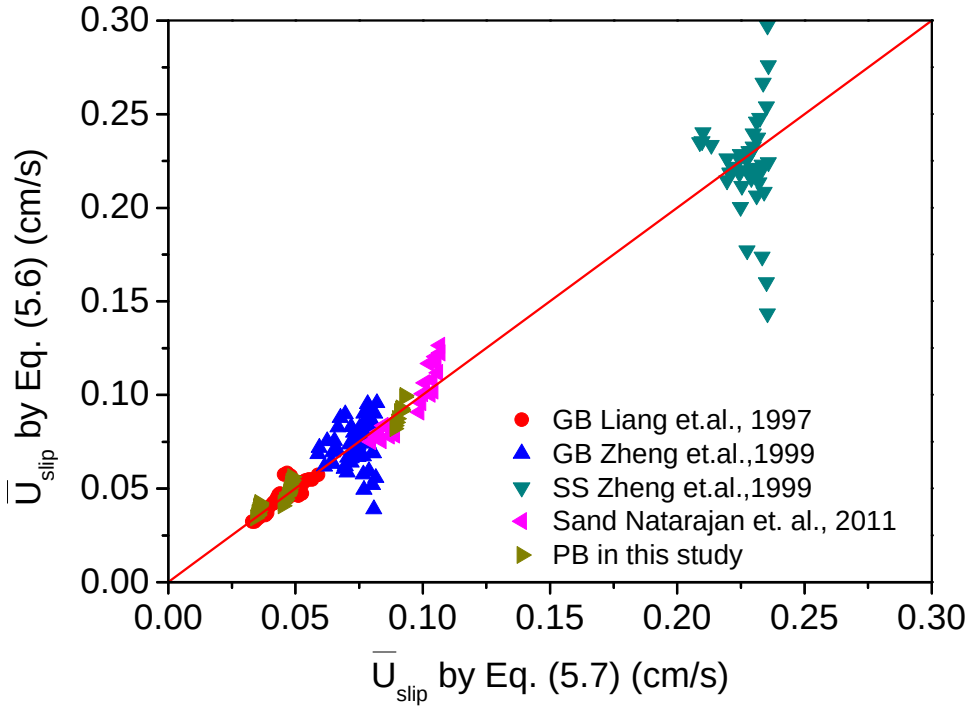

Fig. 5.5 Comparisons of average slip velocities by different definitions.

By combining Eq. (5.4) or Eq. (5.5) and Eq. (5.6) with Eq. (5.3), there is

$$\bar{\varepsilon}_s = \frac{U_s}{\frac{U_l}{1-\bar{\varepsilon}_s} - 1.2U_t(1-\bar{\varepsilon}_s)^{n-1}} \tag{5.8}$$

In Eq. (5.8), the only unknown parameter is $\bar{\varepsilon}_s$. By solving this equation with bisection method in matlab, $\bar{\varepsilon}_s$ can be calculated with the limitation that solids holdup lies between 0 and 1.

The predicted average solids holdups by Eq. (5.8) are compared with the experimental data from this work and other reported studies (Zheng, 1999; Liang et. al., 1997, Natarajan et. al., 2011). It is shown in Fig. 5.6 that there is good correlation between the predicted results by Eq. (5.8) and the experimental results. In Fig. 5.6, the predicted average solids holdups correspond well with the experimental results with the accuracy larger than 80%. It is worth mentioning that the dimensions of LSCFB risers (summarized in Table 5.1) are quite different for this research work and other reported studies (Zheng, et. al., 1999; Liang et. al., 1997, Natarajan et. al., 2011). Therefore, Eq. (5.8) serves well to predict average solids holdup in different LSCFB risers.

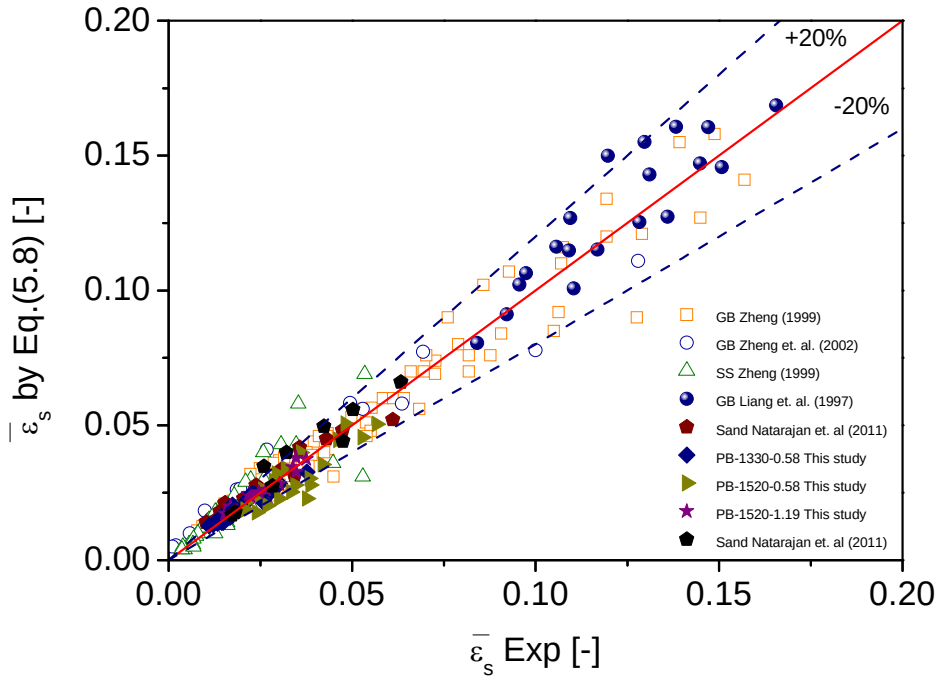

Fig. 5.6 Comparison of predicted average solids holdup with experimental results.

5.6 The effects particle property on solids holdup by model prediction

Based on Eq. (5.8), the detailed comparisons of the particle property effects on average solids holdup can be conducted quantitatively. In our previous work (Chapter 4), average solids holdups are plotted against particle properties under different parameters including U_l, U_l/U_t and U_l-U_t. Following the same idea, the model predicted results by Eq. (5.8) are compared with particle properties under those 3 parameters respectively in this section.

5.6.1 The effects of the particle density on solids holdup by model prediction

Fig. 5.7 shows the variations of average solids holdup and average particle velocity as a function of the particle density ranging from 1500 kg/m^3 to 7000 kg/m^3 when d_p=0.58 mm and U_s=0.4 cm/s. The comparisons were conducted under U_l, U_l/U_t and U_l-U_t respectively. Fig. 5.7a shows that under fixed U_l, average solids holdup increases rapidly with increasing particle density, especially at lower superficial liquid velocity (U_l),

e.g. U_l =20 cm/s. When average solids holdup is compared under U_l/U_t shown in Fig. 5.7b, it decreases dramatically with increasing particle density, which is a reverse effect on solids holdup when compared with the results shown in Fig. 5.7a. Meanwhile, from Fig. 5.7c it can be noted that for fixed U_l -U_t , particle density has very little effect on solids holdup when the comparisons are conducted under U_l-U_t, even the particle densities increase from 1500 kg/m^3 to 7000 kg/m^3. Similar results were also reported in our previous work (Chapter 4).

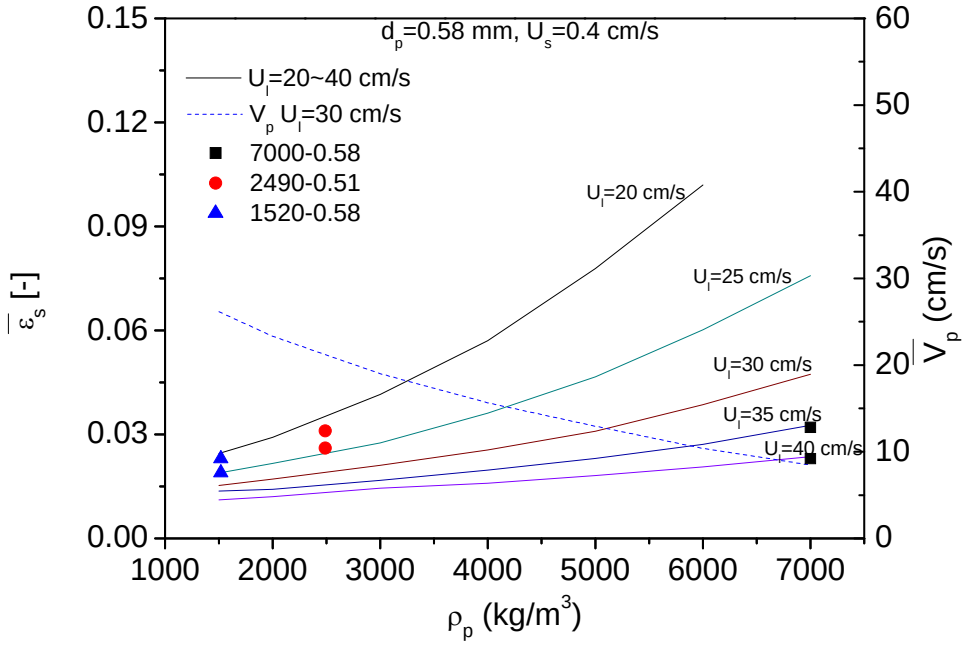

(a)

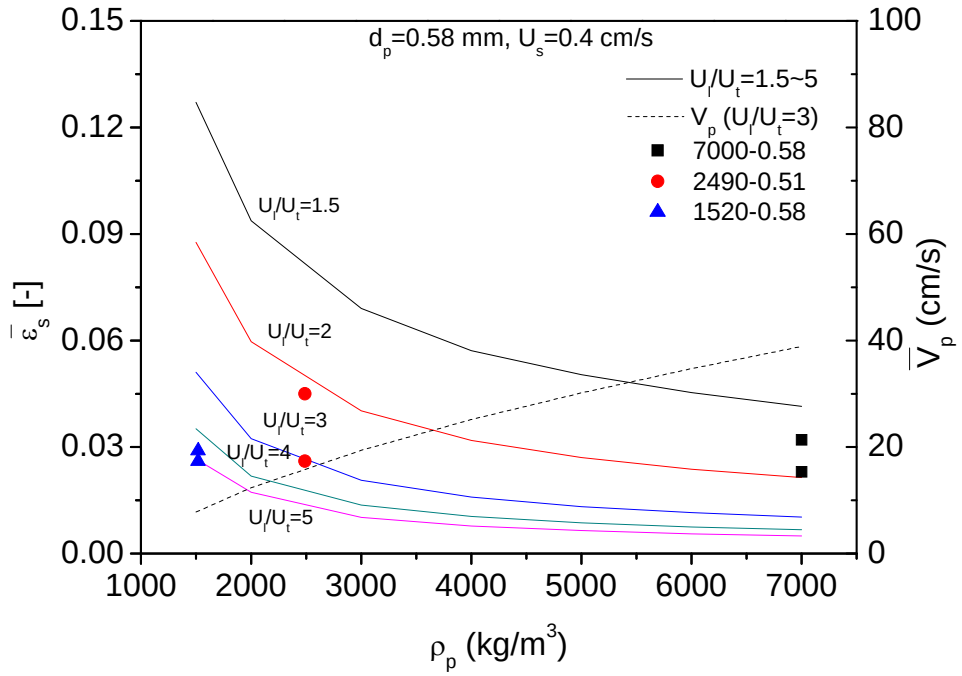

(b)

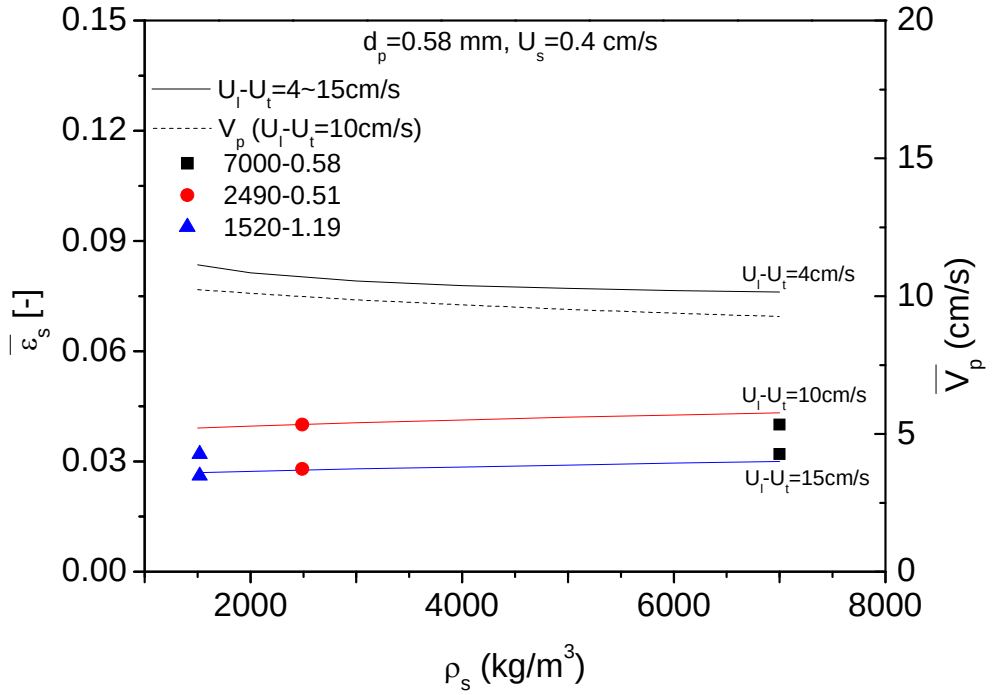

(c)

Fig. 5.7 The effects of the particle density on the average solids holdup ($\overline{\varepsilon_s}$) based on (a) U_l; (b) U_l/U_t; (c) U_l-U_t.

Though the effects of particle density are different when compared under three different parameters, these trends actually follow the same mechanism: average solids holdup ($\bar{\varepsilon}_s$) increases with decreasing particle velocity (V_p) as seen in Fig. 5.7a and 5.7b according to Eq. (5.1). Interestingly, under given U_l-U_t , the particle velocity (V_p) almost does not change with the particle density.

5.6.2 The effects of the particle size on solids holdup by model prediction

The effects of the particle size on solids holdup under different parameters are shown in Fig. 5.8 with particle size varying from 0.2 mm to 1.9 mm for $\rho_p = 2500\ \mathrm{kg/m^3}$ and U_s=0.4 cm/s. It is shown that the effects of the particle size are similar with those of the particle density: when the comparisons are conducted under U_l, solids holdup increases with particle sizes (Fig. 5.8a) due to the decreasing particle velocity (V_p); under fixed U_l /U_t, solids holdup decreases with particle sizes (Fig. 5.8b) due to the increasing particle velocity (V_p); while under fixed U_l -U_t, particle size almost has no effect on the solids holdup (Fig. 5.8c) as V_p is almost constant.

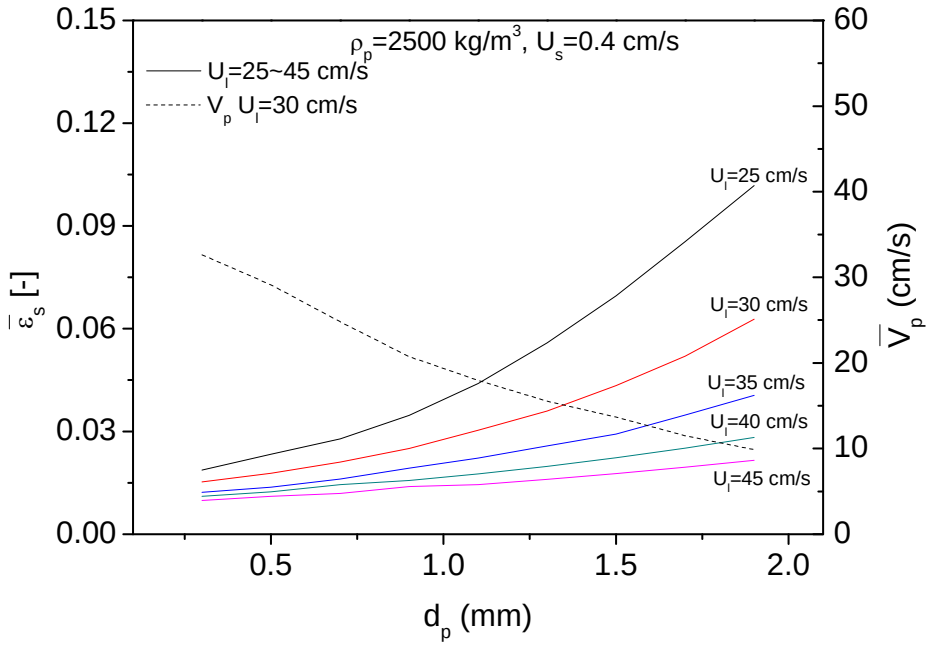

(a)

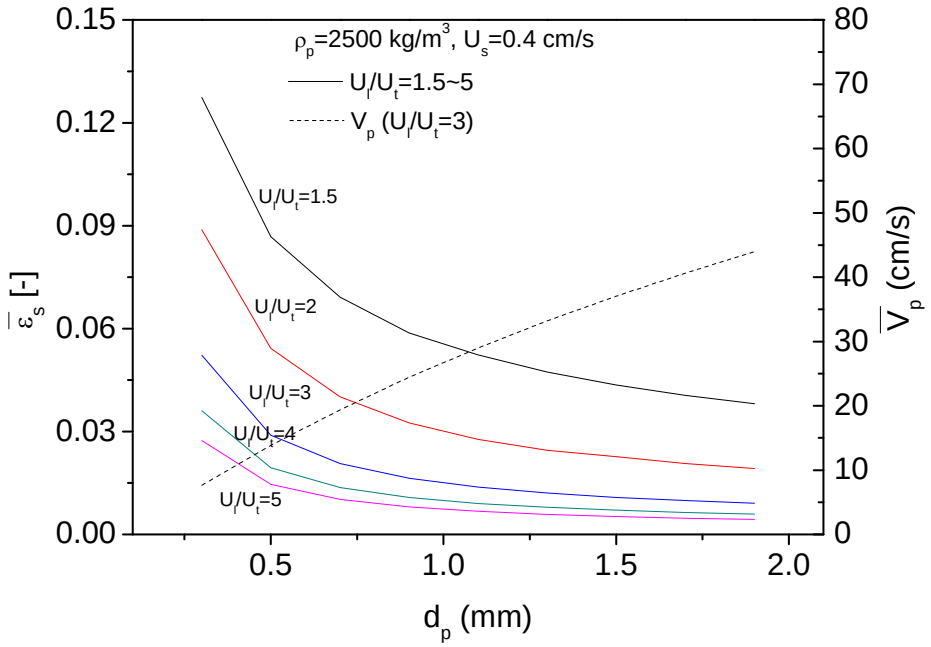

(b)

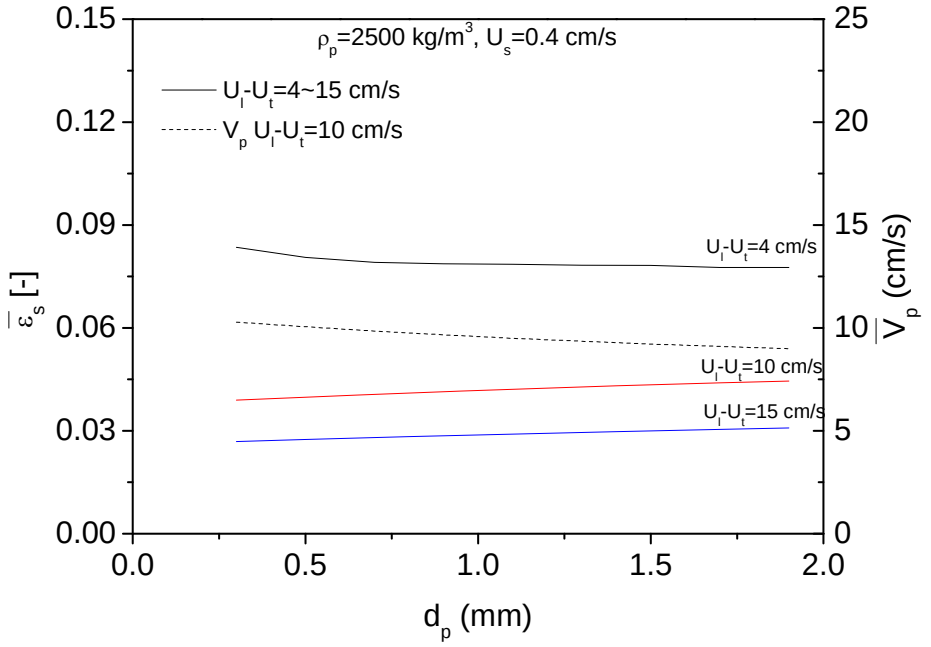

(c)

Fig. 5.8 The effects of the particle size on the average solids holdup ($\overline{\varepsilon_s}$) based on (a) U_l; (b) U_l/U_t; (c) U_l-U_t.

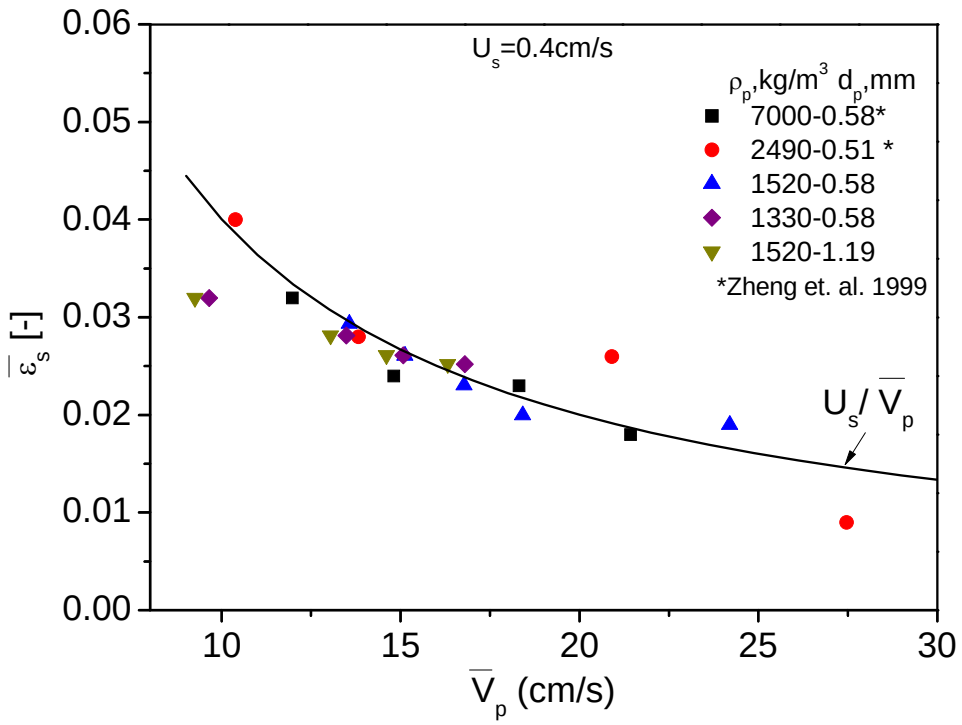

Fig. 5.9 The average solids holdup against the average particle velocity.

According to the above results, average solids holdup is closely related to average particle velocity, which can be expressed as $U_l/(1-\bar{\varepsilon}_s)-1.2U_t(1-\bar{\varepsilon}_s)^{n-1}$ based on Eq. (5.9). For further investigation, the experimental data shown in Fig. 5.3 is replotted in terms of average solids holdup ($\bar{\varepsilon}_s$) vs. the average particle velocity ($\bar{V}_p$) as shown in Fig. 5.9. It can clearly be seen that the scattered data in Fig. 5.3 is nicely lined up in Fig. 5.9, indicating that the solids holdup is only a function of the average particle velocity ($\bar{V}_p$) under the same superficial solids velocity (U_s), regardless of the particle properties.

5.6.3 The effects of the particle sphericity on solids holdup by model prediction

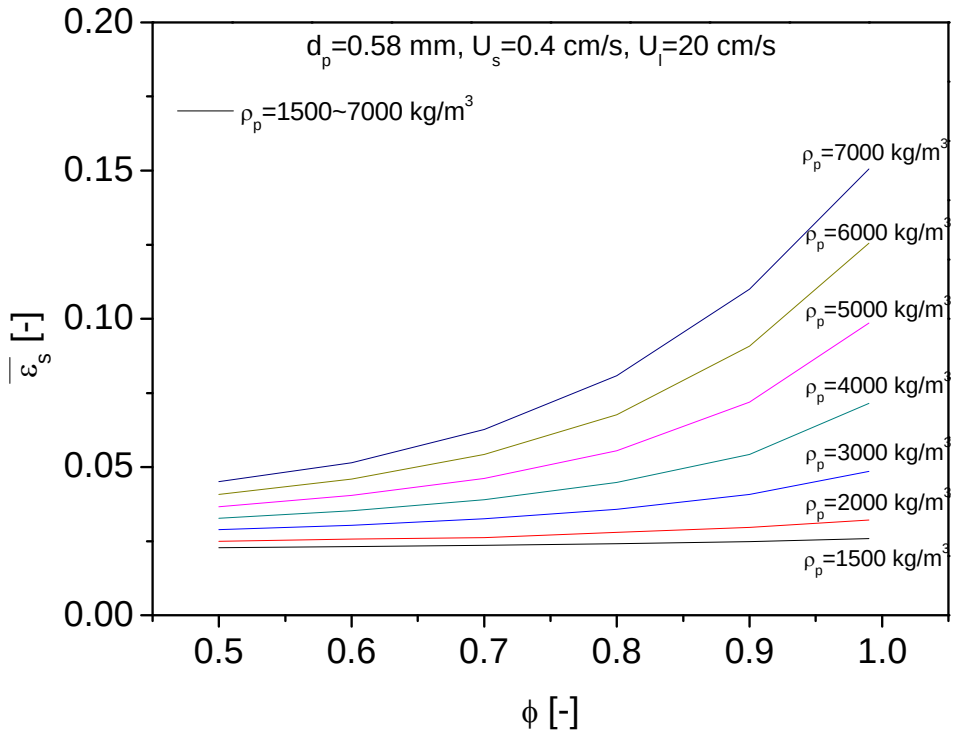

(a)

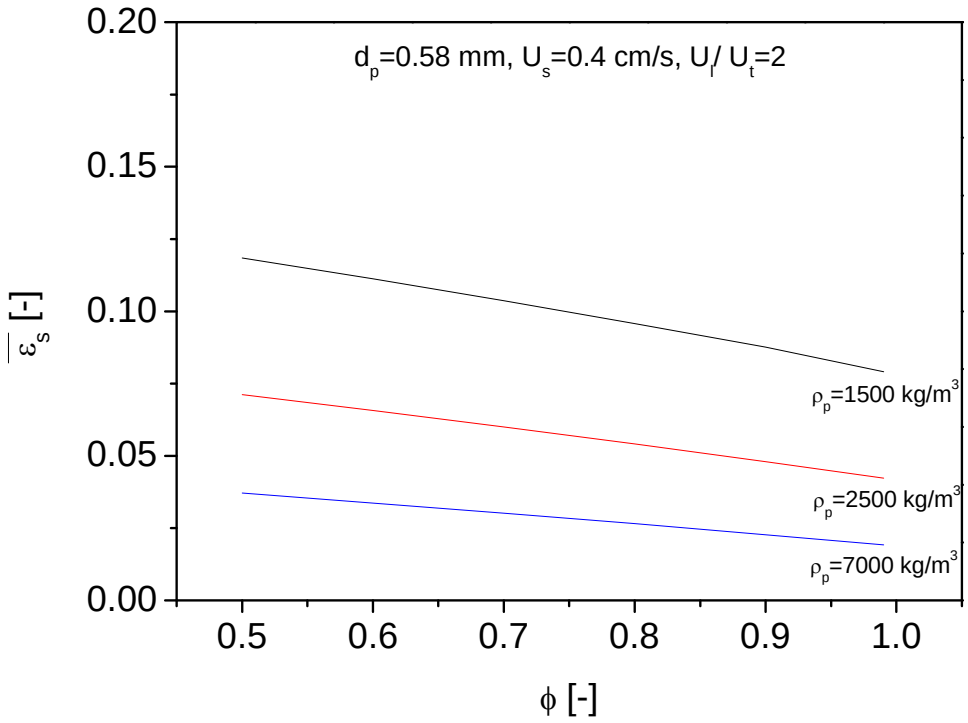

(b)

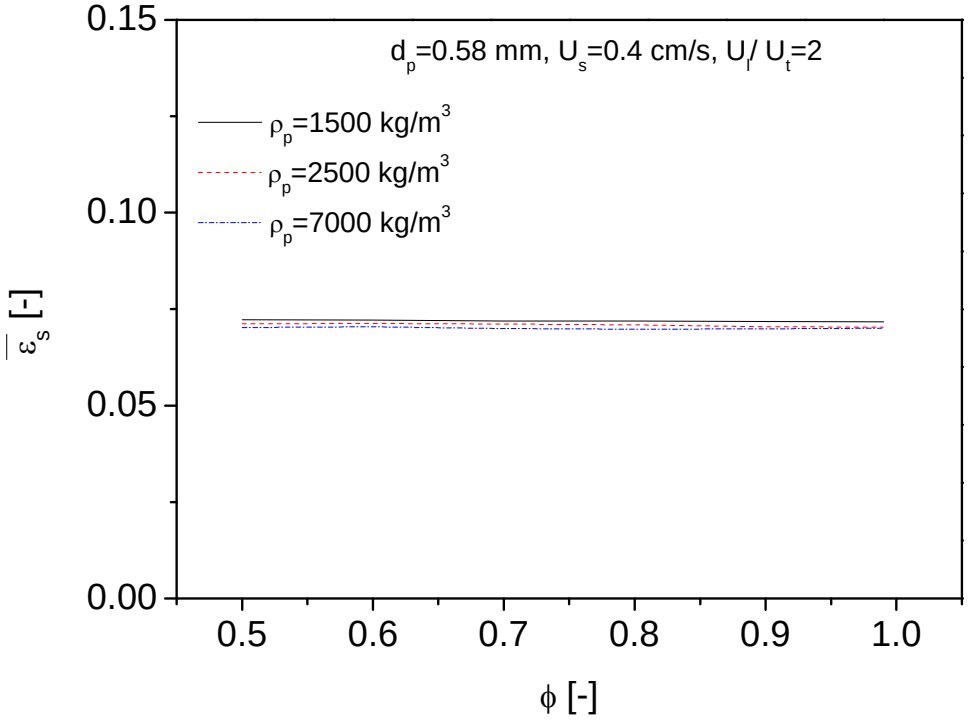

(c)

Fig. 5.10 The effects of particle sphericity on the average solids holdup ($\overline{\varepsilon}_s$) based on (a) U_l, (b) Ul/U_t and (c) U_l-U_t

The effects of the particle sphericity on the average solids holdup ($\bar{\varepsilon}_s$) are shown in Fig. 5.10 based on U_l, U_l /U_t and U_l-U_t respectively. One could note that the similar trends are observed when compared with the effects of the particle density and size. Fig. 5.10a shows that at lower liquid velocity (U_l), the effect of particle sphericity is quite obvious, but such effect is reduced at larger liquid velocity (U_l). Meanwhile, the effect of the sphericity also relates to the particle density, increasing of which makes the effect of particle shape become more dominant on the solids holdup, as the terminal velocity increases rapidly with increasing sphericity for heavier particles compared with that for the lighter particles leading a fast increase of solids holdup with the increasing particle sphericity for heavier particles. Therefore, the particle shape should be considered especially when superficial liquid velocity (U_l) is low or particle is heavy. Fig. 5.10b shows that the average solids holdup ($\bar{\varepsilon}_s$) decreases with increasing sphericity based on the same U_l /U_t, while based on same U_l-U_t, the average solids holdup is independent of particle properties.

5.7 Determination of critical transition velocity demarcating the circulating fluidization regime and the transport regime

The discussions in Section 5.3 have proven that Eq. (5.8) could provide good estimation on solids holdup under various operating conditions. On the other hand, when the solid holdup and superficial solids velocity is known in advance, Eq. (5.8) could serve as the determination of the superficial liquid velocity. Following this logic, the critical superficial liquid velocity (U_{cv}) demarcating the circulating fluidization regime and the transport regime can be determined because solids holdup is always below 1% under the transport regime. Then

$$U_{cv} = \frac{U_s}{\bar{\varepsilon}_s} + 1.2U_t(1-\bar{\varepsilon}_s)^{n-1} = \frac{U_s}{1\%} + 1.2U_t(1-1\%)^{n-1} \approx 100U_s + 1.2U_t \qquad (5.9)$$

It can be noted that the transition velocity (U_{cv}) is a function of the terminal velocity (U_t) and the superficial solids velocity (U_s), proving the reports by Liang et. al. (1997).

This transition velocity (U_{cv}) determined by Eq. (5.9) can be validated with several sets of experimental data done by Zheng et. al. (1999, 2002). The detailed comparisons are shown in Table 5.2 and Fig. 5.11. One can notice that the transition velocity (U_{cv}) for glassbeads is 29.8 cm/s by Eq. (5.9). When the superficial liquid velocity (U_l) is smaller than transition velocity (U_{cv}), i.e, U_l =28 cm/s, which is very close to the transition velocity (U_{cv}) but still lower than it, the flow is still in the circulating fluidization regime because the non-uniform radial solids holdup distribution is existing as seen in Table 5.2. Only when the superficial liquid velocity (U_l) beyond the transition velocity (U_{cv}), the flow enters the transport regime and the uniform radial solids holdup distribution can be observed. The similar results can also be observed in the steel shots results. Thus the flow regime map in LSCFB is completed quantitatively as seen in Fig. 5.11.

Table 5.2 The comparison of the U_{cv} determined by Eq. (5.9) with the experimental results reported by Zheng et. al. (1999, 2002)

Particle	U_l (cm/s)	U_s (cm/s)	U_t (cm/s)	U_{cv} (cm/s)	$\overline{\varepsilon}_s$ (Pre)	$\overline{\varepsilon}_s$ (Exp)	Radial ε_s
GB	15	0.2	7.1	29.8	0.0395	0.0383	Non-uniform
	28	0.2	7.1	29.8	0.011	0.013	Non-uniform
	42	0.2	7.1	29.8	0.006	0.005	Uniform
SS	38	0.196	19.5	39.1	0.012	0.012	----
	45	0.196	19.5	39.1	0.008	0.0084	----
	48.4	0.196	19.5	39.1	0.006	0.007	----
	51.9	0.189	19.5	38.4	0.005	0.006	----
	31.1	0.12	19.5	32	0.012	0.011	----
	38	0.11	19.5	31.1	0.009	0.008	----
	41.5	0.98	19.5	31	0.006	0.006	----
	45	0.09	19.5	28.5	0.004	0.004	----
	48.4	0.095	19.5	29	0.005	0.004	----
	51.9	0.98	19.5	31	0.004	0.004	----

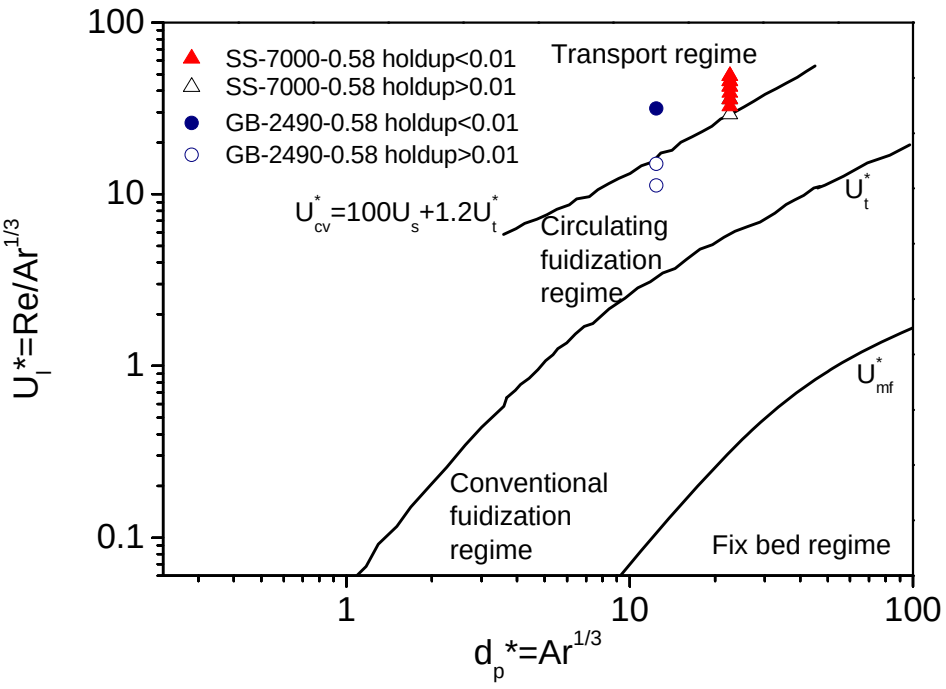

Fig. 5.11 Completed flow regime map for LSCFB.

5.8 Conclusions

An analytical model, which incorporates particle slip velocity, operating conditions and solids properties in terms of terminal velocity (U_t), is proposed to estimate average solids holdup regardless of the dimensions of LSCFB risers, showing satisfactory agreement with the experimental results. By this model, the effects of the particle properties including particle density, size and sphericity can be determined quantitatively, revealing solids holdup is closely related to the particle velocity, increasing of which contributed to lower solids holdup. Then the transition velocity from the Circulating fluidized regime to the Transport regime is determined to finalize the flow regime map in LSCFB.

Nomenclature

Ar	Archimedes number defined by $d^3 g(\rho_p - \rho_l)\rho_l / \mu^2$
a	Slip velocity coefficient U_{slip} / U_t
C_D	Particle drag coefficient
d_p	Particle diameter (mm)
d_p^*	Dimensionless particle size defined by $Ar^{1/3}$
D	Column diameter (m)
F_b, F_d, F_g	Buoyancy force, drag force and gravity
G_s	Solids circulation rate (kg/(m^{2}s))
g	Gravity acceleration
H	Bed height
n	Richardson and Zaki index
N_D	Best number
P	Pressure (Pa)
Q	Volumetric flowrate (m^3 / s)
Re	Reynolds number defined by $Ud\rho_l / \mu$
Re_t	Particle terminal Reynolds number defined by $U_t d\rho_l / \mu$
t	Residence time (s)
U_a	Auxiliary liquid velocity (cm/s)
U_{cr}	Transition velocity from Particulate fluidization regime to Circulating fluidization regime (cm/s)
U_{cv}	Transition velocity from Circulating fluidization regime to Transport regime (m/s)
U_l	Total superficial liquid velocity (cm/s)
U_i	Extrapolated value of U as ε approaches 1
U_l^*	Dimensionless superficial velocity defined by $Re / Ar^{1/3}$
U_s	Superficial particle velocity (cm/s)

U_{slip}	Slip velocity (cm/s)
U_t	Particle terminal velocity (cm/s)
U_t^*	Dimensionless transition velocity defined by Re_t / $Ar^{1/3}$
V_l, V_p	Local liquid velocity and local particle velocity
$\overline{V}_l, \overline{V}_p$	Average liquid velocity and average particle velocity

Greek letters

$\overline{\varepsilon}$	Average bed voidage
$\overline{\varepsilon}_s$	Average solids holdup
ϕ	Particle sphericity
μ_l	Liquid viscosity (mPas)
ρ_p	Particle density (kg/m^3)
ΔP	Pressure drop

Subscripts

l	Liquid
p	Particle
s	Solids

References

Denn, M. M. (1980). Process fluid mechanics. N.J., Englewood Cliffs.

Haider, A. and O. Levenspiel (1989). Drag coefficient and terminal velocity of spherical and nonspherical particles. Powder Technology 58(1): 63-70.

Karamanev, D. G. (1996). Equations for calculation of the terminal velocity and drag coefficient of solid spheres and gas bubbles. Chemical Engineering Communications 147(Compendex): 75-84.

Kwauk, M. (1963). Generalized fluidization I, steady state motion. Scienta Sinica 12: 587-612.

Lan, Q., J. X. Zhu, A. S. Bassi, A. Margaritis, Y. Zheng and G. E. Rowe (2000). Continuous protein recovery using a liquid - Solid circulating fluidized bed ion exchange system: Modelling and experimental studies. Canadian Journal of Chemical Engineering 78(Compendex): 858-866.

Liang, W., S. Zhang, J.-X. Zhu, Y. Jin, Z. Yu and Z. Wang (1997). Flow characteristics of the liquid-solid circulating fluidized bed. Powder Technology 90(2): 95-102.

Mazumder, J., J. Zhu, A. S. Bassi and A. K. Ray (2009). Modeling and simulation of liquid–solid circulating fluidized bed ion exchange system for continuous protein recovery. Biotechnology and Bioengineering 104(1): 111-126.

Natarajan, P., V. Ramalingam, G. Ramadoss and R. V. Seeniraj (2011). Study of slip velocity and application of drift-flux model to slip velocity in a liquid-solid circulating fluidized bed. Advanced Powder Technology 22(Compendex): 77-85.

Natarajan, P., R. Velraj and R. V. Seeniraj (2008). Application of drift-flux model in liquid-solid circulating fluidized bed. Chemical Engineering Communications 195(Compendex): 1144-1158.

Richardson, J. F. and W. N. Zaki (1954). Sedimentation and fluidisation. Institution of Chemical Engineers -- Transactions 32(1): 35-52.

Zhang, H., P. M. Johnston, J. X. Zhu, H. I. de Lasa and M. A. Bergougnou (1998). A novel calibration procedure for a fiber optic solids concentration probe. Powder Technology 100(2-3): 260-272.

Zheng, Y. (1999). Flow Structure in a Liquid Solid Circulating Fluidized Bed. Chemical and Biochemical Engineering. London, University of Western Ontario. Ph.D.

Zheng, Y., J.-X. Zhu, N. S. Marwaha and A. S. Bassi (2002). Radial solids flow structure in a liquid-solids circulating fluidized bed. Chemical Engineering Journal 88(1-3): 141-150.

Zhu, J.-X., D. G. Karamanev, A. S. Bassi and Y. Zheng (2000). (Gas-)liquid-solid circulating fluidized beds and their potential applications to bioreactor engineering. The Canadian Journal of Chemical Engineering 78(1): 82-94.

Chapter 6

6 Comparisons of Fluidization in Inverse and Upwards Liquid-Solid Fluidized Bed

6.1 Introduction

The hydrodynamic characteristics in the liquid-solid fluidization systems have attracted popularitiy due to a number of their merits: such as significantly high mass and heat transfer rates, improved liquid-solid contact efficiency and easy control of large quantity of particles etc. (Zhu et al. 2000). Generally, the solids are fluidized upwards in the fluidized bed when the density of the particles is higher than that of the surrounding liquid, such as in the Liquid-Solid Fluidized Bed (LSFB) and the Liquid-Solid Circulating Fluidized Bed (LSCFB). When the density of the solids is lower than that of the surrounding liquid, the downwards fluidization is necessary and referred to as the inverse fluidization. Compared to other light particle systems, the inverse conventional fluidization has its advantages, including the efficient control of the bioprocess (Nikolov and Karamanev 1987; Karamanev and Nikolov 1996) and of biofilm thickness (Karamanev and Nikolov 1992), higher rate of mass transfer (Nikolov and Nikov 1994), and possibility for re-fluidization (Renganathan and Krishnaiah 2003). Due to those merits, the inverse fluidization already has some applications in waste water treatment (Karamanev and Nikolov 1996; Sowmeyan and Swaminathan 2008).

A good understanding of the hydrodynamics of the inverse fluidization system is crucial to the design, mathematical modeling and optimizing of inverse fluidized bed bioreactor (Chavarie and Karamanev 1986). Some experimental and modeling works have been done to investigate the hydrodynamics in the Inverse Liquid-Solid Fluidized Bed (ILSFB), for example, the bed voidage (Karamanev and Nikolov 1992; Renganathan and Krishnaiah 2005), the minimum fluidization velocity (Karamanev and Nikolov 1992; Vijaya et al. 2000; Renganathan and Krishnaiah 2003), drag coefficient and particle terminal velocity in Newtonian fluids (Karamanev and Nikolov 1992) and non-Newtonian fluids (Dewsbury et al. 2000), flow regimes and pressure drops across the bed

(Ulaganathan and Krishnaiah 1996), voidage waves (Howley and Glasser 2004), and layer inversion of binary particle system (Escudie et al. 2007), were well studied experimentally or theoretically. Some other related characteristics such as heat transfer (Cho et al. 2002; Lu et al. 2006) and mass transfer (Nikolov and Nikov 1994) were also studied.

Comparing the upwards and inverse fluidization, there are many hydrodynamic similarities between the inverse and upwards fluidization, for example, the flow behaviors of particles are quite similar when particle terminal Reynolds number Re_t<130, so that the net forces exerted on the particles are the same but with different directions (Karamanev and Nikolov 1992; Yang and Renken 2003). However, when Re_t>130, the drag force on the "light" particles becomes different due to the violation of the standard drag curve, leading to different particle flow behaviors (Karamanev and Nikolov 1992). Such similarities and differences make the comparison of inverse and upwards fluidization become necessary. Richardson and Zaki equation might serve as the theoretical guidance to achieve the above mentioned comparison under certain conditions, however, it has obvious limitations (Karamanev and Nikolov 1992; Andalib et al. 2012).

In this paper, a mathematical model for predicting the bed voidage under the inverse conventional fluidization regime is proposed based on force balance of particles. The predicted bed voidage then is validated with the experimental results in the inverse fluidization systems (this work and Karamanev and Nikolov (1992)) and the upwards fluidization systems (Loeffler and Ruth 1959; Hoffman et al. 1960; Wen and Yu 1966; Hirata and Bulos 1990; Subramanian and Kannan 1997). By this model, the dimensionless bed expansion is also determined and compared with the experimental data.

6.2 Materials and methods

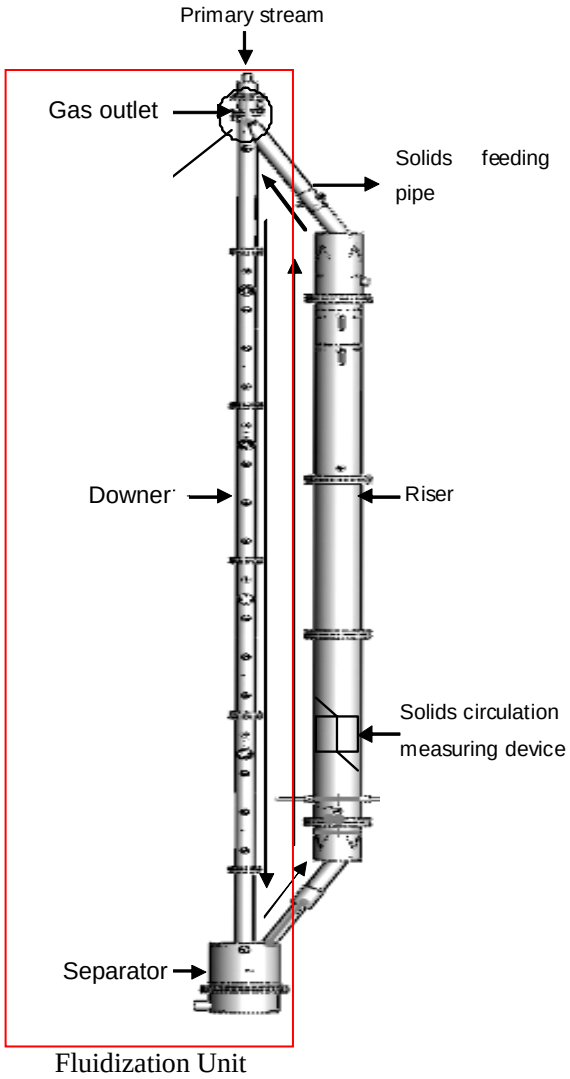

Fig. 6.1 The schematic diagram of the ILSFB apparatus.

The set-up of the ILSFB system is shown schematically in Fig. 6.1. The system mainly consists of a 0.076 m ID and 5.4 m Plexiglas downer column, where the inverse fluidization takes place, a liquid–solid separator and a storage column. This downer is connected to the 0.2 m ID Plexiglas storage through a solids returning pipe at the bottom and a solids feeding pipe at the top, so that the amount of the particles in the downer can be adjusted inside the fluidized bed conveniently without taking/adding particles out/in the system. At the top of the downer, there are two distributors: the main liquid

distributor made of seven stainless steel tubes occupying 19.5% of the total downer cross-sectional area and extending 0.2 m into the downer, and the auxiliary liquid distributor made of a porous plate with 4.8% opening area at the top of the downer.

All experiments were carried out at ambient temperature. Tap water was used as the fluidization media and four types of "light" particles were employed as shown in Table 6.1. Particle density was measured by determining the volume and mass: place the particles with known weight (m_p) into a cylinder with scale and add a certain amount of water (with known weight m_w); push a plug that fits snugly into the cylinder with known volumes (V_{plug}) into the measuring cylinder to prevent particles from floating to the surface; then tap the measuring vessel to remove any air bubbles; after reading off the total volume (V), the particle density can be calculated as $\rho_p = m_p / \left(V - (V_{plug} + m_w / \rho_w)\right)$.

In each run, water was pumped to the top of the downer through a calibrated rotameter at a known flowrate to fluidize the pre-loaded particles downwards until reaching a steady state. Then the bed voidage and bed expansion can be measured by the manometers and visual observation respectively. The same procedure was followed with different particle sizes and densities for various static bed height and water flowrates.

The experimental results for the upwards conventional fluidization in some previous studies (Loeffler and Ruth 1959; Hoffman et al. 1960; Wen and Yu 1966; Hirata and Bulos 1990; Subramanian and Kannan 1997) summarized in Table 6.2 are also incorporated into this study.

Table 6.1 Summary of particle properties used in this study and previously published works in inverse fluidization systems

Researchers	Particles	Density (kg/m^3)	Size (mm)	*Ar* ($\times 10^6$)	U_t (based on *Ar*) (cm/s)	U_t (Reported)
This work	SF46-0.8	46	0.8	0.009	10.8	----
	SF15-5	15	5	3.31	30.8	----
	HGB790-2.5	790	2.5	0.032	9.63	----
	HDPE940-3.5	940	3.5	0.0252	5.89	----
Karamanev and Nikolov (1992)	SF 159-5.77	159	5.77	1.58	25.8	21.3
	SF 75-3.46	75	3.46	0.376	21	18.4
	SF 314-2.33	314	2.33	0.108	12	12.8
	SF 427-2.75	427	2.75	0.117	14.7	13.3
	SF 201-5.35	201	5.35	1.2	24.3	20.6
	SF 96-7.24	96	7.24	3.39	30	24.3
	SF 155-2.4	155	2.4	0.115	16.7	15.2
	SF 650-1.31	650	1.31	0.008	7.95	7.3
	SF 705-3.16	705	3.16	0.091	11.3	10.3
	SF 854-3.03	854	3.03	0.04	7.8	7.9
	PE 930-3.57	930	3.57	0.032	5.87	6

Table 6.2 Summary of particle properties used in previously published works in upwards fluidization systems

Researchers	Particles	Density (kg/m^3)	Size (mm)	*Ar* ($\times 10^6$)	U_t (based on *Ar*) (cm/s)	U_t (Reported)
Subramanian and Kannan (1997)	GB 2490-1.87	2490	1.87	0.09	25.3	25.7
Hirata and Bulos (1990)	GB 2470-0.267	2470	0.267	0.000274	3.3	3.75
	GB 2470-0.631	2470	0.631	0.00362	9.03	----
	GB 2470-1.88	2470	1.88	0.00952	25.2	25.5
	GB 2470-2.36	2470	2.36	0.189	30.2	29.9
Loeffler and Ruth (1959)	GB 2630-0.659	2630	0.659	0.00457	10.1	----
Hoffman et.al. (1960)	GB 2524-0.19	2524	0.19	0.000132	2.1	----
Wen and Yu (1966)	GB 2450-2.03	2450	2.03	0.119	26.7	----
	GB 2460-5	2460	5	1.79	49.1	----
	GB 2360-6.35	2360	6.35	3.42	53.8	----
	SS 7840-2.38	7840	2.38	0.905	72.1	----

6.3 The conventional inverse fluidization regime

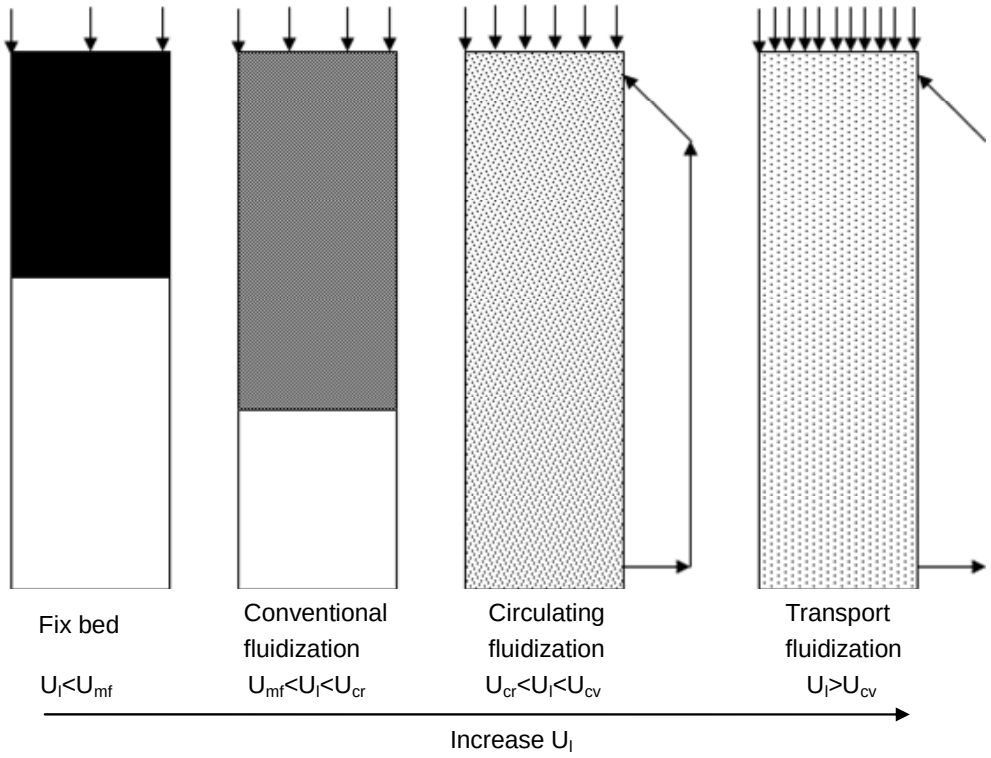

Fig. 6.2 Flow regimes in ILSCFB with increasing of superficial liquid velocity.

As shown in Fig. 6.2, since the particles have lower density than that of the fluidization media (water), they form a packed bed at the top of the downer supported by the liquid distributor due to the buoyancy. With increasing superficial liquid velocity (U_l), the liquid-solid system experiences several flow regimes: at low superficial liquid velocity (U_l) (lower than the minimum fluidization velocity (U_{mf})), the particles remain packed and stay in stationary; by further increasing the superficial liquid velocity (U_l) beyond the minimum fluidization velocity (U_{mf}), the particles start to fluidize to form a conventional fluidized bed where there exists a clear boundary between the top dense region and the bottom freeboard region. Within this regime, an increase in the liquid flowrate causes the dense phase to expand more and raises the dense-dilute phase boundary. This flow regime is quite similar to its counterpart in the upwards fluidization. The theoretical and experimental work in this chapter focuses on this flow regime. With a further increase of the liquid velocity larger than the terminal velocity (U_t), the fluidization will enter a new

flow regime, referred to as circulating fluidization regime, which will be discussed in detail in the next chapter.

6.4 Mathematical model for bed expansion

The different models for correlation of bed expansion with superficial liquid velocity can be classified into three main categories (Fan et al. 1982) in the conventional fluidized bed. Type I model is based on correlations between U/U_i and ε. The Richardson and Zaki model (1954) is the most popular in this group. Type II gives ε as a function of *Ar* and *Re*. The Ramamurthy and Subbaraju model (Ramamurthy and Subbaraju 1973) is typical for this group. The third group of models is based on the dependence between ε and the main variables of the fluidized bed as in the Wen and Yu (1966) correlation. Among all the models, the Richardson and Zaki model (Richardson and Zaki 1954) is most popular due to its simplicity and its accuracy of predicting the experimental data. Theoretically, the flow behavior of free rising particles is identical to the free settling ones. Ideally, the Richardson and Zaki equation in the upwards fluidization system is suppose to be valid in the inverse fluidization system as well. However, Karamanev and Nikolov (1992) found that there were large deviations between the experimental results and the predicted ones of the Richardson and Zaki equation in the inverse system, because the free rising of the lighter particles deviate from the standard drag curve when $Re > 130$ or $\rho_p < 300\text{Kg/m}^3$. Furthermore, the Richardson and Zaki equation adopted a compromised method of determining the bed expansion index (*n*) based on the particle terminal velocity Reynolds number, resulting in a discontinuity and complexity.

Yang and Renken (2003) proposed the idea of the force balance for multi-particle system and developed their own correlation based on the Richardson and Zaki equation. However, extra parameters were introduced, making their model more complex. In addition to the fact that since their model is for upwards fluidization, it cannot govern the inverse fluidization.

In the inverse fluidization system where the density of particles is lower than that of the surrounding liquid, the forces acting on each particle include gravity (F_g), drag (F_d), buoyancy (F_b) and the random inter-particle forces which are minor compared with those three forces. In the case of a single particle in an infinite expansion state ($\varepsilon = 1$), the force balance can be expressed as:

$$F_g + F_d = F_b \tag{6.1}$$

For spherical particles, Eq. (6.1) is expressed as:

$$\frac{1}{6}\pi d_p^3 \rho_p g + \frac{1}{2} C_D \rho_l v^2 \frac{1}{4}\pi d_p^2 = \frac{1}{6}\pi d_p^3 \rho_l g \tag{6.2}$$

Rearranging Eq. (6.2),

$$\frac{1}{2} C_D \rho_l v^2 \frac{1}{4}\pi d_p^2 = \frac{1}{6}\pi d_p^3 g\left(\rho_l - \rho_p\right) \tag{6.3}$$

Eq. (6.3) shows that for a single particle in an infinite expansion state ($\varepsilon = 1$), the ratio $F_d / F_G = 1$ with the apparent drag force $F_d = C_D\left(\rho_l v^2 / 2\right)\left(\pi d_p^2 / 4\right)$ and the effective gravitational force $F_G = \pi d_p^3 g\left(\rho_l - \rho_p\right)/6$. Introducing the voidage function for multi-particle system (Felice 1995), F_d / F_G should be a function of the bed voidage expressed as $F_d / F_G \sim f\left(\varepsilon\right)$. Then Eq. (6.3) becomes:

$$\frac{1}{2} C_D \rho_l v^2 \frac{1}{4}\pi d_p^2 = \frac{1}{6}\pi d_p^3 g\left(\rho_p - \rho_l\right) f\left(\varepsilon\right) \tag{6.4}$$

Combining the similar force balance expression in upwards system (Yang and Renken 2003), then

$$\frac{1}{2} C_D \rho_l v^2 \frac{1}{4}\pi d_p^2 = \frac{1}{6}\pi d_p^3 g \Delta\rho f\left(\varepsilon\right) \tag{6.5}$$

where $\Delta\rho = \rho_p - \rho_l$ for upwards fluidization and $\Delta\rho = \rho_l - \rho_p$ for downwards fluidization.

The dimensionless form of Eq. (6.5) is then expressed as:

$$\frac{3}{4}C_D\frac{Re^2}{Ar}=f(\varepsilon) \tag{6.6}$$

which can serve to predict the bed voidage under the conventional fluidization regime by knowing the drag coefficient (C_D) and voidage function ($f(\varepsilon)$).

When determining the drag coefficient (C_D), most of equations are based on the terminal Re_t number rather than Ar number, leading to an implicit expression to obtain this parameter. Only in Karamanev (1996) the C_D is determined based on Ar number explicitly:

$$C_D=\frac{432}{Ar}(1+0.0470Ar^{\frac{2}{3}})+\frac{0.517}{1+154Ar^{-\frac{1}{3}}} \tag{6.7}$$

valid for both free falling and free rising particles, but when $Ar>1.18\times10^6 d_p^2$, $C_D=0.95$ for free rising particles (Karamanev 1996).

In order to determine the voidage function ($f(\varepsilon)$), many previous studies (Felice 1995) have been done to obtain its proper expressions in the upwards fluidization system. However, there is no attempt to investigate the voidage function ($f(\varepsilon)$) in the inverse conventional fluidization system. In this study, the experimental data in this work and in the literature (Karamanev and Nikolov 1992) for inverse fluidization and the experimental data in the literatures (Loeffler and Ruth 1959; Hoffman et al. 1960; Wen and Yu 1966; Hirata and Bulos 1990; Subramanian and Kannan 1997) for upwards fluidization, are plotted in the terms of $3C_DRe^2/(4Ar)$ vs. ε as shown in Fig. 6.3. The particle properties are listed in Table 6.1 and 6.2. It is shown that $f(\varepsilon)=\varepsilon^n$ could provide the best fitting but the results are dependent on the value of bed expansion index (n), which may vary depending on the particle properties and operating conditions

as shown in Fig. 6.3 and 6.4. It is also obvious that constant value of bed expansion index (*n*) cannot provide accurate estimation.

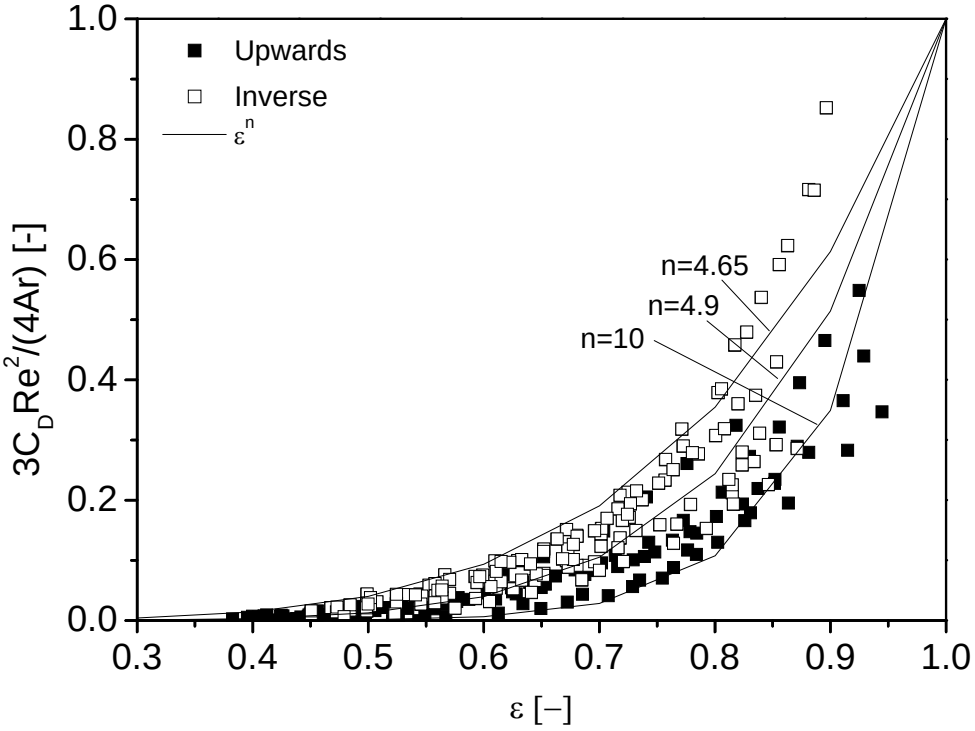

Fig. 6.3 The fitting of $3C_DRe^2/(4Ar)$ as a function of the bed voidage.

Then Eq. (6.6) can be expressed as

$$\frac{3}{4}C_D\frac{Re^2}{Ar}=\varepsilon^n \tag{6.8}$$

According to Eq. (6.7) and (6.8), it is reasonable to correlate the bed expansion index (*n*) with *Ar* and *Re* in the form of: *n=f (Ar)*, *n=f (Re)* or *n=f (Ar, Re)*.

Following the aforementioned logic, Eq. (6.9) is obtained through non-linear curve fitting as shown in Fig. 6.4a to give the best predictions to the bed expansion index (*n*) based on *Ar* number:

$$n=8.8Ar^{-0.04} \tag{6.9}$$

And Eq. (6.10) is obtained through non-linear curve fitting as shown in Fig. 6.4b to give the best predictions to the bed expansion index (n) based on Re number:

$$n = 9.4Re^{-0.1} \tag{6.10}$$

Both Eq. (6.9) and Eq. (6.10) can serve to determine the bed expansion index (n) based on Ar number and Re number respectively. However, it can be noted that the bed expansion index (n) is fixed value in Eq. (6.9) and Fig. 6.4a for same type of particles, without incorporating the operating conditions. Whereas, the bed expansion index (n) in Eq. (6.11) and Fig. 6.4b only varies with the operation conditions without considering the particle properties. Therefore, it is more appropriate to correlate the bed expansion index (n) with both Ar and Re numbers.

In this study, it is considered that the Ar term and Re term contribute the same to the bed expansion index (n), so that Eq. (6.11) can be obtained.

$$n = 4.4Ar^{-0.04} + 4.7Re^{-0.1} \tag{6.11}$$

With Eq. (6.8) and Eq. (6.11), the bed voidage can be calculated explicitly based on Ar and Re. The validations of these two equations are carried out in the next section.

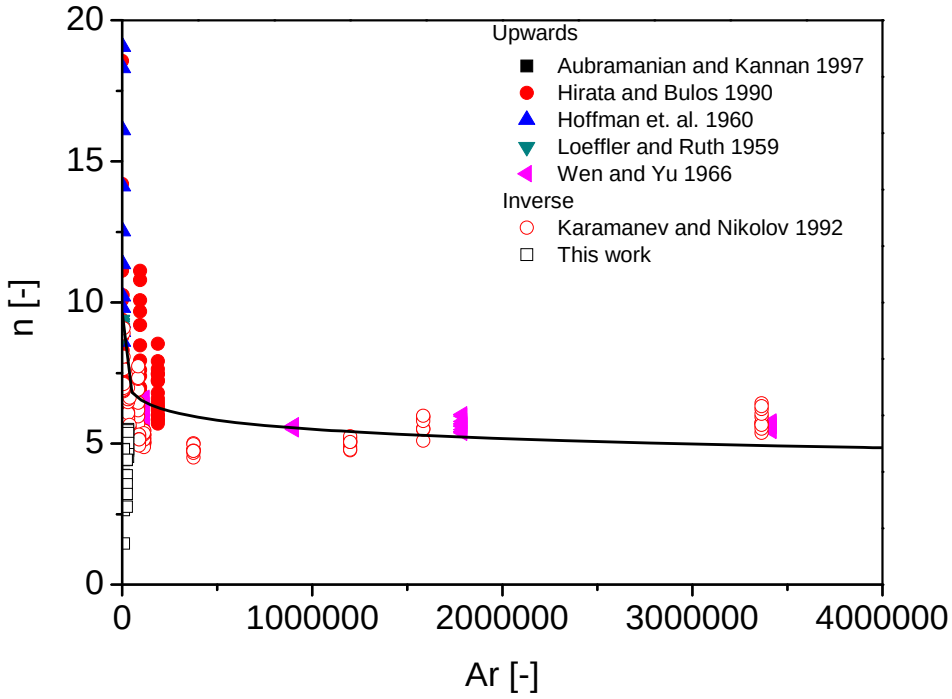

(a)

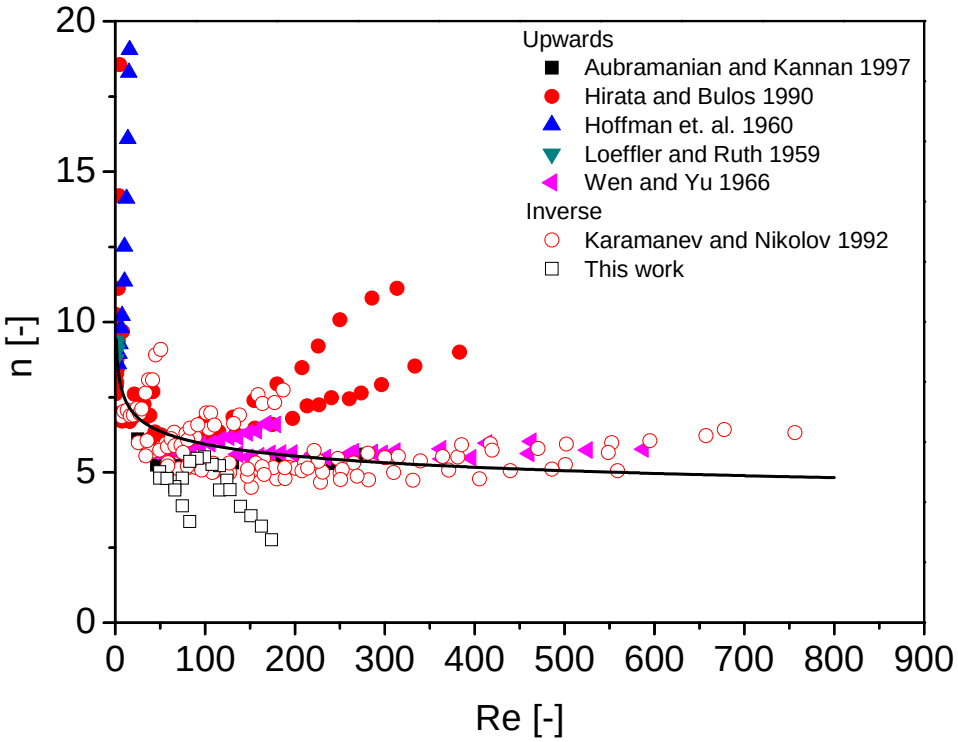

(b)

Fig. 6.4 The bed expansion index (*n*) as a function of (a) *Ar* and (b) *Re* number.

6.5 Prediction of bed voidage in the inverse and upwards liquid-solid conventional fluidization system

Before validating the proposed Eq. (6.8) and Eq. (6.11) with experimental data, the experimental results of inverse conventional fluidization (4 types of particles in the current study and 2 types of particles in the studies by Karamanev and Nikolov (1992)) and upwards conventional fluidization (Loeffler and Ruth 1959; Hoffman et al. 1960; Wen and Yu 1966; Hirata and Bulos 1990; Subramanian and Kannan 1997) are plotted in Fig. 6.5 under various fluidization conditions (U_l =0~25 cm/s). The selected particle densities and sizes can be referred in Table 6.1 and 6.2. It is obvious that the variations of the bed voidage in inverse and upwards systems are quite similar. For all particles, the bed voidage increases when the superficial liquid velocity (U_l) increases because much energy is provided to entrain the particles, leading to larger bed viodage. By introducing the particle terminal velocity (U_t) that incorporates particle properties (density, size, sphericity), the direct comparison among different types of particles having different densities and sizes can be achieved.

Then Eq. (6.8) and Eq. (6.11) can be validated with the experimental data as shown in Fig. 6.6. The comparison shows that the newly proposed equations could predict the bed voidage for both inverse and upwards conventional fluidization with enough accuracy (>85%) and have better performance compared to the Richardson and Zaki Equation.

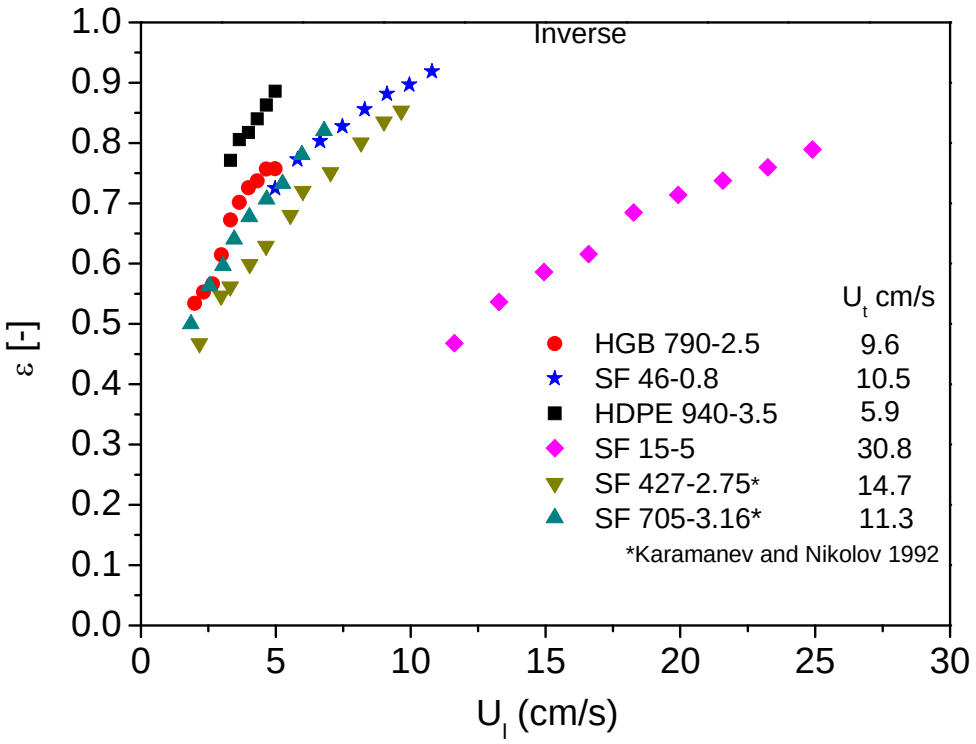

(a)

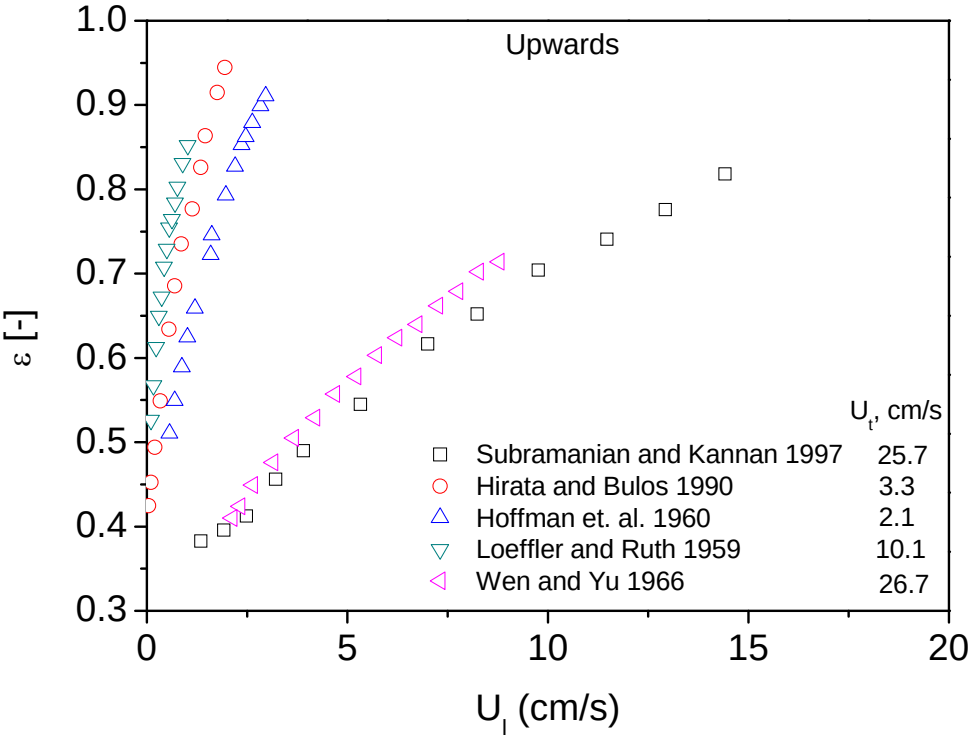

(b)

Fig. 6.5 The bed voidage as a function of the superficial liquid velocity (U_l) in (a) inverse and (b) upwards fluidization systems.

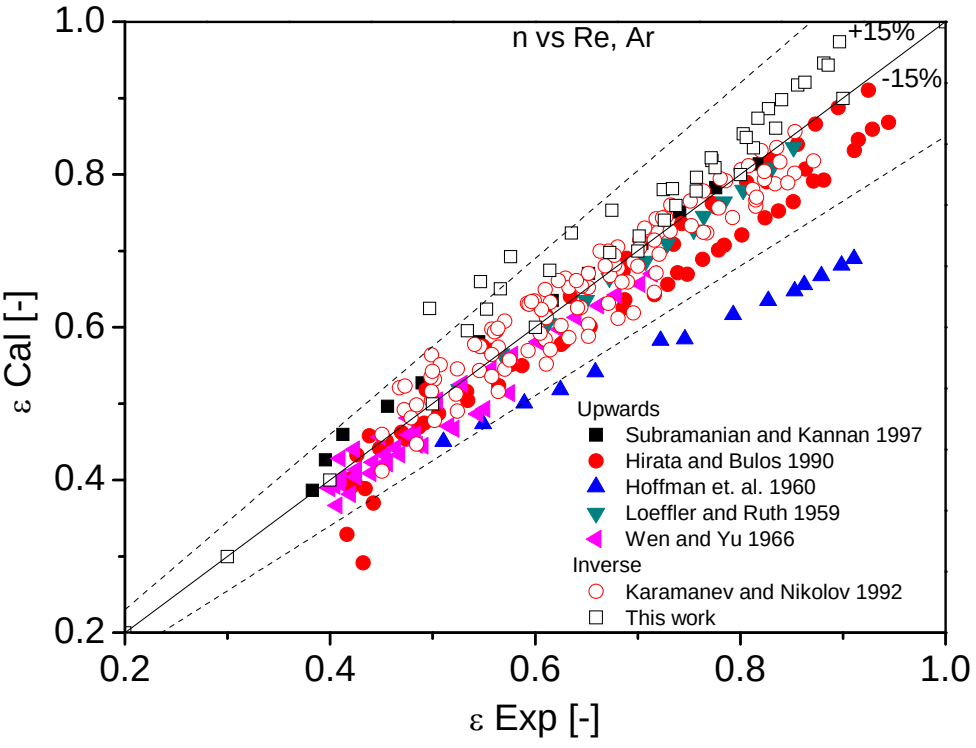

(a)

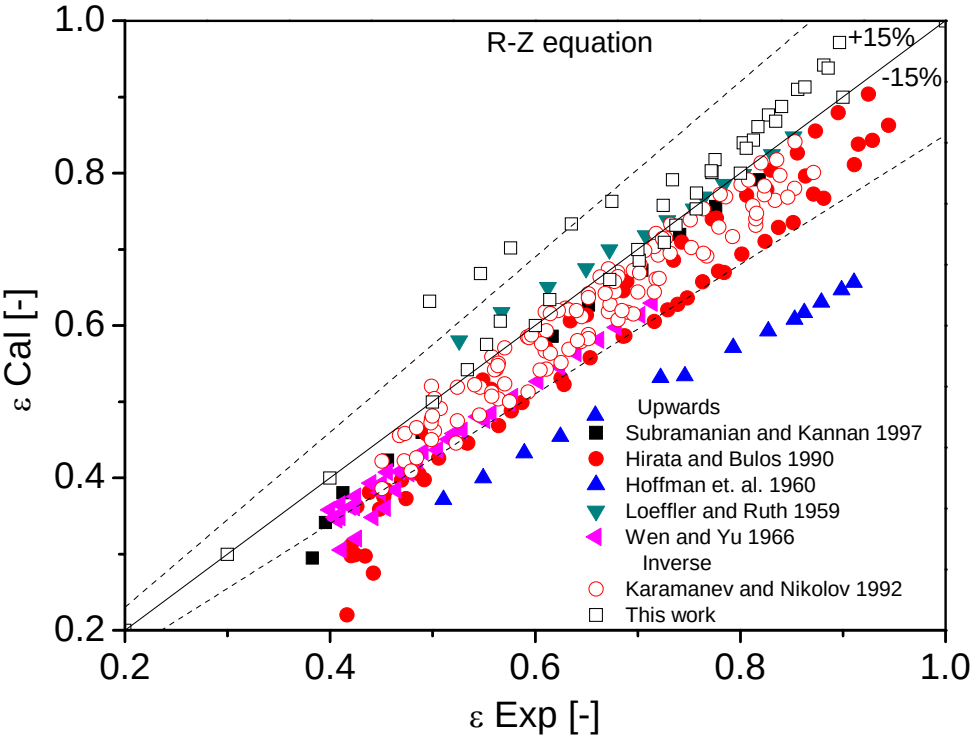

(b)

Fig. 6.6 The predicted bed voidage against the experimental results based on (a) Eq. (6.11), (b) Richardson and Zaki Equation.

6.6 Prediction of dimensionless bed expansion in the inverse liquid-solid fluidization system

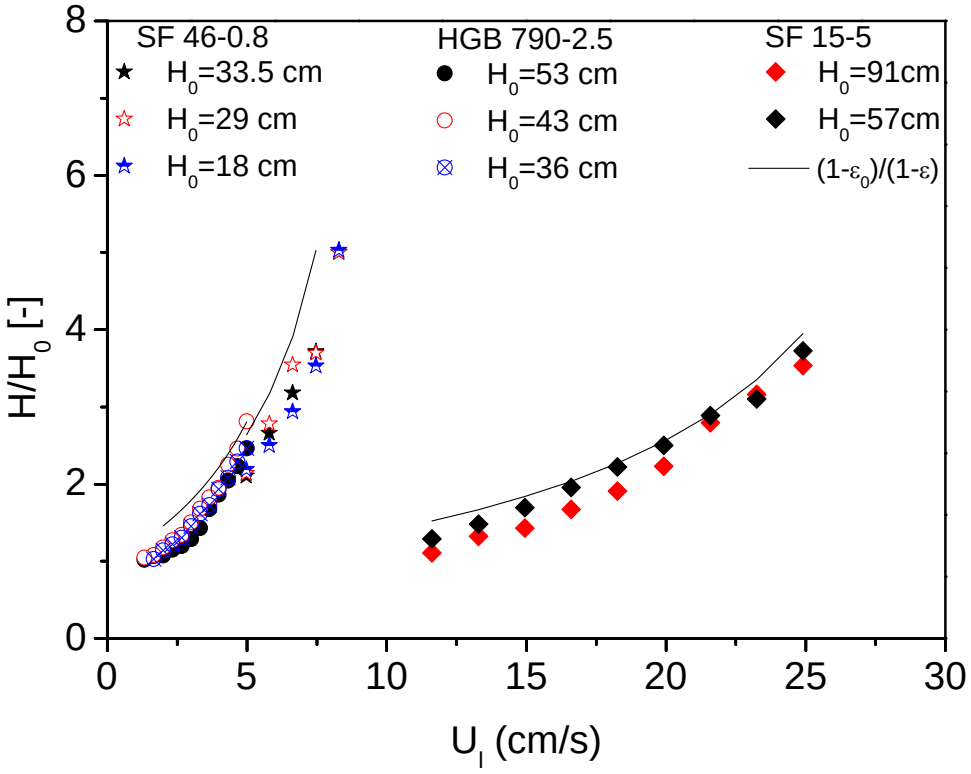

Fig. 6.7 The dimensionless bed expansion as a function of superficial liquid velocity (U_l) under different initial bed height for 3 different types of particles.

Another important parameter in the inverse fluidization is the dimensionless bed expansion (H_T/H_0). According to the definitions of bed voidage and dimensionless bed expansion:

$$\frac{H_T}{H_0} = \frac{1-\varepsilon_0}{1-\varepsilon} \tag{6.12}$$

where ε_0 is the fixed bed voidage and $\varepsilon_0 = 0.43$ (Lewis and Bowerman 1952; Loeffler and Ruth 1959; Hoffman et al. 1960; Karamanev and Nikolov 1992), ε is the bed voidage under specific superficial liquid velocity (U_l).

By Eq. (6.12), the dimensionless bed expansion (H_T/H_0) can be predicted from the bed voidage obtained from Eq. (6.8) and (6.11) under various superficial liquid velocity (U_l).

In order to validate Eq. (6.12) with the experimental results, the experimental dimensionless bed expansions (H_T/H_0) are plotted in Fig. 6.7. It is shown that the variations of dimensionless bed expansion (H_T/H_0) are quite similar with those in the upwards fluidization system. The dimensionless bed expansion (H_T/H_0) is independent of initial bed height for the whole range of operation conditions. Meanwhile, for all types of particles, the dimensionless bed expansion (H_T/H_0) increases with superficial liquid velocity (U_l) and its variation is corresponding to the variation of the bed voidage: under similar superficial liquid velocity (U_l): the particles with smaller terminal velocity (U_t) lead to larger bed expansion and vice versa.

The comparisons of the predicted dimensionless bed expansion (H_T/H_0) by Eq. (6.12) and the experimental dimensionless bed expansion (H_T/H_0) are shown in Fig. 6.7 and 6.8. It is obvious that the predicted and experimental dimensionless bed expansions (H_T/H_0) are in good correlation with each other within the accuracy of 85%.

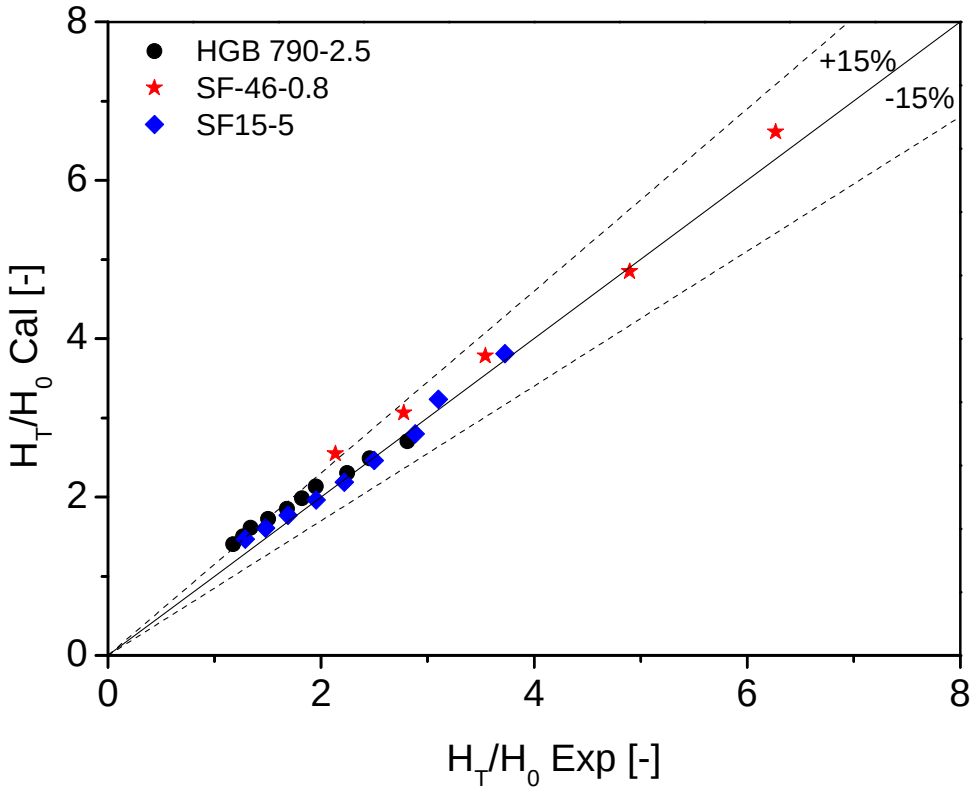

Fig. 6.8 The comparisons of predicted dimensionless bed expansion (H_T/H_0) by this work and the experimental results.

6.7 Conclusions

The different flow regimes for the inverse fluidization system have been discussed. By increasing of the superficial liquid velocity (U_l), the bed is experiencing fixed bed regime, conventional fluidization regime, circulating fluidization regime and transport regime.

A new mathematical model is proposed to predict the bed voidage and dimensionless bed expansion for both inverse and upwards liquid-solid fluidization systems based on force balance of particle in terms of Archimedes number and Reynolds number. The results are validated with experimental data, showing adequate accuracy within a wide range of operating conditions.

The bed voidage and dimensionless bed expansion are investigated and predicted under various liquid flowrate for inverse conventional fluidization regime of 4 different types of particles. Both the bed vodiage and dimensionless bed expansion increase with superficial liquid velocity (U_l); for fixed superficial liquid velocity (U_l), lower particle density leads to smaller bed voidage so as to smaller bed expansion, while larger particle size leads to smaller bed viodage so as to smaller bed expansion. Such comparisons can be conducted in terms of particle terminal velocity (U_t) incorporating different particle properties (density, size, sphericity). Under similar superficial liquid velocity (U_l), the particles with smaller terminal velocity (U_t) lead to larger bed voidage as well as bed expansion, and vice versa.

Nomenclature

Ar	Archimedes number defined by $d^3 g(\rho_p - \rho_l)\rho_l / \mu^2$
a	Slip velocity coefficient U_{slip} / U_t
C_D	Particle drag coefficient
d_p	Particle diameter (mm)
d_p^*	Dimensionless particle size defined by $Ar^{1/3}$
D	Column diameter (m)
F_b, F_d, F_g	Buoyancy force, drag force and gravity
G_s	Solids circulation rate (kg/(m^{2}s))
g	Gravity acceleration
H	Bed height
n	Richardson and Zaki index
N_D	Best number
P	Pressure (Pa)
Q	Volumetric flowrate (m^3 / s)
Re	Reynolds number defined by $Ud\rho_l / \mu$
Re_t	Particle terminal Reynolds number defined by $U_t d\rho_l / \mu$
t	Residence time (s)
U_a	Auxiliary liquid velocity (cm/s)
U_{cr}	Transition velocity from Particulate fluidization regime to Circulating fluidization regime (cm/s)
U_{cv}	Transition velocity from Circulating fluidization regime to Transport regime (m/s)
U_l	Total superficial liquid velocity (cm/s)
U_i	Extrapolated value of U as ε approaches 1
U_l^*	Dimensionless superficial velocity defined by $Re / Ar^{1/3}$
U_s	Superficial particle velocity (cm/s)

U_{slip}	Slip velocity (cm/s)
U_t	Particle terminal velocity (cm/s)
U_t^*	Dimensionless transition velocity defined by Re_t / $Ar^{1/3}$
V_l, V_p	Local liquid velocity and local particle velocity
$\overline{V}_l, \overline{V}_p$	Average liquid velocity and average particle velocity

Greek letters

$\overline{\varepsilon}$	Average bed voidage
$\overline{\varepsilon}_s$	Average solids holdup
ϕ	Particle sphericity
μ_l	Liquid viscosity (mPas)
ρ_p	Particle density (kg/m^3)
ΔP	Pressure drop

Subscripts

l	Liquid
p	Particle
s	Solids

References

Andalib, M., J. Zhu and G. Nakhla (2012). A new definition of bed expansion index and voidage for fluidized biofilm-coated particles. Chemical Engineering Journal 189-190: 244-249.

Chavarie, C. and D. Karamanev (1986). Use of inverse fluidization in biofilm reactors. Int. Syrup. on Bioreactor Fluid Dynamics. Cambridge, England**:** 181-190.

Cho, Y. J., H. Y. Park, S. W. Kim, Y. Kang and S. D. Kim (2002). Heat transfer and hydrodynamics in two- and three-phase inverse fluidized beds. Industrial and Engineering Chemistry Research 41(8): 2058-2063.

Dewsbury, K. H., D. G. Karamanev and A. Margaritis (2000). Dynamic behavior of freely rising buoyant solid spheres in non-newtonian liquids. AIChE Journal 46(1): 46-51.

Escudie, R., N. Epstein, J. R. Grace and H. T. Bi (2007). Layer inversion and bed contraction in down-flow binary-solid liquid-fluidized beds. Canadian Journal of Chemical Engineering 85(1): 25-35.

Fan, L.-S., K. Muroyama and S. H. Chern (1982). Hydrodynamic Characteristics of Inverse Fluidization in Liquid-Solid and Gas-Liquid-Solid Systems. The Chemical Engineering Journal V 24(N 2): 143-150.

Felice, R. D. (1995). Hydrodynamics of liquid fluidisation, Review article number 47 Chemical Engineering Science 50(8): 1213-1245.

Hirata, A. and F. B. Bulos (1990). Predicting bed voidage in solid-liquid fluidization. Journal of Chemical Engineering of Japan 23(5): 599-604.

Hoffman, R. F., L. Lapidus and J. C. Elgin (1960). The mechanics of vertical moving fluidized systems: IV. Application to batch-fluidized systems with mixed particle sizes. AIChE Journal 6(2): 321-324.

Howley, M. A. and B. J. Glasser (2004). A comparison of one-dimensional traveling waves in inverse and normal fluidized beds, Austin, TX, United states, American Institute of Chemical Engineers.

Karamanev, D. G. (1996). Equations for calculation of the terminal velocity and drag coefficient of solid spheres and gas bubbles. Chemical Engineering Communications 147: 75-84.

Karamanev, D. G. and L. N. Nikolov (1992). Bed Expansion of Liquid-Solid Inverse Fluidization. Aiche Journal 38(12): 1916-1922.

Karamanev, D. G. and L. N. Nikolov (1996). Application of inverse fluidization in wastewater treatment: From laboratory to full-scale bioreactors. Environmental Progress 15(3): 194-196.

Lewis, E. W. and E. W. Bowerman (1952). Fluidization of solid particles in liquids. Chemical Engineering Progress 48(12): 603-610.

Loeffler, J. A. L. and B. F. Ruth (1959). Particulate fluidization and sedimentation of spheres. A.I.Ch.E. Journal 5(3): 310-314.

Lu, P., Y. Cao, A. Wu and W.-P. Pan (2006). Experimental study of heat transfer in a horizontal swirling fluidized bed, Pittsburgh, PA, United states, International Pittsburgh Coal Conference.

Nikolov, L. and D. Karamanev (1987). Experimental Study of the Inverse Fluidized Bed Biofilm Reactor. Canadian Journal of Chemical Engineering 65(2): 214-217.

Nikolov, V. R. and I. Nikov (1994). Liquid-solid mass transfer in three-phase inverse fluidized bed (TPIFB). Hungarian Journal of Industrial Chemistry 22(2): 125-128.

Ramamurthy, K. and K. Subbaraju (1973). Bed Expansion Characteristics of Annular Liquid Fluidized. 12(2): 184-189.

Renganathan, T. and K. Krishnaiah (2003). Prediction of minimum fluidization velocity in two and three phase inverse fluidized beds. Canadian Journal of Chemical Engineering 81(3-4): 853-860.

Renganathan, T. and K. Krishnaiah (2005). Voidage characteristics and prediction of bed expansion in liquid-solid inverse fluidized bed. Chemical Engineering Science 60(10): 2545-2555.

Richardson, J. and W. Zaki (1954). Sedimentation and fluidization: Part I. Transactions of the Institution of Chemical Engineers 32(8): 35-53.

Sowmeyan, R. and G. Swaminathan (2008). Performance of inverse anaerobic fluidized bed reactor for treating high strength organic wastewater during start-up phase. Bioresource Technology 99(14): 6280-6284.

Subramanian, B. and C. S. Kannan (1997). Slip velocity characteristics in liquid-solid fluidized beds. Hungarian Journal of Industrial Chemistry 25(1): 17-20.

Ulaganathan, N. and K. Krishnaiah (1996). Hydrodynamic characteristics of two-phase inverse fluidized bed. Bioprocess and Biosystems Engineering 15(3): 159-164.

Vijaya, L. A. C., M. Balamurugan, M. Sivakumar, S. T. Newton and M. Velan (2000). Minimum fluidization velocity and friction factor in a liquid-solid inverse fluidized bed reactor. Bioprocess and Biosystems Engineering 22(5): 461-466.

Wen, C. Y. and Y. H. Yu (1966). Mechanics of fluidization. Chemical Engineering Progress Symposium, 1966.

Yang, J. and A. Renken (2003). A generalized correlation for equilibrium of forces in liquid-solid fluidized beds. Chemical Engineering Journal 92(1-3): 7-14.

Zhu, J.-X., D. G. Karamanev, A. S. Bassi and Y. Zheng (2000). (Gas-)liquid-solid circulating fluidized beds and their potential applications to bioreactor engineering. The Canadian Journal of Chemical Engineering 78(1): 82-94.

Chapter 7

7 Hydrodynamics in Inverse Liquid-Solid Circulating Fluidized Bed Downer

7.1 Introduction

Generally, the solids are fluidized upwards in the fluidized bed when the density of the particles is higher than that of the surrounding liquid, such as in the Liquid-Solid Fluidized Bed (LSFB) and the Liquid-Solid Circulating Fluidized Bed (LSCFB). Whereas, when the density of the solids is lower than that of the surrounding liquid, the downwards fluidization is necessary, and referred to as the inverse fluidization.

A good understanding of hydrodynamics in the inverse conventional fluidization system is crucial to the design operation, mathematical modeling and optimizing of the inverse fluidized bed reactors such as bioreactors (Chavarie and Karamanev 1986). Some previous experimental and modeling research has been done to investigate the hydrodynamics in the conventional Inverse Liquid-Solid Fluidized Bed (ILSFB). For example, the bed voidage (Karamanev and Nikolov 1992; Renganathan and Krishnaiah 2005), the minimum fluidization velocity (Karamanev and Nikolov 1992; Vijaya et al. 2000; Renganathan and Krishnaiah 2003), drag coefficient and particle terminal velocity in Newtonian fluids (Karamanev and Nikolov 1992) and non-Newtonian fluids (Dewsbury et al. 2000), flow regimes and pressure drops across the bed (Ulaganathan and Krishnaiah 1996), voidage waves (Howley and Glasser 2004), and layer inversion of binary particle system (Escudie et al. 2007), were all well studied experimentally or mathematically. Some other related characteristics such as heat transfer (Cho et al. 2002; Lu et al. 2006) and mass transfer (Nikolov and Nikov 1994) were also studied.

However, all the above mentioned studies focused only on the conventional fluidization regime under which the superficial liquid velocity is lower than that of the particle terminal velocity. When the superficial liquid velocity is larger than the particle terminal velocity, the particles will be fluidized under the circulating fluidization regime, which

has unfortunately, not been reported by any research work in the aspect of hydrodynamics.

In this paper, a new type of fluidized bed called Inverse Liquid-Solid Circulating Fluidized Bed (ILSCFB) has been developed to investigate the hydrodynamics in the inverse circulating fluidization regime by fluidizing two different types of particles whose densities are lower than that of the fluidization media. The axial and radial solids holdup distributions are studied under various operating conditions. Comparisons of ILSCFB and LSCFB are also made based on force balance analysis, facilitating the direct prediction of the average solids holdup in ILSCFB.

7.2 Materials and methods

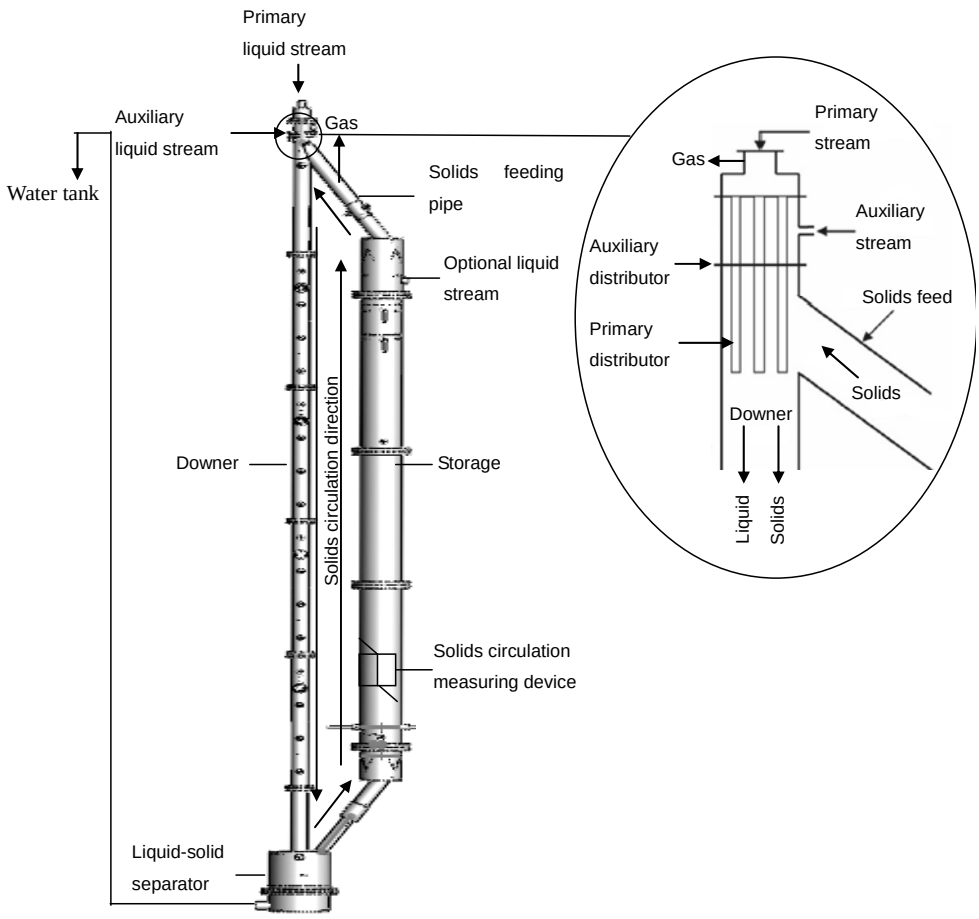

Fig. 7.1 The schematic diagram of ILSCFB apparatus.

The set-up of ILSCFB system is shown schematically in Fig. 7.1. The system mainly consists of a 0.076 m ID Plexiglas downer column, where the inverse fluidization takes place, a liquid–solid separator, storage column, and a device for measuring the solids circulation rate at the bottom of storage. This downer is connected to the 0.2 m ID Plexiglas storage column through a solids returning pipe at the bottom and a solids feeding pipe at the top. There are two distributors: the main liquid distributor made of seven stainless steel tubes occupying 19.5% of the total downer cross-sectional area and extending 0.2 m down to the downer, and the auxiliary liquid distributor made of a porous plate with 4.8% opening area at the top of the downer. With such configuration, particles introduced into the downer top are carried downwards to the bottom of the downer by the combined liquid flow (the primary liquid flow plus the auxiliary liquid

flow) and separated by the cylindrical liquid–solid separator at the bottom. Liquid is then returned to the liquid reservoir for reuse while the particles are returned to the storage after passing through the solids circulation rate measuring device and re-introduced into the downer top via the solid feeding pipe to re-fluidize. Therefore, the light particles are continuously circulating inside ILSCFB system.

The liquid and solids flow rates can be controlled independently by adjusting the primary and the auxiliary liquid flow rates. The auxiliary liquid stream controls the quantity of the particles recirculating from the storage column to the downer: when the auxiliary flow is set to zero, no particles are able to enter the downer and no continuous particle circulation could be formed. Introducing the auxiliary liquid flow, solids do not begin to flow immediately. Only when the auxiliary liquid flow reaches a threshold flow rate, solids will begin to flow, following that, additional liquid added to the downer top cause more particles to enter the downer.

The local solids holdup and particle velocity is measured by using an optical fiber probe model PV-6, produced by the Institute of Process Engineering, Chinese Academy of Sciences. For details of this probe, please refer to some earlier papers by our group (Zhang et al. 1998; Zheng et al. 2002). The calibration of this probe for the liquid–solid systems could be carried out on site. With the fluidized bed operated in the conventional fluidization regime, where the solids holdup is considered homogeneous in both the axial and the radial direction, the output voltage signal from the probe is calibrated against the solids holdup data obtained from pressure gradient measurements. Such calibration is always conducted in the middle section of the fluidized bed so that the “end effect” is eliminated. A linear relationship was found between the voltage signal and the solids holdup for each type of the particle.

The local liquid velocity was measured with a pulse injection of saturated NaCl and carbon black electrolyte solution at the upstream of two bronze conductivity probes connecting to a conductivity meter. Given the very small volume of the injection (about 0.5 ml), the effects of injection on the flow structure are negligible. The distance between

the injection point and the conductivity probe is 25 cm. When the electrolyte solution is just injected into the downer, there is no signal change indicated by the conductivity meter. Then when the electrolyte solution travels downstream and reaches the point of conductivity probe, the signal indicated by the conductivity meter starts to change. The traveling of the electrolyte solution can also be observed from the traveling of the carbon black. By recording the time interval of the signal change and knowing the distance from the injection point to the conductivity probe, the local liquid velocity at various locations in the bed can be obtained. The injection was traversed in the radial direction to obtain the radial distribution of liquid velocity. All the radial distributions of liquid velocity reported in this study were at the axial position of 4 m below the main distributor, which is in the fully developed flow region.

All experiments were carried out at ambient temperature. Tap water was used as the fluidizing liquid and the Styrofoam and Hollow Glassbeads were employed as the circulating particles in this study. The detailed particle properties are summarized in Table 7.1. Particle density was measured by determining the volume and mass: place the particles with known weight (m_p) into a cylinder with scale and add a certain amount of water (with known weight m_w); push a plug that fits snugly into the cylinder with known volumes (V_{plug}) into the measuring cylinder to prevent particles from floating to the surface; then tap the measuring vessel to remove any air bubbles; after reading off the total volume (V), the particle density can be calculated as $\rho_p = m_p / \left(V - (V_{plug} + m_w / \rho_w)\right)$.

In each run, the local solids holdup was measured at different radial positions but given axial position by traversing the probe horizontally, after the ILSCFB unit was brought to a steady operation. During initial measurements, the probe was traversed from one wall to the other and no significant asymmetry was found in the radial holdup profile. Therefore, measurements were taken only at one side of the downer, at seven radial locations between the center and the wall (r/R =0, 0.2034, 0.492, 0.6396, 0.7615, 0.8641, 0.9518). At 4 different levels the same procedure was repeated for different solids circulation rates and liquid velocities. For each measurement location, the column section from about 0.3 m above to 0.3 m below the probe was wrapped with a black plastic sheet

to prevent external light from penetrating into the downer and interfering with the measurements.

Table 7.1 Particle properties

Particles	Density (kg/m3)	Size (mm)	*Ar* (×10^6)	U_t (cm/s)*
SF 46-0.8	46	0.8	0.009	10.5
HGB 790-2.5	790	2.5	0.032	9.63

*$U_t = \sqrt{\frac{4(\rho_p - \rho_l)gd}{3\rho_l C_D}}$, $C_D = \frac{432}{Ar}(1 + 0.0470 Ar^{\frac{2}{3}}) + \frac{0.517}{1 + 154 Ar^{-\frac{1}{3}}}$, valid for both free falling and free rising particles, but when $Ar > 1.18 \times 10^6 d_p^2$, $C_D = 0.95$ for free rising particles (Karamanev 1996).

7.3 The operation of ILSCFB

7.3.1 Flow regimes

Similar to the upwards fluidization system, there are different flow regimes when the superficial liquid velocity is increasing from zero. In order to show the different characteristics under each flow regime, the variation of the axial solids holdup with an increase of superficial liquid velocity (U_l) is shown in Fig. 7.2 for SF46-0.8 particles. When the superficial liquid velocity (U_l) is lower than that of the particle terminal velocity (U_t=10.5 cm/s), for example U_l=5 cm/s, the bed is under the conventional fluidization regime where a clear distinction exists between the dense region with uniform solids holdup distribution and the free board region. With increasing superficial liquid velocity (U_l), the particles expanded downwards and the distinction between the dense phase and the dilute phase gradually becomes unclear. For example, at U_l =9.96 cm/s, close but still lower than the U_t, some smaller particles begin to be entrained out of the bed. At this time, the fluidized bed is in the transition from conventional fluidization to circulating fluidization. With ever increasing superficial liquid velocity (U_l) beyond the particle terminal velocity (U_t), the axial solids holdup distribution becomes uniform throughout the whole bed and large quantity of particles are transported out of the bed and solids circulation rate is increased sharply. At this point, the bed has entered the

circulating fluidization regime and it is essential to continuously feed particles into the downer top to maintain the bed.

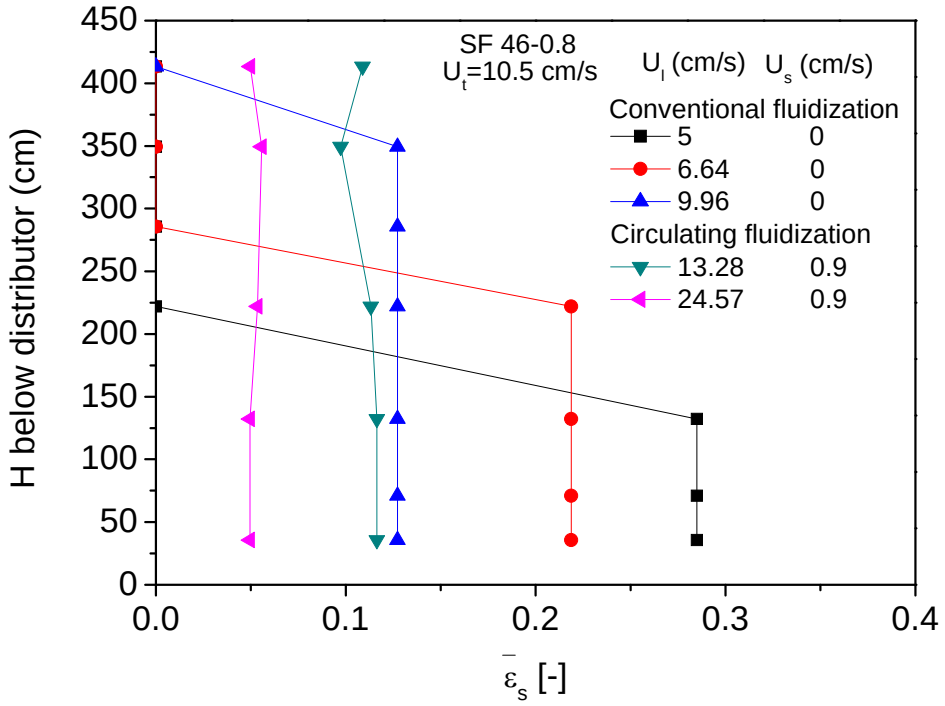

Fig. 7.2 The variation of the axial average solids holdup distribution under the conventional and circulating fluidization regimes for SF46-0.8.

7.3.2 The control of superficial solids velocity U_s

Superficial solids velocity (U_s) is defined as the downwards velocity of the solids phase alone where there is no liquid present in the downer. Solids circulation rate (G_s) is the mass flow rate of solids circulating into the downer at steady-state operation and the relation between the two is $U_s = G_s / \rho_p$. Although both parameters could be employed to describe the amount of solids circulating from the downer to the storage column at unit time per unit area, it is more appropriate to use the superficial solids velocity (U_s) when different types of particles with different solids densities (ρ_p) are involved. It is important when conducting comparisons such as solids holdup under different operating conditions, to ensure the superficial solids velocity (U_s) is the same, otherwise the

comparisons are not on the same basis. This is due to the fact that superficial solids velocity (U_s) could be different even when the solids circulation rate (G_s) is set to be the same for particles of different density.

Fig. 7.3 shows that the superficial solids velocity (U_s) then can then be controlled by the combined superficial liquid velocity (U_l) and the auxiliary liquid velocity (U_a) for SF46-0.8 and HGB790-2.5. For both types of particles, at different auxiliary liquid velocities (U_a), superficial solids velocity (U_s) initially increases with combined superficial liquid velocity (U_l). This is because solids circulation tends to be limited by the entrainment capacity of the combined liquid velocity rather than the particle mobility at the exit of the feeding pipe at the downer top controlled by the auxiliary liquid velocity (U_a). Beyond the initial stage, the solids circulation is more controlled by the auxiliary liquid velocity (U_a), so the superficial solids velocity (U_s) is constant for each auxiliary liquid velocity (U_a) though the combined superficial liquid velocity (U_l) keeps increasing and the solids circulation is considered to be fully developed. Similar observation was also reported by Zheng et. al. (1999). On the other hand, at this stage, the superficial solids velocity (U_s) increases with the auxiliary liquid velocity (U_a) for a fixed superficial liquid velocity (U_l) since more particles are introduced into the downer with higher auxiliary liquid velocity (U_a).

By adjusting the auxiliary liquid velocity (U_a), similar superficial solids velocity (U_s) could be achieved. As a result, when conducting the comparisons, it is important to keep the superficial solids velocity (U_s) fixed, rather than the auxiliary liquid velocity (U_a). Otherwise the comparisons are not valid since the solids holdup increase with the superficial solids velocity (U_s) when other operating conditions are the same.

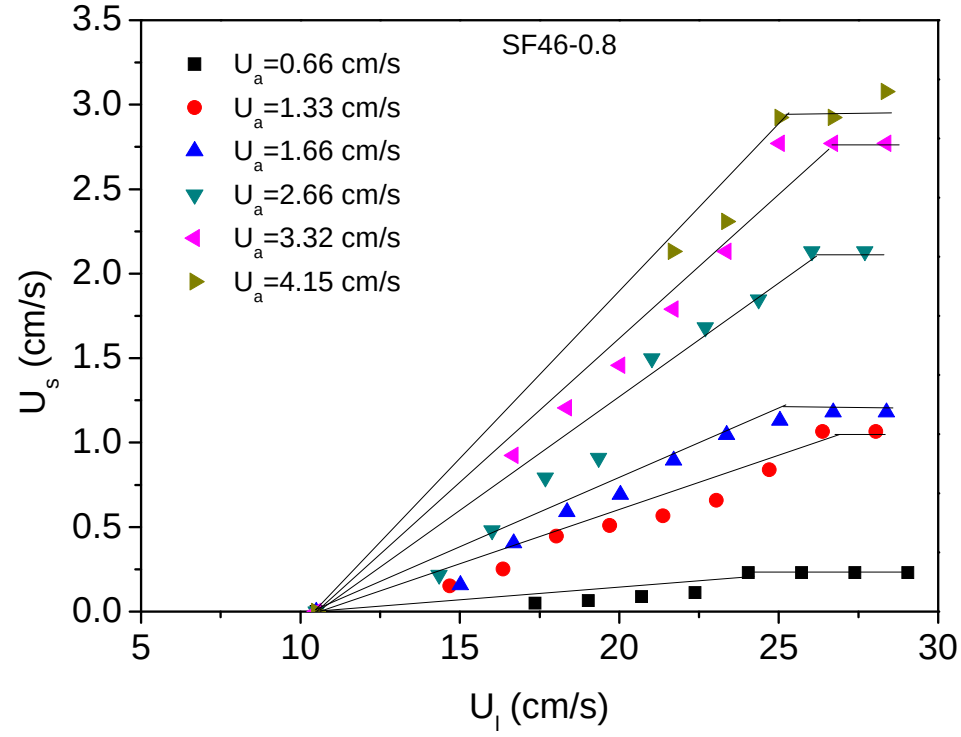

(a)

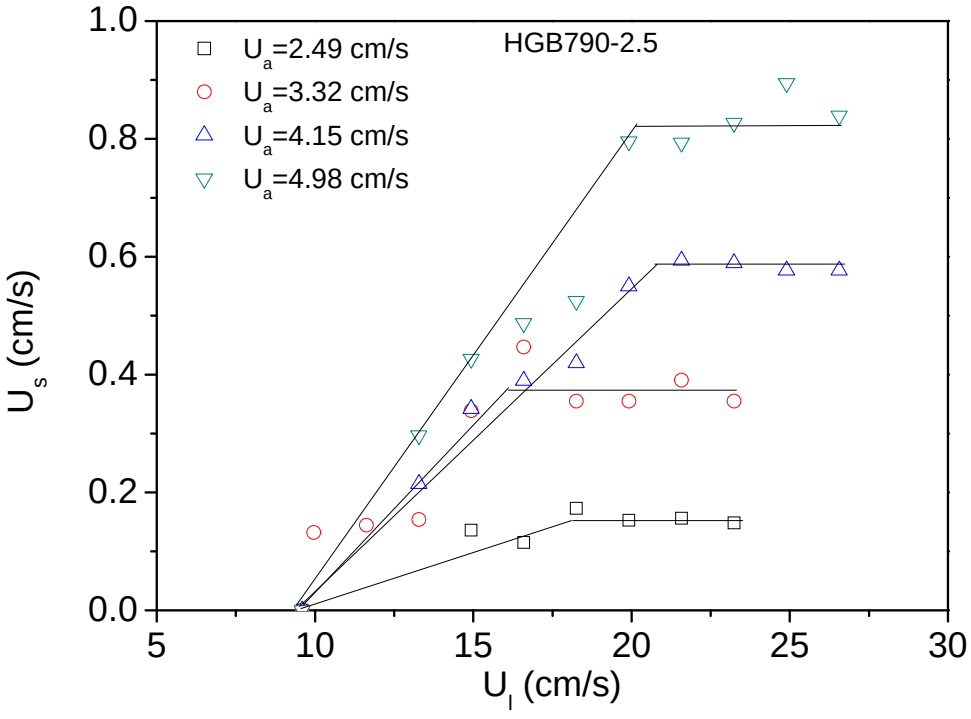

(b)

Fig. 7.3 The superficial solids velocity (U_s) as a function of combined superficial liquid velocity (U_l) for (a) SF46-0.8 and (b) HGB790-2.5 under different auxiliary liquid velocity (U_a).

7.4 The hydrodynamics in the ILSCFB

7.4.1 The variations of average solids holdup

The average solids holdups ($\overline{\varepsilon}_s$) of the 2 types of particles are plotted against the superficial liquid velocity (U_l) in Fig. 7.4 under different superficial solids velocity (U_s). For all particles under similar superficial solids velocity, the average solids holdup ($\overline{\varepsilon}_s$) decreases when the superficial liquid velocity (U_l) increases. This is because much energy is provided to entrain the particles, which leads to a lower solids concentration. While for all particles under similar superficial liquid velocity (U_l), the average solids holdup ($\overline{\varepsilon}_s$) increases with increasing superficial solids velocity (U_s) because of increasing solids flux. In order to show the effects of the superficial solids velocity on the average solids holdup ($\overline{\varepsilon}_s$) explicitly, it is also plotted against the superficial solids velocity (U_s) in Fig. 7.5. It is clear that for all superficial liquid velocity (U_l), the average solids holdup ($\overline{\varepsilon}_s$) increases with superficial solids velocity (U_s) and there appear to be a linear relation existing between those two parameters under the same superficial solids velocity (U_l). Similar results were also found in the upwards LSCFB system (Zheng 1999; Zheng et al. 1999; Sang and Zhu 2012). Such variation of solids holdup can be explained quantitatively by $\overline{\varepsilon}_s = U_s / \overline{V}_p$, the average solids holdup ($\overline{\varepsilon}_s$) is in inverse proportion to the average particle velocity ($\overline{V}_p$) and proportional to the superficial solids velocity (U_s). From the particle velocity study (Chapter 4 and Chapter 8), average particle velocity ($\overline{V}_p$) is primarily determined by the superficial liquid velocity (U_l) not the superficial solids velocity (U_s). Therefore, under the same superficial liquid velocity (U_l) solids holdup ($\overline{\varepsilon}_s$) increases with superficial solids velocity (U_s) linearly.

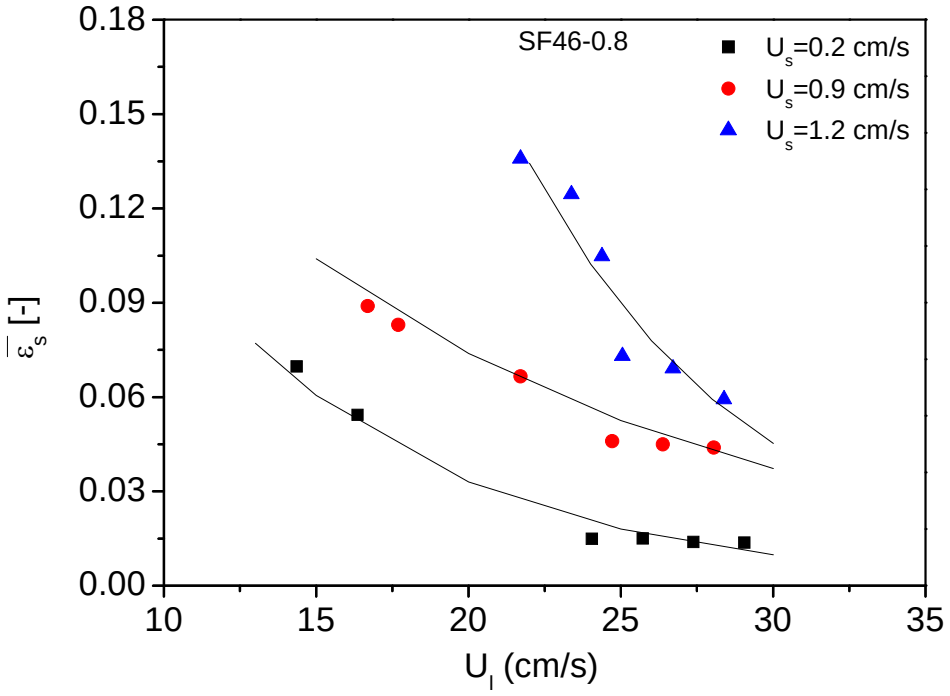

(a)

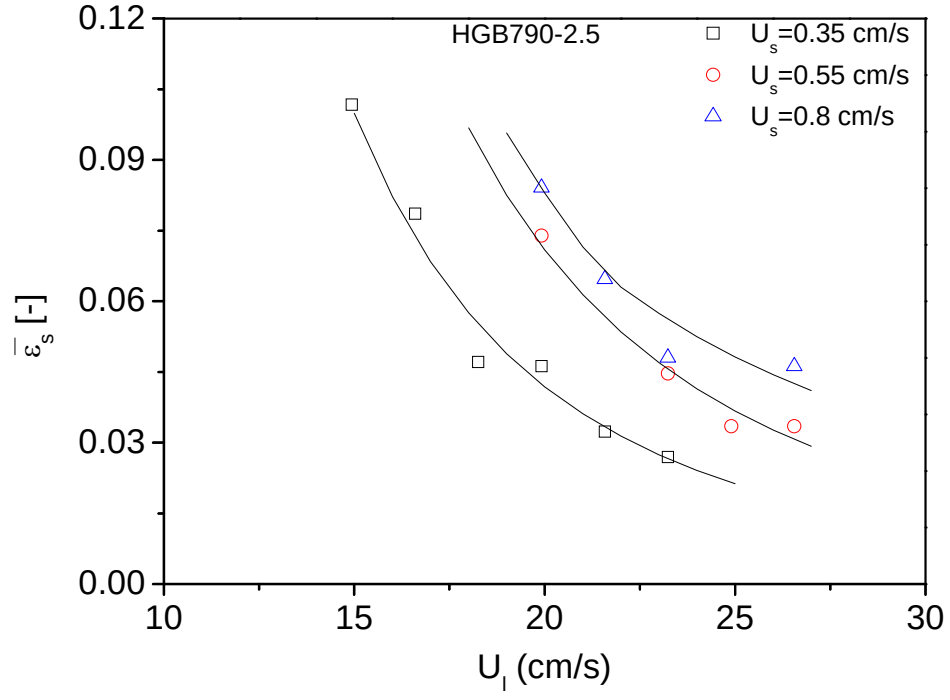

(b)

Fig. 7.4 The average solids holdups ($\bar{\varepsilon}_s$) against the superficial liquid velocity (U_l) under various superficial solids velocities (U_s) for (a) SF46-0.8 and (b) HGB790-2.5.

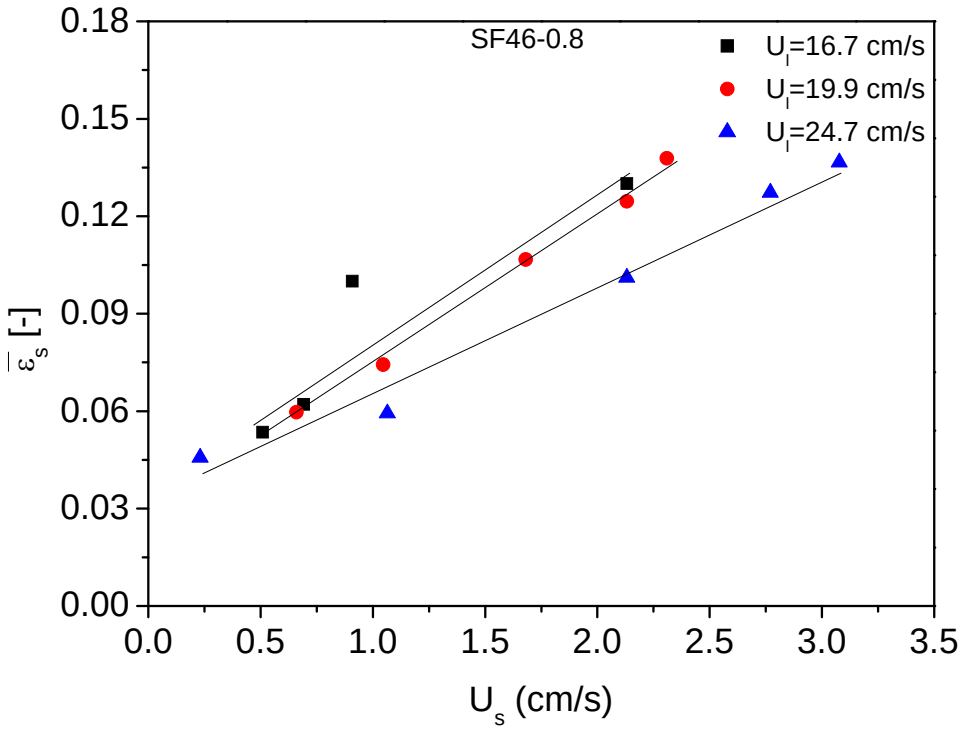

(a)

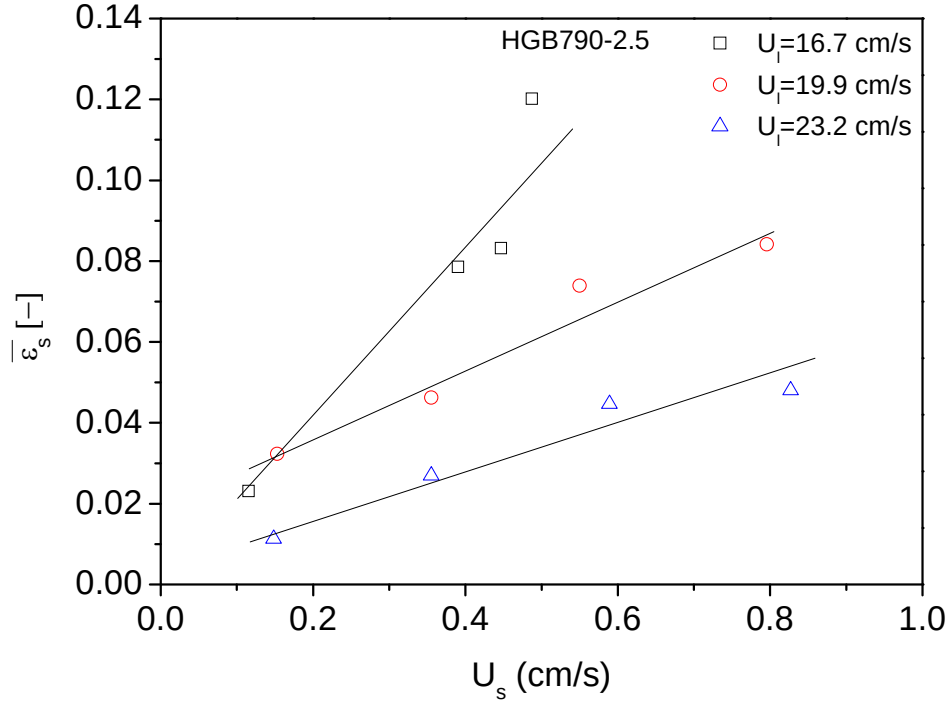

(b)

Fig. 7.5 The average solids holdups ($\bar{\varepsilon}_s$) against the superficial solids velocity (U_s) under various superficial liquid velocities (U_l) for (a) SF46-0.8 and (b) HGB790-2.5.

7.4.2 Axial solids holdup distribution

The average solids holdup distributions along the height of the downer below the main liquid distributor are shown in Fig. 7.6 and Fig. 7.7 for the 2 types of particles under various operating conditions. It can be noted that there is a similar flow structure along the height of ILSCFB, indicating a rather uniform axial flow under high superficial liquid velocity. However, under lower superficial liquid velocity, for example, U_l=14.94 cm/s, the average solids holdup distribution has less uniformity. Similar observations were also reported in other studies (Liang et al. 1997; Zheng 1999; Zheng et al. 2002) in the upwards LSCFB systems. The minor non-uniformity is attributed to the acceleration distance of the particles from nearly zero velocity upon entering the downer to the "normal" particle velocity by the down flowing liquid. Lower liquid velocity leads to longer acceleration distance because less energy is provided for particle acceleration, and therefore less uniformity of solids holdup distribution. However, such non-uniformity in both ILSCFB and LSCFB is not as large as that in the gas-solid circulating fluidized bed because of smaller density differences between the particles and the fluidization media.

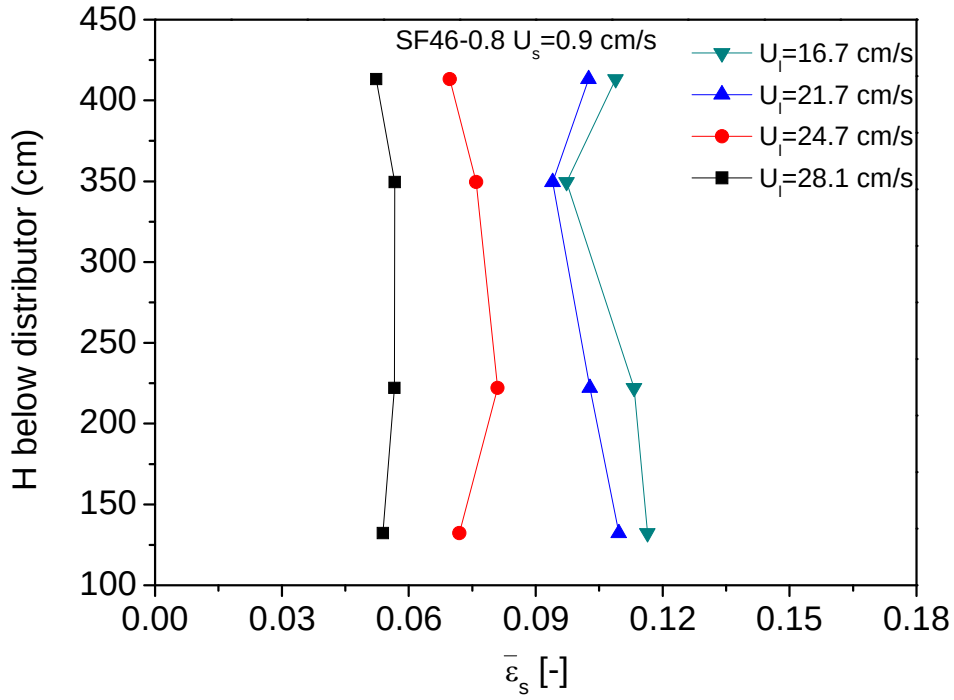

(a)

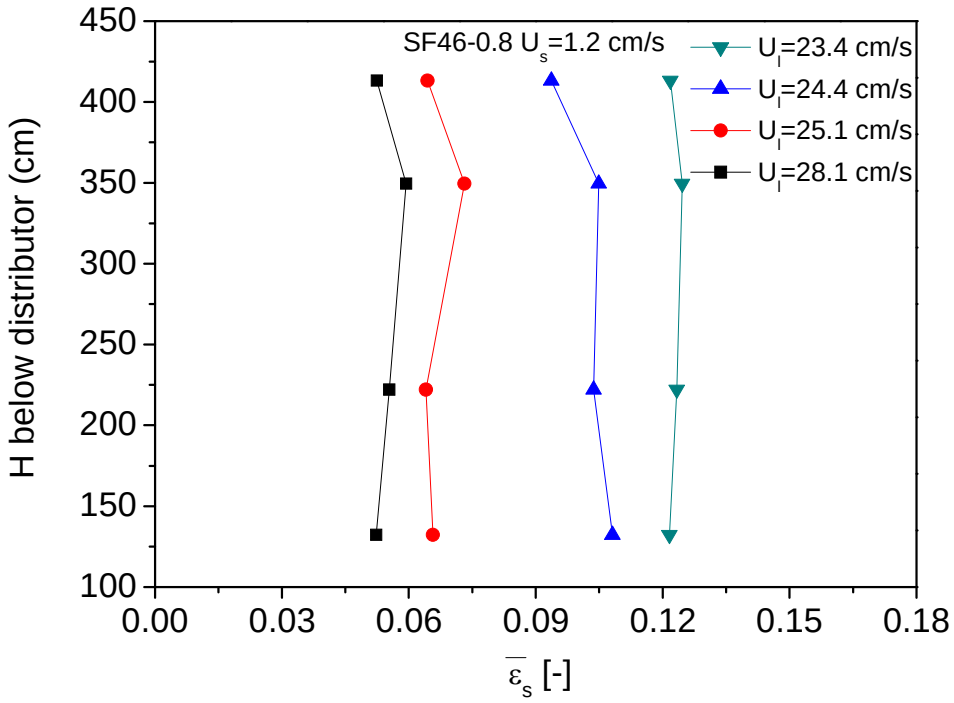

(b)

Fig. 7.6 The variations of the axial solids holdup for the SF46-0.8 under various superficial liquid velocity when (a) U_s=0.9 cm/s and (b) U_s =1.2 cm/s.

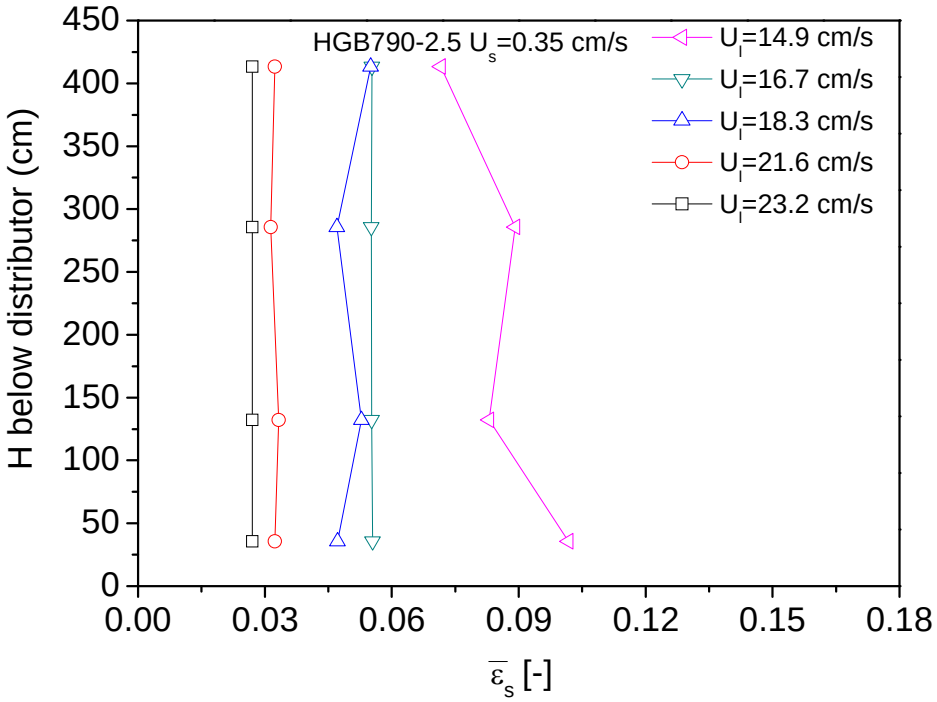

(a)

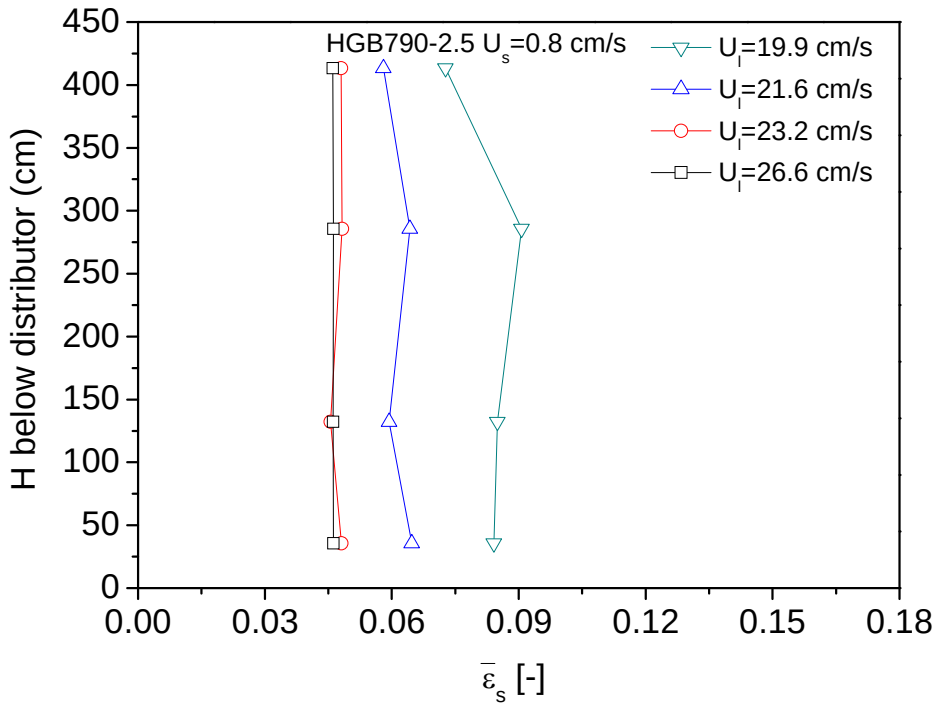

(b)

Fig. 7.7 The variations of the axial solids holdup for the HGB790-2.5 under various superficial liquid velocity when (a) U_s=0.35 cm/s and (b) U_s =0.8 cm/s.

7.4.3 Radial solids holdup distribution

The corresponding local solids holdup profiles along the radial direction at a typical location in the fully developed region (H=2.86 m) is plotted in Fig. 7.8 under various superficial liquid velocity (U_l) when U_s=0.9 cm/s and 1.2 cm/s respectively. It can be seen that the radial distribution of solids holdup is quite uniform across the downer and only with slight increasing near the wall under each superficial liquid velocity (U_l), indicating that there is no obvious “core-annulus” flow structure in ILSCFB. Such uniformity is closely related to the wall effects and the local liquid velocity (V_l) profile. As shown in Fig. 7.9, the local liquid velocity is almost the same through the radial direction, only with slight decreasing adjacent to the wall, leading to slight increase in local solids holdup at the corresponding radial position when U_s =0.9 cm/s under different superficial liquid velocity (U_l). A detailed explanation will be provided in the later section.

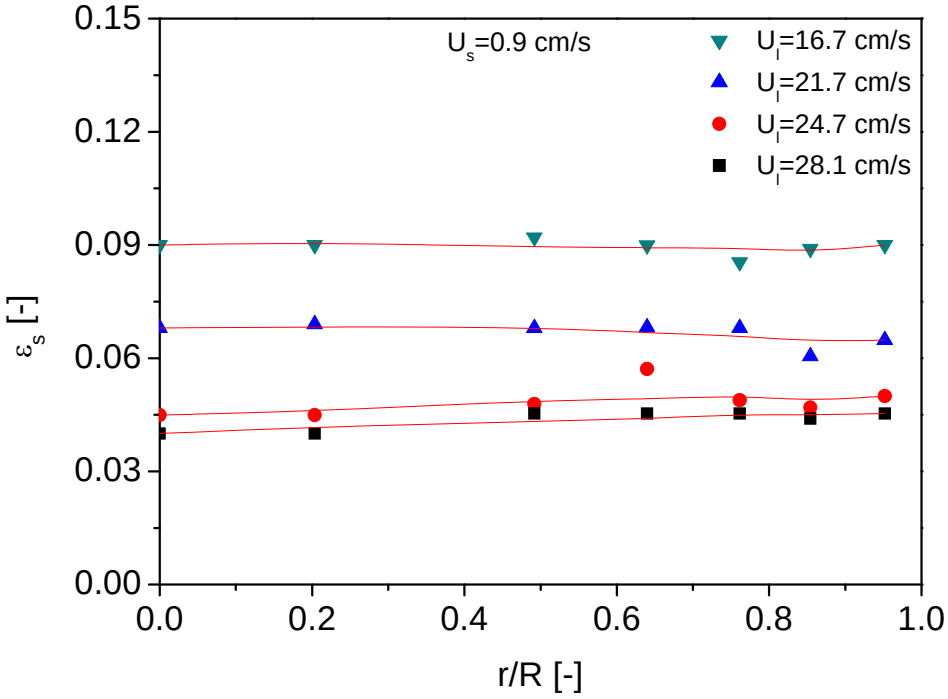

(a)

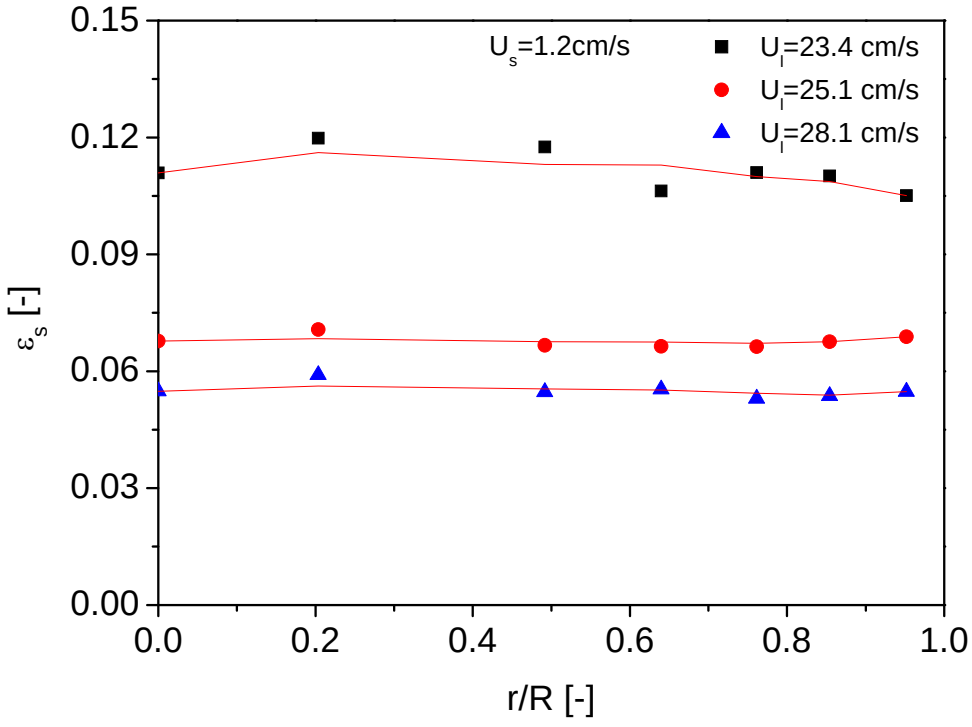

(b)

Fig. 7.8 Local solids holdup distribution radial positions under various superficial liquid velocity (U_l) when (a) U_s=0.9 cm/s and (b) U_s=1.2 cm/s.

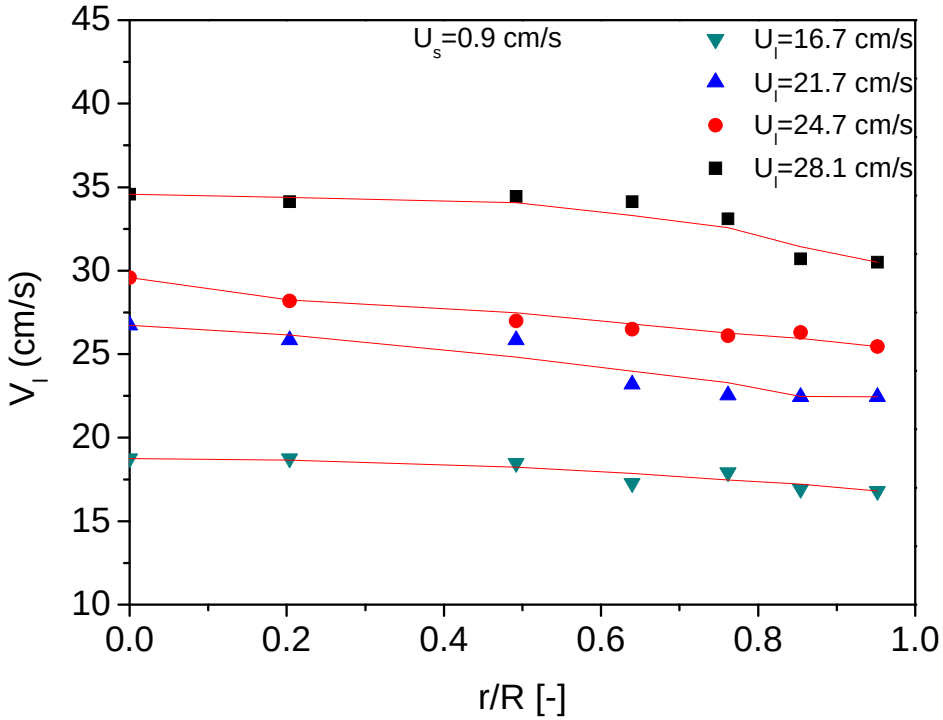

Fig. 7.9 Local liquid velocity distribution at different dimensionless radial positions under various superficial liquid velocity (U_l) when U_s=0.9 cm/s.

7.5 Comparisons of ILSCFB and LSCFB

7.5.1 Average solids holdup

In the upwards fluidization system where the density of particles is higher than that of the surrounding liquid, the forces acting on each particle include gravity (F_g), drag (F_d), buoyancy (F_b) and the random inter-particle forces which are minor compared with those three forces. Therefore, in the case of a single particle in an infinite expansion state ($\varepsilon = 1$), the force balance can be expressed as:

$$F_g = F_d + F_b \tag{7.1}$$

For spherical particles, Eq. (7.1) is expressed as:

$$\frac{1}{6}\pi d_p^3 \rho_p g = \frac{1}{2} C_D \rho_l v^2 \frac{1}{4}\pi d_p^2 + \frac{1}{6}\pi d_p^3 \rho_l g \tag{7.2}$$

Rearranging Eq. (7.2),

$$\frac{1}{2}C_D\rho_l v^2\frac{1}{4}\pi d_p^2=\frac{1}{6}\pi d_p^3 g\left(\rho_p-\rho_l\right) \tag{7.3}$$

While in the downwards fluidization system when the density of particles is lower than that of the surrounding liquid, under the conventional fluidization regime, the nature of the forces acting on the free rising spheres are the same as those acting on the free settling spheres with the only difference being the direction of the net force (upwards in the first case and downwards in the second case). Then for the downward fluidization,

$$F_b=F_g+F_d \tag{7.4}$$

Rearranging Eq. (7.4),

$$\frac{1}{2}C_D\rho_l v^2\frac{1}{4}\pi d_p^2=\frac{1}{6}\pi d_p^3 g\left(\rho_l-\rho_p\right) \tag{7.5}$$

Therefore, one can expect that for both upwards and downward fluidization system, the same expressions of force balance should apply:

$$\frac{1}{2}C_D\rho_l v^2\frac{1}{4}\pi d_p^2=\frac{1}{6}\pi d_p^3 g\Delta\rho \tag{7.6}$$

where $\Delta\rho=\rho_p-\rho_l$ for upwards fluidization and $\Delta\rho=\rho_l-\rho_p$ for downwards fluidization.

From the above discussion, due to the similarity in the force balance in the upwards and downwards circulating fluidization systems, it can be concluded that the mathematical expressions based on the force balance valid in the upwards circulating fluidization system should also be valid in the downwards counterpart. Sang and Zhu (Chapter 5) proposed a model to predict average solids holdups for the upwards circulating fluidization shown as:

$$\bar{\varepsilon}_s = \frac{U_s}{\frac{U_l}{1-\bar{\varepsilon}_s} - 1.2U_t(1-\bar{\varepsilon}_s)^{n-1}} \tag{7.7}$$

Then the predicted average solids holdup by Eq. (7.7) are compared with the downwards fluidization experimental results in this work as shown in Fig. 7.10. It can be noted there is a good correlation between the predicted average solids holdup by Eq. (7.7) and the experimental results for both types of particles.

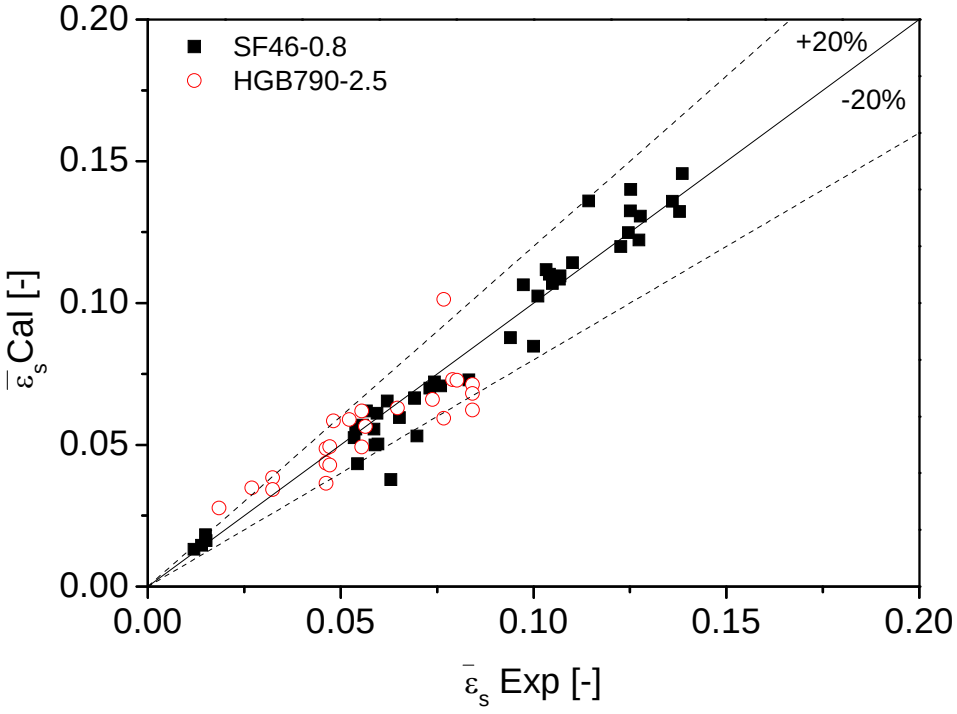

Fig. 7.10 Comparisons of the predicted average solids holdup from Eq. (7.7) valid for LSCFB with the experimental data in ILSCFB.

7.5.2 Local solids holdup

As shown in Section 7.3 and Fig. 7.11, there is no obvious “core-annulus” structure observed in ILSCFB, compared with its counterpart in LSCFB. Thus the radial solids holdup distribution is more uniform in ILSCFB than that in LSCFB. Such phenomenon is attributed to the wall friction effect expressed as (Rose and Duckworth 1969):

$$F_{friction} = \frac{1}{2} f_{sa} \rho_p \varepsilon_s V_l^2 \tag{7.8}$$

where f_{sa} is friction factor between particles and wall.

It is shown that the friction is quite dependent on the particle density. Then the detailed comparisons are presented in Fig. 7.11. It can be seen that the radial distribution of solids holdup for the SF46-0.8 particles are more uniform than PB1520-1.19 and GB2490-0.51 particles, because the density of SF46-0.8 is much lower than those of PB1520-1.19 and GB2490-0.51 particles, so as to smaller wall friction effects. Therefore, there is no obvious increase in solids holdup adjacent to the wall in the ILSCFB compared with the LSCFB.

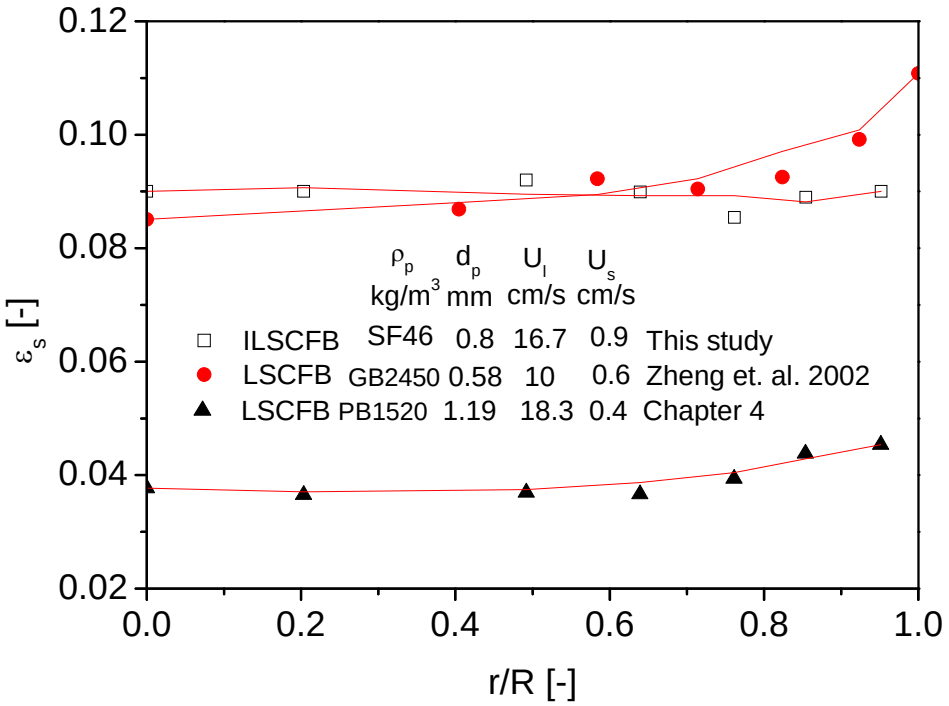

Fig. 7.11 Comparisons of local solids holdup in ILSCFB and LSCFB.

7.6 Generalized flow regime map

It is logical to presume that the flow regimes in the inverse fluidization system are quite similar to those of the upwards fluidization systems. Based on the flow regime map in the

upwards fluidization (Liang et. al., 1997; Zhu et. al., 2000; Chapter 5), there are fixed bed regime, conventional fluidization regime, circulating fluidization regime and transport regime. The fixed bed flow regime and the conventional fluidization regime are demarcated by the minimum fluidization velocity (U_{mf}), while the conventional fluidization regime and the circulating fluidization regime are demarcated by the particle terminal velocity (U_t); the transition velocity (U_{cv}) demarcates the circulating fluidization regime and the transport regime. The generalized flow regime map is proposed in terms of dimensionless superficial velocity and dimensionless particle size which are defined as $U_l^* = U_l \left[\rho_l^2 / (\mu g \Delta\rho) \right]^{1/3} = Re / Ar^{1/3}$ and $d_p^* = d_p \left(\rho_s g \Delta\rho / \mu^2 \right)^{1/3} = Ar^{1/3}$ (Grace 1986) respectively (shown in Fig. 7.12).

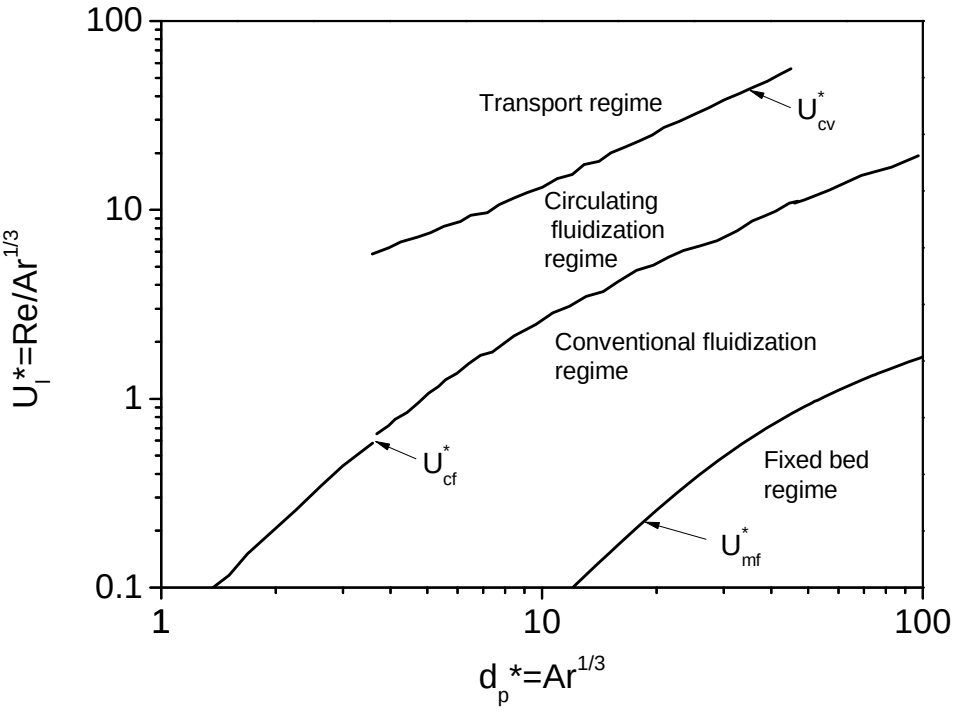

Fig. 7.12 Generalized flow regime map for both inverse and upwards fluidization systems.

In order to quantitatively determine the flow regime and its corresponding flow conditions, the mathematical correlations for each critical velocity (U_{mf}, U_t and U_{cv}) are compared and reviewed in the following parts.

7.6.1 Determination of U_{mf}

The Wen and Yu correlation (Wen and Yu 1966) is discussed to determine the inverse U_{lmf}*.

$$Re_{mf} = \sqrt{33.7^2 + 0.0408Ar} - 33.7 \tag{7.9}$$

Limited by

$$Re_{mf} = \frac{Ar}{1650} \qquad when\ Re_{mf} < 20$$

$$Re_{mf} = \frac{Ar^{0.5}}{4.95} \qquad when\ Re_{mf} > 100$$

By dividing $Ar^{1/3}$ on both side of Eq. (7.9), the following equation can be obtained in terms of U_l^* vs. d_p^* as defined previously:

$$U_{lmf}^* = \sqrt{\left(\frac{33.7}{Ar^{1/3}}\right)^2 + 0.0408Ar^{1/3}} - \frac{33.7}{Ar^{1/3}} \tag{7.10}$$

$$U_{lmf}^* = \frac{\left(Ar^{1/3}\right)^2}{1650} \qquad when\ Re_{mf} < 20$$

$$U_{lmf}^* = \frac{\left(Ar^{1/3}\right)^{0.5}}{4.95} \qquad when\ Re_{mf} > 100$$

7.6.2 Determination of U_t

For a free falling particle, its terminal velocity U_t could be calculated as (Denn 1980):

$$U_t = \sqrt{\frac{4\left(\rho_p - \rho_l\right)gd}{3\rho_l C_D}} \tag{7.11}$$

where the drag coefficient C_D is determined from (Karamanev 1996).

$$C_D = \frac{432}{Ar}(1+0.0470Ar^{\frac{2}{3}}) + \frac{0.517}{1+154Ar^{-\frac{1}{3}}} \tag{7.12}$$

The dimensionless form of Eq. (7.11) is then expressed as:

$$U_{lt}^{*} = \left(\frac{4Ar}{3C_D}\right)^{1/2} = \left(\frac{324}{Ar^2}(1+0.0470Ar^{2/3}) + \frac{0.38775}{Ar+154Ar^{2/3}}\right)^{-1/2} \tag{7.13}$$

7.6.3 Prediction of U_{cv}

Sang and Zhu (Chapter 5) proposed that when solids holdup is below 1%, the flow regime is considered as the transport regime, so that based on their developed average solids holdup model, the critical velocity demarcating the circulating fluidization regime and the transport regime can be obtained by the following equation:

$$U_{cv} = \frac{U_s}{\bar{\varepsilon}_s} + 1.2U_t(1-\bar{\varepsilon}_s)^{n-1} = 100U_s + 1.2U_t \tag{7.14}$$

7.7 Conclusions

The hydrodynamic characteristics in the downer of an Inverse Liquid-Solid Circulating Fluidized Bed (ILSCFB) were investigated experimentally by the fluidization of Styrofoam and Hollow Glassbeads both with densities lower than that of the fluidization media. For both types of particles, axial solids holdup distribution is quite uniform under various operating conditions, while radial solids holdup distributions are somewhat non-uniform with a slight increase in solids holdup adjacent to the wall but not significant enough to be considered as an obvious “core-annulus” structure. Such solids holdup distribution pattern is closely related to the wall effects.

The comparisons of the hydrodynamics in ILSCFB and LSCFB show that the mathematical models based on the force balance valid in the upwards circulating fluidization system is also valid in the downwards counterpart.

The generalized flow regime map for both the inverse and upwards fluidization systems are proposed in terms of dimensionless superficial velocity and dimensionless particle size. With increasing superficial liquid velocity, there are fixed bed regime, conventional fluidization regime, circulating fluidization regime and transport regime. The demarcations of the different flow regimes are also quantitatively determined from the minimum fluidization velocity, particle terminal velocity and transition velocity.

Nomenclature

Ar	Archimedes number defined by $d^3 g(\rho_p - \rho_l)\rho_l / \mu^2$
a	Slip velocity coefficient U_{slip} / U_t
C_D	Particle drag coefficient
d_p	Particle diameter (mm)
d_p^*	Dimensionless particle size defined by $Ar^{1/3}$
D	Column diameter (m)
F_b, F_d, F_g	Buoyancy force, drag force and gravity
G_s	Solids circulation rate (kg/(m^{2}s))
g	Gravity acceleration
H	Bed height
n	Richardson and Zaki index
N_D	Best number
P	Pressure (Pa)
Q	Volumetric flowrate (m^3 / s)
Re	Reynolds number defined by $Ud\rho_l / \mu$
Re_t	Particle terminal Reynolds number defined by $U_t d\rho_l / \mu$
t	Residence time (s)
U_a	Auxiliary liquid velocity (cm/s)
U_{cr}	Transition velocity from particulate fluidization regime to circulating fluidization regime (cm/s)
U_{cv}	Transition velocity from circulating fluidization regime to transport regime (cm/s)
U_l	Total superficial liquid velocity (cm/s)
U_i	Extrapolated value of U as ε approaches 1
U_l^*	Dimensionless superficial velocity defined by $Re / Ar^{1/3}$
U_s	Superficial particle velocity (cm/s)

U_{slip}	Slip velocity (cm/s)
U_t	Particle terminal velocity (cm/s)
U_t^*	Dimensionless transition velocity defined by Re_t / $Ar^{1/3}$
V_l, V_p	Local liquid velocity and local particle velocity
$\overline{V}_l, \overline{V}_p$	Average liquid velocity and average particle velocity

Greek letters

$\overline{\varepsilon}$	Average bed voidage
$\overline{\varepsilon}_s$	Average solids holdup
ϕ	Particle sphericity
μ_l	Liquid viscosity (mPas)
ρ_p	Particle density (kg/m^3)
ΔP	Pressure drop

Subscripts

l	Liquid
p	Particle
s	Solids

References

Chavarie, C. and D. Karamanev (1986). Use of inverse fluidization in biofilm reactors. Int. Syrup. on Bioreactor Fluid Dynamics. Cambridge, England**:** 181-190.

Cho, Y. J., H. Y. Park, S. W. Kim, Y. Kang and S. D. Kim (2002). Heat transfer and hydrodynamics in two- and three-phase inverse fluidized beds. Industrial and Engineering Chemistry Research 41(8): 2058-2063.

Denn, M. M. (1980). Process fluid mechanics. N.J., Englewood Cliffs.

Dewsbury, K. H., D. G. Karamanev and A. Margaritis (2000). Dynamic behavior of freely rising buoyant solid spheres in non-newtonian liquids. AIChE Journal 46(1): 46-51.

Escudie, R., N. Epstein, J. R. Grace and H. T. Bi (2007). Layer inversion and bed contraction in down-flow binary-solid liquid-fluidized beds. Canadian Journal of Chemical Engineering 85(1): 25-35.

Grace, J. R. (1986). Contacting modes and behaviour classification of gas-solid and other two-phase suspensions. The Canadian Journal of Chemical Engineering 64(3): 353-363.

Howley, M. A. and B. J. Glasser (2004). A comparison of one-dimensional traveling waves in inverse and normal fluidized beds, Austin, TX, United states, American Institute of Chemical Engineers.

Karamanev, D. G. (1996). Equations for calculation of the terminal velocity and drag coefficient of solid spheres and gas bubbles. Chemical Engineering Communications 147: 75-84.

Karamanev, D. G. and L. N. Nikolov (1992). Bed Expansion of Liquid-Solid Inverse Fluidization. Aiche Journal 38(12): 1916-1922.

Liang, W., S. Zhang, J.-X. Zhu, Y. Jin, Z. Yu and Z. Wang (1997). Flow characteristics of the liquid-solid circulating fluidized bed. Powder Technology 90(2): 95-102.

Lu, P., Y. Cao, A. Wu and W.-P. Pan (2006). Experimental study of heat transfer in a horizontal swirling fluidized bed, Pittsburgh, PA, United states, International Pittsburgh Coal Conference.

Nikolov, V. R. and I. Nikov (1994). Liquid-solid mass transfer in three-phase inverse fluidized bed (TPIFB). Hungarian Journal of Industrial Chemistry 22(2): 125-128.

Renganathan, T. and K. Krishnaiah (2003). Prediction of minimum fluidization velocity in two and three phase inverse fluidized beds. Canadian Journal of Chemical Engineering 81(3-4): 853-860.

Renganathan, T. and K. Krishnaiah (2005). Voidage characteristics and prediction of bed expansion in liquid-solid inverse fluidized bed. Chemical Engineering Science 60(10): 2545-2555.

Rose, R. H. and R. A. Duckworth (1969). Transport of solid particles in liquids and gases. The Engineer 227: 392-396, 430-433,478-483.

Sang, L. and J. Zhu (2012). Experimental investigation of the effects of particle properties on solids holdup in an LSCFB riser. Chemical Engineering Journal 197: 322-329 (Chapter Four of this thesis).

Ulaganathan, N. and K. Krishnaiah (1996). Hydrodynamic characteristics of two-phase inverse fluidized bed. Bioprocess and Biosystems Engineering 15(3): 159-164.

Vijaya, L. A. C., M. Balamurugan, M. Sivakumar, S. T. Newton and M. Velan (2000). Minimum fluidization velocity and friction factor in a liquid-solid inverse fluidized bed reactor. Bioprocess and Biosystems Engineering 22(5): 461-466.

Wen, C. Y. and Y. H. Yu (1966). Mechanics of Fluidization. Chem. Eng. Prog.
.

Zhang, H., P. M. Johnston, J. X. Zhu, H. I. de Lasa and M. A. Bergougnou (1998). A novel calibration procedure for a fiber optic solids concentration probe. Powder Technology 100(2-3): 260-272.

Zheng, Y. (1999). Flow Structure in a Liquid Solid Circulating Fluidized Bed. Chemical and Biochemical Engineering. London, University of Western Ontario. Ph.D.

Zheng, Y., J.-X. Zhu, N. S. Marwaha and A. S. Bassi (2002). Radial solids flow structure in a liquid-solids circulating fluidized bed. Chemical Engineering Journal 88(1-3): 141-150.

Zheng, Y., J.-X. Zhu, J. Wen, S. A. Martin, A. S. Bassi and A. Margaritis (1999). The axial hydrodynamic behavior in a liquid-solid circulating fluidized bed. Canadian Journal of Chemical Engineering 77(Compendex): 284-290.

Chapter 8

8 Local Particle and Liquid Velocities in Inverse Liquid-Solid Circulating Fluidized Bed Downer

8.1 Introduction

The characteristics and the applications of the Liquid-Solid Circulating Fluidized Beds (LSCFBs), where the solids are fluidized upwards, have been intensively investigated in many previous studies in the Particle Technology Research Center (PTRC) at Western University (Liang et al. 1997; Zheng et al. 1999; Zhu et al. 2000; Zheng et al. 2002) and others (Natarajan et al. 2009). However, when the density of the solids lower than that of the surrounding liquid, the downwards circulating fluidization is necessary, referred to as the inverse circulating fluidization (Chapter 7). Although inverse circulating fluidization is novel, the advantages of inverse conventional fluidization has been studied due to its in the past, including the efficient control of the bioprocess (Nikolov and Karamanev 1987; Karamanev and Nikolov 1996) and of biofilm thickness (Karamanev and Nikolov 1992), higher rate of mass transfer (Nikolov and Nikov 1994), and possibility for re-fluidization (Renganathan and Krishnaiah 2003). Combing the benefits of inverse fluidization and the concept of circulating fluidization, Sang and Zhu (Chapter 7) proposed a novel Inverse Liquid-Solid Circulating Fluidized Bed (ILSCFB), which enables continuous solids circulation, and conducted intensive research on local and average solids holdup distributions under the circulating fluidization regime. In order to reveal the fluidization mechanisms in ILSCFB systems, local liquid, particle and slip velocities should also be investigated systematically. Unfortunately, no such study has been carried out in the ILSCFB systems. Only few researchers from our group (Liang et al. 1996; Zheng 1999) reported the measurement of the local liquid velocity in LSCFB and neither of them measured the particle velocity.

In this paper, the local liquid and particle velocities are measured in a pilot scale ILSCFB downer by utilizing conductivity probe and optical fiber probe respectively. The slip velocity derived from the liquid and particle velocities is then determined.

8.2 Materials and methods

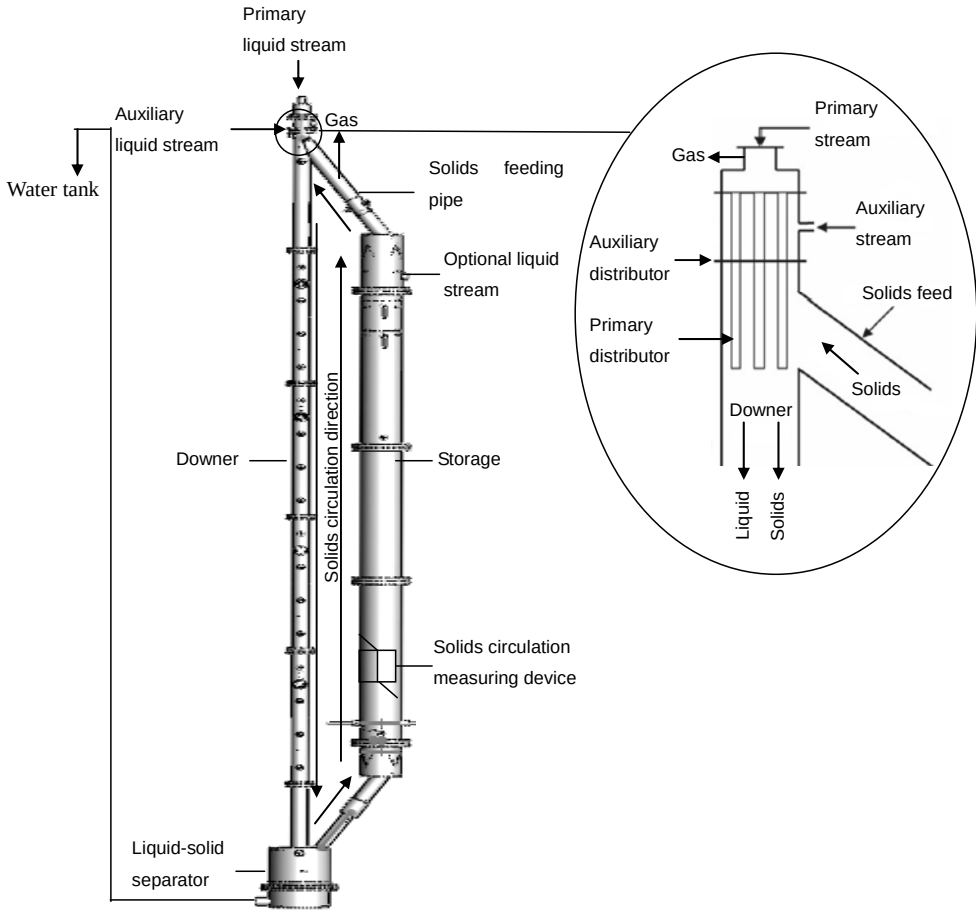

Fig. 8.1 The schematic diagram of ILSCFB apparatus.

The set-up of ILSCFB system is shown schematically in Fig. 8.1. The system mainly consists of a 0.076 m ID Plexiglas downer column, where the inverse fluidization takes place, a liquid–solid separator, storage column and a device for measuring the solids circulation rate at the bottom of storage. This downer is connected to the 0.2 m ID Plexiglas storage column through a solids returning pipe at the bottom and a solids feeding pipe at the top. There are two distributors: the main liquid distributor made of seven stainless steel tubes occupying 19.5% of the total downer cross-sectional area and extending 0.2 m down to the downer, and the auxiliary liquid distributor made of a porous plate with 4.8% opening area at the top of the downer. With this configuration, particles introduced into the downer top are carried downwards to the bottom of the

downer by the combined liquid flow (the primary liquid flow plus the auxiliary liquid flow) and separated by the cylindrical liquid–solid separator at the bottom. Liquid is then returned to the liquid reservoir for reuse while the particles are returned to the storage after passing through the solids circulation rate measuring device and re-introduced into the downer top via the solid feeding pipe to re-fluidize. Therefore, the light particles are continuously circulating inside ILSCFB system.

The liquid and solids flow rates can be controlled independently by adjusting the primary and the auxiliary liquid flow rates as shown in Fig. 8.2. At different auxiliary liquid velocities (U_a), superficial solids velocity (U_s) initially increases with combined superficial liquid velocity (U_l). Beyond the initial stage, the solids circulation is more controlled by the auxiliary liquid velocity (U_a), so that the superficial solids velocity (U_s) is constant for each auxiliary liquid velocity (U_a) though the combined superficial liquid velocity (U_l) keeps increasing and the solids circulation is considered to be fully developed. On the other hand, at this stage, the superficial solids velocity (U_s) increases with the auxiliary liquid velocity (U_a) for a fixed superficial liquid velocity (U_l) since more particles are introduced into the downer with higher auxiliary liquid velocity (U_a).

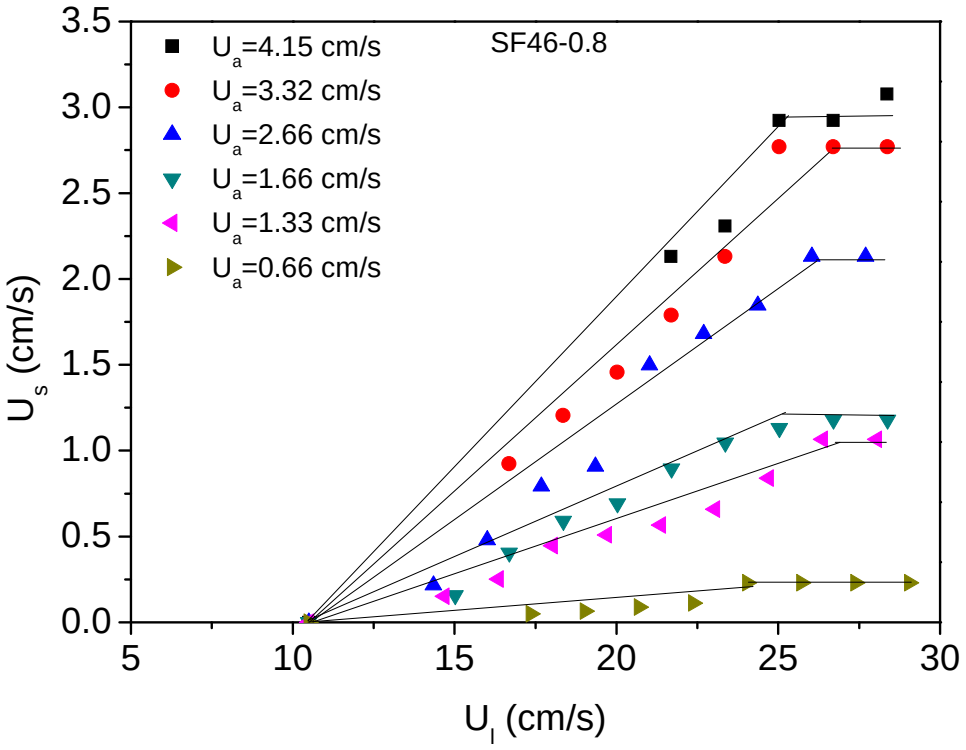

Fig. 8.2 The superficial solids velocity (U_s) as a function of combined superficial liquid velocity (U_l) and the auxiliary liquid velocity (U_a).

The local solids holdup and particle velocity is measured by using an optical fiber probe model PV-6, produced by the Institute of Process Engineering, Chinese Academy of Sciences. For details of this probe, please refer to some earlier research papers from PTRC (Zhang et al. 1998; Zheng et al. 2002). The calibration of this probe for the liquid–solid systems could be carried out on site. With the fluidized bed being operated in the conventional fluidization regime, where the solids holdup is considered homogeneous in both the axial and the radial direction, the output voltage signal from the probe is calibrated against the solids holdup data obtained from pressure gradient measurements. Such calibration is always conducted in the middle section of the fluidized bed so that the "end effect" is eliminated. A linear relationship was found between the voltage signal and the solids holdup for each type of the particles. A cross-correlation between two light receiving channels must be applied to obtain the particle velocity (Horio et al. 1988).

The local liquid velocity was measured with a pulse injection of saturated NaCl and carbon black electrolyte solution at the upstream of two bronze conductivity probes connecting to a conductivity meter. Given the very small volume of the injection (about 0.5 ml), the effects of injection on the flow structure can be neglected. The distance between the injection point and the upper conductivity probe is 25 cm. When the electrolyte solution is just injected into the downer, there is no signal change indicated by the conductivity meter. Then when the electrolyte solution travels to downstream and reaches the point of conductivity probe, the signal indicated by the conductivity meter starts to change. The traveling of the electrolyte solution can also be observed from the traveling of the carbon black. By recording the time interval of the signal change and knowing the distance from the injection point to the conductivity probe, the local liquid velocity at various locations in the bed can be obtained. The injection was traversed in the radial direction to obtain the radial distribution of liquid velocity. All the radial distributions of liquid velocity reported in this study were at the axial position of 4 m below the main distributor, which is in the fully developed flow region.

All experiments were carried out at ambient temperature. Tap water was used as the fluidizing liquid and the Styrofoam, whose density and size are 46 kg/m^3 and 0.8 mm respectively, is employed as the circulating particles in this study. Particle density was measured by determining the volume and mass: place the particles with known weight (m_p) into a cylinder with scale and add a certain amount of water (with known weight m_w); push a plug that fits snugly into the cylinder with known volumes (V_{plug}) into the measuring cylinder to prevent particles from floating to the surface; then tap the measuring vessel to remove any air bubbles; after reading off the total volume (V), the particle density can be calculated as $\rho_p = m_p / \left(V - (V_{plug} + m_w / \rho_w)\right)$.

In each run, local solids holdup and particle velocity were measured at different radial positions but given axial position by traversing the probe horizontally, after ILSCFB unit was brought to a steady operation. In initial measurements, the probe was traversed from one wall to the other and no significant asymmetry was found in the radial holdup profile. Therefore, measurements were taken only at one side of the downer, at seven radial

locations between the center and the wall (r/R =0, 0.2034, 0.492, 0.6396, 0.7615, 0.8641, 0.9518). At 4 different levels the same procedure was repeated for different solids circulation rates and liquid velocities. For each measurement location, the column section from about 0.3m above to 0.3m below the probe was wrapped with a black plastic sheet to prevent external light from penetrating into the downer and interfering with the measurements.

8.3 Solids holdup distribution in ILSCFB downer

The solids holdup distributions in the axial and radial directions are plotted in Fig. 8.3a and Fig. 8.3b respectively under various superficial liquid velocities (U_l) when U_s=0.9 cm/s. It can be seen that the axial and radial local solids holdup (ε_s) decreases with increasing superficial liquid velocity (U_l) under same superficial solids velocity (U_s). Meanwhile, the axial solids distribution is quite uniform especially at higher superficial liquid velocity (U_l), while the radial distribution of solids holdup is uniform only slightly increasing near the wall under each superficial liquid velocity (U_l). More detailed results can be referred to in Chapter 7.

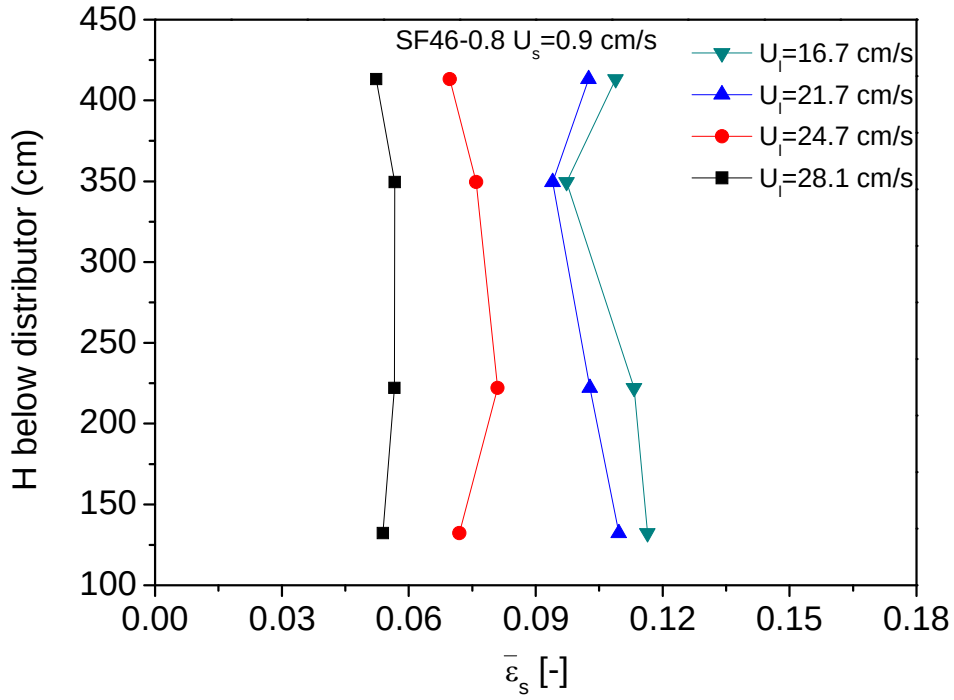

(a)

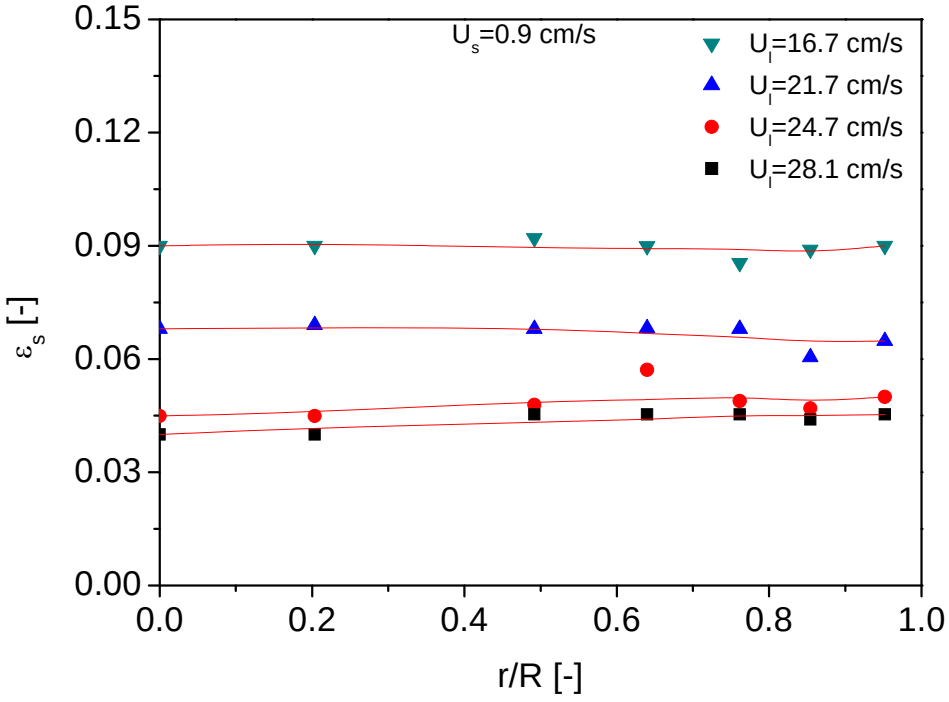

(b)

Fig. 8.3 Solids holdup distributions (a) axial and (b) radial when U_s=0.9 cm/s.

8.4 Axial and radial distributions of local particle velocity

The axial and radial distributions of local particle velocity (V_p) are shown in Fig. 8.4a and Fig. 8.4b respectively under various superficial liquid velocity (U_l) when U_s=0.9 cm/s. It has been shown that both the axial and the local particle velocity (V_p) increases with increasing superficial liquid velocity (U_l) but it is always lower than the superficial liquid velocity (U_l). In the axial direction, there is a similar flow structure along the height of ILSCFB downer, indicating a rather uniform axial flow under high superficial liquid velocity. However, under lower superficial liquid velocity, for example, U_l=16.7 cm/s, the average particle velocity distribution has less uniformity. The minor non-uniformity is attributed to the acceleration distance of the particles from nearly zero velocity upon entering the downer to the “normal” particle velocity by the down flowing liquid. Lower liquid velocity leads to longer acceleration distance because less energy is provided for particle acceleration. Such phenomenon also affects the axial solids holdup distribution as shown in Fig. 8.3a. In the radial direction, similar to the radial distribution of local liquid velocity (to be discussed in the next section) under the same operating conditions, the local particle velocity is higher at the central region and lower near the wall region. However, an increase in superficial solids velocity (U_s) leads to a slight increase of local particle velocity (V_p) at the central region and decrease near wall region as shown in Fig. 8.4c under the similar superficial liquid velocity (U_l).

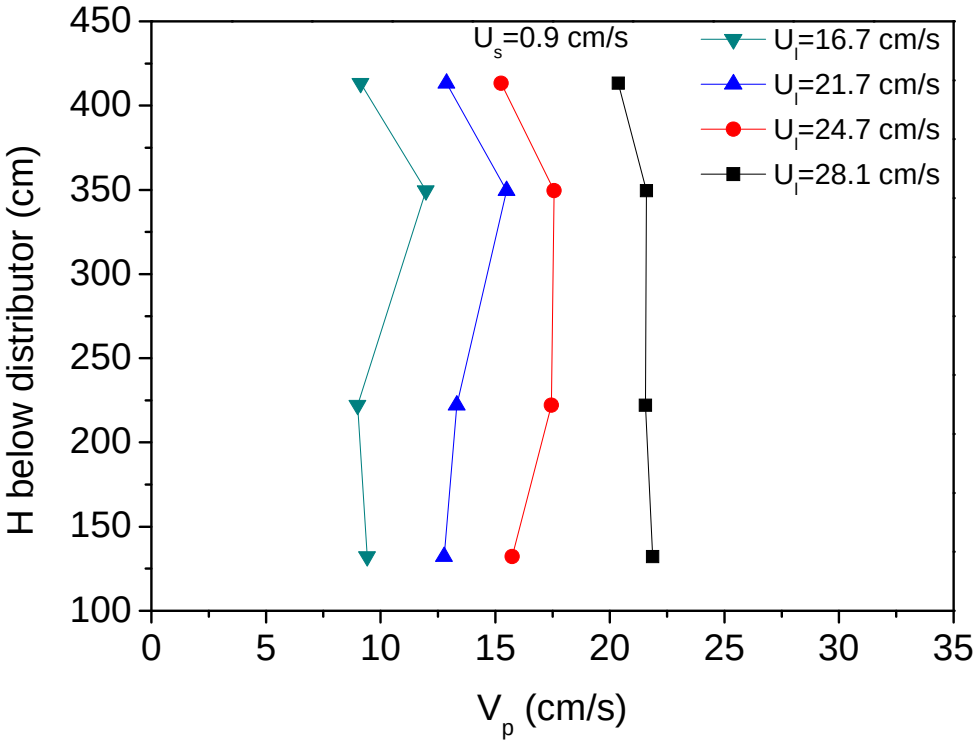
U_s=0.9 cm/s
U_l=16.7 cm/s
U_l=21.7 cm/s
U_l=24.7 cm/s
U_l=28.1 cm/s
H below distributor (cm)
V_p (cm/s)
450
400
350
300
250
200
150
100
0
5
10
15
20
25
30
35

(a)

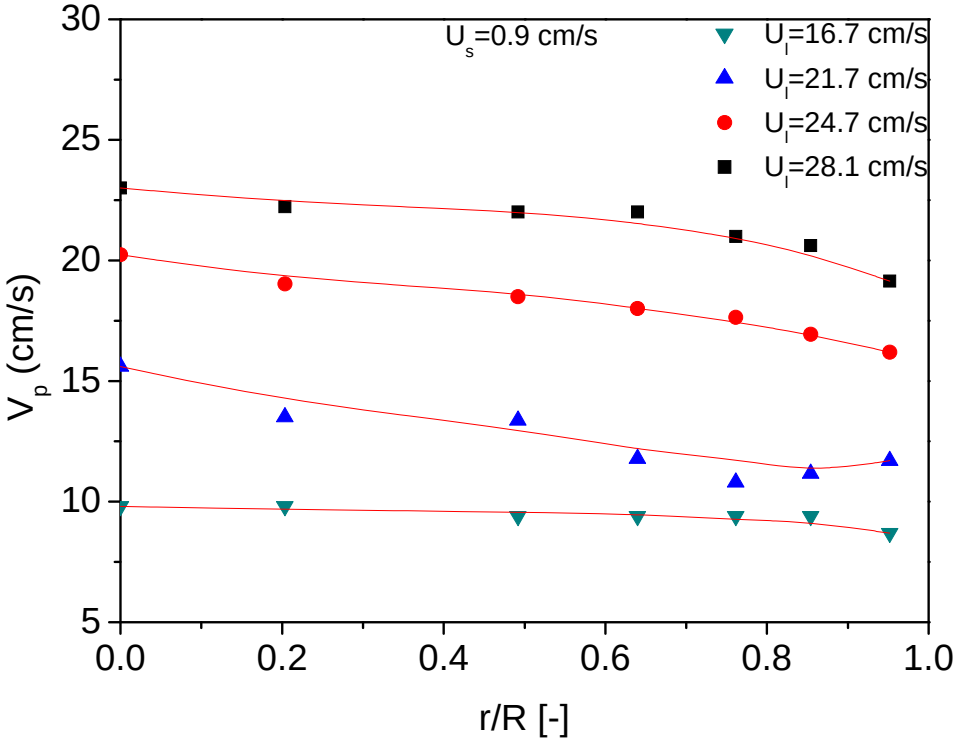
U_s=0.9 cm/s
U_l=16.7 cm/s
U_l=21.7 cm/s
U_l=24.7 cm/s
U_l=28.1 cm/s
V_p (cm/s)
r/R [-]
30
25
20
15
10
5
0.0
0.2
0.4
0.6
0.8
1.0

(b)

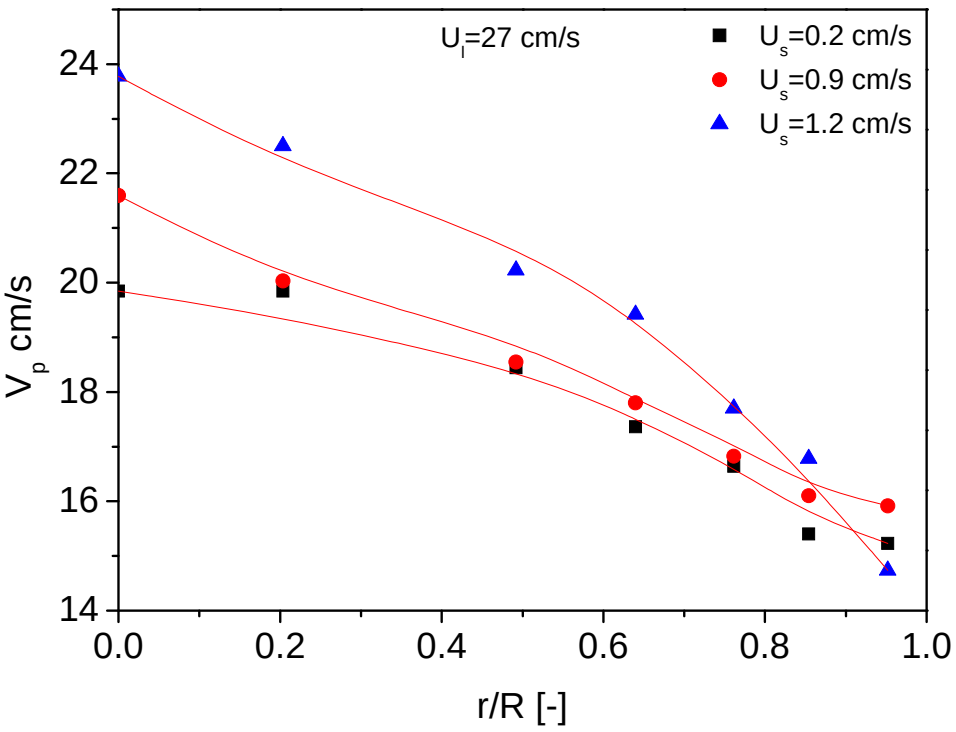

(c)

Fig. 8.4 Particle velocity distribution in (a) axial direction, (b) radial positions when U_s=0.9 cm/s, (c) radial positions when U_l=27 cm/s but various superficial solids velocities.

In order to show the effects of the superficial liquid velocity (U_l) and superficial solids velocity (U_s) on the particle velocity (V_p) explicitly, the average particle velocity ($\bar{V}_p$) is calculate from the local particle velocity (V_p) and local solids holdup based on the following equation:

$$\bar{V}_p = \frac{1}{\pi R^2 \bar{\varepsilon}_s} \int_0^R V_p(r)\varepsilon_s(r) 2\pi r dr \qquad (8.1)$$

where ε_s and $\bar{\varepsilon}_s$ are the local solids holdup and average solids holdup respectively.

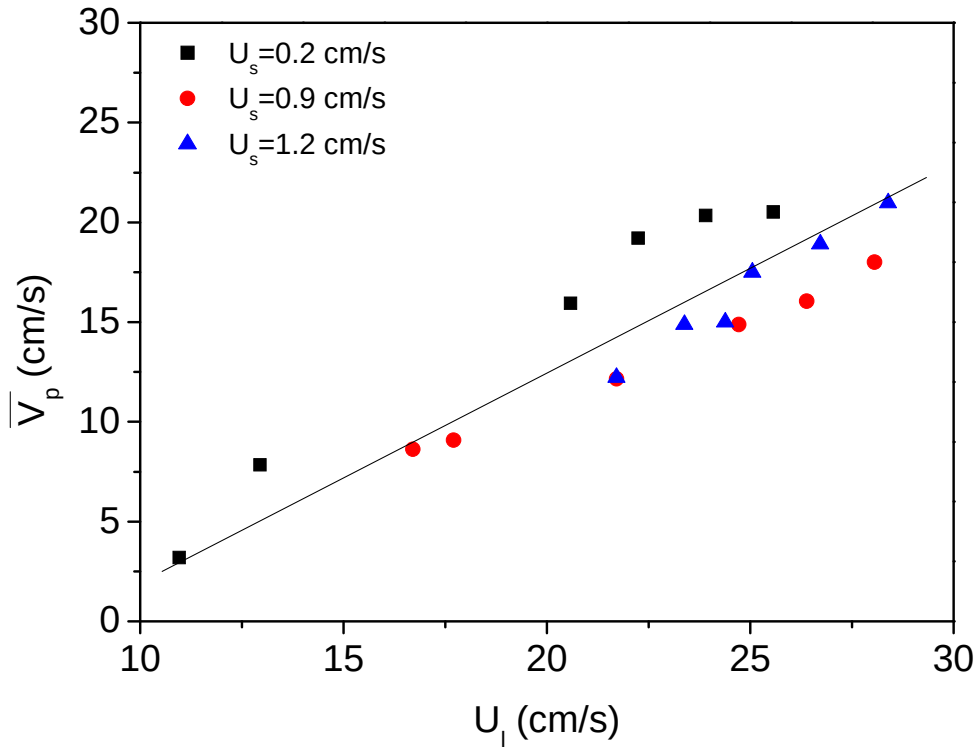

Fig. 8.5 Average particle velocity ($\overline{V}_p$) as a function of superficial liquid velocity (U_l) under different superficial solids velocity (U_s).

The calculated average particle velocity ($\overline{V}_p$) is plotted as a function of the superficial liquid velocity (U_l) shown in Fig. 8.5 under different superficial solids velocity (U_s). One can note that the average particle velocity ($\overline{V}_p$) increases with superficial liquid velocity (U_l) monotonously, however, the superficial solids velocity (U_s) has little effects on the average particle velocity ($\overline{V}_p$). Therefore, the particle velocity is more dominant by the liquid velocity (U_l) rather than superficial solids velocity (U_s). Similar results are also observed in the LSCFB (Chapter 4).

To validate the measurement of the local particle velocity (V_p), the superficial solids velocity (U_s) is also calculated by the following equation (Yang et al. 1993) from the local particle velocity (V_p) and local solids holdup (ε_s) and compared with that from the readings obtained by butterfly valve:

$$U_s = \frac{1}{\pi R^2}\int_0^R V_p(r)\varepsilon_s(r)2\pi r dr \qquad (8.2)$$

The comparisons plotted in Fig. 8.6 show good agreement between the calculated and measured superficial solids velocity (U_s), verifying the feasibility of the present measurement methods.

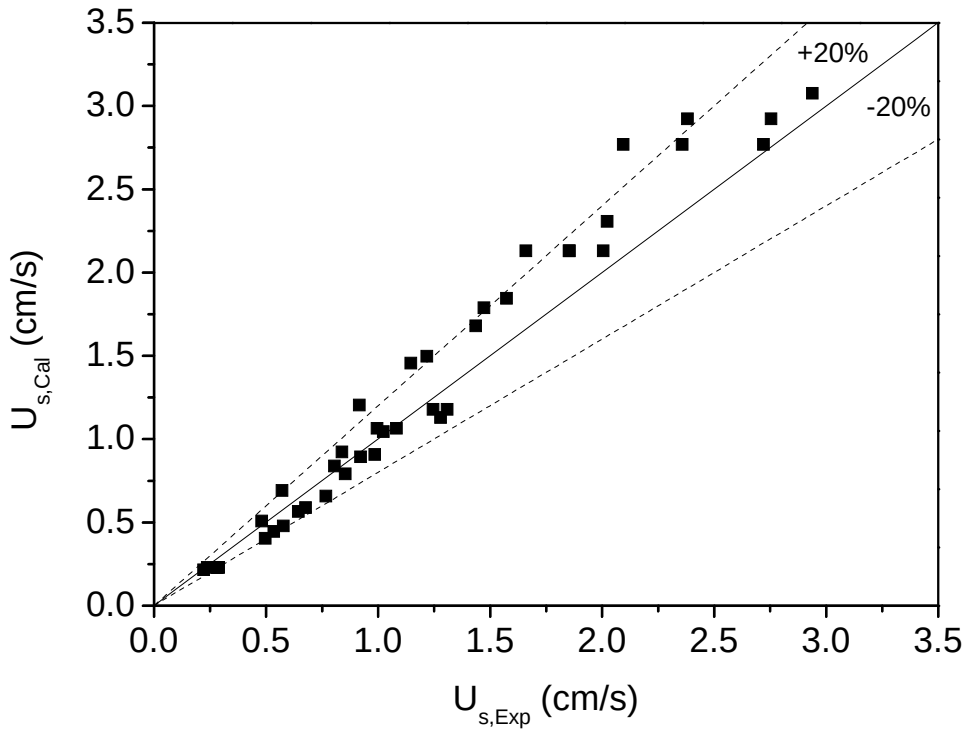

Fig. 8.6 Comparisons of measured and calculated superficial solids velocity based on local particle velocity.

8.5 Radial distribution of local liquid velocity

The radial distributions of liquid velocity (V_l) are shown in Fig. 8.7 under various superficial liquid velocity (U_l) and superficial solids velocity (U_s). It can be seen from Fig. 8.7a that, the radial distribution of local liquid velocity (V_l) is quite uniform from the center to the wall when there is no particle involved. By introducing the solids circulation at U_s=0.9 cm/s, under the circulating fluidization regime, the radial distribution of local liquid velocity (V_l) becomes slightly non-uniform with lower value adjacent to the wall.

Similar observation was also reported by Zheng (Zheng 1999) in LSCFB riser. However, the local liquid velocity distribution in ILSCFB is more uniform than that in LSCFB, because of the smaller wall friction exerted on lighter particles (Chapter 7). Besides, the local liquid velocity (V_l) at each position is almost equal to the superficial liquid velocity (U_l) when there is no particle involved as shown in Fig. 8.7a. Whereas, the local liquid velocity (V_l) at each position is larger than the superficial liquid velocity (U_l) when solids circulation is introduced as shown in Fig. 8.7b. This is reasonable because the calculation of the superficial liquid velocity (U_l) from the flowmeter is based on pure liquid flow, while the cross-sectional area of ILSCFB downer is occupied by both liquid and solid during fluidization, thus the local liquid velocity (V_l) calculated as $U_l / (1-\varepsilon_s)$ is larger than the superficial liquid velocity (U_l).

For a given superficial liquid velocity (U_l), under the circulating fluidization regime, the variation of the radial distribution of local liquid velocity (V_l) is presented in Fig. 8.7c with different superficial solids velocity (U_s). Obviously, the effect of the superficial solids velocity (U_s) is minor on the local liquid velocity, only with a slight increasing at the center region and decreasing near the wall, though the solids circulation rate is doubled.

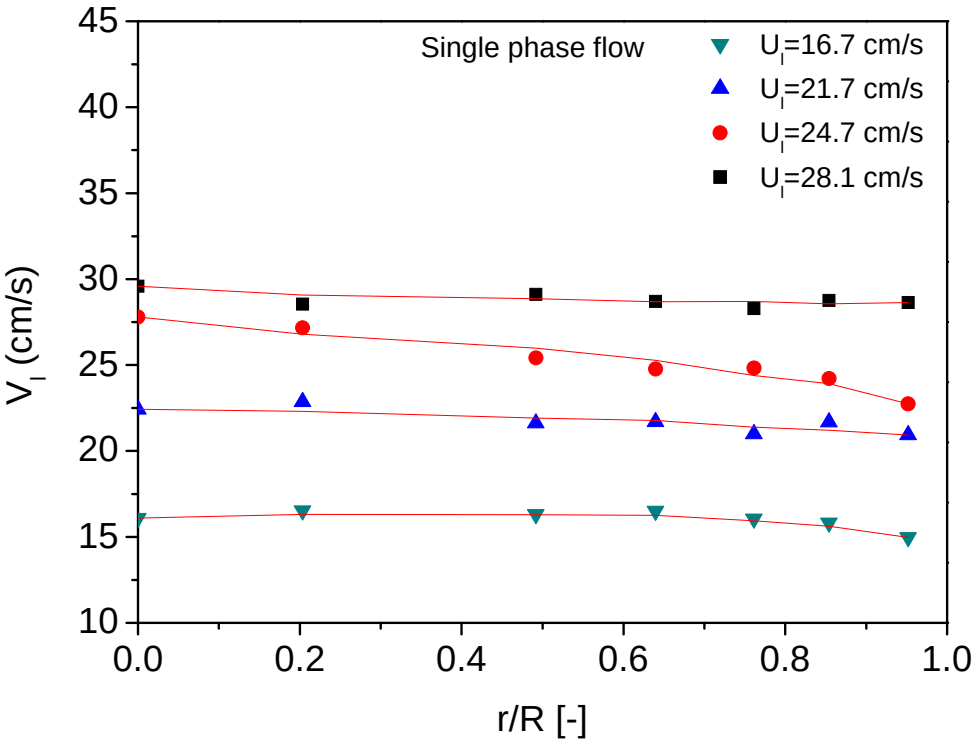
Single phase flow
U_l=16.7 cm/s
U_l=21.7 cm/s
U_l=24.7 cm/s
U_l=28.1 cm/s
V_l (cm/s)
r/R [-]
45
40
35
30
25
20
15
10
0.0
0.2
0.4
0.6
0.8
1.0

(a)

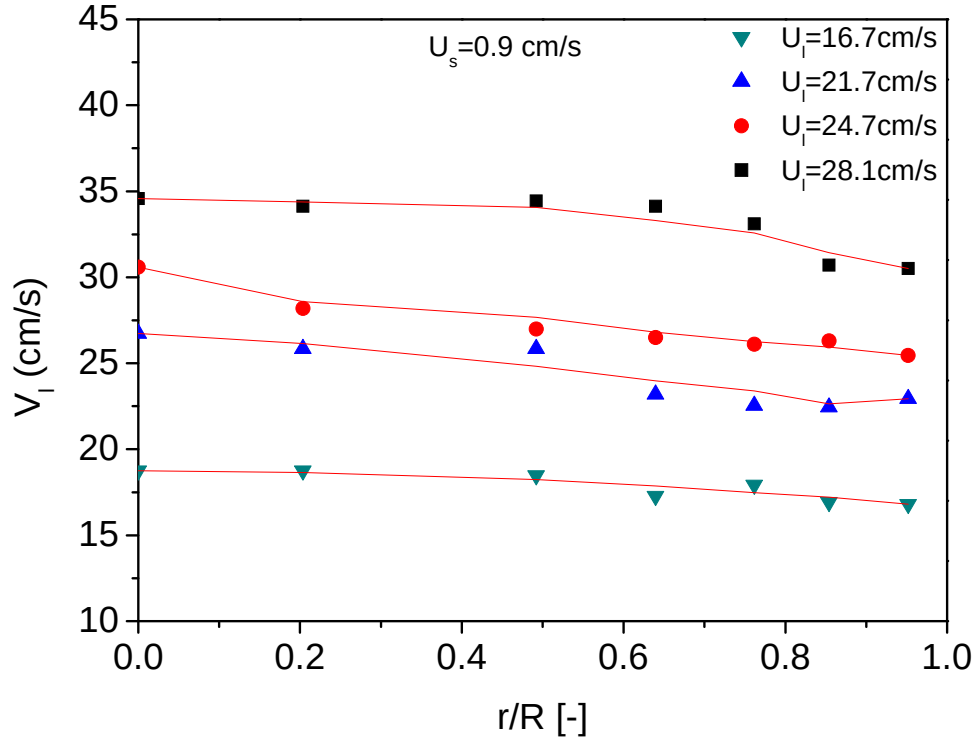
U_s=0.9 cm/s
U_l=16.7cm/s
U_l=21.7cm/s
U_l=24.7cm/s
U_l=28.1cm/s
V_l (cm/s)
r/R [-]
45
40
35
30
25
20
15
10
0.0
0.2
0.4
0.6
0.8
1.0

(b)

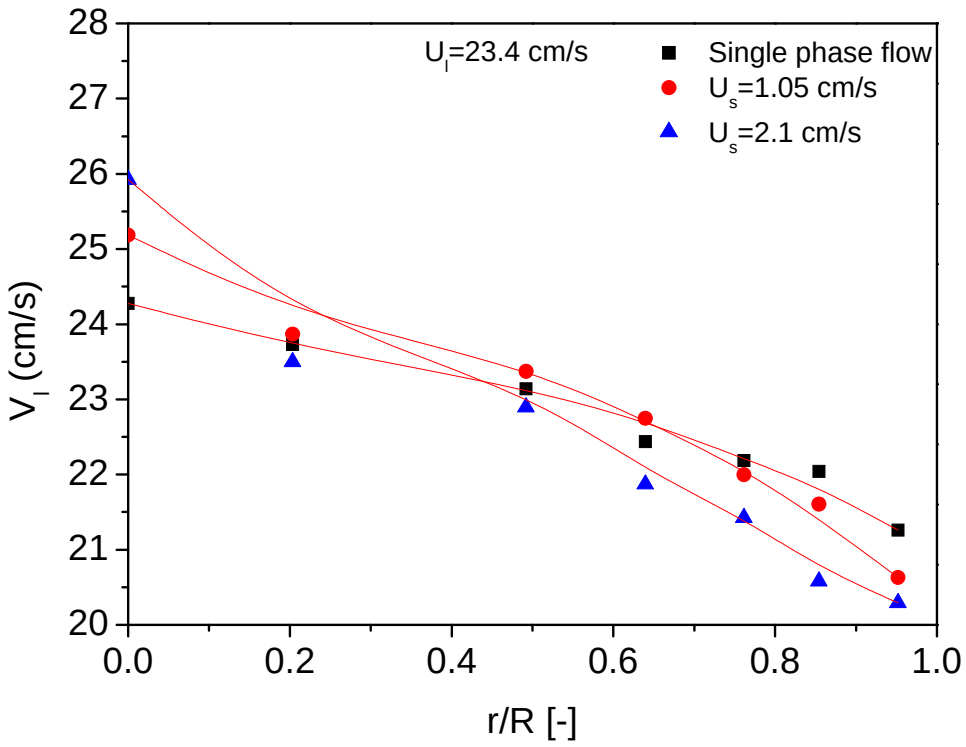

(c)

Fig. 8.7 Local liquid velocity distribution across the radial positions under various operating conditions (a) single phase flow (b) U_s=0.9 cm/s (c) U_l=23.4 cm/s.

To validate the measurement of the local liquid velocity, the superficial liquid velocity (U_l) is also calculated by the following equation (Yang et al. 1993) from the local liquid velocity (V_l) and local solids holdup (ε_s), and compared with that from rotameter readings:

$$U_l = \frac{1}{\pi R^2 \left(1-\overline{\varepsilon}_s\right)} \int_0^R V_l(r)\left[1-\varepsilon_s(r)\right] 2\pi r dr \qquad (8.3)$$

where U_l is the superficial liquid velocity, V_l is the local liquid velocity, ε_s and $\overline{\varepsilon}_s$ are the local solids holdup and average solids holdup respectively. The comparison is plotted in Fig. 8.8, which shows very good agreement between the calculated and measured superficial liquid velocity (U_l).

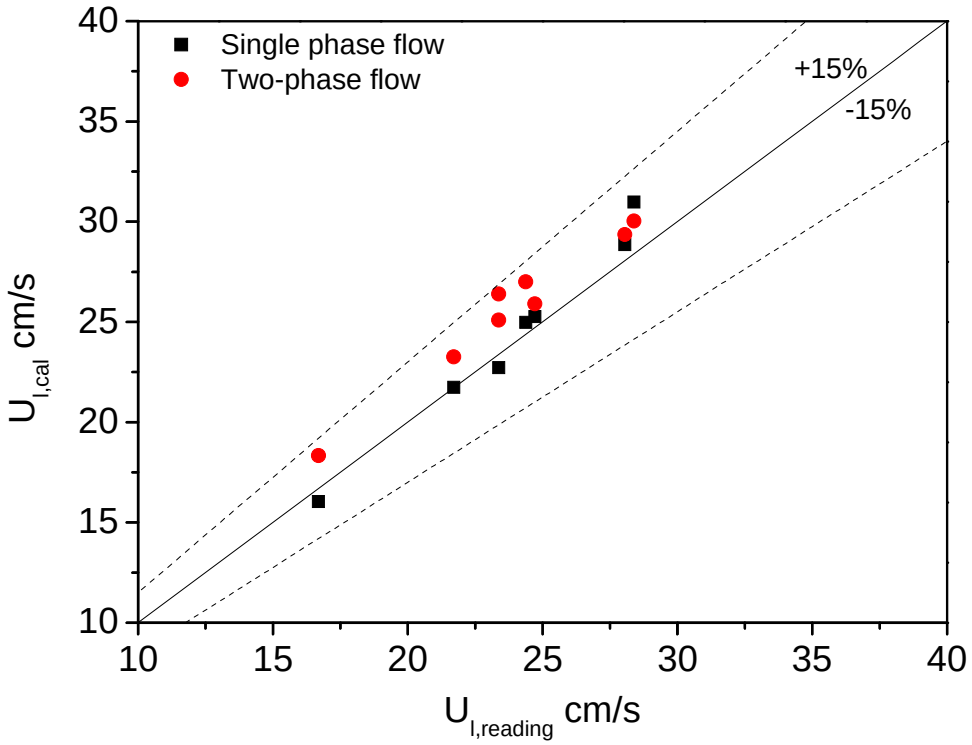

Fig. 8.8 The comparisons of measured and calculated superficial liquid velocity (U_l) based on local liquid velocity (V_l).

8.6 Radial distribution of local slip velocity

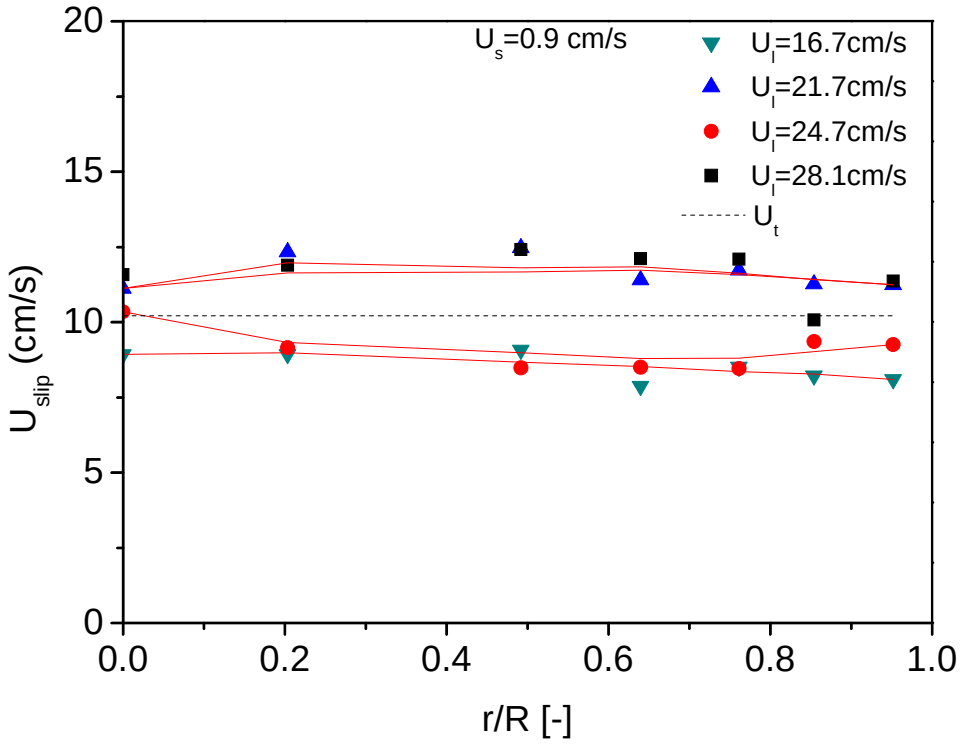

Fig. 8.9 Local slip velocity (U_{slip}) across the radial positions for U_s=0.9 cm/s under various superficial liquid velocity.

Local slip velocity (U_{slip}) is defined as the relative velocity between liquid and solids:

$$U_{slip} = V_l - V_p \tag{8.4}$$

indicating the interaction between liquid and solids. Then the local slip velocity (U_{slip}) can be determined by Eq. (8.4) based on the measured local liquid and particle velocities.

The radial distribution of local slip velocity (U_{slip}) for U_s=0.9 cm/s is shown in Fig. 8.9 under various superficial liquid velocity (U_l). One can note that the local slip velocity distribution is quite uniform from the downer center to the wall though there are slight fluctuations related to the fluctuations of liquid and particle velocities as shown in Fig. 8.4 and Fig. 8.7. By comparing these three figures, it can be seen that all local slip velocities (U_{slip}) are very close to the particle terminal velocity (U_t) and independent of

the operating conditions. Such observations are reasonable because there is no obvious clustering phenomenon under the circulating fluidization regime in ILSCFB, so that the slip velocity of the particles is similar to the particle terminal velocity (U_t).

In order to further investigate the slip velocity behavior in ILSCFB system, Fig. 8.10 shows comparisons of the measured local slip velocities and calculated slip velocities by different definitions.

$$\overline{U}_{slip} = \frac{U_l}{1-\overline{\varepsilon}_s} - \frac{U_s}{\overline{\varepsilon}_s} \tag{8.5}$$

$$\overline{U'}_{slip} = \frac{2}{R^2}\int_0^R U_{slip}(r) r dr = \frac{2}{R^2}\int_0^R \left[V_l(r) - V_p(r)\right] r dr \tag{8.6}$$

Eq. (8.5) is called apparent slip velocity based on the one-dimensional pseudo-homogeneous model, while Eq. (8.6) is the uniform voidage slip velocity based on the cross-sectional average of local slip velocities without considering the radial particle segregation (Yang et al. 1993). The comparisons in Fig. (8.10) show that there are no major differences for slip velocities obtained by experiment and different definitions, indicating that there is no obvious clustering or segregation phenomenon in ILSCFB. Therefore, the slip velocity can be determined easily and accurately by Eq. (8.5) in ILSCFB system by knowing the average solids holdup.

The slip velocity in Gas-Solid Circulating Fluidized (GSCFB) Bed shows quite different behaviors compared with that in the ILSCFB and LSCFB. The value of slip velocity in GSCFB is larger than that of single particle terminal velocity but significantly lower than the apparent slip velocity obtained from Eq. (8.5) because of the clustering and segregation phenomenon (Yang et al. 1993). Therefore, Eq. (8.6) is more appropriate for estimating the slip velocity in GSCFB.

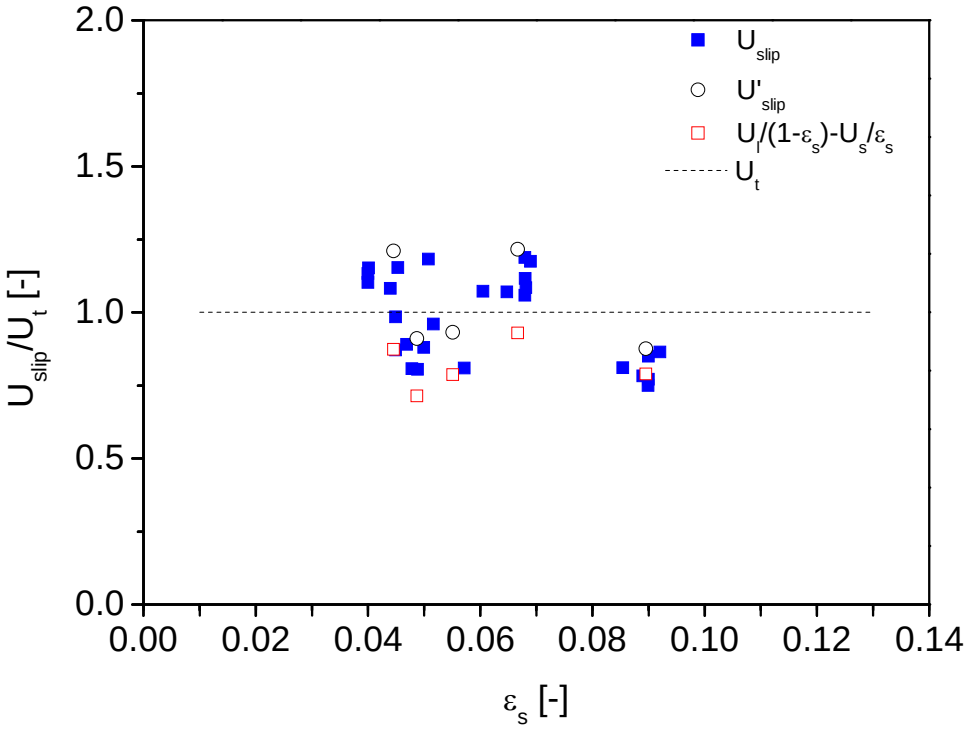

Fig. 8.10 Comparisons of slip velocity under different definitions.

8.7 Conclusions

Local particle and liquid velocities are measured in the downer of a pilot scale ILSCFB by using optical fiber probe and conductivity probe respectively. The radial profiles of both particle velocity and liquid velocity are slightly non-uniform with higher particle and liquid velocities in the center region and lower ones adjacent to the wall. Such non-uniformity is affected by solids circulation rate but not obviously influenced by the superficial liquid velocity. At fixed liquid velocity, the non-uniformity of both particle and liquid velocities radial distributions increase with increasing superficial solids velocity, increasing in the core region and decreasing near the wall. However, such non-uniformity observed in ILSCFB is less than that observed in LSCFB due to the fact that the lower particle density in the ILSCFB causes a weaker wall friction effect to occur.

Local slip velocity calculated from the local particle and liquid velocities are also investigated. It is found that all the local slip velocity distributions follow similar trend

under various operating conditions: the values of local slip velocity are very close to the single particle terminal velocity, suggesting no obvious clustering phenomenon and solids segregation in the ISLCFB downer, so that there are no major differences for average slip velocities obtained by different definitions, indicating the similar slip velocity behavior in LSCFB and ILSCFB.

Nomenclature

Ar	Archimedes number defined by $d^3 g(\rho_p - \rho_l)\rho_l / \mu^2$
a	Slip velocity coefficient U_{slip} / U_t
C_D	Particle drag coefficient
d_p	Particle diameter (mm)
d_p^*	Dimensionless particle size defined by $Ar^{1/3}$
D	Column diameter (m)
F_b, F_d, F_g	Buoyancy force, drag force and gravity
G_s	Solids circulation rate (kg/(m^{2}s))
g	Gravity acceleration
H	Bed height
n	Richardson and Zaki index
N_D	Best number
P	Pressure (Pa)
Q	Volumetric flowrate (m^3 / s)
Re	Reynolds number defined by $Ud\rho_l / \mu$
Re_t	Particle terminal Reynolds number defined by $U_t d\rho_l / \mu$
t	Residence time (s)
U_a	Auxiliary liquid velocity (cm/s)
U_{cr}	Transition velocity from Particulate fluidization regime to Circulating fluidization regime (cm/s)
U_{cv}	Transition velocity from Circulating fluidization regime to Transport regime (m/s)
U_l	Total superficial liquid velocity (cm/s)
U_i	Extrapolated value of U as ε approaches 1
U_l^*	Dimensionless superficial velocity defined by $Re / Ar^{1/3}$
U_s	Superficial particle velocity (cm/s)

U_{slip}	Slip velocity (cm/s)
U_t	Particle terminal velocity (cm/s)
U_t^*	Dimensionless transition velocity defined by Re_t / $Ar^{1/3}$
V_l, V_p	Local liquid velocity and local particle velocity
$\overline{V}_l, \overline{V}_p$	Average liquid velocity and average particle velocity

Greek letters

$\overline{\varepsilon}$	Average bed voidage
$\overline{\varepsilon}_s$	Average solids holdup
ϕ	Particle sphericity
μ_l	Liquid viscosity (mPas)
ρ_p	Particle density (kg/m^3)
ΔP	Pressure drop

Subscripts

l	Liquid
p	Particle
s	Solids

References

Horio, M., K. Morishita, O. Tachibana and N. Murata (1988). Solids distribution and movement in circulating fluidized beds. Circulating Fluidized Bed Technology II, Toronto, Pergamon Press.

Karamanev, D. G. and L. N. Nikolov (1992). Bed Expansion of Liquid-Solid Inverse Fluidization. Aiche Journal 38(12): 1916-1922.

Karamanev, D. G. and L. N. Nikolov (1996). Application of inverse fluidization in wastewater treatment: From laboratory to full-scale bioreactors. Environmental Progress 15(3): 194-196.

Liang, W., S. Zhang, J.-X. Zhu, Y. Jin, Z. Yu and Z. Wang (1997). Flow characteristics of the liquid-solid circulating fluidized bed. Powder Technology 90(2): 95-102.

Liang, W. G., J. X. Zhu, Y. Jin, Z. Q. Yu, Z. W. Wang and J. Zhou (1996). Radial nonuniformity of flow structure in a liquid-solid circulating fluidized bed. Chemical Engineering Science 51(10 pt A): 2001-2010.

Natarajan, P., R. Velraj and R. V. Seeniraj (2009). Studies on regime transition, operating range and system stability in a liquid-solid circulating fluidized bed. Chemical Engineering and Technology 32(4): 572-579.

Nikolov, L. and D. Karamanev (1987). Experimental Study of the Inverse Fluidized Bed Biofilm Reactor. Canadian Journal of Chemical Engineering 65(2): 214-217.

Nikolov, V. R. and I. Nikov (1994). Liquid-solid mass transfer in three-phase inverse fluidized bed (TPIFB). Hungarian Journal of Industrial Chemistry 22(2): 125-128.

Renganathan, T. and K. Krishnaiah (2003). Prediction of minimum fluidization velocity in two and three phase inverse fluidized beds. Canadian Journal of Chemical Engineering 81(3-4): 853-860.

Yang, Y. L., Y. Jin, J. X. Zhu and H. Bi (1993). Local slip behaviors in the circulating fluidized bed. AIChE symposium series 89: 81-90.

Zhang, H., P. M. Johnston, J. X. Zhu, H. I. de Lasa and M. A. Bergougnou (1998). A novel calibration procedure for a fiber optic solids concentration probe. Powder Technology 100(2-3): 260-272.

Zheng, Y. (1999). Flow Structure in a Liquid Solid Circulating Fluidized Bed. Chemical and Biochemical Engineering. London, University of Western Ontario. Ph.D.

Zheng, Y., J.-X. Zhu, N. S. Marwaha and A. S. Bassi (2002). Radial solids flow structure in a liquid-solids circulating fluidized bed. Chemical Engineering Journal 88(1-3): 141-150.

Zheng, Y., J.-X. Zhu, J. Wen, S. A. Martin, A. S. Bassi and A. Margaritis (1999). The axial hydrodynamic behavior in a liquid-solid circulating fluidized bed. Canadian Journal of Chemical Engineering 77(Compendex): 284-290.

Zhu, J.-X., D. G. Karamanev, A. S. Bassi and Y. Zheng (2000). (Gas-)liquid-solid circulating fluidized beds and their potential applications to bioreactor engineering. The Canadian Journal of Chemical Engineering 78(1): 82-94.

Chapter 9

9 Conclusions and Recommendations

9.1 Conclusions

In this study, a comprehensive investigation is conducted on inverse conventional fluidization and Inverse Liquid-Solid Circulating Fluidized Bed (ILSCFB), as well as upwards Liquid-Solid Circulating Fluidized Bed (LSCFB).

In the ILSCFB, under the conventional fluidization regime and circulating fluidization regime, a systematic understanding of the hydrodynamics is established by examining the variations of solids distributions, liquid and particle velocities and slip velocity experimentally and theoretically.

Under the conventional fluidization regime, the bed voidage and dimensionless bed expansion are investigated under various liquid flowrate for 4 different types of particles. Both the bed vodiage and dimensionless bed expansion increase with superficial liquid velocity. With regards to the effects of particle properties, for fixed superficial liquid velocity, lower particle density leads to smaller bed voidage so as to smaller bed expansion, while larger particle size leads to smaller bed viodage so as to smaller bed expansion. Such comparisons can be conducted in terms of particle terminal velocity which incorporates particle properties (density, size, sphericity): under similar superficial liquid velocity, the particles with smaller terminal velocity lead to larger bed voidage as well as bed expansion, and vice versa. A new mathematical model is proposed to predict the bed voidage and dimensionless bed expansion for both inverse and upwards liquid-solid fluidization systems based on force balance of particle in terms of Archimedes number and Reynolds number. The results are validated with experimental data, showing adequate accuracy within a wide range of operating conditions to provide a simple way to estimate the bed voidage so as to bed expansion.

Under the circulating fluidization regime, the solids holdup distributions in the downer of a pilot scale Inverse Liquid-Solid Circulating Fluidized Bed (ILSCFB) are investigated experimentally by fluidization of Styrofoam and Hollow Glassbeads whose densities are lower than that of fluidization media. For both types of particles, axial solids holdup distribution is quite uniform under various operating conditions, while radial solids holdup distributions are somehow non-uniform with a slight increase in solids holdup adjacent to the wall under various operating conditions but not significant to be considered as an obvious “core-annulus” structure. Such solids holdup distribution pattern is closely related to the wall friction effects. The comparisons of the hydrodynamics in ILSCFB and LSCFB show that the mathematical expression based on the force balance valid in the upwards circulating fluidization system is also valid in the downwards counter part. The generalized flow regime map for both the inverse and upwards fluidization system is proposed in terms of dimensionless superficial velocity and dimensionless particle size. The demarcations of different flow regimes are also quantitatively determined from the minimum fluidization velocity, particle terminal velocity and transition velocity.

Furthermore, the local particle and liquid velocities are measured in the same ILSCFB downer by using optical fiber probe and conductivity probe respectively. The radial profiles of both particle velocity and liquid velocity are slightly non-uniform with higher particle and liquid velocities in the center region and lower ones adjacent to the wall. However, the average particle velocity is mainly determined by superficial liquid velocity rather than superficial solids velocity. Local slip velocity calculated from the local particle and liquid velocities are also investigated. It is found that all the slip velocity distributions follow similar trend under various operating conditions: the values of local slip velocity are very close to the single particle terminal velocity, suggesting no obvious clustering phenomenon and solids segregation in the ISLCFB downer, so that there are no major differences for average slip velocities obtained by different definitions, indicating the similar slip velocity behavior in ILSCFB and LSCFB.

In the LSCFB, the effects of particle properties on the solids holdup distribution are investigated experimentally and analytically.

The average and local solids holdups of 5 different types of particles are compared under various operating conditions to investigate the effects of the particle properties based on 3 parameters: the superficial liquid velocity (U_l), the normalized superficial liquid velocity (U_l/U_t) and the excess superficial liquid velocity (U_l-U_t). At fixed superficial solids velocity (U_s), the solids holdup increases with increasing particle density or size based on the superficial liquid velocity (U_l); whereas, the solids holdup decreases with increasing particle density or size based on the normalized superficial liquid velocity (U_l/U_t). When the comparison is based on the excess superficial liquid velocity (U_l-U_t), particle properties has little effects on the solids holdup, so that the excess superficial liquid velocity (U_l-U_t) is a more appropriate parameter to evaluate the effects of the particle properties compared to the superficial liquid velocity (U_l) and the normalized superficial liquid velocity (U_l/U_t). A discussion on the force balance of the particles reveals that the excess superficial liquid velocity (U_l-U_t) is approximately equivalent to the average particle velocity ($\overline{V}_P$) when the solids holdup is less than 0.1. Furthermore, the solids holdup is a function of the particle velocity (V_p) and the superficial solids velocity (U_s), which could be expressed quantitatively as $\overline{\varepsilon}_s = U_s / (U_l - U_t)$ when $\overline{\varepsilon}_s < 0.1$. This equation enables the quick estimation of the average solids holdup directly from the operation conditions in the industrial LSCFB systems for different types of particles having different densities and sizes. However, when $\overline{\varepsilon}_s > 0.1$, the predicted results would deviate from the experimental results.

An analytical model incorporating particle slip velocity, operating conditions and solids properties in terms of terminal velocity, is proposed to estimate average solids holdup regardless the dimensions of LSCFB risers, showing satisfactory agreement with the experimental results. By this model, the effects of the particle properties including particle density, size and sphericity can be determined quantitatively, revealing solids holdup is closely related to the particle velocity, increasing of which contributed to lower

solids holdup. Then the transition velocity from the circulating fluidized regime to the transport regime is determined to finalize the flow regime map in LSCFB.

9.2 Recommendations

This study provides comprehensive experimental results and systematic understanding on the hydrodynamics in LSCFB and ILSCFB. However, there are still some areas where further research is needed.

In this study, only two types of “light” particles, whose size is smaller than 3 mm, are fluidized under the circulating fluidization regime due to the limited spaces around the primary liquid distributors. More types of particles with different densities and sizes are needed to investigate the effects of the particle properties in ILSCFB.

This study only focuses on the macro flow in ILSCFB. With the currently available experimental data of hydrodynamic parameters, some micro flow characteristics can be investigated.

Only two phase fluidization is experimentally studied. In the future work, the gas phase can be introduced into the downer of ILSCFB to develop a three phase Inverse Gas-Liquid-Solid Circulating Fluidized Bed (IGLSCFB).

Appendices

A1 An example of error bars for solid holdup, liquid velocity and particle velocity measurements

In order to ensure the accuracy of solids holdup, liquid and particle velocity measurements, preliminary measurements and analyses of standard error were taken for SF46-0.8 particles under U_l=21.7 cm/s, U_s=0.9 cm/s at axial level H=2.48 m. 10 measurements were taken for every one of 7 radial positions. Fig.A1 shows an example of error bars for solid holdup, liquid and particle velocity measurements respectively.

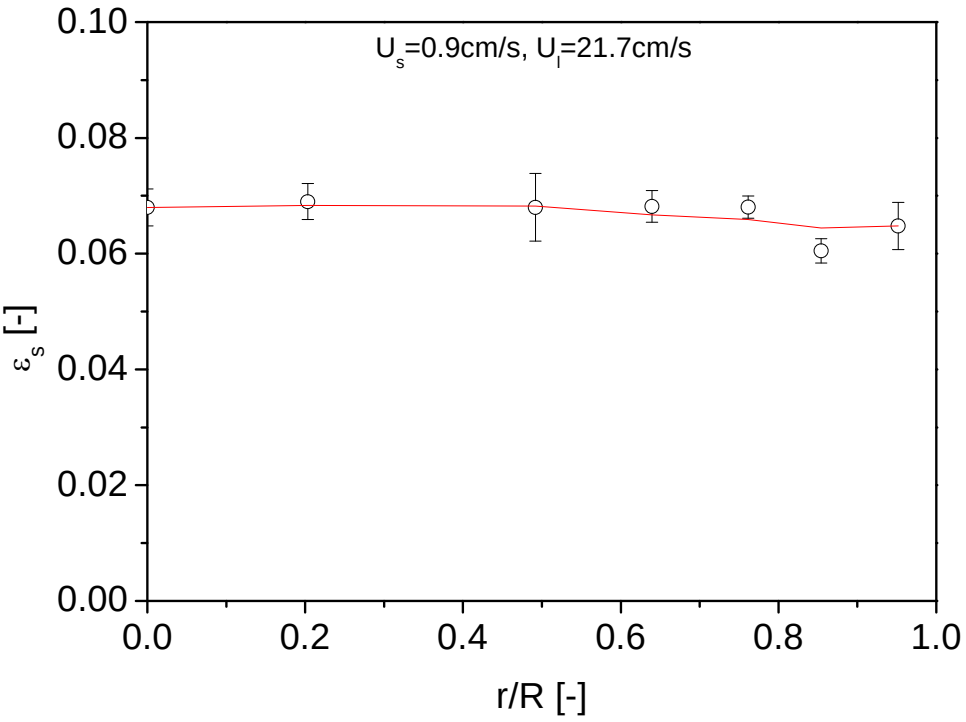

(a)

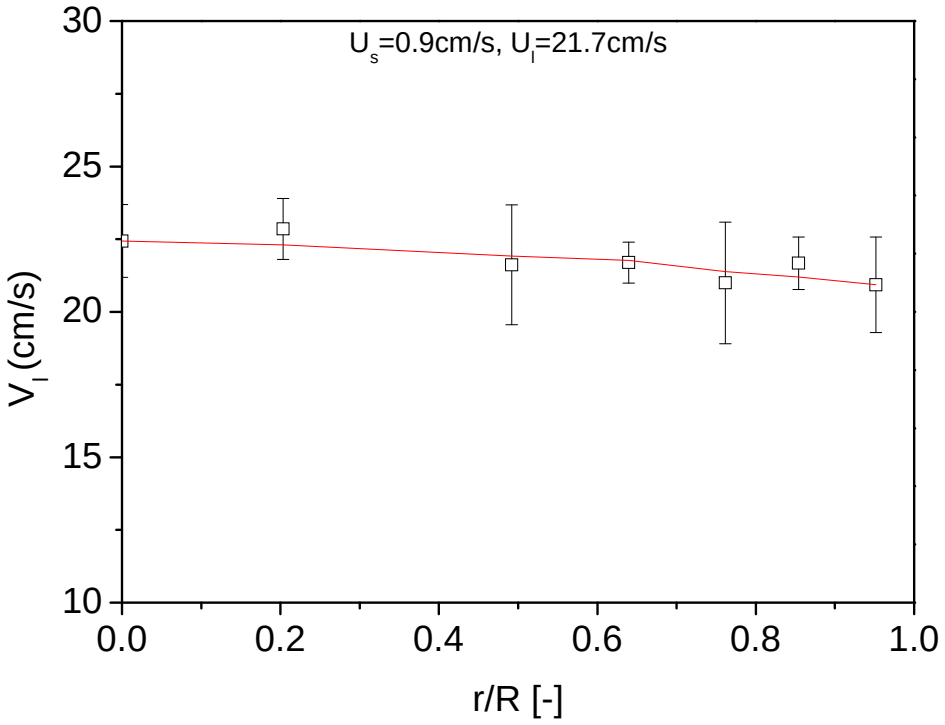

(b)

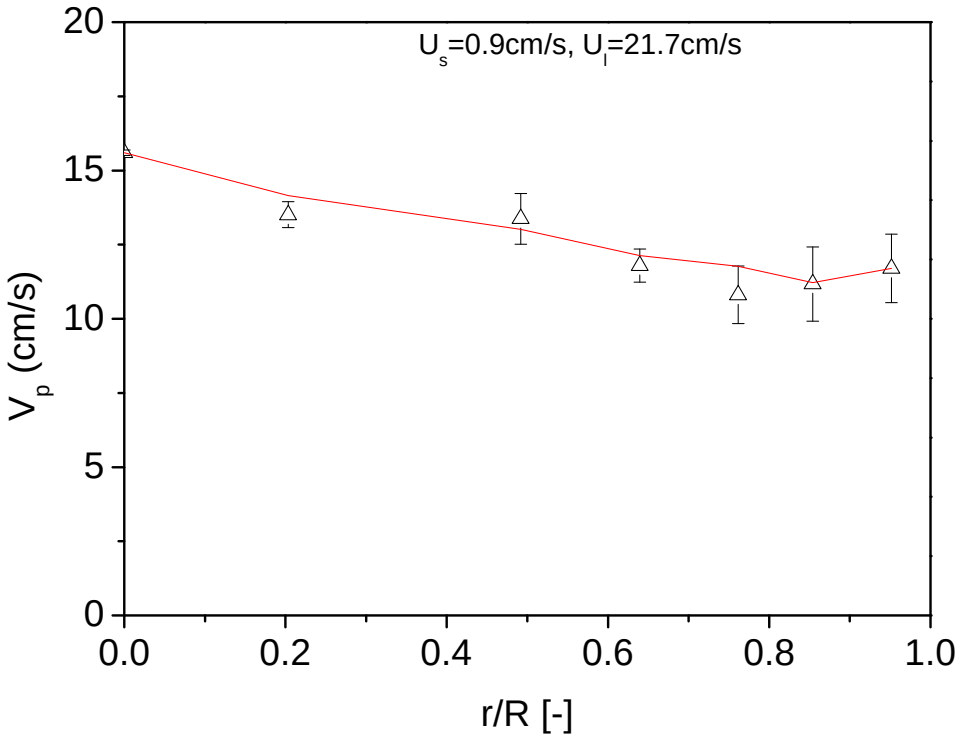

(c)

Fig. A.1 Error bars for (a) solid holdup; (b) liquid velocity; (c) particle velocity.

B1 Superficial solids velocity (U_s) in LSCFB and ILSCFB

LSCFB

PB1330-0.58

U_l (cm/s) U_a=1.33	U_s (cm/s)	U_l (cm/s) U_a=1.66	U_s (cm/s)
2.5	0.00	2.5	0.00
5.65	0.10	6.65	0.18
7.31	0.13	8.31	0.39
8.97	0.19	9.97	0.42
10.63	0.25	11.63	0.48
12.30	0.29	13.29	0.52
13.96	0.32	14.95	0.56
15.62	0.37	16.61	0.58
17.28	0.42	18.28	0.59
18.94	0.42	19.94	0.59
20.60	0.42	21.60	0.59

PB1520-0.58

U_l (cm/s) U_a=1.33	U_s (cm/s)	U_l (cm/s) U_a=1.66	U_s (cm/s)
4.32	0	4.32	0
5.65	0.06	6.65	0.12
7.31	0.19	8.31	0.23
8.97	0.23	9.97	0.25
10.63	0.23	11.63	0.29
12.30	0.26	13.29	0.36
13.96	0.29	14.95	0.38
15.62	0.34	16.61	0.48
17.28	0.37	18.28	0.48
18.94	0.38	19.94	0.48
20.60	0.38	21.60	0.48
22.26	0.38	23.26	0.48

PB1520-1.19

U_l (cm/s) U_a=1.66	U_s (cm/s)	U_l (cm/s) U_a=2.66	U_s (cm/s)	U_l (cm/s) U_a=3.32	U_s (cm/s)
9.97	0	10	0	18.28	0.59
11.63	0.02	11.8	0.1	19.94	0.6
13.29	0.06	13.46	0.19	21.6	0.61
14.95	0.11	15.12	0.27	23.26	0.57
16.61	0.19	16.78	0.3	24.92	0.63
18.28	0.22	18.44	0.37		
19.94	0.24	20.1	0.4		
21.6	0.23	21.77	0.42		
23.26	0.23	23.43	0.41		
24.92	0.23	25.09	0.42		

ILSCFB

SF46-0.8

U_l (cm/s) U_a=4.15	U_s (cm/s)	U_l (cm/s) U_a=3.32	U_s (cm/s)	U_l (cm/s) U_a=2.66	U_s (cm/s)
10.5	0	10.5	0	10.5	0
21.69	2.13	16.68	0.92	14.35	0.22
23.36	2.31	18.35	1.2	16.02	0.48
25.03	2.92	20.02	1.46	17.69	0.79
26.7	2.92	21.69	1.79	19.36	0.91
28.37	3.08	23.36	2.13	21.03	1.5
		25.03	2.77	22.7	1.68
		26.7	2.77	24.37	1.85
		28.37	2.77	26.04	2.13
				27.71	2.13
U_l (cm/s) U_a=1.66	U_s (cm/s)	U_l (cm/s) U_a=1.33	U_s (cm/s)	U_l (cm/s) U_a=0.66	U_s (cm/s)
10.5	0	10.5	0	10.5	0
15.02	0.16	14.69	0.15	17.36	0.05
16.69	0.4	16.36	0.25	19.03	0.06
18.36	0.59	18.03	0.45	20.7	0.09
20.03	0.69	19.7	0.51	22.37	0.11
21.7	0.89	21.37	0.57	24.04	0.23
23.37	1.05	23.04	0.66	25.71	0.23
25.04	1.13	24.71	0.84	27.38	0.23
26.71	1.18	26.38	1.07	29.05	0.23
28.38	1.18	28.05	1.07		

HGB790-2.5

U_l (cm/s) U_a=2.49	U_s (cm/s)	U_l (cm/s) U_a=3.32	U_s (cm/s)	U_l (cm/s) U_a=4.15	U_s (cm/s)	U_l (cm/s) U_a=4.98	U_s (cm/s)
9.60	0	9.60	0	9.60	0	9.60	0
14.94	0.14	9.96	0.13	13.28	0.21	13.28	0.30
16.60	0.12	11.62	0.14	14.94	0.34	14.94	0.43
18.26	0.17	13.28	0.15	16.60	0.39	16.60	0.49
19.92	0.15	14.94	0.34	18.26	0.42	18.26	0.52
21.58	0.16	16.60	0.45	19.92	0.55	19.92	0.80
23.24	0.15	18.26	0.36	21.58	0.59	21.58	0.79
--	--	19.92	0.36	23.24	0.59	23.24	0.83
--	--	21.58	0.39	24.90	0.58	24.90	0.89
--	--	23.24	0.36	26.56	0.58	26.56	0.84

B2 Local and average solids holdup in LSCFB

Average solids holdup as a function of U_l

PB-1330-0.58

U_l (cm/s)	$\overline{\varepsilon}_s$	U_s (cm/s)
17.3	0.023	0.4
18.9	0.022	0.4
20.6	0.020	0.4
22.3	0.018	0.4
28.0	0.013	0.4

PB-1520-0.58

U_l (cm/s)	$\overline{\varepsilon}_s$	U_s (cm/s)
17.3	0.029	0.4
18.9	0.026	0.4
20.6	0.023	0.4
22.3	0.020	0.4
28.0	0.019	0.4

PB-1520-1.19

U_l (cm/s)	$\overline{\varepsilon}_s$	U_s (cm/s)
18.0	0.032	0.4
21.8	0.028	0.4
23.4	0.026	0.4
25.1	0.025	0.4

Average solids holdup as a function of U_l/U_t

PB-1330-0.58

U_l/U_t	$\overline{\varepsilon}_s$	U_s (cm/s)
6.41	0.023	0.4
7.00	0.022	0.4
7.63	0.020	0.4
8.26	0.018	0.4
10.37	0.013	0.4

PB-1520-0.58

U_l/U_t	$\overline{\varepsilon}_s$	U_s (cm/s)
4.51	0.029	0.4
4.92	0.026	0.4
5.36	0.023	0.4
5.81	0.020	0.4
7.29	0.019	0.4

PB-1520-1.19

U_l/U_t	$\overline{\varepsilon}_s$	U_s (cm/s)
2.12	0.032	0.4
2.57	0.028	0.4
2.76	0.026	0.4
2.96	0.025	0.4

Average solids holdup as a function of U_l-U_t

PB-1330-0.58

U_l-U_t (cm/s)	$\overline{\varepsilon}_s$	U_s (cm/s)
9.52	0.032	0.4
13.32	0.028	0.4
14.92	0.026	0.4
16.62	0.025	0.4

PB-1520-0.58

U_l (cm/s)	$\overline{\varepsilon}_s$	U_s (cm/s)
13.46	0.029	0.4
15.06	0.026	0.4
16.76	0.023	0.4
18.46	0.020	0.4
24.16	0.019	0.4

PB-1520-1.19

U_l (cm/s)	$\overline{\varepsilon}_s$	U_s (cm/s)
9.52	0.032	0.4
13.32	0.028	0.4
14.92	0.026	0.4
16.62	0.025	0.4

Average solids holdup as a function of ρ_p under different U_l

U_l (cm/s)	$\overline{\varepsilon}_s$ ρ_p =1330kg/m^3	$\overline{\varepsilon}_s$ ρ_p =1520kg/m^3	U_s (cm/s)	d_p (mm)
18.9	0.022	0.026	0.4	0.58
20.6	0.020	0.023	0.4	0.58
22.3	0.018	0.020	0.4	0.58
28.0	0.013	0.019	0.4	0.58

Average solids holdup as a function of ρ_p under different U_l/U_t

U_l/U_t	$\overline{\varepsilon}_s$ ρ_p =1330kg/m^3	$\overline{\varepsilon}_s$ ρ_p =1520kg/m^3	U_s (cm/s)	d_p (mm)
2.2	0.066	0.050	0.2	0.58
5.0	0.040	0.029	0.4	0.58

Average solids holdup as a function of ρ_p under different U_l-U_t

U_l-U_t (cm/s)	$\overline{\varepsilon}_s$ ρ_p =1330kg/m^3	$\overline{\varepsilon}_s$ ρ_p =1520kg/m^3	U_s (cm/s)	d_p (mm)
3.5	0.044	0.05	0.1	0.58
14.9	0.014	0.018	0.2	0.58
15.6	0.026	0.028	0.4	0.58

Local solids holdup

U_l=28cm/s

r/R	$\overline{\varepsilon}_s$ ρ_p =1330kg/m^3	$\overline{\varepsilon}_s$ ρ_p =1520kg/m^3	U_s (cm/s)	d_p (mm)
0	0.012	0.011	0.4	0.58
0.2034	0.011	0.012		
0.492	0.011	0.014		
0.6396	0.010	0.014		
0.7615	0.010	0.014		
0.8541	0.011	0.014		
0.9518	0.016	0.018		

U_l/U_l =5

r/R	$\overline{\varepsilon}_s$ ρ_p =1330kg/m^3	$\overline{\varepsilon}_s$ ρ_p =1520kg/m^3	U_s (cm/s)	d_p (mm)
0	0.036	0.025	0.4	0.58
0.2034	0.037	0.022		
0.492	0.037	0.027		
0.6396	0.037	0.027		
0.7615	0.037	0.030		
0.8541	0.040	0.030		
0.9518	0.057	0.041		

U_l-U_l =3.5cm/s

r/R	$\overline{\varepsilon}_s$ ρ_p =1330kg/m^3	$\overline{\varepsilon}_s$ ρ_p =1520kg/m^3	U_s (cm/s)	d_p (mm)
0	0.030	0.040	0.1	0.58
0.2034	0.035	0.041		
0.492	0.033	0.036		
0.6396	0.036	0.038		
0.7615	0.042	0.039		
0.8541	0.044	0.042		
0.9518	0.069	0.052		

U_l-U_l =15.6cm/s

r/R	$\overline{\varepsilon}_s$ ρ_p =1330kg/m^3	$\overline{\varepsilon}_s$ ρ_p =1520kg/m^3	U_s (cm/s)	d_p (mm)
0	0.025	0.023	0.4	0.58
0.2034	0.023	0.022		
0.492	0.022	0.022		
0.6396	0.023	0.022		
0.7615	0.022	0.023		
0.8541	0.024	0.023		
0.9518	0.037	0.038		

B3 Local solids holdup in ILSCFB

U_s=0.9 cm/s

U_l=16.7 cm/s

r/R	*H*=132cm	*H*=222cm	*H*=349cm	*H*=413cm
0	0.083	0.090	0.096	0.090
0.2034	0.083	0.090	0.121	0.114
0.492	0.110	0.092	0.116	0.092
0.6396	0.097	0.090	0.100	0.090
0.7615	0.104	0.085	0.105	0.085
0.8541	0.083	0.089	0.105	0.080
0.9518	0.116	0.090	0.099	0.087

U_l=21.7 cm/s

r/R	*H*=132cm	*H*=222cm	*H*=349cm	*H*=413cm
0	0.068	0.068	0.065	0.082
0.2034	0.069	0.069	0.066	0.078
0.492	0.065	0.068	0.064	0.079
0.6396	0.072	0.068	0.066	0.068
0.7615	0.068	0.068	0.064	0.068
0.8541	0.063	0.060	0.064	0.060
0.9518	0.062	0.065	0.063	0.065

U_l=24.7 cm/s

r/R	*H*=132cm	*H*=222cm	*H*=349cm	*H*=413cm
0	0.053	0.045	0.045	0.050
0.2034	0.053	0.045	0.045	0.063
0.492	0.061	0.048	0.048	0.057
0.6396	0.062	0.057	0.057	0.048
0.7615	0.051	0.049	0.049	0.048
0.8541	0.051	0.047	0.047	0.067
0.9518	0.047	0.050	0.050	0.046

U_l=28.1 cm/s

r/R	*H*=132cm	*H*=222cm	*H*=349cm	*H*=413cm
0	0.052	0.054	0.040	0.054
0.2034	0.048	0.056	0.040	0.069
0.492	0.051	0.056	0.051	0.059
0.6396	0.045	0.044	0.045	0.047
0.7615	0.042	0.040	0.040	0.043
0.8541	0.042	0.048	0.052	0.051
0.9518	0.043	0.045	0.044	0.045

U_s=1.2 cm/s

U_l=23.4 cm/s

r/R	*H*=132cm	*H*=222cm	*H*=349cm	*H*=413cm
0	0.124	0.138	0.111	0.113
0.2034	0.118	0.138	0.120	0.106
0.492	0.113	0.123	0.118	0.113
0.6396	0.112	0.109	0.106	0.115
0.7615	0.106	0.115	0.111	0.100
0.8541	0.106	0.099	0.110	0.109
0.9518	0.120	0.105	0.105	0.126

U_l=25.1 cm/s

r/R	*H*=132cm	*H*=222cm	*H*=349cm	*H*=413cm
0	0.063	0.066	0.068	0.060
0.2034	0.057	0.064	0.071	0.060
0.492	0.059	0.061	0.067	0.058
0.6396	0.062	0.054	0.066	0.059
0.7615	0.059	0.059	0.066	0.061
0.8541	0.059	0.054	0.068	0.060
0.9518	0.066	0.063	0.069	0.058

U_l=28.1 cm/s

r/R	*H*=132cm	*H*=222cm	*H*=349cm	*H*=413cm
0	0.049	0.056	0.055	0.049
0.2034	0.053	0.050	0.059	0.050
0.492	0.053	0.052	0.055	0.052
0.6396	0.048	0.052	0.055	0.051
0.7615	0.048	0.048	0.053	0.047
0.8541	0.045	0.050	0.054	0.045
0.9518	0.042	0.053	0.055	0.044

B4 Local particle velocity in ILSCFB

U_s=0.9 cm/s

U_l=16.7 cm/s

r/R	*H*=132cm	*H*=222cm	*H*=349cm	*H*=413cm
0	10.03	9.16	10.24	9.81
0.2034	8.83	9.16	10.80	9.81
0.492	9.39	8.69	12.61	9.40
0.6396	8.65	8.68	12.54	9.40
0.7615	9.11	8.47	14.50	9.40
0.8541	8.54	9.58	11.85	9.40
0.9518	9.37	9.16	11.34	8.69

U_l=21.7 cm/s

r/R	*H*=132cm	*H*=222cm	*H*=349cm	*H*=413cm
0	17.02	17.41	15.88	15.60
0.2034	12.19	16.45	16.45	13.51
0.492	14.62	14.50	17.58	13.37
0.6396	11.73	11.16	18.40	11.79
0.7615	10.56	11.57	14.86	10.81
0.8541	11.17	10.16	13.27	11.17
0.9518	12.88	12.01	12.01	11.70

U_l=24.7 cm/s

r/R	*H*=132cm	*H*=222cm	*H*=349cm	*H*=413cm
0	14.71	20.80	20.24	20.24
0.2034	15.31	18.91	19.04	19.04
0.492	14.93	18.05	16.48	18.50
0.6396	14.73	16.42	19.45	18.00
0.7615	15.20	18.05	15.20	17.64
0.8541	14.43	16.05	15.94	16.94
0.9518	17.45	13.87	16.64	16.20

U_l=28.1 cm/s

r/R	*H*=132cm	*H*=222cm	*H*=349cm	*H*=413cm
0	23.00	27.17	25.27	23.00
0.2034	20.02	27.17	22.23	22.23
0.492	20.40	24.24	22.01	22.01
0.6396	20.30	18.07	23.38	22.01
0.7615	19.40	16.74	18.50	21.00
0.8541	18.46	18.73	20.62	20.62
0.9518	21.00	18.73	19.14	19.14

U_l=27 cm/s

r/R	U_s=1.2 cm/s	U_s=0.9 cm/s	U_s=0.2 cm/s
0	23.78	21.60	19.84
0.2034	22.50	20.03	19.84
0.492	20.23	18.55	18.44
0.6396	19.42	17.80	17.36
0.7615	17.70	16.82	16.64
0.8541	16.78	16.10	15.40
0.9518	14.73	15.91	15.23

B5 Local liquid velocity in ILSCFB

Single phase flow

r/R	U_l=16.7 cm/s	U_l=21.7 cm/s	U_l=24.7 cm/s	U_l=28.1 cm/s
0	16.10	22.43	27.79	29.58
0.2034	16.53	22.86	27.16	28.55
0.492	16.31	21.62	25.41	29.11
0.6396	16.50	21.69	24.76	28.70
0.7615	16.06	21.00	24.82	28.29
0.8541	15.82	21.68	24.22	28.76
0.9518	14.98	20.93	22.75	28.65

U_s=0.9 cm/s

r/R	U_l=16.7 cm/s	U_l=21.7 cm/s	U_l=24.7 cm/s	U_l=28.1 cm/s
0	18.74	26.72	30.59	34.59
0.2034	18.74	25.85	28.19	34.13
0.492	18.48	25.85	26.98	34.43
0.6396	17.28	23.19	26.50	34.12
0.7615	17.92	22.54	26.10	33.10
0.8541	16.92	22.44	26.30	30.70
0.9518	16.80	22.94	25.45	30.52

U_l=23.4 cm/s

r/R	Single phase	U_s=0.9 cm/s	U_s=1.2 cm/s
0	24.28	25.18	25.92
0.2034	23.73	23.87	23.50
0.492	23.14	23.37	22.90
0.6396	22.44	22.75	21.87
0.7615	22.18	22.00	21.43
0.8541	22.04	21.61	20.58
0.9518	21.26	20.63	20.29

B6 Bed voidage and bed expansion under the conventional fluidization regime in inverse liquid-solid fluidized bed

Hollow Glassbeads (HGB 790-2.5)

Initial bed height H_0=53cm

U_l (cm/s)	ε	H_T/H_0
4.98	0.72	2.46
4.65	0.71	2.23
4.32	0.70	2.05
3.98	0.68	1.86
3.65	0.67	1.68
3.32	0.65	1.43
2.99	0.57	1.29
2.66	0.52	1.19
2.32	0.49	1.15
1.99	0.47	1.07
1.66	0.62	1.07

Initial bed height H_0=43cm

U_l (cm/s)	ε	H_T/H_0
4.98	0.72	2.81
4.65	0.70	2.46
4.32	0.69	2.25
3.98	0.69	1.95
3.65	0.64	1.82
3.32	0.61	1.68
2.99	0.57	1.51
2.66	0.52	1.34
2.32	0.48	1.27
1.99	0.45	1.18
1.66	0.40	1.08

Initial bed height H_0=36cm

U_l (cm/s)	ε	H_T/H_0
4.98	0.72	2.46
4.65	0.75	2.29
4.32	0.71	2.08
3.98	0.69	1.93
3.65	0.66	1.73
3.32	0.62	1.62
2.99	0.54	1.45
2.66	0.47	1.31
2.32	0.49	1.22
1.99	0.48	1.14
1.66	0.60	1.03

Styrofoam (SF 46-0.8)

Initial bed height H_0=34cm

U_l (cm/s)	ε	H_T/H_0
4.98	0.72	2.10
5.81	0.77	2.66
6.64	0.78	3.18
7.47	0.81	3.72
8.30	0.84	5

Initial bed height H_0=29cm

U_l (cm/s)	ε	H_T/H_0
4.98	0.73	2.14
5.81	0.78	2.78
6.64	0.81	3.54
7.97	0.83	4.90
8.30	0.85	5.00

Initial bed height H_0=18cm

U_l (cm/s)	ε	H_T/H_0
4.98	0.73	2.19
5.81	0.78	2.50
6.64	0.82	2.94
7.47	0.85	3.53
8.30	0.88	5.03

Styrofoam (SF 15-5)

Initial bed height H_0=91cm

U_l (cm/s)	ε	H_T/H_0
11.62	0.50	1.11
13.28	0.55	1.32
14.94	0.58	1.43
16.60	0.64	1.67
18.26	0.67	1.91
19.92	0.73	2.23
21.58	0.78	2.79
23.24	0.81	3.16
24.90	0.83	3.54

Initial bed height H_0=57cm

U_l (cm/s)	ε	H_T/H_0
11.62	0.47	1.29
13.28	0.54	1.48
14.94	0.59	1.69
16.60	0.62	1.96
18.26	0.68	2.22
19.92	0.71	2.50
21.58	0.74	2.89
23.24	0.76	3.10
24.90	0.79	3.73

Curriculum Vitae

Name: Long Sang

Post-secondary Education and Degrees:

Department of Chemical and Biochemical Engineering
The University of Western Ontario
London, Ontario, Canada
2009-2013, Ph.D.

Department of Fluid Machinery and Engineering
China Agricultural University
Haidian, Beijing, China
2004-2009, Ph.D.
2000-2004, B.E.

Honours and Awards:

Graduate Student Fellowship, The University of Western Ontario
2009-2013

Rain Bird Scholarship, China Agricultural University
2005-2006

Bao Steel Scholarship, China Agricultural University
2003-2004

Dow Scholarship, China Agricultural University
2002-2003

Excellent Student Scholarship, China Agricultural University
2001-2004

Related Work Experience

Research Assistant
Teaching Assistant
The University of Western Ontario
2009-2013

Research Assistant
Teaching Assistant
China Agricultural University
2004-2009

Publications:

Sang L and Zhu JX (2012), Experimental investigation of the effects of particle properties on solids holdup in an LSCFB riser, Chemical Engineering Journal, 197: 322-329

Sang L, Hong YP, Wang FJ (2009), Investigation of viscosity effect on droplet formation in T-shaped microchannels by numerical and analytical methods, Microfluidics and Nanofluidics, 6 (5): 621-635

Sang L, Hong YP, Wang FJ (2008), Lattice Boltzmann Simulations of Droplet Formation in A Co-Flowing Microchannel, In: Proceedings of FEDSM, ASME 5th Joint ASME/JSME Fluids Engineering Conference, San Diego, CA, USA, July 30-August 2, 2007: 415-421